

Inaugural dissertation
for
obtaining the doctoral degree
of the
Combined Faculty of Mathematics, Engineering and Natural Sciences of
the
Ruprecht - Karls - University
Heidelberg

Presented by
Katrín Leonie Ganzenberg, M.Sc.
Born in Böblingen, Germany
Oral examination: June 13th, 2022

Investigating tumor cell-specific barriers
for immunotherapy

Referees:

Prof. Dr. Peter Angel

Prof. Dr. Darjus Tschaharganeh

Acknowledgments

This dissertation would not have been possible without the help of my supervisors, colleagues, family, and friends, who provided constant support throughout the last years. Therefore, I would like to express my deepest gratitude to:

Prof. Dr. Darjus Tschaharganeh, who entrusted me with this exciting project, supported my professional and personal growth within his team, and assisted the realization of my dissertation with valuable insights and constant feedback.

The Helmholtz International Graduate School of Cancer Research, the German-Israeli Helmholtz International Research School in Cancer Biology, and the team around Lindsay Murrels for funding as well as administrative advice and mentoring.

Prof. Dr. Peter Angel for agreeing to act as faculty supervisor and providing helpful scientific feedback during TAC meetings.

Prof. Dr. Mathias Heikenwalder for his great scientific support and enthusiasm as thesis advisor and collaborator.

Prof. Dr. Gunter Hammerling, who provided useful feedback as part of my thesis advisory committee.

Prof. Dr. Ralf Bartenschlager and Dr. Richard Harbottle for kindly agreeing to act as examiners in my defense committee and reading my dissertation.

Dr. Rafael Carretero, who offered invaluable scientific advice and generously shared protocols and material, as well as all other collaborative partners at DKFZ and Institute of Pathology who provided scientific support.

My colleagues Dr. Steffie Revia, Dr. Julian Mochayedı, Dr. Mathias Meister, Lena Wendler-Link, Luise Butthof, Philip Ohland, and all current and former members of the Tschaharganeh Lab for their technical, scientific, and emotional support during the last years.

Stephan Krieg, my “honorary thesis advisor”, who played an essential role in my pursuit of a doctorate through endless scientific and non-scientific discussions and sharing all kinds of experiences, worries, and laughter.

My parents, supporting me throughout my life in more ways I can imagine. They taught me to have confidence in my abilities and myself, so that I was always certain I could achieve my goals, no matter how challenging.

My family and friends, who fully understood when I was occupied with my work but still found ways to help me recharge and enjoy my time outside the lab.

My husband Hans-Peter for his endless support, constant encouragement, and loving care throughout the years. I could always rely on his rational judgement in times of doubt and kind words of comfort when I felt discouraged, helping me to overcome every obstacle within my path. Thank you for everything.

Abstract (English)

The notion of harnessing the patient's intrinsic immune system to target tumor cells has sparked the development of immunotherapy as a promising new approach to treat cancer. However, only a minority of patients benefit from currently available immunotherapeutic approaches, as many tumors escape immune attacks and develop immune evasion mechanisms. Hence, it is crucial to identify cellular factors that influence the success of immune cell-mediated tumor clearance.

In this project, I developed a genetically defined autochthonous liver cancer mouse model with conditional neoantigen expression for the investigation of neoantigen-mediated immune responses and immunotherapeutic treatments. In addition to that, I used primary neoantigen-expressing tumor cells and antigen-specific T cells to establish a co-culture assay in order to study mechanisms of cytotoxic T cell-mediated killing. This assay was further used to perform a lentiviral CRISPR/Cas9 screen, which identified new tumor cell-specific mediators of T cell-dependent killing, among others *Activin A receptor type I (Acvr1)*. Additional experiments validated the role of *Acvr1*, a type I receptor serine kinase of the bone morphogenetic protein (BMP) pathway, in T cell-mediated killing. Moreover, I could show that *Acvr1* knock-out reduced T cell killing efficiency by downregulating the expression of the death receptor *Fas*, thus reducing FAS ligand (FASLG)-mediated apoptosis induction.

In summary, this study included the establishment of new *in vivo* and *in vitro* model systems for the investigation of neoantigen-specific immune responses and tumor cell clearance. With that, I was able to identify *Acvr1* as new mediator of T cell-dependent tumor cell killing and prospective drug target. These findings offer the opportunity to further explore and improve immunotherapeutic approaches to potentially enhance the success rate of immunotherapies in the future.

Zusammenfassung (deutsch)

Die Vorstellung, das körpereigene Immunsystem des Patienten zur gezielten Beseitigung von Tumorzellen zu nutzen, hat die Entwicklung der Immuntherapie als vielversprechenden neuen Ansatz zur Behandlung von Krebs in Gang gesetzt. Von den derzeit verfügbaren immuntherapeutischen Ansätzen profitiert jedoch nur eine Minderheit der Patienten, da viele Tumore den Angriffen des Immunsystems entgehen und Mechanismen zur Immunevasion entwickeln. Daher ist es von entscheidender Bedeutung, zelluläre Faktoren zu identifizieren, die den Erfolg der Immunzell-vermittelten Tumorbekämpfung beeinflussen.

In diesem Projekt habe ich ein genetisch definiertes, autochthones Leberkrebs-Mausmodell mit kontrollierter Neoantigen-Expression entwickelt, um Neoantigen-spezifische Immunantworten und immuntherapeutische Behandlungsmethoden zu untersuchen. Zusätzlich verwendete ich primäre Neoantigen-exprimierende Tumorzellen und Antigen-spezifische T-Zellen, um einen Co-Kultur-Assay zu etablieren und die Mechanismen der zytotoxischen T-Zell-vermittelten Abwehr zu untersuchen. Dieser Assay wurde anschließend zur Durchführung eines lentiviralen CRISPR/Cas9-Screens verwendet, mit dem neue Tumorzell-spezifische Faktoren der T-Zell-abhängigen Tötung identifiziert wurden, unter anderem *Activin A receptor type I* (*Acvr1*). Weitere Experimente bestätigten die Rolle von *Acvr1*, einer Typ-I-Rezeptor-Serin-Kinase des BMP-Signalwegs (*bone morphogenetic protein*), bei der T-Zell-vermittelten Abwehr. Darüber hinaus konnte ich zeigen, dass der Knock-out von *Acvr1* die Effizienz der T-Zell-Tötung reduziert, indem er die Expression des Todesrezeptors *Fas* herunterreguliert und damit die FAS-Ligand (FASLG)-vermittelte Einleitung der Apoptose verringert.

Im Rahmen dieser Studie wurden neue *in vivo* und *in vitro* Modellsysteme zur Untersuchung Neoantigen-spezifischer Immunantworten und der Eliminierung von Tumorzellen entwickelt. Dadurch konnte ich *Acvr1* als neuen Vermittler der T-Zell-abhängigen Tumorzell-Tötung und potenziellen Arzneimittelkandidaten identifizieren. Diese Erkenntnisse bieten die Möglichkeit, immuntherapeutische Ansätze weiter zu erforschen und zu verbessern, um so die Erfolgsrate von zukünftigen Immuntherapien zu erhöhen.

Table of contents

List of tables.....	viii
List of figures	ix
List of abbreviations	x
1 Introduction.....	1
1.1 Cancer as genetic disease	1
1.1.1 The role of genetic aberrations in cancer	1
1.1.2 Oncogenes and tumor suppressor genes.....	1
1.1.2.1 Oncogenes	1
1.1.2.2 Tumor suppressor genes	2
1.1.3 Liver cancer	3
1.1.3.1 Hepatocellular carcinoma.....	3
1.1.3.2 Intrahepatic cholangiocarcinoma.....	4
1.1.3.3 Mouse models to study liver cancer <i>in vivo</i>	4
1.2 Cancer therapies	6
1.2.1 Established cancer treatments.....	6
1.2.2 Immunotherapy	6
1.2.2.1 Recognition and elimination of tumor cells by cytotoxic T cells	7
1.2.2.2 Immune checkpoint blockade	8
1.2.2.3 Adoptive T cell therapy.....	9
1.2.2.4 Other immunotherapeutic approaches	10
1.2.2.5 Limitations and challenges of immunotherapy.....	10
1.3 The role of the bone morphogenetic protein (BMP) pathway in cancer and immunotherapy...	13
1.3.1 The canonical TGF β and BMP pathway	13
1.3.2 The role of TGF β and BMP signaling in cancer and immunotherapy	14
1.4 Aims of the project.....	15
2 Material and methods.....	17
2.1 Molecular biology	17
2.1.1 Overview of used plasmids.....	17
2.1.2 Molecular cloning	18
2.1.2.1 Generation of CRISPR/Cas9 guide plasmids.....	18
2.1.2.2 HiFi Assembly.....	20
2.1.2.3 Transformation of heat competent <i>E. coli</i>	20
2.1.3 Plasmid DNA purification (Mini and Midi prep)	20

TABLE OF CONTENTS

2.1.4	Isolation of gDNA	20
2.1.5	T7 endonuclease I assay	21
2.1.6	Isolation of RNA	22
2.1.7	Reverse transcription and quantitative real-time PCR (qRT-PCR)	23
2.2	Protein analysis	24
2.2.1	Protein isolation	24
2.2.2	Bradford assay	25
2.2.3	SDS-PAGE and Western blot	25
2.3	Cell culture methods	27
2.3.1	General remarks	27
2.3.2	Isolation of murine primary hepatocytes	27
2.3.3	Production of viral particles	27
2.3.4	Stable transduction of primary hepatocytes	28
2.3.5	Proliferation assay	28
2.3.6	Colony formation assay	28
2.3.7	Cell surface staining for flow cytometry	28
2.3.8	Cleaved caspase 3/7 assay	29
2.3.9	OT-I T cell killing assay	29
2.3.10	Lentiviral CRISPR/Cas9 screen	30
2.3.11	RNA sequencing and differential gene expression analysis	32
2.4	Animal experiments	32
2.4.1	Hydrodynamic tail vein injection (HTVI)	32
2.4.2	Magnetic resonance imaging (MRI)	32
2.4.3	Adoptive T cell transfer and immune checkpoint blockade	32
2.4.4	Immunohistochemistry (IHC)	33
3	Results	34
3.1	Generating genetically defined liver tumors with conditional neoantigen expression	34
3.2	Establishment of a T cell killing assay to identify tumor cell-specific barriers for immunotherapy	38
3.2.1	Characterization of tumor-derived primary cell lines to investigate neoantigen-specific tumor cell killing <i>in vitro</i>	38
3.2.2	Establishment of a neoantigen-specific T cell killing assay	39
3.2.3	A lentiviral CRISPR/Cas9 screen reveals modulators of T cell-mediated tumor cell killing	40
3.3	<i>Acvr1</i> KO leads to reduced antigen-specific tumor cell killing	44
3.4	<i>Acvr1</i> KO leads to changes in BMP signaling	47
3.5	ACVR1 re-expression reverses the effects of <i>Acvr1</i> KO on T cell-mediated killing	50
3.6	Investigating the effect of BMP signaling pathway pre-activation on T cell-mediated killing	51

3.7	Unravelling the mechanistic effect of <i>Acvr1</i> on antigen-specific tumor cell killing	53
3.7.1	<i>Acvr1</i> KO does not affect antigen presentation in tumor cells.....	53
3.7.2	<i>Acvr1</i> KO diminishes <i>Fas</i> upregulation and leads to reduced apoptosis induction	53
3.8	Investigating the effect of other BMP signaling effectors on antigen-specific tumor cell killing	58
3.9	KO of the ACVR1 downstream target <i>Id1</i> does not affect T cell killing efficiency.....	60
3.10	The effect of ACVR1 KO on T cell killing efficiency in a human MART-1-specific killing assay	62
4	Discussion	64
4.1	A genetically defined autochthonous liver cancer model for the investigation of neoantigen-specific immune responses.....	64
4.2	A novel T cell killing assay identifies new mediators of tumor cell clearance.....	68
4.2.1	A novel T cell killing assay to study T cell-mediated tumor cell killing	68
4.2.2	A lentiviral CRISPR/Cas9 screen identifies new modulators of T cell-mediated tumor cell killing.....	69
4.3	The role of <i>Acvr1</i> in T cell-mediated tumor cell killing.....	71
4.3.1	<i>Acvr1</i> as new mediator of T cell-mediated cytotoxicity.....	71
4.3.2	The role of other BMP signaling effectors on T cell-mediated tumor cell killing	73
4.3.3	A potential mechanism of <i>Acvr1</i> -mediated resistance to T cell killing involves <i>Fas</i> and NFκB signaling.....	74
4.4	Unravelling the role of BMP signaling in different cellular contexts	75
4.5	Clinical applications for ACVR1 as mediator of antigen-specific tumor cell killing.....	76
5	Conclusion	78
6	References.....	79
7	Appendix.....	100

List of tables

Table 2.1. Overview of used plasmids.	17
Table 2.2. sgRNA sequences used in this study.	18
Table 2.3. Primer sequence for HiFi Assembly.	20
Table 2.4. Overview of PCR primers used for T 7 Endonuclease I assay.	21
Table 2.5. Reverse transcription reaction.	23
Table 2.6. Overview qPCR reaction.	23
Table 2.7. Overview qPCR primers.	23
Table 2.8. Composition of cell lysis buffer for protein extraction.	24
Table 2.9. Composition of phosphatase inhibitor cocktail.	24
Table 2.10. Composition of PAA gels.	25
Table 2.11. Composition of buffers used for SDS-PAGE and Western blotting.	25
Table 2.12. Overview of antibodies used for immunoblotting.	26
Table 2.13. Overview of antibiotics used for selection after viral transduction.	28
Table 2.14. Antibodies used for flow cytometrical analysis.	29
Table 2.15. PCR primer sequences for analysis of the CRISPR/Cas9 screen.	30
Table 3.1. Overview of the 10 highest ranked hits of the CRISPR/Cas9 screen.	43
Table 7.1. List of genes included in the sgRNA surface library.	100
Table 7.2. Genes identified as hits in the CRISPR/Cas9 screen.	106

List of figures

Figure 1.1. Mechanism of DNA uptake by hepatocytes via hydrodynamic tail vein injection [80].	5
Figure 1.2. Mechanism of T cell activation and cytotoxicity.	8
Figure 1.3. Mechanism of immune checkpoint blockade therapy.	9
Figure 1.4. Overview of the canonical TGF β and BMP signaling pathway.	14
Figure 3.1. Generation of genetically defined autochthonous liver tumors.	35
Figure 3.2. DOX-dependent neoantigen expression in primary liver cancer cell lines.	37
Figure 3.3. DOX-dependent neoantigen expression in primary liver cancer cell lines.	38
Figure 3.4. Establishment of an antigen-specific T cell killing assay.	39
Figure 3.5. A pooled CRISPR/Cas9 screen to identify modulators of antigen-specific tumor cell killing.	41
Figure 3.6. Validation of hits identified in the CRISPR/Cas9 screen.	44
Figure 3.7. <i>Acvr1</i> KO leads to reduced T cell-mediated killing in MYC/sgTrp53 cells.	45
Figure 3.8. <i>Acvr1</i> KO leads to reduced T cell-mediated killing in <i>Kras</i> ^{G12D} /sgTrp53 cells.	46
Figure 3.9. Activation of ACVR1 downstream targets is reduced in <i>Acvr1</i> KO cells.	48
Figure 3.10. Gene expression analysis in <i>Acvr1</i> KO cells.	49
Figure 3.11. Expression of catalytically active ACVR1 versions reverses the effect of <i>Acvr1</i> KO on T cell-mediated killing in MYC/sgTrp53 cells.	50
Figure 3.12. The effect of BMP7 treatment on T cell-mediated killing.	52
Figure 3.13. Neoantigen presentation in <i>Acvr1</i> KO cells.	53
Figure 3.14. <i>Fas</i> surface presentation and gene expression in <i>Acvr1</i> KO and <i>ACVR1</i> -expressing cells.	54
Figure 3.15. Cleaved caspase 3/7 assay with <i>Acvr1</i> KO and <i>ACVR1</i> -expressing cells.	56
Figure 3.16. The impact of <i>Acvr1</i> on STAT1 and NF κ B signaling.	57
Figure 3.17. The effect of other BMP signaling receptor KOs on T cell-mediated killing in MYC/sgTrp53 cells.	59
Figure 3.18. KO of the ACVR1 downstream target <i>Id1</i> does not affect T cell killing efficiency.	61
Figure 3.19. Human MART-1 co-culture assay with <i>ACVR1</i> KO COLO800 cells.	63

List of abbreviations

Acvr1	Activin A receptor type 1
Acvr2	Activin A receptor type 2
ALK	Activin receptor-like kinase
APC	Adenomatous polyposis coli
APC	Antigen-presenting cell
Approx.	Approximately
APS	Ammonium persulfate
B2M	Beta-2 microglobulin
Bche	Butyrylcholinesterase
BMP	Bone morphogenetic protein
BMPR	Bone morphogenetic protein receptor
bp	Base pair
BRCA1/2	Genes encoding Breast cancer type 1/2 susceptibility protein
BSA	Bovine serum albumin
c-Myc	Cellular Myc
C3ar1	Complement C3a receptor 1
caACVR1	Constitutively active <i>ACVR1</i> , mutated at Q207D
Cacng8	Calcium voltage-gated channel auxiliary subunit gamma 8
CAF	Cancer-associated fibroblast
CAR	Chimeric antigen receptor
Cas9	Clustered regularly interspaced short palindromic repeats associated protein 9
CCl ₄	Carbon tetrachloride
CD	Cluster of differentiation
CDK	Cyclin-dependent kinase
CMV	Cytomegalovirus
Col6a5	Collagen type VI alpha 5 chain
CRES	CAR T cell-related encephalopathy syndrome
CRISPR	Clustered regularly interspaced short palindromic repeats
CRS	Cytokine release syndrome
CTL	Cytotoxic T lymphocyte
CTLA4	Cytotoxic T lymphocyte antigen 4
CTNNB1	Beta-Catenin
DC	Dendritic cell
ddH ₂ O	Double-distilled water
DEN	Diethylnitrosamine

DIPG	Diffuse intrinsic pontine glioma
DKFZ	Deutsches Krebsforschungszentrum
DMEM	Dulbecco's Modified Eagle Medium
DMSO	Dimethyl sulfoxide
DNA	Deoxyribonucleic acid
DOX	Doxycycline hyclate
E-boxes	Enhancer box elements
<i>e.g.</i>	<i>Exempli gratia</i> , for example
ECM	Extracellular matrix
EDTA	Ethylenediamine tetraacetic acid
Egfr	Epidermal growth factor receptor
EMT	Epithelial mesenchymal transition
Ephb4	Ephrin type-B receptor 4
ER	Endoplasmic reticulum
ERK	Extracellular signal-regulated kinase
<i>et al.</i>	<i>Et alii</i> , and others
EV	Empty vector
FASLG	FAS ligand
FCS	Fetal calf serum
FDA	Food and Drug Administration
FITC	Fluorescein isothiocyanate
FOP	Fibrodysplasia ossificans progressiva
G12D/G12V	Base substitution at position 12 from glycine to aspartate/valine
GDF	Growth differentiation factor
gDNA	Genomic deoxyribonucleic acid
GFP	Green fluorescent protein
GM-CSF	Granulocyte-macrophage colony-stimulating growth factor
Gpc1	Glypican 1
GSEA	Gene Set Enrichment Analysis
GTPase	Guanosine triphosphatase
GZM	Granzyme
h	Hour
H&E	Hematoxylin & eosin
HBV	Hepatitis B virus
HCC	Hepatocellular carcinoma
HCV	Hepatitis C virus
HLA	Human leukocyte antigen
HPV	Human papilloma virus

LIST OF ABBREVIATIONS

HRP	Horse radish peroxidase
HTVI	Hydrodynamic tail vein injection
<i>i.e.</i>	<i>Id est</i> , that is
I κ B α	NFKB inhibitor alpha
ICC	Intrahepatic cholangiocarcinoma
ID1-4	Inhibitor of differentiation/DNA binding 1-4
IFN γ	Interferon gamma
Igln5	IgLON family member 5
Igsf8	Immunoglobulin superfamily member 8
IHC	Immunohistochemistry
IKK	Inhibitor of nuclear factor kappa-B kinase
IL-10	Interleukin-10
IL-2	Interleukin-2
Indels	Insertions and deletions
IPA	Ingenuity Pathway Analysis
IR/DR	Inverted repeats/direct repeats
IRES	Internal ribosomal entry site
JAK	Janus kinase
JNK	c-Jun N-terminal kinase
kdACVR1	Kinase-dead <i>ACVR1</i> , mutated at K235R
KO	Knock-out
KRAS	Kirsten rat sarcoma virus
l	Liter
LAG3	Lymphocyte activation gene 3
Ldlr	Low density lipoprotein receptor
Lrrc4b	Leucine rich repeat containing 4B
MAPK	Mitogen-activated protein kinase
MART-1	Melanoma antigen recognized by T-cells
MAX	MYC-associated factor X
MDSC	Myeloid-derived suppressor cell
MFI	Mean fluorescent intensity
mg	Milligram
MHC	Major histocompatibility complex
min	Minute
ml	Milliliter
MOI	Multiplicity of infection
MRI	Magnetic resonance imaging
mRNA	Messenger ribonucleic acid

MSCV	Murine stem cell virus
NASH	Non-alcoholic steatohepatitis
NES	Normalized enrichment score
NF κ B	Nuclear factor kappa-light-chain-enhancer of activated B cells
ng	Nanogram
NGS	Next generation sequencing
NK cell	Natural killer cell
Nlgn2	Neurologin 2
o/n	Overnight
PAA	Polyacrylamide
PBS	Phosphate buffered saline
Pcdh15	Protocadherin related 15
PCR	Polymerase chain reaction
PD1	Programmed cell death protein 1
PDL1/2	Programmed cell death protein 1 ligand 1/2
PEI	Polyethyleneimine
PI3K	Phosphatidylinositol 3-kinase
PP2A	Protein phosphatase 2A
PRF1	Perforin 1
Ptpn2	Protein tyrosine phosphatase non-receptor type 2
PVDF	Polyvinylidene
qRT-PCR	Quantitative real-time PCR
RAS	Rat sarcoma virus
RB	Retinoblastoma
RB1	RB transcriptional corepressor 1
rIL-2	Recombinant Interleukin-2
RNA	Ribonucleic acid
RNAi	Ribonucleic acid interference
RT	Room temperature
rtTA3	Reverse tetracycline-regulated transactivator gene 3
SB	Sleeping Beauty
s.d.	Standard deviation
Sdk2	Sidekick cell adhesion molecule 2
SDS	Sodium dodecyl sulfate
SDS-PAGE	Sodium dodecyl sulfate-polyacrylamide gel electrophoresis
sec	Seconds
sgRNA	Single guide ribonucleic acid
shRNA	Short-hairpin ribonucleic acid

LIST OF ABBREVIATIONS

SIINFEKL	Ovalbumin-derived neoantigen with amino acid sequence SIINFEKL
Slc12a9	Solute carrier family 12 member 9
SMAD	Small/Mothers against Decapentaplegic
SMURF1	SMAD ubiquitination regulatory factor-1
Sorcs3	Sortilin-related VPS10 domain containing receptor 3
Sostdc	Sclerostin Domain Containing 1
STAT1	Signal transducer and activator of transcription 1
TGFBR	Transforming growth factor beta receptor
TAA	Tumor-associated antigen
TAK1	TGF β -activated kinase
TCR	T cell receptor
TERT	Telomerase reverse transcriptase
TGF β	Transforming growth factor beta
TIL	Tumor-infiltrating lymphocyte
TIM3	T cell immunoglobulin 3
T _m	Melting temperature
TMB	Tumor mutational burden
TME	Tumor microenvironment
TNF α	Tumor necrosis factor alpha
TP53	Tumor protein p53
TRE	Tetracycline response element
Treg	Regulatory T cell
tRFP	Turbo red fluorescent protein
TRP53	Transformation-related protein 53
TSA	Tumor-specific antigen
UV	Ultraviolet
v/w	Volume per weight
VEGF	Vascular endothelial growth factor receptor
VISTA	V-domain immunoglobulin suppressor of T cell activation
Vs.	<i>Versus</i>
Wnt	Wingless-related integration site
Wt	Wildtype
wtACVR1	Wildtype ACVR1
μ g	Microgram
μ l	Microliter

1 Introduction

1.1 Cancer as genetic disease

1.1.1 The role of genetic aberrations in cancer

Cancer is a family of diseases that are characterized by uncontrolled growth of malignant cells leading to the formation of neoplastic lesions, tissue invasion, and metastases. Taken together, cancer accounts for approx. 10 million deaths in 2020 worldwide, making it the second leading cause of death [2,3]. Hanahan and Weinberg postulated common acquired characteristics of cancer cells, which explain how cancer arises and why treatment options are still limited. These hallmarks of cancer include sustaining proliferative signaling, evading growth suppressors, replicative immortality, resistance to cell death, induction of angiogenesis, invasion and metastasis, immune evasion, tumor-promoting inflammation, dysregulated cellular metabolism, and genomic instability and mutation [4,5]. Since these acquired properties are consequences of genetic alterations or gene mutations in cells, cancer has been widely accepted to be a genetic disease [6]. Genetic alterations leading to cancer can be either hereditary germ line mutations, *e.g.*, mutations in the breast cancer prevalence genes encoding Breast cancer type 1 and 2 susceptibility proteins (*BRCA1* and *BRCA2*), or acquired mutations in somatic cells that were triggered by external factors like smoking, diet, or UV radiation [7,3]. Different classes of molecular alterations or gene mutations have been identified and described in tumor genomes and range from single nucleotide variations to large chromosomal rearrangements, like large-scale deletions or copy number alterations [6,8,9]. Additionally, beside direct changes in the genomic DNA sequence, cancer can arise through epigenetic dysregulation, such as hypo- or hypermethylation of CpG islands, which promote aberrant gene activation or silencing, respectively [10,11]. Moreover, several genes of viral origin are known to cause cancer (*e.g.*, human papilloma virus, HPV) [12,13]. Generally, altered genes that drive tumorigenesis can be categorized as oncogenes or tumor suppressor genes, which will be discussed hereafter.

1.1.2 Oncogenes and tumor suppressor genes

Consistent with the notion that cancer is a genetic disease, a large number of genes has been identified that lead to tumorigenesis if they are altered or mutated. These genes can be categorized according to their tumorigenic mode of action in (proto-)oncogenes and tumor suppressor genes.

1.1.2.1 Oncogenes

In healthy cells, proto-oncogenes fulfill various roles in fundamental cellular processes like proliferation, cell survival, and differentiation [14]. During tumorigenesis, proto-oncogenes undergo genetic alterations, which lead to aberrantly increased gene expression or hyperactivation of the encoded protein. These abnormally activated genes are then dubbed oncogenes and cause uncontrolled cell growth and proliferation, thus driving tumorigenesis [15].

Several different molecular mechanisms lead to oncogene activation. One of them are mutations in the coding sequence of a proto-oncogene which cause hyperactivation of the expressed protein. A well-described example is the oncogene Kirsten rat sarcoma virus (*KRAS*), which is part of the *RAS* gene family [16].

KRAS mutations are often found in pancreatic, colorectal, and lung adenocarcinomas, making it one of the most frequent mutated oncogenes in humans [17]. *KRAS* encodes a GTPase which acts as an activator of several signaling pathways associated with tumorigenesis, including the mitogen-activated protein kinase (MAPK) and the phosphatidylinositol 3-kinase (PI3K) pathway [18,19]. Under healthy conditions, *KRAS* alternates between a GTP-bound activated state, in which it is able to transduce activating signals to downstream effectors, and a GDP-bound inactivated state, which occurs after hydrolysis of GTP to GDP by *KRAS* [20]. Oncogenic *KRAS* is often found to have a point mutation at position G12, which leads to the substitution of the amino acid glycine to aspartate (G12D) or valine (G12V) [21]. As a consequence, *KRAS* is not able to hydrolyze GTP, which causes permanent activation of *KRAS*. This results in constitutive activation of signaling pathways associated with proliferation and cell survival, ultimately leading to tumorigenesis [22,16].

A second type of molecular event causing oncogene activation are large chromosomal rearrangements that lead to increased oncogene expression. One oncogene that is activated in this manner is *MYC* (also known as *c-Myc* (cellular Myc)). *MYC* is part of a family of *Myc* transcription factors including *MYC*, *l-Myc*, and *n-Myc* [23]. *MYC* targets at least 15 % of all human genes and regulates a multitude of cellular processes like cell cycle progression, proliferation, cell survival, cell growth, and differentiation [24,25]. Accordingly, aberrantly expressed *MYC* is one of the most frequent oncogenes found in many different tumor types [26]. In order to initiate gene expression, *MYC* forms heterodimers with the *MYC*-associated factor X (*MAX*) and binds DNA at enhancer box elements (E-boxes). This is mediated by the basic helix-loop-helix and leucine zipper motifs found in both *MYC* and *MAX* [27,28]. Different mechanisms of *MYC* oncogene activation have been described. For instance, chromosomal translocations placing *MYC* under the control of strong enhancer elements like the immunoglobulin heavy chain enhancer have been identified in approx. 80 % of Burkitt's lymphomas [29,30]. Furthermore, copy number alterations can result in the amplification of the *MYC* gene on chromosome 8q [31,32]. Remarkably, *MYC* is estimated to be amplified in 21 % of all cancer types [33].

1.1.2.2 Tumor suppressor genes

Tumor suppressor genes are regulators for cell cycle progression and proliferation and can induce cell cycle arrest or apoptosis. Unlike oncogenes, they exert their tumor promoting role upon aberrant inactivation rather than upregulation [34]. If tumor suppressor genes lose their regulatory function, cell cycle progression and proliferation can occur uncontrolled, which results in genomic instability and formation of malignant cells. Several molecular alterations can lead to the loss of a tumor suppressor gene, including complete loss of the gene (large-scale deletion), point mutations, or epigenetic silencing [35]. Since tumor-promoting mutations of tumor suppressor genes lead to a loss of function, both alleles need to be affected for the formation of malignant cells (also known as Knudson's two-hit hypothesis) [36,35].

The first identified tumor suppressor gene was found in both hereditary and sporadic cases of retinoblastomas (RB) and was therefore named RB transcriptional corepressor 1 (*RB1*) [37]. In healthy cells, the gene product of *RB1* suppresses the transcription of E2F transcription factor target genes, which are essential for cell cycle progression and proliferation [38]. *RB1* is inactivated through phosphorylation by Cyclin-dependent kinase 4 (CDK4)/Cyclin D complexes, leading to cell cycle progression and proliferation. Hence, if the function of *RB1* is lost, cells can divide uncontrollably and promote tumorigenesis. Dysregulated or mutated *RB1* is often found in retinoblastomas, osteosarcomas, and small-cell lung cancer [38].

The tumor protein p53 (*TP53*) is a tumor suppressor gene that is estimated to play a role in 50 % of all cancers [34]. Germline mutations of *TP53* are the cause of the Li-Fraumeni syndrome, a hereditary disease that leads to development of tumors in young age [39,40]. In healthy cells, TP53 is activated upon DNA damage or oncogene expression in order to arrest cell cycle progression or to induce apoptosis [41,42]. Therefore, *TP53* is also dubbed the “guardian of the genome”, as it prevents cells harboring potentially tumorigenic DNA damage from proliferating and forming neoplastic lesions. In healthy cells, detection of DNA damage leads to rapid upregulation of TP53, which in turn activates the expression of genes associated with cell cycle arrest, DNA repair, apoptosis, and senescence [43]. One major target of TP53 is the CDK inhibitor p21 [44]. Inhibition of CDK/Cyclin complexes by p21 leads to cell cycle arrest until DNA damage is repaired [34]. Additionally, DNA damage-induced activation of TP53 can lead to induction of apoptosis in order to eliminate cells with DNA damage.

In tumors, *TP53* is often mutated in the DNA binding domain of the gene [45], leading to missense mutations and altered protein function [46]. Loss of function of *TP53* leads to reduced DNA damage repair and increased genome instability, thus ultimately promoting tumorigenesis [34].

1.1.3 Liver cancer

Liver cancer is the third most frequent cause of cancer-related death worldwide [47]. The two most common primary liver cancer subtypes are hepatocellular carcinoma and intrahepatic cholangiocarcinoma.

1.1.3.1 Hepatocellular carcinoma

Hepatocellular carcinoma (HCC) is the most frequent form of liver cancer, accounting for approx. 75 % of all primary liver cancers [48]. HCC is generally considered to originate from hepatocytes, although the scientific discourse of the origin of HCC is still ongoing and proposes several hepatic progenitor cell types as cells of origin [49]. Major risk factors for HCC development are chronic infections with hepatitis B and C viruses, cirrhosis, obesity- or diabetes- induced non-alcoholic steatohepatitis (NASH), and excessive alcohol consumption [50]. Hepatitis B virus (HBV) infections account for 60 % of all HCC cases in Asia and Africa and 20 % of all HCC cases in the West [51]. HBV is a DNA virus that integrates into the genome of the host, thereby causing oncogene activation [52]. On the other hand, hepatitis C virus (HCV) is an RNA virus and leads to HCC development indirectly by inducing chronic liver damage and cirrhosis [50]. Liver cirrhosis, caused by viral infections, alcohol consumption, or NASH, is found in more than 80 % of all HCC cases [53]. Notably, 90 % of all HCC cases develop in the context of chronic liver disease or cirrhosis and it was shown that chronic inflammation, dysregulated immune surveillance, and a cirrhotic microenvironment promote tumorigenesis in HCC [54–56].

The mutational landscape of HCC is highly heterogeneous and still under investigation [57]. Frequent mutational drivers of HCC include activating mutations of Telomerase reverse transcriptase (*TERT*) (found in 60 % of all HCC), genetic alterations leading to activation of the Wnt- β -Catenin pathway (*e.g.*, mutations in *CTNNB1*, *AXIN1*, or *APC*, approx. 50 %), and loss-of-function mutations of *TP53* (20-25 %) [58,57,50]. Additionally, the MAPK pathway is altered in 43 % of all HCC cases, with activating mutations of *KRAS* making up for 1.6 % [57,58]. Activating alterations of the oncogene *MYC* are found in 12 % of HCC [59–61]. However, even though many tumor-driving genes causing HCC have been identified, only 20-25 % of all HCC

patients are found to have a potentially actionable mutation, highlighting the need for new therapy approaches [50].

1.1.3.2 Intrahepatic cholangiocarcinoma

Intrahepatic cholangiocarcinoma (ICC) arises from cholangiocytes of intrahepatic bile ducts. It accounts for 12-15 % of all liver cancers and is the second most frequent liver cancer entity after HCC [48]. Common risk factors for developing ICC are the same as for HCC, namely HBV and HCV infections, alcohol consumption, obesity, and NASH. Accordingly, chronic inflammation of the biliary epithelium is observed in many cases of ICC [62,63].

The mutational landscape of ICC comprises genetic alterations that lead to dysregulation of *WNT-CTNNB1*, *MYC*, *ERBB*, *TNF*, and *VEGF* signaling [62]. *KRAS* mutations are present approx. 8 % of ICC, while amplifications of the *MYC* oncogene could be found in approx. 20 % [64,65]. Furthermore, mutations in the tumor suppressor *TP53* have been reported in 12.5 % of studied ICC cases [65]. 50 % of all cholangiocarcinoma harbor genetic driver mutations that can be targeted by drugs and offer new possibilities for targeted therapy approaches for optimized treatment of ICC [62].

1.1.3.3 Mouse models to study liver cancer *in vivo*

Mice are often used as *in vivo* models owing to their relatively cost- and time-effective husbandry and their genetic similarity to humans [66]. In cancer research, mouse models are utilized to gain deeper insights into biological mechanisms of tumorigenesis and cancer therapies. For that, they need to be able to mimic molecular changes and pathophysiological processes of tumorigenesis and tumor progression in a reproducible and reliable manner. For liver cancer research, a variety of mouse models has been established that differ in the mode of cancer initiation, tumor incidence, and time of tumor development [67].

Several dietary models have been described that are able to recapitulate liver tumorigenesis caused by obesity or the metabolic syndrome. For instance, mice fed with a choline-deficient diet develop hepatosteatosis and HCC [68]. High-fat or Western diets contain high percentages of fats, fructose, and cholesterol, and cause similar symptoms as the metabolic syndrome found in humans (*e.g.*, obesity and insulin resistance), resulting in hepatic steatosis with chronic inflammation, fibrosis, and ultimately HCC [69–73]. Dietary mouse models have a relatively long tumor incidence of approx. 12 months and closely mimic the human pathophysiology of NASH-associated chronic inflammation and fibrosis, which eventually leads to HCC development [67].

Additionally, tumor induction by chemotoxins like diethylnitrosamine (DEN) or carbon tetrachloride (CCl₄) has been used for several decades and has been well described. Chemotoxins and their metabolites lead to tumorigenesis by causing DNA damage, oxidative stress, and liver damage and result in tumor induction within 9-24 months [67,74–77].

Being a genetic disease, numerous genetically-engineered mouse models are used in liver cancer research that aim to emulate genetic alterations found in HCC. For instance, several transgenic mouse strains have been established that harbor mutations causing overexpression of *Myc* [67]. By coupling oncogenes or tumor suppressor genes with the albumin receptor or the Cre-lox system, it is possible to achieve liver-specific gene expression or gene knock-out (KO). Transgenic mouse strains frequently used to study HCC include

genetic manipulations of the Wnt- β -Catenin pathway, or KO of *Trp53* or *Pten*. In these models, the time of tumor development and incidence vary depending on the tumor-driving mutation [67]. However, the establishment of genetically-engineered mouse strains is time- and cost-intensive and requires gene modification in embryonic stem cells and extensive cross-breeding.

Therefore, hydrodynamic tail vein injection (HTVI) has become a cheap and straight-forward alternative to traditional methods of generating transgenic mice. HTVI is used to quickly deliver naked DNA into liver cells. This is achieved through rapid injection of a large amount of DNA (up to 50 μ g) in saline solution (10 % v/w of the body weight) into the tail vein within 7-10 seconds. The solution enters the *inferior vena cava* and leads to increased intravascular pressure. After reaching the heart, the high volume of the injection stretches the myocardial fibers and causes cardiac congestion. This results in a retrograde flow via the *inferior vena cava* into hepatic vessels. Due to the high endothelial pressure, the endothelial fenestrations in the hepatic sinusoids are transiently expanded and mediate the uptake of DNA by hepatocytes (Figure 1.1) [78,79].

Using this method, between 10 % and 40 % of all hepatocytes are transiently transfected [67,80]. By combining HTVI with plasmids encoding Sleeping Beauty (SB) transposase elements, genetic information can be stably integrated into the genome of hepatocytes. The SB system consists of the SB transposase, a synthetic recombinase, and transposable elements flanked by specific inverted repeats/direct repeats (IR/DR) sequences [81]. The transposase recognizes and binds to the IR/DR regions and leads to transposition of the transposon element into the genome in a cut-and-paste manner [82]. By designing transposon elements that harbor genetic information of oncogenes or short-hairpin RNA (shRNA), the SB system can be

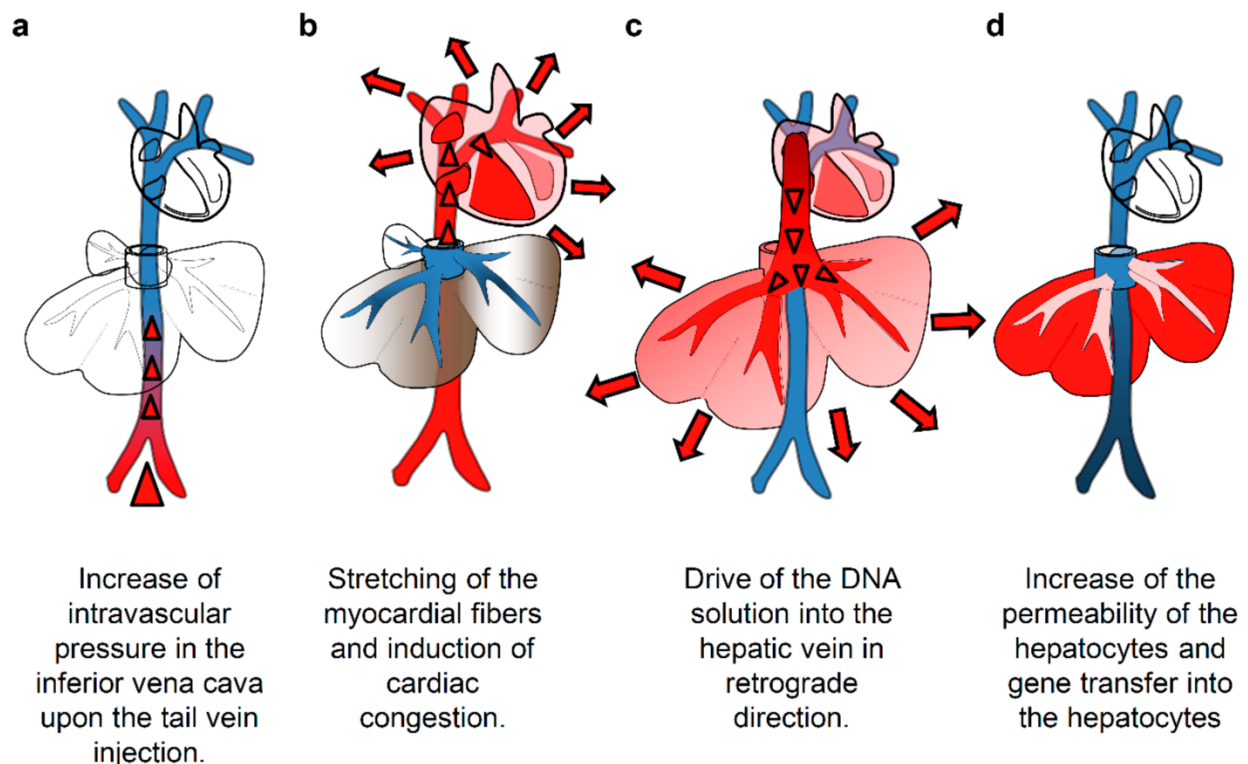


Figure 1.1. Mechanism of DNA uptake by hepatocytes via hydrodynamic tail vein injection [80].

used to induce expression of oncogenes or RNA interference (RNAi)-mediated knock-down of tumor suppressor genes, which leads to rapid and aggressive tumor development [82]. Furthermore, transposon elements can be designed to contain tetracycline-responsive gene promoters, thus achieving conditional transgene or shRNA expression [83]. In addition to that, HTVI can be used to deliver plasmids encoding for components of various CRISPR systems allowing targeted gene editing like gene KO, base editing, or gene activation in hepatocytes [84]. Through combined use of transposon and CRISPR/Cas9 plasmids with HTVI, it is possible to simultaneously generate stable oncogene expression and tumor suppressor gene KO in hepatocytes. This leads to rapid formation of liver tumors within several weeks or months, depending on the cancer-driving genes [85].

Taken together, this highly flexible model allows the generation of genetically defined autochthonous liver tumors and is therefore well suited to investigate the impact of specific genes on liver tumorigenesis and tumor progression.

1.2 Cancer therapies

1.2.1 Established cancer treatments

For a long time, standard medical interventions to treat cancer were limited to surgical resection of the tumor mass, radiation therapy, and untargeted chemotherapy. However, these approaches are often not feasible, ineffective, or caused severe adverse effects due to systemic toxicity [86].

With the advent of personalized medicine, targeted anti-cancer drugs have been developed that allowed to match the treatment to the underlying disease-conferring cellular mechanisms. Unlike classical chemotherapy, which targets all fast-proliferating cells regardless of their malignant state, targeted therapies aim to inhibit specific cellular functions that contribute to the cancerous phenotype of tumor cells [87]. For example, the multikinase inhibitor Sorafenib (Nexavar®) is used for the treatment of unresectable advanced HCC, renal cell carcinoma, and thyroid cancer [88,89]. Sorafenib targets receptor tyrosine kinases like vascular endothelial growth factor receptor (VEGFR) and the intracellular serine/threonine kinases of the MAPK pathway, thus inhibiting angiogenesis and tumor cell proliferation [90]. Moreover, targeted hormonal therapies can be used to treat hormone-sensitive tumors, like certain breast cancer types, by binding to hormone receptors and inhibiting hormone-induced growth signals (*e.g.*, Tamoxifen (Nolvadex®)) [91]. Since targeted therapies specifically inhibit individual cellular processes of tumor cells, many tumors develop drug resistance over time [87]. Therefore, targeted anti-cancer therapies are often combined with other therapy approaches, such as chemotherapy, radiation, or immunotherapy [87,92].

1.2.2 Immunotherapy

The notion to harness the patient's immune system to attack malignant cells has become increasingly significant over the last three decades. In 2018, the inventors of immune checkpoint blockade therapy James P. Allison and Tasuko Honjo were awarded with the Nobel Prize of Medicine, underlining the importance and therapeutic potential of immunotherapies [93].

Immunotherapeutic approaches can be divided into four categories: immune checkpoint blockade, adoptive T cell-based therapies, cancer vaccines, and immune system modulators [94,95]. Immunotherapeutic

approaches are mainly based on the function of cytotoxic T lymphocytes, which are able to recognize and kill cells expressing specific antigens.

1.2.2.1 Recognition and elimination of tumor cells by cytotoxic T cells

Malignant tumor cells can be eliminated through the cytotoxic effects of activated CD8⁺ T cells (cytotoxic T lymphocytes, CTLs). For that, CD8⁺ T cells have to undergo three activation steps. First, tumor cells are recognized by T cells through specific binding of antigen: major histocompatibility class I complexes (MHC class I) to antigen-specific T cell receptors. This initiates the cellular mechanism of T cell activation, which ultimately results in the implementation of cytotoxic effector functions to kill target cells.

Initially, T cells have to be able to recognize tumor cells as abnormal. This is accomplished by the presentation of tumor-specific or tumor-associated antigens (TSAs or TAAs) complexed with MHC class I on the surface of tumor cells. TSAs, also referred to as neoantigens, are antigens that are uniquely expressed on the surface of tumor cells and originate from the expression and processing of mutated proteins that arise during the neoplastic progression of tumor cells [96]. TAAs, on the other hand, derive from unmutated proteins that are overexpressed or abnormally expressed on tumor cells [97,98]. The precursors of TAAs and TSAs are endogenous proteins that are translated in the cytosol and subsequently undergo proteasomal degradation. The degraded peptides are then transported into the endoplasmic reticulum (ER) via the transporter associated with antigen processing (TAP), where they bind to MHC class I. Next, the peptide-loaded complex is shuttled to the cell membrane, where it presents the loaded antigen to CD8⁺ T cells [99]. CD8⁺ T cells specifically bind to peptide:MHC class I complexes through direct interaction of the co-receptor CD8 and MHC class I [100], thus being able to recognize antigens on all nucleated cells in the body [101]. Upon binding of the antigen-specific T cell receptor of naïve CD8⁺ T cells to antigen:MHC class I complexes, T cell activation is initiated (**Figure 1.2**).

The activation of T cells is a two-step process and starts with the interaction of the T cell receptor (TCR) to its cognate antigen:MHC class I complex on antigen-presenting cells (APCs). Secondly, the co-stimulatory receptor CD28 on the T cell engages with the ligands B7-1 (CD80) or B7-2 (CD86) on the APC. This second step is necessary to initiate activating signaling in T cells and serves as a control mechanism to prevent immune reactions to self-antigens [102,103]. Activated T cells expand rapidly and undergo transcriptional changes, thereby differentiating into CTLs. When activated CTLs encounter their cognate antigen in the context of an MHC class I complex, they exert their cytotoxic function in three different ways. First, they secrete the inflammatory cytokines Interferon gamma (IFN γ) and Tumor necrosis factor alpha (TNF α), which increase antigen presentation and induce apoptotic pathways in target cells [104,105]. Second, CTLs initiate exocytosis of cytosolic granules. These granules comprise cytotoxic proteins like Perforin 1 (PRF1) and Granzymes (GZMs) that are released to the interaction site of target cell and CTL (also known as immunological synapse) [106]. PRF1 acts by forming pores in the cell membrane of target cells, which on the one hand enables GZMs to enter the cell and on the other hand is thought to induce cell lysis to kill target cells directly [107,108]. GZMs act as serine proteases and lead to the activation of apoptotic pathways in target cells, *e.g.*, through cleavage of caspase-3 by GZM B [109]. In addition to exocytosis of cytotoxic granules, CTLs secrete the ligand of the FAS cell surface death receptor, FASLG. FASLG binds to the death receptor FAS (CD95) on the surface of target cells, which consequently initiates the extrinsic apoptotic pathway and leads to apoptotic cell death in target cells [110,111].

Taken together, the activation of CTLs is tightly regulated and depends on cognate antigen recognition and co-activation via B7 ligand binding. Once activated, CTLs exert their cytotoxic functions through several mechanisms, leading to rapid and effective target cell killing.

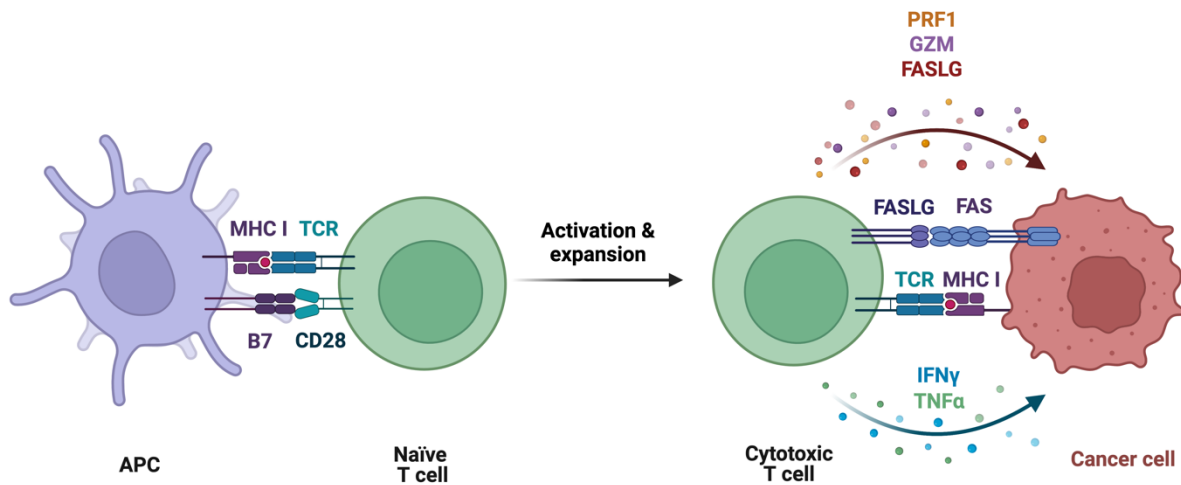


Figure 1.2. Mechanism of T cell activation and cytotoxicity. The activation of T cells is a two-step process and involves binding of the cognate antigen:MHC class I complex to the specific T cell receptor (TCR) as well as co-stimulatory engagement of CD28 with B7 receptors (B7-1 or B7-2, left panel). Once naïve T cells are activated, they proliferate massively and differentiate into cytotoxic T lymphocytes (CTLs, right panel). Upon antigen recognition on target cells, CTLs exert their cytotoxic function through secretion of immunomodulatory cytokines, exocytosis of Perforin1 (PRF1)- and Granzyme (GZM)-containing vesicles, and induction of FASLG-mediated apoptosis. (Adapted from “T cell Activation in Cancer”, by BioRender.com (2022). Retrieved from <https://app.biorender.com/biorender-templates>)

1.2.2.2 Immune checkpoint blockade

Immune checkpoints are negative feedback regulators of activated T lymphocytes that are needed in healthy conditions to prevent excessive T cell activity and autoimmunity. Upon T cell activation, the immune checkpoint molecules Cytotoxic T lymphocyte antigen 4 (CTLA4) and Programmed cell death protein 1 (PD1) are upregulated and act as a negative regulators of T cell activation via two distinct mechanisms: CTLA4 is a receptor with close similarities to the co-stimulatory protein CD28 and binds the same ligands B7-1 and B7-2, but with a higher affinity and avidity than CD28. Consequently, this disrupts the co-stimulatory binding of CD28 and its B7 ligands, thereby restricting T cell activation and effector cell function [103,112]. PD1, on the other hand, binds to its ligands PD1 ligand 1 (PDL1) and PD1 ligand 2 (PDL2), which are expressed on professional APCs [113]. Establishment of the PD1-PDL axis leads to intracellular signaling which counteracts T cell activation and effector cell function [114]. Interestingly, PDL1 and PDL2 can also be expressed in non-hematopoietic tissue, and (over-)expression of PDLs by tumor cells has been described as a mechanism of immune evasion [115,116] (**Figure 1.3**).

Monoclonal antibodies targeting CTLA4 or the PD1-PDL axis have shown remarkable success in clinical research and have been approved for the treatment of numerous cancer types, including melanoma, lung cancer, and HCC (e.g., Ipilimumab, Nivolumab) [117,118]. As immune checkpoint blockade therapies unleash the full power of activated T lymphocytes, reported side effects are mainly immune-related adverse events including dermatological, gastrointestinal, hepatic, and pulmonary autoimmune toxicity [119]. The discovery of additional checkpoint regulators like T cell immunoglobulin 3 (TIM3), Lymphocyte activation

gene 3 (LAG3), or V-domain immunoglobulin suppressor of T cell activation (VISTA) presents new potential targets for checkpoint blockade therapy and additional checkpoint inhibitors are being developed for future use as anti-cancer treatments [94,120–122].

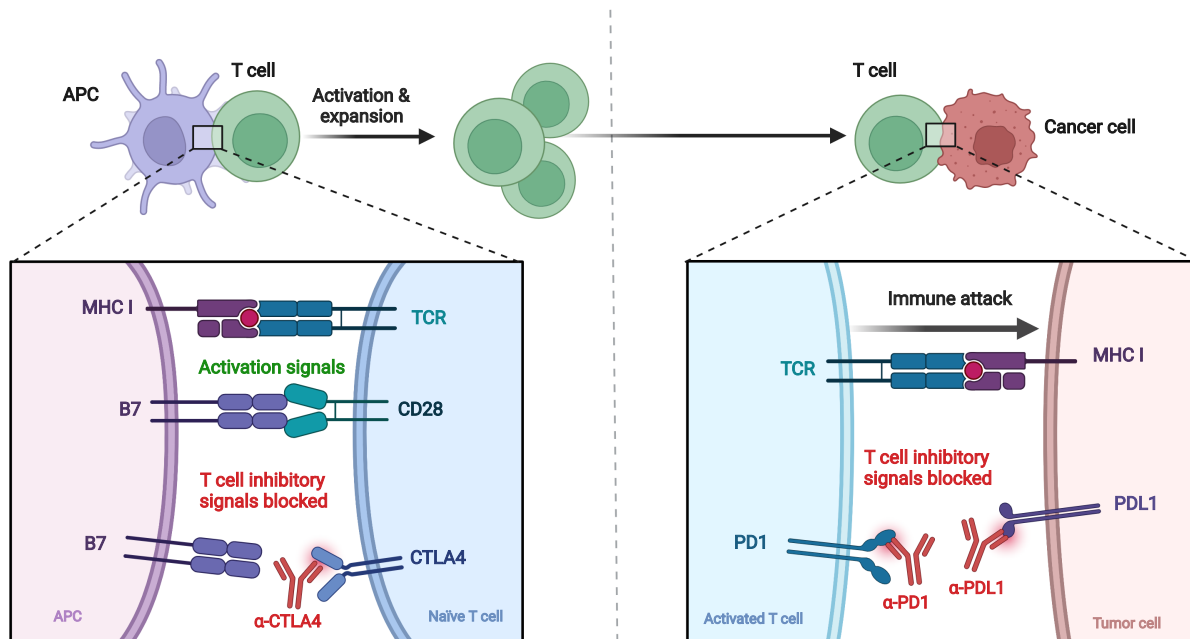


Figure 1.3. Mechanism of immune checkpoint blockade therapy. Left panel: Mechanism of immune checkpoint blockade with CTLA4-targeting antibodies that prevent competitive binding of CTLA4 with co-stimulatory B7 receptors. Right panel: Mechanism of immune checkpoint blockade with PD1- and PDL1-targeting antibodies that block PD1-PDL1-axis formation and downstream immune-inhibitory signaling. (Adapted from “Blockade of CTLA-4 or PD1 Signaling in Tumor”, by BioRender.com (2022). Retrieved from <https://app.biorender.com/biorender-templates>)

1.2.2.3 Adoptive T cell therapy

For adoptive T cell therapies, T lymphocytes are isolated and expanded *ex vivo* before they are transferred into the patient. Two T cell-based approaches can be distinguished, namely the transfer of tumor-infiltrating lymphocytes (TILs) and the transfer of genetically engineered chimeric antigen receptor (CAR) T cells.

The underlying idea behind adoptive TIL therapy is that T cells that are found at the tumor site are already reactive against TAAs and display anti-tumor toxicity [123]. Therefore, TILs are isolated from tumor biopsies, massively expanded *ex vivo* through cytokine stimulation, and re-injected into the patient’s system [124]. TIL therapies are considered to display very low off-target toxicity, as T lymphocytes have already undergone negative TCR selection during development in the thymus [124]. So far, TIL therapies are not FDA-approved and their application is still under investigation in clinical trials for the treatment of several cancer types like melanoma, non-small cell lung cancer, or head and neck cancer [124]. Major obstacles that need to be overcome in the development of TIL therapies are that TILs often display an exhausted phenotype after long-time stimulation *in vitro*, consequently causing only small response rates, and the laborious and cost-intensive manufacturing of patient-specific TIL therapies, which further limits the applicability of these therapies [124–126].

CAR T cell therapy uses autologous or allogenic donor T lymphocytes, which are genetically modified *in vitro* to express CAR, massively expanded and then administered to the patient [94]. In contrast to MHC-restricted TCRs, CARs do not rely on the antigen to be bound by an MHC molecule, but are able to identify molecules and elicit an immune response independent of the MHC status of the tumor cell [94]. The first generation of CARs consisted of the variable region of antibodies which are linked to the signal-transducing CD3 ζ -chain of the TCR [127]. Subsequent developments of newer CAR generations aimed at increasing T cell activation by including co-stimulatory factors like CD28 or 4-1BB, or by adding chimeric cytokine receptors that are able to overcome an immunosuppressive microenvironment [94,128–132]. CAR T cell therapies have been approved for the treatment of certain B cell malignancies, all of them targeting the B cell marker CD19 [133]. The identification of appropriate CAR targets is one of the major challenges in CAR T cell development, as they need to be tissue-restricted and expressed specifically on the surface of tumor cells [94]. Current research is focusing on the discovery of new CAR targets, particularly tumor-associated neoantigens, for the development of new CAR T cell therapies [94,134,135]. The most frequent adverse events of T cell-based therapies are the cytokine release syndrome (CRS) and CAR T cell-related encephalopathy syndrome (CRES), which occur after rapid activation and proliferation of CAR T cells. The symptoms of CRS and CRES are usually mild, however, in rare cases, they make further intensive-care interventions necessary or can even be fatal [136].

Taken together, adoptive T cell therapy approaches show highly promising results in clinical research and continue to be the subject of extensive studies aimed at developing new therapies.

1.2.2.4 Other immunotherapeutic approaches

In addition to checkpoint inhibition and adoptive T cell therapies, several other types of immunotherapies have been established. For instance, personalized cancer vaccines are developed based on the specific mutational landscape of individual tumors. For that, tumor biopsies are first characterized via next generation sequencing (NGS) in order to identify tumor-specific neoantigens. Based on these neoantigens, vaccines are produced and applied to the patient in order to induce immune responses directed against cells presenting neoantigens, *i.e.*, tumor cells [94]. Different formulations are used to produce cancer vaccines, like synthetic peptides, mRNA, DNA plasmids, or antigen-loaded dendritic cells (DCs) [137]. However, the identification of suitable neoantigens that are able to elicit sufficient immune responses and the cost and time intensive manufacturing of autologous vaccines remains challenging [94].

Furthermore, non-specific modulators of the immune system that are used to increase overall immune responses in cancer patients are used in cancer treatment. For example, treatment with IFN α or Interleukin-2 (IL-2) is approved for several cancer types [138]. Other substances that are used as non-specific immune modulators are hematopoietic growth factors such as granulocyte-macrophage colony-stimulating growth factor (GM-CSF), which stimulates the proliferation of leukocytes, and biological response modifiers [95]. Biological response modifiers, *e.g.*, Thalidomide (Thalomid[®]), stimulate the immune system indirectly by inducing IL-2 secretion in immune cells and inhibiting angiogenesis [95,139].

1.2.2.5 Limitations and challenges of immunotherapy

Even though immunotherapeutic approaches have shown remarkable success in a subset of cancer patients, the majority of patients has been unresponsive to available immunotherapies [140,141]. The

underlying mechanisms of how tumors acquire immune resistance and evade attacks of the immune system are under ongoing investigation and the inactivation of immune evasion mechanisms is a promising approach to overcome immune resistance in the future [142–145]. Tumors have developed a variety of strategies to sabotage T cell-mediated tumor cell clearance, including the recognition of tumor cells by the immune system, the recruiting of immune cells to the tumor site, and activation and regulation of immune cells within the tumor. Players that contribute to manipulating the immune system are tumor cells, regulatory immune cells, and other factors of the tumor microenvironment [142,144].

Antigenicity of tumor cells. One mechanism of how tumor cells evade the immune system is the reduction or elimination of their antigenicity. Consequently, immune cells are not able to recognize tumor cells as malignantly transformed and will not mount an immune attack against the tumor. This masking can be achieved through several mechanisms affecting the antigen-processing and -presenting machinery [142]. For example, tumor cells can avoid immune recognition through loss or downregulation of Human leukocyte antigen (HLA) genes or Beta-2 microglobulin (B2M), genetic or transcriptional disruption of the proteasome or TAP, or loss of immunogenic mutations or antigens [142,143]. Accordingly, it was shown that reduced expression of HLA and B2M correlates with reduced levels of tumor-infiltrating lymphocytes in lung cancer and that patients with impaired antigen presentation and reduced immune cell infiltrates were less responsive to checkpoint inhibitor treatment [146,147]. Therefore, the antigenicity of a tumor is considered to be a predictive biomarker for the outcome of immunotherapy. One potential biomarker being investigated is the tumor mutational burden (TMB), as higher TMB has been associated with better response to checkpoint inhibitor blockade [148]. However, the determinants of sufficient antigenicity are largely unknown and still under investigation [142].

Immunogenicity. Another mechanism of immune evasion is to decrease the extent of T cell effector function by reduced T cell activation or increased T cell exhaustion. Through chronic antigen exposure at the tumor site or disturbed activating and regulatory signals in the tumor microenvironment, TILs can acquire an exhausted or dysfunctional phenotype. This is associated with the expression of inhibitory immune checkpoint receptors like PD1 or CTLA4, disturbed cytokine production, and defective proliferation [144,149]. Decrease in CTL effector function at the tumor site is accomplished through the increased expression of checkpoint ligands and immune regulatory cytokines by regulatory immune cells or tumor cells [145]. The use of PDL1 expression as predictive biomarker for immunotherapy is under investigation, but led to contradicting results, so that further research will be needed to identify robust biomarkers [142,150,151].

Shaping of the tumor microenvironment. The tumor microenvironment (TME) constitutes a highly heterogeneous milieu that influences tumor growth, angiogenesis, metastasis, and immune cell recruitment and function [152,153]. It consists of a variety of extracellular molecules forming the extracellular matrix (ECM) and different cell types, including endothelial cells, fibroblasts, TILs, macrophages, DCs, and myeloid-derived suppressor cells (MDSCs) [152,154,155]. The components of the TME contribute to the recruitment, activation, regulation, and dysfunction of immune cells and are thereby critical factors for the immunogenicity of a tumor and immune evasion mechanisms.

Especially tumor-infiltrating regulatory immune cells play a crucial role in establishing an immunosuppressive microenvironment. For instance, regulatory T cells (Tregs) downregulate T cell activation and effector

function by secreting immunosuppressive cytokines like Interleukin-10 (IL-10) or Transforming growth factor beta (TGF β) and expressing high-affinity IL-2 receptors, thereby depriving activated T cells of IL-2 [152,156,157]. Additionally, through the expression of checkpoint receptors, Tregs interact with APCs in the microenvironment, thus further contributing to an immunosuppressive milieu [158,159]. Another type of regulatory immune cells are MDSCs, which are a heterogenic group of immature myeloid cells and act by creating a chronic inflammatory environment and mediate tumor progression, angiogenesis, and metastasis [152]. MDSCs exert their immunosuppressive potential by releasing nitric oxide, arginase, and reactive oxygen species, which leads to suppression of T cell proliferation and activation [160]. Moreover, tumor-associated macrophages can act either pro-inflammatory and contribute to tumor cell killing (M1 subtype), or play an immunosuppressive role (M2 subtype). The M2 subtype of macrophages acts anti-inflammatory and tumor-promoting by inducing angiogenesis and contributes to metastasis by mediating the degradation of the ECM. Additionally, M2 macrophages recruit Tregs to the tumor site by releasing immunosuppressive cytokines [153,161].

In addition to immune cells, stromal cells influence the TME. Especially cancer-associated fibroblasts (CAFs) impact the TME by affecting immune cell recruitment and inflammation through the release of growth factors, chemokines, and immunosuppressive cytokines [153]. Additionally, CAFs interact with regulatory immune cells and are able to convert T cells in Tregs, inhibit natural killer (NK) and T cell function, and activate M2 macrophages, thereby contributing to an immunosuppressive TME [153].

Based on immunohistological observations, it was possible to differentiate three different TME subtypes with regard to the inflammatory milieu and infiltrating immune cells [162]. The first subtype describes inflamed tumors, which are characterized by high levels of TILs, PD1/PDL1 expression, and an intact antigen presenting machinery. Secondly, in the immune-excluded TME subtype, immune cells accumulate at the periphery of the tumor mass, but are not able to penetrate the tumor entirely. This phenomenon is believed to be the result of immune cells being attracted by the tumor via chemokines, but not being able to infiltrate the tumor due to mechanical or functional barriers [163]. This subtype is marked by high TGF β signaling in the tumor, the presence of MDSCs, and induction of angiogenesis [162]. The third subtype, the immune desert or immune ignorant TME, is completely devoid of immune infiltrates and is accompanied by a high tumor cell proliferation rate [162]. While tumors of the inflamed subtype have been shown to respond well to immune checkpoint blockade in clinical studies, immune-excluded and immune desert tumors respond only poorly to immunotherapy [143,164,165].

Therefore, several different approaches have aimed at further classifying the TME and link TME subtypes to the outcome of immunotherapy [164–167]. It was found that a variety of different factors influence the inflammatory landscape of tumors, including immune cell infiltrates, tumor stroma, vasculature, and specific gene signatures. However, the complex interplay of influential factors is still not fully understood, and further investigations are needed to unravel the underlying mechanisms of immune evasion and to identify reliable predictive biomarkers for immunotherapy.

1.3 The role of the bone morphogenetic protein (BMP) pathway in cancer and immunotherapy

Even though immunotherapy has shown great success in some patients, a majority of patients does not respond to immunotherapy. The mechanisms of immune evasion are manifold and still under investigation and involve the infiltration or exclusion of immune cells, antigen presentation, regulatory immune cells, and inflammatory cytokine signatures (see 1.2.2.5, [142–144]). Additionally, immune-modulating signaling pathways have been in the focus of immunotherapy and immune evasion research. One pathway that has gained relevance in immuno-oncology research is the bone morphogenetic protein (BMP) pathway, and its involvement in cancer progression and immune evasion is subject of current investigations [168–172].

1.3.1 The canonical TGF β and BMP pathway

The BMP signaling pathway has been originally found to play a role in bone and cartilage formation, but it has since then been shown to impact a multitude of processes, including embryonal development, adult tissue homeostasis, apoptosis, differentiation, wound healing, and angiogenesis [173–178]. BMPs are part of the Transforming growth factor beta superfamily, which also includes Activin signaling molecules and growth differentiation factors (GDF), or Nodal. Analogous to the TGF β signaling pathway, BMPs transmit their signal by binding to transmembrane serine/threonine kinase receptors, which can be categorized into type I and type II receptors. Ligand binding induces the formation of type I and II heterotetramers. As a consequence, the constitutively active kinase domain of the type II receptor is able to phosphorylate the GS-rich domain of type I receptors, which leads to activation of the type I receptor kinase domain [178,179]. In turn, activated type I receptors phosphorylate downstream effectors known as R-SMADs (Receptor-Small/Mothers against Decapentaplegic), which then associate with the co-SMAD (SMAD4) and translocate into the nucleus, where they function as transcription factors [179]. Typical target genes of BMP signaling include the Inhibitor of differentiation/DNA binding genes *ID1-ID4* and inhibitory I-SMADs (*SMAD6* and *SMAD7*), which act as negative signaling regulators of the pathway (**Figure 1.4**) [180,181].

Even though the signaling pathways of TGF β and BMPs follow the same mechanistic principles, they differ with respect to the receptors that they bind, as well as the R-SMADs that associate with SMAD4 and lead to gene expression in the nucleus. For instance, TGF β -1, -2, and -3 bind to the TGF β receptors 1 and 2 (TGFBR1/ALK5 and TGFBR2) in order to activate SMAD2/3, while BMP2 forms signaling complexes with BMP receptor 1A or 1B (BMPR1A/ALK3 or BMPR1B/ALK6) and BMP receptor 2 (BMPR2), leading to phosphorylation of SMAD1/5/9 [182]. Additionally, the combination of different ligands and type I and type II receptors allows for ligand-specific signaling and differentially regulated gene expression [182]. For example, Activin leads to the formation of the signaling complex consisting of Activin A receptor type 2A (ACVR2A) and Activin A receptor type 1B (ACVR1B/ALK4) and results in activation of SMAD2/3, while BMP2, 6, and 7 bind to ACVR2A:BMPR1A or ACVR2A:BMPR1B heterotetramers and signal via phosphorylation of SMAD1/5/9 [182,183]. In total, seven type I and five type II receptors are known that can interact with more than 30 TGF β superfamily ligands to regulate and initiate gene expression, suggesting receptor and signaling redundancy [169]. However, the combinatorial interactions of type I and II receptors with different ligands result in distinct and specific gene regulation through TGF β or BMP signaling [182].

Moreover, non-canonical SMAD-independent signaling activates several pathways, including the Extracellular signal-regulated kinase (ERK), c-Jun N-terminal kinases (JNK), and p38 MAPK pathways [184–189]. TGF β - and BMP-induced signaling has been reported to activate the TGF β -activated kinase (TAK1), which is an upstream regulator of JNK and p38 [190,191]. Additionally, members of the TGF β superfamily have been observed to activate PI3K signaling and Protein phosphatase 2A (PP2A) [1,192]. Taken together, however, very little is known about the molecular mechanisms that lead to SMAD-independent signaling [191].

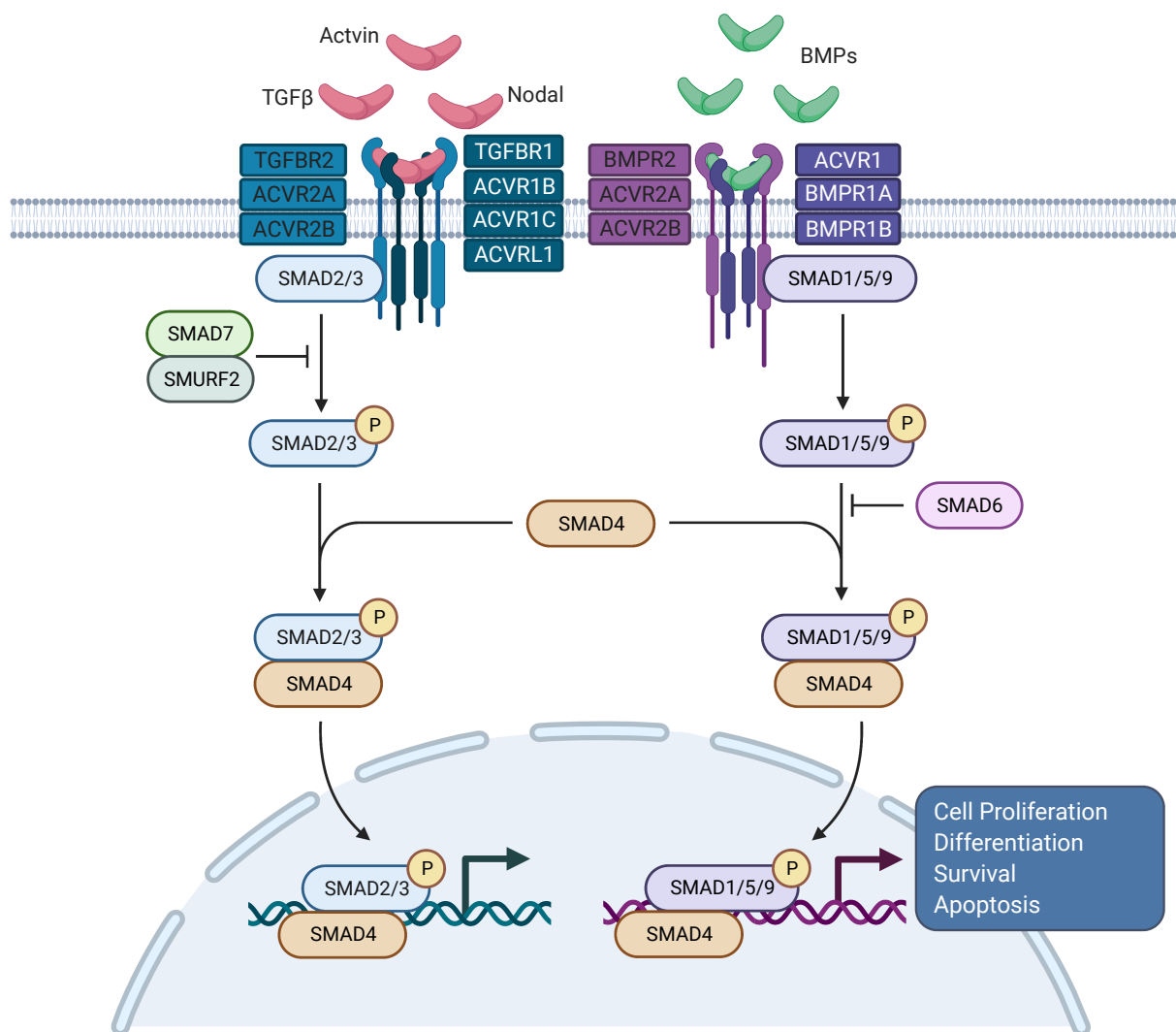


Figure 1.4. Overview of the canonical TGF β and BMP signaling pathway. (Adapted from “TGF-Beta and BMP Signaling Pathway”, by BioRender.com (2022). Retrieved from <https://app.biorender.com/biorender-templates>)

1.3.2 The role of TGF β and BMP signaling in cancer and immunotherapy

The role of TGF β signaling in tumorigenesis and cancer progression is well described and encompasses tumor-suppressive as well as tumor-promoting mechanisms. In healthy cells and early stages of tumorigenesis, TGF β signaling acts anti-tumorigenic by inducing cell cycle arrest and apoptosis [193]. In later stages

of cancer progression, however, TGF β promotes epithelial-mesenchymal transition (EMT), metastasis, chemoresistance, angiogenesis, and immune cell suppression [193]. Increased TGF β signaling is found in many cancer types and correlates with poor prognosis [194–196]. The tumor-promoting effects of TGF β signaling have prompted several clinical studies investigating TGF β as a target for cancer therapy, which have revealed promising anti-tumor effects of TGF β -targeting agents [193,197,198].

While affecting similar cell functions as TGF β , BMP signaling has been proposed to play an opposing role to TGF β -mediated signaling by causing antagonistic effects [199]. Compared to TGF β signaling, BMP signaling is less investigated, but has been connected to tumor cell proliferation, invasion, EMT, and metastasis [169,200–203]. Additionally, BMPs can act tumor-suppressive by inducing apoptosis in tumor cells and reducing metastatic potential [204,205]. Therefore, BMPs have been suggested to play a dual role in cancer development and progression by influencing pro- as well as anti-tumorigenic mechanisms [168]. In addition to direct consequences on tumor cell functions, BMP signaling has immunoregulatory effects in the TME and can affect growth, activation, and cytokine secretion of macrophages, as well as DC, MDSC, NK, and T cell activity [169,171,172,205–210]. BMP signaling effectors have been suggested as biomarkers for tumor progression and cancer therapy outcome, since BMP expression is reported in many cancer types and is generally associated with poor prognosis [168,211–214]. Additionally, BMP signaling is investigated as a target for cancer therapy [171]. For instance, blockade of BMP signaling was shown to increase TILs in the TME and decrease the metastatic potential [215].

Taken together, growing evidence suggests that BMP signaling plays a crucial role in tumorigenesis, tumor progression, and therapy outcome. However, due to the dual role and pleiotropic effects in cancer, the effect of BMP signaling in tumors is still not fully understood. Several studies report contradictory functions of BMP signaling, thus implying that BMP signaling is context- and cell type-dependent [168,216]. Hence, further investigations will be needed to comprehensively unravel the role of BMP signaling in cancer and immunotherapy.

1.4 Aims of the project

Immunotherapy has shown great success in the treatment of various cancer types. However, to this date, only a minority of cancer patients benefit from cancer immunotherapy. The underlying mechanisms that promote immune evasion and resistance are poorly understood and subject of current investigations. In order to shed light on how cellular processes in tumor cells impact the outcome of immunotherapeutic approaches, this project aimed at identifying new tumor cell-specific barriers for immunotherapy. This was realized by addressing three main objectives:

First, I investigated immune responses caused by neoantigen expression in liver tumors *in vivo*. For that, a murine model was established that allowed for the generation of genetically defined liver tumors with conditional neoantigen expression. This model was further used to study neoantigen-specific immune responses in the context of immunotherapeutic interventions.

Second, based on tumor-derived primary murine cell lines, I established an *in vitro* system that allows investigating neoantigen-dependent tumor cell killing in controlled conditions. Subsequently, this assay was

used to perform a lentiviral CRISPR/Cas9 screen in order to identify new tumor cell-specific genes that impact T cell-mediated tumor cell killing.

Lastly, genes that were identified in the CRISPR/Cas9 screen were further investigated to validate their proposed role in T cell-mediated tumor cell killing. Additionally, I selected the most promising gene candidate to elucidate the mechanistic foundation that confers resistance to immune cell-mediated tumor cell killing.

Overall, this study aimed at identifying new modulators of antigen-dependent tumor cell killing. The principal purpose of this project is to join the shared scientific effort of unravelling biological mechanisms of immune escape and resistance, thereby contributing to improve the outcome of future immunotherapeutic approaches for cancer patients.

2 Material and methods

2.1 Molecular biology

2.1.1 Overview of used plasmids

All plasmids used in this study are listed in **Table 2.1**.

Table 2.1. Overview of used plasmids.

Plasmid	Description	Origin
<i>Plasmids used for production of viral particles</i>		
psPAX2	2 nd generation lentiviral packaging plasmid	Addgene #12260, gift from Didier Trono
pMD.2G	VSV-G envelope expression plasmid	Addgene #12259, gift from Didier Trono
<i>Plasmids used for CRISPR-mediated gene knockout in vitro</i>		
lentiCas9-Blast	Lentiviral plasmid expressing SpCas9 and Blasticidin resistance from EFS promoter	Addgene #52962, gift from Feng Zhang [217]
pLenti-U6-sgRNA-improved scaffold-EFS-puromycin-P2A-tRFP (pUSEPR)	Lentiviral backbone with improved sgRNA scaffold expressing sgRNA under U6 promoter, EFS-dependent expression of puromycin resistance and tRFP	Tschaharganeh Lab, DKFZ, Heidelberg
lentiCRISPR v2	Lentiviral backbone expressing SpCas9 and P puromycin resistance from EFS promoter and sgRNA from U6 promoter	Addgene #52961, gift from Feng Zhang [217]
lentiCRISPR v2-Blast	Modified lentiCRISPR v2 with blasticidin resistance	Tschaharganeh Lab, DKFZ, Heidelberg
<i>Plasmids used for stable gene expression in vitro</i>		
pMSCV-PGK-Hygro	Retroviral plasmid for the expression of cDNAs and Hygromycin resistance	Tschaharganeh Lab, DKFZ, Heidelberg
pcDNA3-ALK2 wt	Mammalian expression of ALK2/ACVR1 wt	Addgene #80870, gift from Aristidis Moustakas [218]
pcDNA3-ALK2 Q207D	Mammalian expression of ALK2/ACVR1 Q207D	Addgene #80871, gift from Aristidis Moustakas [218]
pcDNA3-ALK2 K235R	Mammalian expression of ALK2/ACVR1 K235R	Addgene #80872, gift from Aristidis Moustakas [218]
<i>Plasmids used for in vivo gene delivery using HTVI</i>		
CMV-SB13	Sleeping Beauty Transposase expression plasmid	Tschaharganeh Lab, DKFZ, Heidelberg
pT3-EF1a-Kras ^{G12D} -IRES-rtTA3	Transposon-based Kras ^{G12D} and rtTA3 expression plasmid	Tschaharganeh Lab, DKFZ, Heidelberg
pT3-EF1a-MYC-IRES-rtTA3	Transposon-based human MYC and rtTA3 expression plasmid	Tschaharganeh Lab, DKFZ, Heidelberg

Plasmid	Description	Origin
pT3-TRE-trFP-miRE-shRen-IRES-OVA-P2A-GFP	Transposon-based expression plasmid of Ovalbumin (OVA), trFP, and GFP under the control of TRE	Tschaharganeh Lab, DKFZ, Heidelberg
pX330-U6-Chimeric_BB-CBh-hSpCas9 (pX330)	Human codon-optimized SpCas9 and chimeric guide RNA expression plasmid	Addgene #42230, gift from Feng Zhang [219]

2.1.2 Molecular cloning

2.1.2.1 Generation of CRISPR/Cas9 guide plasmids

DNA-targeting sgRNAs were designed using the online tool CHOPCHOP [220–223]. Briefly, I used the target gene sequence to create reverse complementary DNA oligonucleotides. To these, 5' overhangs were added that are complementary to the sticky ends resulting from a restriction digest of the sgRNA scaffold with BsmBI (CACC and CAAA, respectively).

The oligonucleotides were phosphorylated using T4 Polynucleotide Kinase (PNK, 10,000 U/ml, NEB) according to the manufacturer's protocol and subsequently annealed by first incubating the reaction at 95°C for 5 min and a stepwise reduction of the temperature to 25°C.

The plasmids used to deliver sgRNAs were digested with BsmBI (NEB) and dephosphorylated with Shrimp Alkaline Phosphatase (rSAP, NEB) according to manufacturer's instructions and purified using the QIAquick PCR Purification Kit (Qiagen). The insert was ligated to the digested plasmid with the T4 DNA Ligase (400,000 U/ml, NEB) for 1 h at room temperature and subsequently used for transformation.

The sgRNA sequences used in this study are shown in **Table 2.2**.

Table 2.2. sgRNA sequences used in this study.

Identifier	Sequence (5' – 3')
<i>murine sgRNAs</i>	
sgRosa26	GAAGATGGGCGGGAGTCTTC
sgTap1	GCCTGGAACGGTGACAGCGT
sgAB124611.1	GGCCCCAGGGGACATCCTAG
sgAB124611.2	GTACATCAGGCCGATCTGAG
sgAcvr1.1	GGGGCTCATCACCACCAATG
sgAcvr1.2	GTATGGACAGTACAATCCGA
sgAcvr1.3	GGTACCTTCCACACTCGGGGA
sgAcvr1.4	GTGTAAGACCCCGCCGTCACC
sgAcvr1.5	GACCAAGCGCTACATGGCTC
sgAcvr1.6	GTTATAAGAGGGTCGATATT
sgAcvr1.7	GTTGTACTIONGTCCATAGCCAG
sgAcvr1.8	GTGGGTACTGGAGTGTCTGG
sgAcvr1.9	GCACCACAAAGACTTAACGG
sgBche.1	GTGAATCTTAGGCTACCCAG
sgBche.2	GTTTCGATGAAGTATAGGGT
sgC3ar1.1	GGGATGGGATAAGTTTGAC
sgC3ar1.2	GGTCCATAATGAACAGATCA
sgCacng8.1	GGCACACTGCCAATCACGCT

Identifier	Sequence (5' – 3')
sgCacng8.2	GTGTACATATCGGCCAACGC
sgCd164.1	GAAGTCAGTGCGGTTACCT
sgCd164.2	GTGCGTCGTCGGGACCACTT
sgCol6a5.1	GGTAACTTACGGGATCCCCCT
sgCol6a5.2	GTGTTGCACGTCACAGTCCG
sgEgfr.1	GATGAATAGGCCAATCCCCAA
sgEgfr.2	GGGGCCTGACTACTACGAAG
sgEgfr.3	GGTCGCATCTCTGACCGGGAG
sgEgfr.4	GGGACCTGCCACGACAGCGAT
sgEphb4.1	GTCTGGTCCAGGTACGCGCA
sgEphb4.2	GATCATGGTGAAGCGTATCG
sgGpc1.1	GCTGCGCCTCTACTACCGTG
sgGpc1.2	GCGCAGGCGCAGTTCTCGAG
sgld1.1	GGTCCCAGCGCAGCGCGAGA
sgld1.2	GAACGGCGAGATCAGTGCCT
sglglon5.1	GCAGACGGTTTTACCTCAGA
sglglon5.2	GGGTAGACCTGAGTGGTGTA
sglgsf8.1	GCCACTGTACGGCCGCTGAG
sglgsf8.2	GCACGCCTCACAGTGCACGA
sglgsf8.3	GAGGAGCGAACTCAGCGGCGT
sglgsf8.4	GTCGGTACCGAATGGTGGTTG
sgLdlr.1	GTGGTCCGGATGAGCCCATCA
sgLdlr.2	GGAGTGTATCCATCGCAGCT
sgLdlr.3	GACAGTCGACATCCCCGTCGC
sgLdlr.4	GCCGCGGATCTGATGCGTCGC
sgLdlr.5	GGGTGTCGTAGGACAAGTTAG
sgLrrc4b.1	GCTGGTGCGAAAGATCGAGG
sgLrrc4b.2	GCAGGTAGCGGGTGTTGACA
sgLrrc4b.3	GGGGTGGCTCCACGATGACCG
sgLrrc4b.4	GCGACACGTTAAGCGTGGCCG
sgLrrc4b.5	GGAAGGCGTTTTCGCTCGATGG
sgNlgn2.1	GCCAGCCGCTCAAGTACACG
sgNlgn2.2	GCTCTTTACCGACCACCAGT
sgNlgn2.3	GGTCCCCTTGTAAATAGAGGG
sgNlgn2.4	GACTACGTCGCCGTCACCCAC
sgPcdh15.1	GGCAGATAGGGATCGAACAC
sgPcdh15.2	GTTCCCTGAATGACTACACCT
sgSdk2.1	GCGCAGAACGTCATCGCCAG
sgSdk2.2	GCTGGTCATCCTGTGACGG
sgSlc12a9.1	GCTAAACATGGACAGAACCG
sgSlc12a9.2	GGGAGCACGTAAAGTTCTGG
sgSlc12a9.3	GATGCCGATCAACACGAGCGG
sgSlc12a9.4	GGATGCCGATCAACACGAGCG
sgSlc12a9.5	GGCGCCGAGGACTACACCACA
sgSorcs3.1	GCGTGGGATCTACTTTACCC

Identifier	Sequence (5' – 3')
sgSorcs3.2	G TTCAGTCCGTATCTCCCCG
sgSorcs3.3	GAGCCGACGAATACCACCGAG
sgSorcs3.4	GGCCGGCGCCGAGATCACTTG
sgSorcs3.5	GCACACCAAGGGTTCGCGAG
sgSostdc1.1	GCCACCAAATACATTTTCGGA
sgSostdc1.2	GTCATCAGGATGCAGAGCAG
<i>human sgRNAs</i>	
TAP1.1	GGGGATCTATAACAACACCA
TAP1.2	GATCATGTCTCGGGTAACAG
ACVR1.1	GCCATCGTTGATGCTCAGTG
ACVR1.2	GTGGGAACAATCCCCGTGT

2.1.2.2 HiFi Assembly

In order to create retroviral pMSCV-ACVR1-PGK-Hygro expression plasmids, I introduced respective DNA sequences of wildtype and mutant *ACVR1* versions into a pMSCV-PGK-Hygro backbone using the NEB-uilider® HiFi DNA Assembly Master Mix (NEB) according to manufacturer’s instructions. Primers used to amplify the inserts are shown in **Table 2.3**.

Table 2.3. Primer sequence for HiFi Assembly.

Identifier	Sequence (5' – 3')	Tm
HiFi_Acvr1 for	CCAGCCCTCACTCCTTCTCTAGGGCGCCGGAATTAGCCACCATGG- TAGATGGAGTGATGATTCTTCCT	65°C
HiFi_Acvr1 rev	TTGGGATCCGCGCCGCCCTCGAGCCTAGGACCCTCTAGAGTCGACCTA- GAGGCTA	65°C

2.1.2.3 Transformation of heat competent *E. coli*

For transformation of bacteria with respective plasmids, I incubated 10-25 µl of NEB® Stable Competent *E. coli* (High Efficiency) bacteria (NEB) with 3 µl of the ligation reaction on ice for 10 min, then at 42°C for 45 sec, and again on ice for 5 additional minutes. The bacteria were then plated on Carbenicillin-containing agar plates (100 µg/ml) and incubated on a bacterial shaker o/n at 32°C.

2.1.3 Plasmid DNA purification (Mini and Midi prep)

Purification of plasmid DNA was done using the QIAprep Spin Miniprep Kit or the QIAGEN Plasmid Plus Midi Kit (Qiagen), according to manufacturer’s protocols. DNA concentration was measured using a NanoDrop ND 100 Spectrophotometer (Thermo Fisher Scientific).

2.1.4 Isolation of gDNA

gDNA isolation was performed using the Gentra Puregene CellKit (Qiagen) according to the manufacturer’s protocol with slight modifications: after adding 300 µl of cell lysis solution, Proteinase K (0.4 mg/ml, Sigma Aldrich) was added and the sample was incubated for 1 h with gentle shaking at 55°C. To inactivate Proteinase K, the sample was incubated at 95°C for 5 min. Next, 1.5 µl RNase A solution were added and subsequently, the manufacturer’s protocol was followed.

2.1.5 T7 endonuclease I assay

In order to detect CRISPR-mediated gene modifications and test for the effectiveness of sgRNAs, I performed T7 Endonuclease I assays. For that, gDNA isolated from modified cells was used to amplify the target region via PCR. PCR reactions were set up using Q5 Hot Start High-Fidelity 2X Master Mix (NEB) according to manufacturer's protocol with 200-400 ng gDNA template and primers listed in **Table 2.4**.

After the correct amplification of DNA fragments had been verified by agarose gel electrophoresis, the PCR reaction was purified using the QIAquick PCR Purification Kit (Qiagen). The purified PCR product was used in a hybridization reaction to form heterduplexes according to manufacturer's instructions. After reannealing, T7 Endonuclease I (NEB) was added and the reaction was incubated at 37°C for 15-30 min. Subsequently, samples were immediately loaded on 3 % agarose or 10% polyacrylamide (PAA) gels to perform a gel electrophoresis.

Table 2.4. Overview of PCR primers used for T 7 Endonuclease I assay.

Primer ID	Sequence (5' – 3')	Product size [bp]	Fragment size [bp]	Tm
<i>Murine PCR primers for T 7 Endonuclease I assay</i>				
sgTap1/2 for #1	GGACTCCTTGCTCTCCACTCA	463	321+142	60°C
sgTap1/2_rev	CTCACCTGAGTGTGCAGGTAAT			
Acvr1_1.3 for	GTCTGGGCCATTGTCTAAATGT	764	375+389	60°C
Acvr1_1.3 rev	GTCTCTAAATTATGGCGGATGC			
Acvr1_2.3 for	CCTCGAAAGAGTATAAAATGCCG	738	376+362	60°C
Acvr1_2.3 rev	CAACTTGCTTTGAAATGCTCAC			
Acvr1_3.1 for	ACCACCAATGTCGTGTTCAA	729	317+412	60°C
Acvr1_3.1 rev	TGGCAGCTCCGAGTACATTTG			
Acvr1_4.4 for	GATGCACAACGTAAGGCAGATA	754	423+331	60°C
Acvr1_4.4 rev	CATACACCCATTTGTGATGACC			
sgAcvr1.5 F1	TATAGCCTCACAATCTGCCTGA	564	278+286	60°C
sgAcvr1.5 R1	TTCGAACAGAATGCCATTACAC			
sgAcvr1.6 F2	ATCAACTGCCCTGTAGGAGAAA	379	184+195	60°C
sgAcvr1.6 R2	ACTGTAAGTCGCGCAAGTATGA			
sgAcvr1.7 F2	GTCGCTGTTCTTTGTTGCCTTTG	411	162+249	60°C
sgAcvr1.7 R2	CCAAATCTGCTATGCAGCACTGTC			
sgAcvr1.8 F2	GTCGCTGTTCTTTGTTGCCTTTG	397	163+234	60°C
sgAcvr1.8 R2	CAGCACTGTCCATTCTTCTTCACCA			
sgAcvr1.9 F2	CGCAAGACTCACAGCTCTACGTATC	509	188+321	60°C
sgAcvr1.9 R2	GCAACGAAGAGTAGATGCAGCC			
Egfr_1.3 for	GGGCTTGAAGGAAGTTGGT	835	495+340	60°C
Egfr_1.3 rev	GTTAACGTGCTCCACCATGC			

MATERIAL AND METHODS

Primer ID	Sequence (5' – 3')	Product size [bp]	Fragment size [bp]	Tm
Egfr_2.3 for	GGAAATTCATATTCAGCAAGGG	843	366+477	60°C
Egfr_2.3 rev	TGCTACCGTGCACTATTGATTC			
Egfr_3.2 for	CACTGCCTGCTTTTCGATCCT	791	395+396	60°C
Egfr_3.2 rev	TTTCTGCTCCGAACGCCTAC			
Egfr_3.4 for	TCCCCTCAGAAATTAACCTCCAA	879	494+385	60°C
Egfr_3.4 rev	GCAGGAAAGTGAGGCAACTAAG			
Sorcs3_1.2 for	TGGCCACTAAAGCCCCCTTAC	756	423+333	59°C
Sorcs3_1.2 rev	TAGCAGCCAGCAATGGAGTT			
Sorcs3_2.3 for	AGAGGGGAAGAGTGTAAGGGAC	849	479+370	60°C
Sorcs3_2.3 rev	CTGTCAGGAGACTAGCGATCTG			
Sorcs3_3.1 for	GGACTGGCACCAGTAGAGTG	759	414+346	60°C
Sorcs3_3.1 rev	GATAGCTACCACCACGTGAGA			
Sorcs3_4.1 for	CAAGATCCAGCTAGCGTTGC	874	508+366	60°C
Sorcs3_4.1 rev	TGTGAGGACGGCTTCCTTTG			
Sorcs3_5.3 for	TTCCCCTGACACACTCGCTA	807	617+190	60°C
Sorcs3_5.3 rev	TTACCGTTACCCTCGGCTGT			
ld1_1_fwd-4	GCGCTCTGCCCTCTCATTG	479	213+266	59 °C
ld1_1_rev-4	G TTCAGGGTGCTGAGCGG			
ld1_2_fwd-3	GGTGGAGATCCTGCAGCATG	466	147+319	60°C
ld1_2_rev-3	CCTCCTGAAGGGCTGGAGTC			
Primer ID	Sequence (5' – 3')	Product size [bp]	Fragment size [bp]	Tm
<i>Human PCR primers for T 7 Endonuclease I assay</i>				
hAcvr1-g1-p1 for	CAAGGTCAACCCCAAACCTCTAC	481	94+387	60°C
hAcvr1-g1-p1 rev	GATGGACATCACCTTGCTTACA			
hAcvr1-g2-p1 for	TGAGAAAGGAAGTGGGTGATT	375	70+305	60°C
hAcvr1-g2-p1 rev	TGAATGCCTATAACTCGACACG			
hTap1_1 #2 fwd	CAGTGTTTCCTTTCTGCTGATG	519	435+84	60°C
hTap1_1 #2 rev	CTGGTTCTGTTGGAAAACTCC			
hTap1_2 #2 fwd	CTCCTTAGAACCCCATGTTGAC	439	138+301	60°C
hTap1_2 #2 rev	GATGGAGAATCAGTAAGGGTGC			

2.1.6 Isolation of RNA

RNA was isolated from cells using the RNeasy Mini Kit (QIAGEN) according to manufacturer's protocol. The concentration of isolated mRNA was measured using the NanoDrop ND 100 Spectrophotometer (Thermo Fisher Scientific) and stored at -80°C.

2.1.7 Reverse transcription and quantitative real-time PCR (qRT-PCR)

1 µg isolated RNA was reversely transcribed into cDNA with the TaqMan® Reverse Transcription Reagents (Thermo Fisher Scientific) in a 20 µl reaction according to **Table 2.5**.

Table 2.5. Reverse transcription reaction.

Reaction	
Reagent	Amount for 1x reaction
10x RT buffer	2 µl
Random hexamer (50 µM)	1 µl
MgCl ₂ (25 mM)	4.4 µl
RNase inhibitor (20 U/µl)	0.4 µl
dNTP mix (10 mM)	4.0 µl
MultiScribe™ RT (50 U/µl)	1 µl
PCR program	
Temperature	Time
25°C	10 min
37°C	30 min
95°C	5 min
4°C	indefinitely

After reverse transcription, the reaction was diluted 1:20 and used for qPCR analysis. For that, the PowerUp™ SYBR™ Green Master Mix (Thermo Fisher Scientific) was used as shown in **Table 2.6**. Each sample was analyzed in triplicate using primers targeting the gene of interest or a housekeeping gene (summarized in **Table 2.7**) using the QuantStudio™ 5 Real-Time PCR System (Applied Biosystems). I determined relative gene expression using the $\Delta\Delta C_T$ method [224].

Table 2.6. Overview qPCR reaction.

Reaction	
Reagent	Amount for 1x reaction (25 µl)
PowerUp™ SYBR™ Green Master Mix (2X)	12.5 µl
Primer forward	1 µl
Primer reverse	1 µl
cDNA (1:20 diluted)	1 µl
H ₂ O	Ad 25 µl
PCR program	
Temperature	Time
50°C	2 min
95°C	10 min
95°C	15 sec
60°C	1 min
4°C	indefinitely

| 40 cycles

Table 2.7. Overview qPCR primers.

Identifier	Sequence (5' – 3')
<i>Murine qPCR primers</i>	
Id1.3 for	AGGTGAACGTCCTGCTCTACGA
Id1.3 rev	CAGGATCTCCACCTTGCTCACT

MATERIAL AND METHODS

Identifier	Sequence (5' – 3')
mFas-qPCR-2 for	CAAACCTGCAGGAAACAAAGTCCCAGA
mFas-qPCR-2 rev	GGTATGGTTTTACGACTGGAGGTTC
mAcvr1_qPCR-3 for	GCGAATGGTGAGCAATGGTATAGTG
mAcvr1_qPCR-3 rev	GCGAATGGTGAGCAATGGTATAGTG
GAPDH for	TGTCCGTCGTGGATCTGAC
GAPDH rev	CCTGCTTCACCACCTTCTTG
<i>Human qPCR primers</i>	
hID1_1 for	CCATTCTGTTTTAGCCAGTCGC
hID1_1 rev	CAGACAGACAGCGCACCAC
hFAS1_1 for	GACCCTTGACCAAATGTGAACATG
hFAS1_1 rev	CCCCAAGTTAGATCTGGATCCTTCC
hACVR1_1 for	CCAAGAGCCTGCATTAAGTTGTACAATG
hACVR1_1 rev	GGGCTTCTCATCTTCCATACTAGGG
β-ACTIN for	CACCATTGGCAATGAGCGGTTC
β-ACTIN rev	AGGTCTTTGCGGATGTCCACGT

2.2 Protein analysis

2.2.1 Protein isolation

Cell lysates were obtained from cell pellets which were resuspended in lysis buffer and incubated on ice for 30 min, while being vortexed every 10 min. The composition of the lysis buffer is shown in **Table 2.8** and

Table 2.9. After incubation, lysates were centrifuged at 13,000 rpm for 10 min. Supernatants were transferred to new reaction tubes and stored at -80°C.

Table 2.8. Composition of cell lysis buffer for protein extraction.

Reagent	Amount for 1 ml
10x cell lysis buffer (CST)	100 µl
10x protease inhibitor (cOmplete™ Mini, Sigma Aldrich)	100 µl
50x phosphatase inhibitor	20 µl
ddH ₂ O	Ad 1 ml

Table 2.9. Composition of phosphatase inhibitor cocktail.

Reagent	Concentration
Sodium fluoride	250 mM
Sodium orthovanadate	50 mM
Sodium pyrophosphate	50 mM
β-glycerophosphate	50 mM

2.2.2 Bradford assay

In order to determine the protein concentration of lysates, I performed Bradford assays using a Protein Assay Dye Reagent (Bio-Rad) according to manufacturer's instructions. Samples were measured in triplicate using a spectrophotometer (SPECTROStar Nano microplate reader, BMG Labtech). Additionally, a bovine serum albumin (BSA, molecular biology grade, NEB) standard curve ranging from 5-25 $\mu\text{g}/\mu\text{l}$ was measured to calculate protein concentrations.

Concentrations were adjusted to 1 $\mu\text{g}/\mu\text{l}$ in 5x Laemmli buffer (100 mM Tris-HCl pH 6.8, 5 % glycerol, 2 % SDS, 5 % β -mercaptoethanol) and samples were denatured for 5 min at 95°C.

2.2.3 SDS-PAGE and Western blot

Denatured cell lysates were used for SDS-PAGE and subsequent Western blot analysis. Briefly, 20 μg of denatured protein were loaded on 10-12 % PAA gels and separated by gel electrophoresis. Then, proteins were transferred in a PVDF membrane by wet transfer and detected by immunoblotting using respective antibodies. Bioluminescent image detection was performed using the ChemiDoc™ Gel Imaging System (BioRad) and SuperSignal™ West Pico PLUS Chemiluminescent Substrate (Thermo Fisher Scientific). The composition of used buffers and gels and an overview of all antibodies used in this study is shown in **Table 2.10** to **Table 2.12**.

Table 2.10. Composition of PAA gels.

Reagent	Amount
Running gel (10-12 %)	
30 % acrylamide	2.3-4 ml
Tris-HCl (1.5 M, pH 8.8)	2.6 ml
10 % SDS	100 μl
10 % APS	100 μl
TEMED	4 μl
ddH ₂ O	3.4-4 ml
Stacking gel	
30 % acrylamide	660 μl
Tris-HCl (1.5 M, pH 6.8)	1 ml
10 % SDS	40 μl
10 % APS	40 μl
TEMED	4 μl
ddH ₂ O	2.3 ml

Table 2.11. Composition of buffers used for SDS-PAGE and Western blotting.

Reagent	Amount
SDS-PAGE running buffer	
Trizma® base (0.25 M)	3.03 g
Glycine (1.92 M)	14.4 g
SDS 1%	1 g
ddH ₂ O	Ad 1 l

MATERIAL AND METHODS

Reagent	Amount
Western blotting buffer	
Trizma® base (0.25 M)	3.4 g
Glycine (1.92 M)	14.4 g
ddH ₂ O	Ad 1 l
TBS/T (pH 7.4)	
Trizma® base (0.25 M)	3 g
NaCl	8 g
KCl	0.2 g
TWEEN® 20	1 ml
ddH ₂ O	Ad 1 l

Table 2.12. Overview of antibodies used for immunoblotting.

Antibody	Source	Dilution (buffer)
Primary antibodies		
Mouse monoclonal anti- β -Actin-Peroxidase antibody (AC-15)	Sigma Aldrich, A3854	1:20000 (5% milk/TBST)
Rabbit monoclonal anti-c-Myc	Abcam, ab32072	1:1000 (5% milk/TBST)
Mouse monoclonal anti-GFP (B2)	Santa Cruz, sc-9996	1:1000 (5% milk/TBST)
Rabbit polyclonal anti-Id1	Proteintech, 18475-1-AP	1:1000 (5% milk/TBST)
Rabbit monoclonal anti-IKK β (D30C6)	CST, #8943	1:1000 (5% BSA/TBST)
Mouse monoclonal anti-IkBa (Amino-terminal Antigen) (L35A5)	CST, #4814	1:1000 (5% BSA/TBST)
Rabbit monoclonal anti-NFkB p65 (D14E12)	CST, #3033	1:1000 (5% BSA/TBST)
Mouse monoclonal anti-p53 (1C12)	CST, #2524	1:1000 (5% milk/TBST)
Rabbit polyclonal anti-phospho-IKK α/β (Ser176/180)	CST, #2694	1:1000 (5% BSA/TBST)
Rabbit monoclonal anti-phospho-NFkB p65 (Ser536) (93H1)	CST, #8242	1:1000 (5% BSA/TBST)
Rabbit monoclonal anti-phospho-Smad1/5/9 (D5B10)	CST, #13820	1:1000 (5% BSA/TBST)
Mouse monoclonal anti-phospho-IkBa (Ser32/36) (5A5)	CST, #9246	1:1000 (5% BSA/TBST)
Rabbit monoclonal anti-phospho-Smad2 (138D4)	CST, #3108	1:1000 (5% BSA/TBST)
Rabbit monoclonal anti-phospho-Stat1 (Y701) (58D6)	CST, #9167	1:1000 (5% BSA/TBST)
Rabbit monoclonal anti-phospho-Stat1 (S727) (D3B7)	CST, #8826	1:1000 (5% BSA/TBST)
Rabbit monoclonal anti-Smad1 (D59D7)	CST, #6944	1:1000 (5% milk/TBST)
Rabbit polyclonal anti-Smad2/3	CST, #3102	1:1000 (5% BSA/TBST)

Antibody	Source	Dilution (buffer)
Primary antibodies		
Rabbit monoclonal anti-Stat1 (D1K9Y)	CST, #14994	1:1000 (5% BSA/TBST)
Mouse monoclonal anti- β -Tubulin (TUB2.1)	Santa Cruz, sc58886	1:300 (5% milk/TBST)
Mouse monoclonal anti-Vinculin (hVIN-1)	Sigma Aldrich, #V9131	1:5000 (5% milk/TBST)
Secondary antibodies		
Goat polyclonal anti-mouse HRP-conjugated secondary antibody	Jackson Immuno Research, 115-035-008	1:20,000
Goat polyclonal anti-rabbit HRP-conjugated secondary antibody	Jackson Immuno Research, 111-035-003	1:20,000

2.3 Cell culture methods

2.3.1 General remarks

All cell culture work was performed under sterile conditions. I cultivated stock cells in respective cultivation medium supplemented with 1 % penicillin/streptomycin (10,000 U/ml penicillin and 10 mg/ml streptomycin, Sigma Aldrich) and 10 % FCS (Sigma Aldrich). Murine primary hepatocytes were cultivated in dishes pre-coated with 30 μ g/ml collagen solution (PureCol[®], Advanced BioMatrix). Stock cultures were split when confluency reached 80-90 % using Trypsin-EDTA solution (0.25%, sterile-filtered, Sigma Aldrich) or Versene[®] (EDTA) (0.02%, Lonza).

For cryopreservation, cells were resuspended in freezing medium (20 % FCS, 10 % DMSO) and frozen on -80°C in cryogenic vials.

2.3.2 Isolation of murine primary hepatocytes

For the isolation of primary hepatocytes from liver tumors, tumors were resected using sterile instruments and washed with sterile PBS. A small piece of tumor tissue (approx. 0.5 cm) was minced and incubated in Collagenase D/Dispase[®] II solution (4 mg/ml in Dulbecco's Modified Eagle Medium (DMEM), all Sigma Aldrich) for 30 min at 37°C with gentle shaking. Dissociated cells were washed with complete DMEM (supplemented with 1 % Penicillin/Streptomycin and 10% FCS) and plated on pre-coated dishes. Isolated hepatocytes were passaged until free from other contaminating cell types.

2.3.3 Production of viral particles

For the production of lentiviral particles, I transiently transfected 80 % confluent HEK293T cells with lentiviral packaging plasmids (0.37 μ g pMD.2G, 1.2 μ g psPAX2) and 1.5 μ g of a lentiviral expression plasmid. For that, I mixed plasmids with 9 μ l polyethylenimine (PEI, 1 μ g/ μ l in ddH₂O, Polysciences) in 150 μ l culture medium without supplements, vortexed for 5 sec, and incubated at RT for 30 min. Then, the plasmid mix was added dropwise on the cells plated in a 6 well plate. 24 h post-transfection, a medium change was performed, and 48 h after transfection, viral particles were collected, passed through a 0.45 μ m cellulose acetate membrane filter (VWR) and stored in aliquots at -80°C.

For the production of retroviral particles, 80 % confluent Phoenix-gp cells were transiently transfected with 0.37 µg pMD.2G and 1.5 µg retroviral expression plasmid incubated with PEI as described above [225–227]. Viral particles were harvested and stored as described above.

2.3.4 Stable transduction of primary hepatocytes

Primary murine hepatocytes were stably transduced using viral particles. For that, cells were incubated with viral particles in the presence of Polybrene (4 µg/ml, Sigma Aldrich) for 2 days. After transduction, cells were selected using respective antibiotics (**Table 2.13**).

Table 2.13. Overview of antibiotics used for selection after viral transduction.

Antibiotic	Final Concentration	Source
Puromycin Dihydrochloride	2 µg/ml	Thermo Fisher Scientific
Blasticidin S HCl	10 µg/ml- 50 µg/ml	Thermo Fisher Scientific
Hygromycin B	0.3-1 mg/ml	Thermo Fisher Scientific
G418-Sulfate (Neomycin)	0.3 mg/ml	biomol

2.3.5 Proliferation assay

To determine differences in proliferation rates, I performed proliferation assays. For that, 200,000-300,000 cells were plated in triplicate in 6 well plates and cultivated until they reached approx. 90 % confluency. Cells were detached using Trypsin and the total amount of cells was determined using the Cellometer Auto T4 Bright Field Cell Counter (Nexcelom). Then, I re-seeded the original number of cells and repeated the process for approx. 14 days.

2.3.6 Colony formation assay

The clonogenic capacity of cells was determined via colony formation assay [228]. Briefly, cells were seeded in a low concentration (500-1000 cells per well) in triplicates in 6 well plates. Medium change was performed every 2-3 days. After 7-21 days, the assay was terminated and cell culture plates were stained using a crystal violet staining solution (0.05 % (w/v) crystal violet, 1 % (v/v) formaldehyde, 1% (v/v) methanol in PBS). For the staining with crystal violet, wells were first washed with PBS and then incubated with crystal violet staining solution for 20 min with gentle shaking at RT. Then, the staining was removed and wells were washed with ddH₂O to remove excess dye and plates were air dried.

2.3.7 Cell surface staining for flow cytometry

In order to analyze cell surface markers via flow cytometry, I stained cells with fluorescently-labeled primary antibodies. For that, adherent cells were harvested using Versene-EDTA and washed once with FACS buffer (PBS with 3 % FCS). If a dead cell staining was performed, cells were incubated with Zombie NIR™ Fixable Viability Dye (Biolegend) diluted 1:1000 in FACS buffer for 15-20 min at RT protected from light. After incubation, cells were washed with FACS buffer and used for antibody staining. For that, cells were resuspended in FACS buffer containing fluorescently-labeled antibodies (**Table 2.14**) for 20-30 min at 4°C protected from light. After another washing step using FACS buffer, stained cells were fixated using the eBioscience™ IC Fixation Buffer (Thermo Fisher Scientific) for 15-20 min at 4°C protected from light. After a final washing

step, cells were resuspended in FACS buffer and stored at 4°C. Analysis was performed using a BD LSRFortessa™ Cell Analyzer (BD Biosciences).

Table 2.14. Antibodies used for flow cytometrical analysis.

Antibody	Conjugate	Dilution	Source
Anti-human CD95 (Fas) [clone: DX2]	FITC	1:100	Biologend
Anti-mouse CD95 (Fas) [clone: SA367H8]	PerCP/Cy5.5	1:100	Biologend
Anti-mouse H-2Kb bound to SIINFEKL [clone: 25-D1.16]	APC	1:100	Biologend
Anti-human HLA-A,B,C [clone: W6/32]	Pacific Blue	1:100	Biologend
Anti-mouse H-2Kb [clone: AF6-88.5]	Pacific Blue	1:100	Biologend

2.3.8 Cleaved caspase 3/7 assay

Cleaved and activated caspase 3/7 was detected using the CellEvent™ Caspase-3/7 Green Detection Reagent (Thermo Fisher Scientific) according to manufacturer's instructions. Briefly, after cells had been treated with apoptosis-inducing agents (Fc (human):FasL, Soluble (human) (rec.), Adipogen Life Sciences), supernatant and cells were harvested and incubated with 5 µM detection reagent for 45 min at 37°C. Afterwards, cells were directly subjected to downstream analysis using the BD LSRFortessa™ Cell Analyzer (BD Biosciences).

2.3.9 OT-I T cell killing assay

I isolated splenocytes from 10-20 weeks old OT-I mice by straining spleens through a 40 µm cell mesh and resuspending the cells in T cell isolation buffer (30 % FCS and 10 mM EDTA pH 8.0 in PBS) [229,230]. Then, cells were pelleted by centrifugation and resuspended in RPMI-1640 medium with supplements (RPMI-1640 (Thermo Fisher Scientific) with 10% FCS, 1 % penicillin/streptomycin, 20 mM HEPES (Thermo Fisher Scientific), 1 mM sodium pyruvate (Thermo Fisher Scientific), and 50 µM β-mercaptoethanol (Thermo Fisher Scientific)). For pre-activation, I plated 2-3 million cells/ml in a cell culture flask and incubated with recombinant IL-2 (rIL-2) (10 U/ml, Biologend) and recombinant SIINFEKL (25 nM, IBA Lifesciences) for 3 days.

Two days before co-culture, I treated tumor cells with IFNγ (300 U/ml, PeproTech) for 2 days in order to stimulate MHC class I surface presentation. One day before co-culture, 40,000 tumor cells were plated in 24 well plates and treated with doxycycline hyclate (DOX, 0.3 µg/ml, Thermo Fisher Scientific).

On the day of the co-culture, I performed a medium change on tumor cell plates. OT-I splenocytes were harvested, washed with PBS, and added to the tumor cells in specific target to effector cell ratios.

One day after co-culture, I removed OT-I splenocytes and dead cells from the plates and stained cells that were still attached either directly with crystal violet (as described in 2.3.6) or cultured for 3-5 more days before crystal violet staining.

Stained plates were scanned using the Epson Perfection 4990 Photo (Epson) and analyzed with the "ColonyArea" ImageJ plugin [231], which determines the relative area of a well covered with stained cells. I calculated relative survival of tumor cells by normalizing the relative stained area of a sample well to the relative stained area of -OT-I control wells.

2.3.10 Lentiviral CRISPR/Cas9 screen

sgRNA library. A lentiviral sgRNA library targeting the surfaceome [232] was cloned into pUSEPR prior to this study. The library comprised a total 5190 sgRNAs targeting 865 genes (6 sgRNAs per gene), 36 non-targeting control sgRNAs, and was split into 10 pools, which were handled as separate samples throughout the course of the experiment. Genes included in the library are listed in **Table 7.1**

Transduction. Viral particles containing the sgRNA library were produced as described in HEK293T cells as described in 2.3.3. To achieve single integration of a viral plasmid, I transduced MYC/sgTrp53 primary hepatocytes expressing lentiCas9-Blast at a multiplicity of infection (MOI) of 0.3, which was determined by assessing the fraction of the tRFP-positive population 48 h post-transduction. Transduction was performed as described, and 48 h after transduction, I selected cells with 2 µg/ml puromycin. Each sgRNA pool was transduced in triplicate.

T cell killing assay. After selection was completed, I subjected cells to the T cell killing assay (2.3.9). For that, splenocytes of three OT-I were isolated, pooled, and cultured with rIL-2 and SIINFKEL as described. Target cells that were not used in the co-culture experiment were washed and stored at -20°C as samples for the reference timepoint T_0 . After co-culture, target cells were cultivated without splenocytes for one week in order to obtain a sufficient number of cells for gDNA isolation (T_1).

gDNA isolation and barcode PCR. I performed gDNA extraction as described in (2.1.4). In order to amplify the sgRNA cassette and to tag amplicons with barcodes for downstream analysis, PCR reactions of each sample were performed using primers shown in **Table 2.15**. To achieve a high coverage (1000x), each sample was amplified in two PCR reactions with 2000 ng template each using Q5 High-Fidelity DNA polymerase (NEB) in 25 PCR cycles. PCR products were purified using the QIAquick Gel Extraction Kit (Qiagen).

Table 2.15. PCR primer sequences for analysis of the CRISPR/Cas9 screen.

Primer ID	Primer Sequence (5' – 3')
REVERSE_01	CAAGCAGAAGACGGCATAACGAGATGTGACTGGAGTTCAGACGTGTGCTCTTCCGATCTTCTACTATTCTTTCCCTGCACTGT
FORWARD_01	AATGATACGGCGACCACCGAGATCTACACTCTTTCCCTACACGACGCTCTTCCGATCT-NNNNNNNNNCGGTTCAATTGTGGAAAAGGACGAAACACCG
FORWARD_02	AATGATACGGCGACCACCGAGATCTACACTCTTTCCCTACACGACGCTCTTCCGATCT-NNNNNNNNNGCTGGATTTTGTGGAAAAGGACGAAACACCG
FORWARD_03	AATGATACGGCGACCACCGAGATCTACACTCTTTCCCTACACGACGCTCTTCCGATCT-NNNNNNNNNTAACTCGGTTGTGGAAAAGGACGAAACACCG
FORWARD_04	AATGATACGGCGACCACCGAGATCTACACTCTTTCCCTACACGACGCTCTTCCGATCT-NNNNNNNNNTAACAGTTTGTGGAAAAGGACGAAACACCG
FORWARD_05	AATGATACGGCGACCACCGAGATCTACACTCTTTCCCTACACGACGCTCTTCCGATCT-NNNNNNNNNTACTCAATTGTGGAAAAGGACGAAACACCG
FORWARD_06	AATGATACGGCGACCACCGAGATCTACACTCTTTCCCTACACGACGCTCTTCCGATCT-NNNNNNNNNGCTGAGAATTGTGGAAAAGGACGAAACACCG
FORWARD_07	AATGATACGGCGACCACCGAGATCTACACTCTTTCCCTACACGACGCTCTTCCGATCT-NNNNNNNNNATTGGAGTTGTGGAAAAGGACGAAACACCG
FORWARD_08	AATGATACGGCGACCACCGAGATCTACACTCTTTCCCTACACGACGCTCTTCCGATCT-NNNNNNNNNNTAGTCTAATTGTGGAAAAGGACGAAACACCG
FORWARD_09	AATGATACGGCGACCACCGAGATCTACACTCTTTCCCTACACGACGCTCTTCCGATCT-NNNNNNNNNCGGTTGACCTTGTGGAAAAGGACGAAACACCG
FORWARD_10	AATGATACGGCGACCACCGAGATCTACACTCTTTCCCTACACGACGCTCTTCCGATCT-NNNNNNNNNNTACAGAGTTGTGGAAAAGGACGAAACACCG

Primer ID	Primer Sequence (5' – 3')
FORWARD_11	AATGATACGGCGACCACCGAGATCTACACTCTTTCCCTACACGACGCTCTTCCGATCT- NNNNNNNNNATTGTCAATTGTGGAAAAGGACGAAACACCG
FORWARD_12	AATGATACGGCGACCACCGAGATCTACACTCTTTCCCTACACGACGCTCTTCCGATCT- NNNNNNNNNTATGTCTTTTGTGGAAAAGGACGAAACACCG
FORWARD_13	AATGATACGGCGACCACCGAGATCTACACTCTTTCCCTACACGACGCTCTTCCGATCT- NNNNNNNNNATTGGATTTTGTGGAAAAGGACGAAACACCG
FORWARD_14	AATGATACGGCGACCACCGAGATCTACACTCTTTCCCTACACGACGCTCTTCCGATCT- NNNNNNNNNATACTCGGTTGTGGAAAAGGACGAAACACCG
FORWARD_15	AATGATACGGCGACCACCGAGATCTACACTCTTTCCCTACACGACGCTCTTCCGATCT- NNNNNNNNNTATGAGAATTGTGGAAAAGGACGAAACACCG
FORWARD_16	AATGATACGGCGACCACCGAGATCTACACTCTTTCCCTACACGACGCTCTTCCGATCT- NNNNNNNNNTAACTCAATTGTGGAAAAGGACGAAACACCG
FORWARD_17	AATGATACGGCGACCACCGAGATCTACACTCTTTCCCTACACGACGCTCTTCCGATCT- NNNNNNNNNCGTGAGCCTTGTGGAAAAGGACGAAACACCG
FORWARD_18	AATGATACGGCGACCACCGAGATCTACACTCTTTCCCTACACGACGCTCTTCCGATCT- NNNNNNNNNATCAGAGGTTGTGGAAAAGGACGAAACACCG
FORWARD_19	AATGATACGGCGACCACCGAGATCTACACTCTTTCCCTACACGACGCTCTTCCGATCT- NNNNNNNNNTATGGAGGTTGTGGAAAAGGACGAAACACCG
FORWARD_20	AATGATACGGCGACCACCGAGATCTACACTCTTTCCCTACACGACGCTCTTCCGATCT- NNNNNNNNNCGTTC AATTGTGGAAAAGGACGAAACACCG
FORWARD_21	AATGATACGGCGACCACCGAGATCTACACTCTTTCCCTACACGACGCTCTTCCGATCT- NNNNNNNNNCGCAAGAATTGTGGAAAAGGACGAAACACCG
FORWARD_22	AATGATACGGCGACCACCGAGATCTACACTCTTTCCCTACACGACGCTCTTCCGATCT- NNNNNNNNNCGACAGCCTTGTGGAAAAGGACGAAACACCG
FORWARD_23	AATGATACGGCGACCACCGAGATCTACACTCTTTCCCTACACGACGCTCTTCCGATCT- NNNNNNNNNCGACTCGGTTGTGGAAAAGGACGAAACACCG
FORWARD_24	AATGATACGGCGACCACCGAGATCTACACTCTTTCCCTACACGACGCTCTTCCGATCT- NNNNNNNNNTACAAGAATTGTGGAAAAGGACGAAACACCG
FORWARD_25	AATGATACGGCGACCACCGAGATCTACACTCTTTCCCTACACGACGCTCTTCCGATCT- NNNNNNNNNCGCAGATTTTGTGGAAAAGGACGAAACACCG
FORWARD_26	AATGATACGGCGACCACCGAGATCTACACTCTTTCCCTACACGACGCTCTTCCGATCT- NNNNNNNNNATTGCTCCTTGTGGAAAAGGACGAAACACCG
FORWARD_27	AATGATACGGCGACCACCGAGATCTACACTCTTTCCCTACACGACGCTCTTCCGATCT- NNNNNNNNNNGCACTCGGTTGTGGAAAAGGACGAAACACCG
FORWARD_28	AATGATACGGCGACCACCGAGATCTACACTCTTTCCCTACACGACGCTCTTCCGATCT- NNNNNNNNNATGTTCTTTTGTGGAAAAGGACGAAACACCG
FORWARD_29	AATGATACGGCGACCACCGAGATCTACACTCTTTCCCTACACGACGCTCTTCCGATCT- NNNNNNNNNATGTCTCCTTGTGGAAAAGGACGAAACACCG
FORWARD_30	AATGATACGGCGACCACCGAGATCTACACTCTTTCCCTACACGACGCTCTTCCGATCT- NNNNNNNNNNGCACTCAATTGTGGAAAAGGACGAAACACCG

Sequencing and analysis. Single-read sequencing was kindly performed by members of the Center for Molecular Pathology (Prof. Dr. Albrecht Stenzinger, Heidelberg University Hospital) using the Illumina NextSeq 500 system together with a NextSeq 500/550 High Output v2 kit (75 cycles) (Illumina). In order to identify hits, I analyzed raw data using CRISPRanalyzer [16, preprint]. Differential readcounts of sgRNAs at T_0 and T_1 were used to calculate the relative enrichment of each sgRNA. Hit gene candidates were called according to following criteria: readcount at T_0 is greater than 100, relative enrichment is greater one in at least three out of 6 gene-specific sgRNAs, relative enrichment could be detected in at least 2 out of 3 replicates. An enrichment score was defined by multiplying the number of enriched sgRNAs per gene by the mean

enrichment for the sgRNAs. Thus, hits were scored according to their degree of enrichment and the highest scoring genes were chosen for downstream validation.

2.3.11 RNA sequencing and differential gene expression analysis

For RNA sequencing, I isolated total RNA from respective cell lines in independent triplicates as described above (2.1.6). Library preparation and RNA sequencing was performed by the Genomics and Proteomics Core Facility at DKFZ. 50 bp single-read sequencing was performed using a HiSeq 4000 system (Illumina). Sequence alignment was performed using STAR (Version 2.5.3a) and GRCm38mm10_PhiX as reference genome. For further analysis, data was processed using HTSeq-count [234] to generate readcount tables and FPKM files and DESeq2 [235] to identify differentially expressed genes.

2.4 Animal experiments

All animal experiments were performed in compliance with regional regulations and in approved by regional authorities (Regierungspräsidium Karlsruhe, Germany).

2.4.1 Hydrodynamic tail vein injection (HTVI)

Hydrodynamic injections were kindly performed by Lena Wendler-Link or Prof. Dr. Darjus Tschaharganeh (Tschaharganeh lab, DKFZ). 7-8 weeks old female C57BL/6N mice (Janvier) were injected with naked DNA plasmids (10 % of body weight, approx. 2 ml) into the tail vein within 5-7 sec [80]. In order to generate genetically defined liver tumors, plasmid mixtures contained 5 µg pT3-EF1a-KrasG12D-IRES-rtTA3 or pT3-EF1a-MYC-IRES-rtTA3, 10 µg pX330-sgp53, 3-5 µg CMV-SB13, and 10-20 µg pT3-TRE-tRFP-miRE-shRen-IRES-OVA-P2A-GFP. I monitored animals daily and euthanized mice via cervical dislocation in accordance with the termination criteria defined in the animal permit.

2.4.2 Magnetic resonance imaging (MRI)

Magnetic resonance imaging (MRI) was carried out by the small imaging core facility at DKFZ (Dr. Manfred Jugold) using a BioSpec 3T or a BioSpec 9.4 T (Bruker).

Data analysis was performed by me using OsiriX Lite Dicom Viewer (Pixmeo).

2.4.3 Adoptive T cell transfer and immune checkpoint blockade

After tumor development had been confirmed via MRI, animals were treated with adoptive T cell transfer using pre-activated OT-I splenocytes, immune checkpoint blockade, or both.

Adoptive T cell transfer. I isolated and activated OT-I splenocytes as described in 2.3.9. 15 million splenocytes were harvested, washed, resuspended in 100 µl NaCl, and injected into the tail vein of tumor-bearing mice.

Immune checkpoint blockade. Tumor-bearing mice were injected intraperitoneally with 250 µg anti-CTLA4 or anti-PD1 (InVivoMAb anti-mouse CTLA-4 (CD152) [clone: BE0164], InVivoMAb anti-mouse PD-1 (CD279) [clone: RMP1-14], both Bio X Cell) twice per week.

2.4.4 Immunohistochemistry (IHC)

Organ samples were fixated using 4 % paraformaldehyde for at least 72 h before embedding in formalin and sectioning into 3 μ m sections.

Deparaffinization was achieved by incubating slides in xylene, followed by rehydration using a descending alcohol series and a washing step using water. Antigen retrieval was performed by boiling slides in a pressure cooker for 8 min using a sodium citrate buffer (10 mM Trisodium citrate dihydrate, 0.5 % (v/v) TWEEN® 20, pH 6.0), followed by cooling down the slides for 5 min under running water. Slides were further incubated in 3 % hydrogen peroxide for 10 min to block endogenous HRP and subsequently washed 1 min under running water and twice with PBS for 2 min each. Sections were blocked with 5 % BSA in PBS with 0.05 % Triton X-100 for 1 h at RT and incubated with the primary antibody diluted in blocking buffer overnight at 4°C (rabbit monoclonal anti-GFP (D5.1), CST #2956, 1:500). Then, slides were washed three times with PBS/Triton X-100 (0.05 %) for 5 min and incubated with ImmPRESS® HRP Horse Anti-Rabbit IgG Polymer Detection Kit, Peroxidase (Vectorlabs) for 30 min at RT, followed by three washing steps with PBS/Triton X-100 (0.05 %). Subsequently, slides were stained with ImmPACT DAB Peroxidase (HRP) Substrate (Vectorlabs) according to manufacturer's instructions and observed under the microscope until desired staining intensity was achieved. Then, slides were counterstained using hematoxylin for 1-2 min, washed with tap water, dehydrated using ascending alcohol series ending with Xylol and mounted using Surgipath Micro-mount Mounting Medium (Leica).

All processes involved in IHC staining and hematoxylin & eosin (H&E) staining were kindly performed by Lena Wendler-Link (Tschaharganeh Lab, DKFZ) and members of the Division of Chronic Inflammation and Cancer (Prof. Dr. Mathias Heikenwälder, DKFZ).

3 Results

3.1 Generating genetically defined liver tumors with conditional neoantigen expression

In order to investigate immune responses mediated by neoantigen expression in liver tumors and to identify genes modulating neoantigen-dependent tumor cell clearance, it is necessary to use an appropriate *in vivo* model that is suitable to address these questions. However, this model needs to fulfil several requirements. Ideally, it should facilitate the generation of tumors that closely resemble human liver tumorigenesis and human tumor characteristics. Moreover, the model should allow to generate autochthonous liver tumors that arise orthotopically from pathologically relevant cells of origins [236]. Additionally, to mimic the heterogeneity observed in human liver carcinogenesis, the respective model should allow for flexible combination and exchange of genetic driver alterations leading to tumorigenesis. Lastly, in order to trigger neoantigen-mediated responses, tumor cells are required to express an immunogenic neoantigen, with neoantigen expression being restricted to tumor cells.

With the purpose of conforming to these requirements, I established a murine model that allows for the generation of genetically defined autochthonous liver tumors with conditional neoantigen expression. For that, hepatocytes of wildtype mice were modified using DNA transposon plasmids and CRISPR/Cas9 technology. This was accomplished through the combination of several DNA plasmids (**Figure 3.1 A**). The first plasmid, pX330-sgTrp53, expresses Cas9 and an sgRNA targeting the tumor suppressor *Trp53*, resulting in the CRISPR-mediated KO of *Trp53*. Secondly, the transposon plasmids pT3-EF1a-MYC-IRES-rtTA3 or pT3-EF1a-KrasG12D-IRES-rtTA3 were used, which lead to the stable expression of either oncogenic *MYC* or *Kras*^{G12D}, both oncogenes known to induce liver cancer [237,238]. Additionally, this plasmid harbors the genetic sequence of the Reverse tetracycline-regulated transactivator gene 3 (*rtTA3*), which is needed to activate the Tetracycline response element (TRE) of the third plasmid, pT3-TRE-tRFP-miRE-shRen-IRES-OVA-P2A-GFP. This transposon plasmid is stably integrated into the genome and expresses the model neoantigen Ovalbumin (*OVA*), the reporter genes GFP and tRFP, and a non-targeting shRNA construct under the control of the TRE promoter. Lastly, the SB transposase expression plasmid (CMV-SB13) was added to the cocktail, which assists the stable integration of the transposon plasmids into the genome of target cells.

The plasmid cocktail was introduced specifically into hepatocytes using hydrodynamic tail vein injection (HTVI). With this method, a high volume (10 % of the body weight) of naked DNA plasmids are rapidly (within approx. 7 sec) injected into the tail vein of mice [80]. As a result of the high pressure in hepatic blood vessels, DNA plasmids are able to enter hepatocytes. Through combined injection of CRISPR/Cas9-expressing and transposon-based DNA plasmids, it is possible to generate genetically defined autochthonous liver tumors which are driven by a CRISPR/Cas9-mediated KO of tumor suppressor genes and a stable overexpression of oncogenes. In combination, these effects result in KO of *Trp53* and stable overexpression of oncogenic *MYC* or *Kras*^{G12D}, leading to rapid tumor formation. Additionally, this model allows for conditional expression of *OVA* as a neoantigen in ON DOX conditions (treatment with Doxycycline), which can be monitored by GFP and tRFP expression.

In order to characterize this mouse model and to investigate neoantigen-dependent immune responses *in*

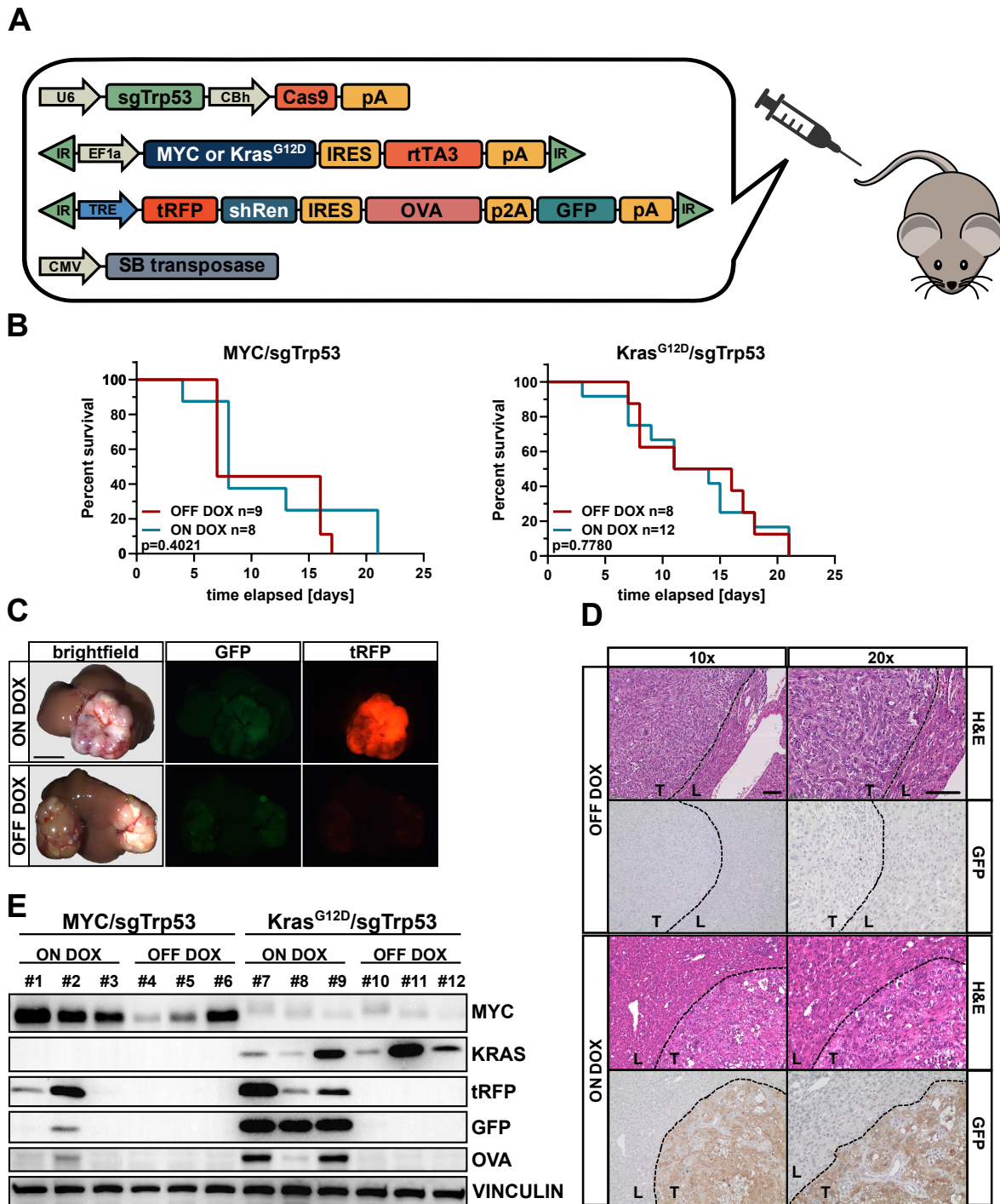


Figure 3.1. Generation of genetically defined autochthonous liver tumors. **A.** Graphic summary of plasmids used to generate genetically defined liver tumors via HTVI. **B.** Survival curves of animals injected with indicated plasmids and fed with DOX-containing or control diet after injection. Statistical analysis was performed using Log-rank test. **C.** Representative stereomicroscopical pictures of livers and tumors of mice injected with MYC/sgTrp53 plasmid mix and fed with DOX-containing or control diet after injection. Scale bar = 1 cm. **D.** Representative immunohistochemical tissue staining of mice injected with Kras^{G12D}/sgTrp53 plasmid mix and fed with regular diet (OFF DOX) or DOX-containing diet (ON DOX). Scale bar = 100 μ m. **E.** Western blot analysis of tumor tissue generated through HTVI. Mice were injected with indicated plasmid mixtures and fed DOX-containing or control diet until euthanized. Data generated jointly with by Sonia Jiménez-Vázquez, DKFZ.

in vivo, 7-8 week old C57BL/6N mice were hydrodynamically injected with plasmid cocktails to generate autochthonous liver tumors. After injection, mice were either fed with regular diet ("OFF DOX") or with Doxycycline-containing diet ("ON DOX") and monitored weekly for tumor development. Mice were euthanized in accordance with local animal welfare protocols and organs and tumors were collected for further analyses. Injection of both plasmid cocktails leading to *Trp53* KO combined with either *MYC* ("MYC/sgTrp53") or *Kras*^{G12D} ("*Kras*^{G12D}/sgTrp53") overexpression resulted in rapid tumor formation and ultimately euthanization of animals within 1-3 weeks after injection (**Figure 3.1 B**). Stereomicroscopical analyses revealed the formation of nodules within the liver, which were GFP- and tRFP-positive in ON DOX mice, but not in OFF DOX mice (**Figure 3.1 C**). H&E staining of formalin-fixed paraffin-embedded liver tissue exposed histopathological changes common in HCC, including atypic cell morphology, trabecular and acinar morphology, and an overall lack of classical hepatic parenchymal architecture [239,240] (**Figure 3.1 D**). Additionally, immunohistochemical staining of tumor tissue showed GFP expression only in dysplastic nodules of ON DOX mice (**Figure 3.1 D**), but not in healthy liver tissue or under OFF DOX conditions. These results demonstrate that the established model can be used to generate genetically defined liver tumors with controlled tumor-specific neoantigen expression within weeks.

To further confirm specific gene expression in tumors generated via HTVI, tumor tissue of MYC/sgTrp53 and *Kras*^{G12D}/sgTrp53 mice were used for Western blot analysis (**Figure 3.1 E**, data generated jointly with by Sonia Jiménez-Vázquez, DKFZ). As expected, MYC/sgTrp53 tumors showed high levels of MYC protein, while *Kras*^{G12D}/sgTrp53 tumor showed high levels of KRAS. Gene expression of the DOX-dependent genes tRFP, GFP, and OVA was only apparent in ON DOX conditions in both MYC/sgTrp53 and *Kras*^{G12D}/sgTrp53 tumors. Surprisingly, DOX-dependent gene expression was not detectable in all ON DOX tumor samples, suggesting a possible silencing or negative selection mechanism of the neoantigen in tumor cells.

In order to investigate the effect of neoantigen expression on overall survival, mice were injected to generate MYC/sgTrp53- or *Kras*^{G12D}/sgTrp53-driven tumors and put ON DOX directly after injection. However, neoantigen expression did not have an effect on survival, as the Kaplan-Meier curves did not differ significantly from respective control groups (**Figure 3.1 B**).

To further determine if the OVA-derived neoantigen SIINFEKL is expressed *in vivo* and elicits an immune response, I investigated the generation of SIINFEKL-specific T cells using MHC:peptide tetramer complexes, which bind to antigen-specific T cells and can be detected via flow cytometry. For this, mice were hydrodynamically injected with a MYC/sgTrp53 plasmid cocktail and tumor formation was monitored via weekly MRI. Once tumors were detectable, mice were put on DOX-containing diet. In parallel, I weekly collected blood from the submandibular vein and examined it for the presence of SIINFEKL-specific T cells using MHC:peptide tetramer staining and flow cytometrical analyses. After 10 days in ON DOX conditions, a distinct population of SIINFEKL-specific CD3⁺ T cells was detectable in peripheral blood of the mice (**Figure 3.2 A**). Importantly, an increase in the antigen-specific T cell population was only found in a subset of DOX-treated mice, suggesting loss of neoantigen. Nevertheless, formation of an antigen-specific T cell population indicates that immune cells encountered SIINFEKL-presenting cells and responded with activation and expansion of the SIINFEKL-specific T cell subset. Consequently, this finding implies that neoantigen presentation induced by DOX treatment can result in an antigen-specific immune response.

The previous results show that this animal model is suited to generate genetically defined liver tumors that lead to immune responses when neoantigen expression is induced. Consequently, I further investigated

whether this model can be used to recapitulate immunotherapeutic interventions that depend on neoantigen-specific T cells. For that, I treated tumor-bearing animals with different immunotherapeutic approaches. Briefly, HTVI was performed to generate MYC/sgTrp53-driven tumors, and tumor formation was monitored via weekly MRI. After tumor detection, mice were put ON DOX and treated with either pre-activated SIINFEKL-specific splenocytes isolated from OT-I mice or an antibody targeting the immune checkpoint CTLA4. 3-4 weeks after the beginning of the treatment, a strong reduction in tumor volume of treated mice was observed, leading to partial or complete tumor regression and prolonged survival (Figure 3.2 B and C). These results demonstrate that this mouse model can be used to challenge neoantigen-expressing tumor cells with T cell-dependent therapeutic approaches, thereby triggering antigen-dependent tumor cell clearance and tumor regression.

In summary, these results show that the newly generated mouse model is well suited for the rapid generation of genetically defined autochthonous liver tumors and that addition of a TRE-dependent OVA-expressing plasmid to the HTVI plasmid cocktail allows for controlled and conditional neoantigen expression in tumors. Thus, this model presents a versatile tool to study neoantigen-dependent mechanisms of tumor formation and therapy approaches *in vivo*.

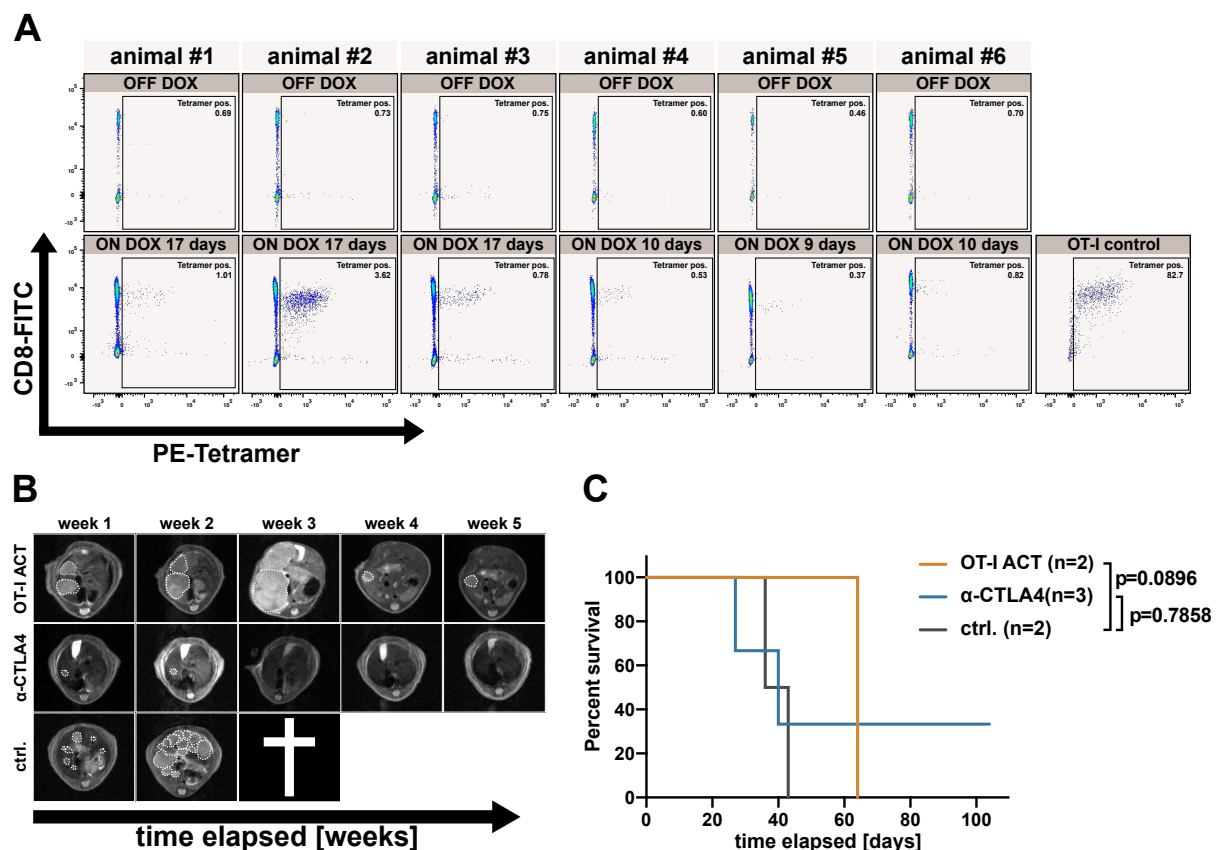


Figure 3.2. DOX-dependent neoantigen expression in primary liver cancer cell lines. **A.** Cell lines generated from HTVI with $Kras^{G12D}$ /sgTrp53 or MYC/sgTrp53 plasmid mixtures were treated with DOX (0.3 μ g/ml) for 3 days and subjected to Western blot analysis. **B.** MYC/sgTrp53 cells with *Tap1* KO and control cells were treated with IFN γ (300 U/ml, 2 days) and DOX (0.3 μ g/ml, 3 days) and stained with antibodies against H-2k B and H-2k B -SIINFEKL for flow cytometrical analysis.

3.2 Establishment of a T cell killing assay to identify tumor cell-specific barriers for immunotherapy

3.2.1 Characterization of tumor-derived primary cell lines to investigate neoantigen-specific tumor cell killing *in vitro*

The previous results demonstrated that the established *in vivo* model can be used to generate immunogenic liver tumors that can be targeted with immunotherapeutic approaches. In order to investigate tumor cell-specific genes mediating immunotherapy in an experimental setting with higher consistency and flexibility, I established an *in vitro* system based on this mouse model with the aim of identifying individual genes that are involved in T cell-mediated killing.

First, I used tumors generated via HTVI to derive primary liver cancer cell lines from respective genotypes. Western blot analyses confirmed that all used cell lines express OVA, tRFP, and GFP only when cultivated in ON DOX conditions (**Figure 3.3 A**). Leakiness of the TRE promotor, which had been described in several publications, was not detectable on protein level under the used experimental conditions [241,242]. Notably, different cell lines, derived from individual tumors, showed varying protein levels for DOX-dependent genes.

Additionally, surface antibody staining of MHC class I (H-2kB) and SIINFEKL bound to MHC class I (H-2kB) revealed that only cells in ON DOX conditions presented SIINFEKL-MHC class I complexes, while cells in OFF DOX conditions demonstrated MHC class I on the surface, but not bound to the antigen SIINFEKL (**Figure 3.3 B**). Furthermore, cells with impaired antigen processing machinery that I generated via CRISPR/Cas9-mediated KO of the Transporter associated with antigen processing I (*Tap1*) showed neither MHC class I nor SIINFEKL bound to MHC class I presentation in ON DOX and OFF DOX conditions (**Figure 3.3 B**).

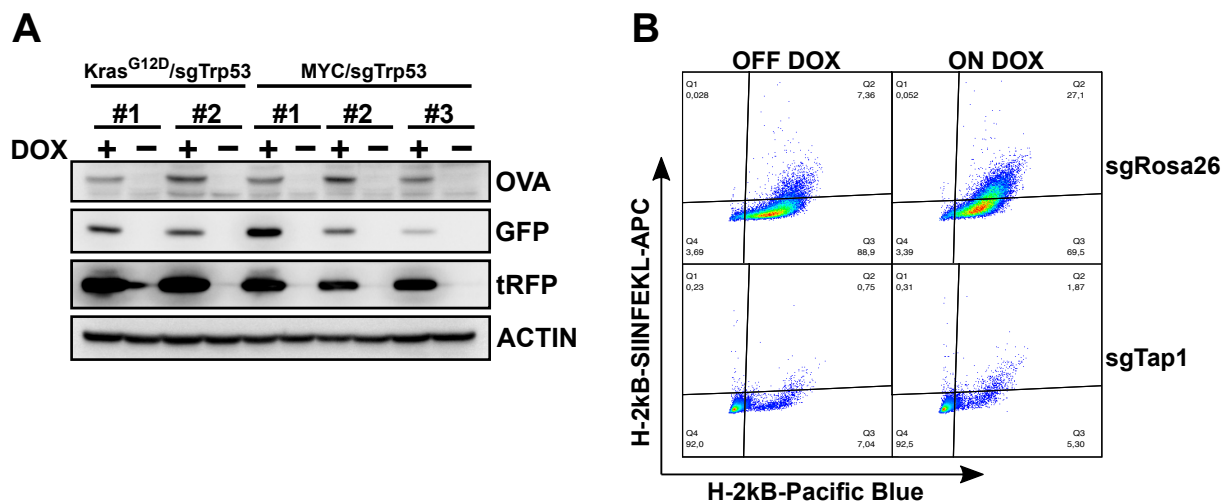


Figure 3.3. DOX-dependent neoantigen expression in primary liver cancer cell lines. **A.** Cell lines generated from HTVI with Kras^{G12D}/sgTrp53 or MYC/sgTrp53 plasmid mixtures were treated with DOX (0.3 µg/ml) for 3 days and subjected to Western blot analysis. **B.** MYC/Trpp53 cells with *Tap1* KO and control cells were treated with IFN γ (300 U/ml, 2 days) and DOX (0.3 µg/ml, 3 days) and stained with antibodies against H-2kB and H-2kB-SIINFEKL for flow cytometrical analysis.

These results show that the generated cell lines express OVA and present SIINFEKL in a DOX-dependent manner, indicating that the tumor-derived primary cell lines can be used as an appropriate *in vitro* model to study neoantigen-dependent tumor cell killing.

3.2.2 Establishment of a neoantigen-specific T cell killing assay

In order to discover new tumor cell-specific modulators of antigen-dependent T cell-mediated killing *in vitro*, I used tumor-derived primary liver cancer cell lines together with SIINFEKL-specific OT-I splenocytes to establish a co-culture assay [229,230]. OT-I splenocytes were pre-activated with recombinant SIINFEKL and rIL-2 for 3 days. In parallel, tumor cells were treated with IFN γ to stimulate MHC class I and antigen surface presentation. For co-culture, I added OT-I splenocytes to tumor cells in defined effector : target cell ratios. After one day in co-culture, remaining tumor cells were stained with crystal violet, serving as an indicator of the amount of tumor cells that survived T cell-mediated killing (Figure 3.4 A).

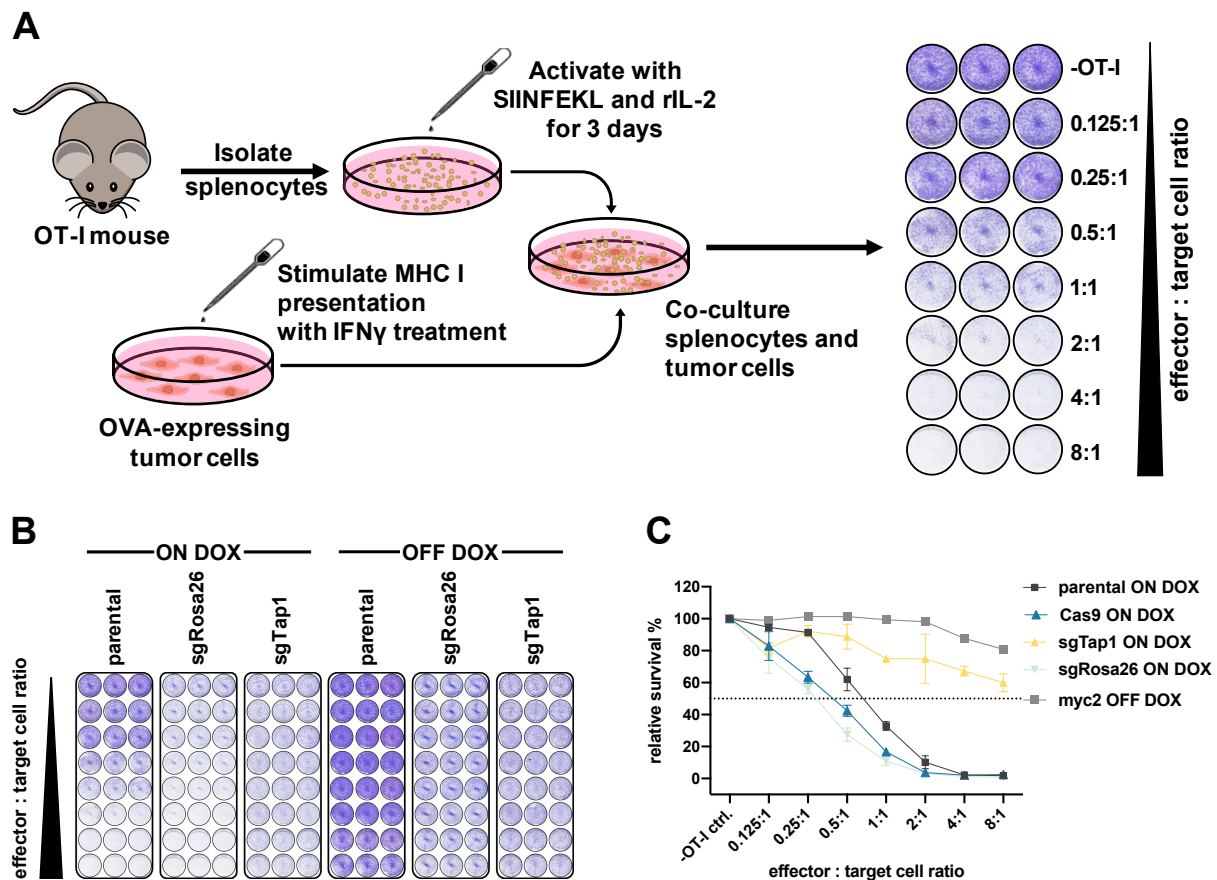


Figure 3.4. Establishment of an antigen-specific T cell killing assay. **A.** Graphic summary of the T cell killing assay. **B.** Overview of T cell killing assay performed with MYC/sgTrp53 cells. Tumor cells were stimulated with IFN γ (300 U/ml, 2 days) and plated in 24 well plates one day prior to co-culture. Activated splenocytes were added in increasing effector : target cell ratios. After one day of co-culture, remaining tumor cells were stained and fixated with crystal violet. **C.** Quantitative analysis of T cell killing assay shown in **B.** Stained wells were scanned and the relative amount of stained area per well was determined. Relative survival was defined as the relative area per well normalized to the relative stained area of untreated control wells (-OT-I). Shown are mean and s.d. of three independent replicates.

Tumor cells were only killed when cultured in ON DOX, but not in OFF DOX conditions, corresponding to decreased crystal violet intensity (**Figure 3.4 B**). Conversely, *Tap1* KO cells were resistant to T cell-mediated killing, independent of DOX conditions. Moreover, the efficiency of tumor cell killing was elevated with increasing effector : target cell ratio. These results indicate that the efficiency of T cell-mediated killing is dependent on the surface presentation of the antigen and the effector : target cell ratio.

To be able to investigate T cell mediated killing in more detail, I used wells stained with crystal violet to quantify the T cell killing efficiency. For that, stained wells were digitalized and the relative stained area of each well was determined. I defined the relative survival by normalizing the relative stained area of each sample to the “-OT-I” negative control (**Figure 3.4 C**). The results confirmed that the relative survival of tumor cells is dependent on the T cell concentration and decreases with increasing effector : target cell ratios. Furthermore, the quantification revealed that even an effector : target cell ratio as small as 0.125:1 was able to achieve measurable T cell-mediated killing with relative survival rates of approx. 80 %. Ratios of 1:1 and 2:1 resulted in relative survival rates ranging from approx. 30 % to 5 %. Additionally, the relative survival of OFF DOX and *Tap1* KO cells remains largely unchanged with increasing effector : target cell ratios, underlining the antigen-specificity of the T cell killing assay. However, at effector : target cell ratios larger than 1:1 - 2:1, the relative survival rates of OFF DOX and *Tap1* KO cells exhibit a slight decrease, which suggests that the T cell-mediated killing becomes unspecific to antigen presentation if T cell concentrations are too high. In summary, these results show that the established assay is able to achieve effective killing in a concentration- and antigen-dependent manner. The relative survival rates indicate that antigen-dependent tumor cell killing is highly specific, since tumor cells without antigen expression (OFF DOX treatment and *Tap1* KO) showed reduced survival rates only in high T cell concentrations. In order to achieve effective and antigen-specific tumor cell killing, I used effector : target cell ratios of 1:1 and 2:1 for further experiments.

Taken together, these findings demonstrate that the T cell killing assay is a useful tool to investigate antigen-specific T cell-mediated tumor cell killing. Furthermore, the flexible design of the assay permits easy genetic manipulation of target cells and allows for combining the T cell killing assay with a CRISPR/Cas9 screen. Therefore, the established T cell killing assay can be further employed to discover new tumor cell specific genes that modulate T cell-mediated killing.

3.2.3 A lentiviral CRISPR/Cas9 screen reveals modulators of T cell-mediated tumor cell killing

The previous results demonstrate that the established T cell killing assay is a reliable system that models neoantigen-dependent tumor cell clearance by cytotoxic lymphocytes. Due to its highly adjustable setup, tumor cells can be genetically modified in order to study genes that influence the efficiency of T cell killing, as demonstrated for *Tap1*. Intriguingly, this assay offers the possibility to modify multiple genes in parallel and identify genes that affect T cell killing efficiency in a pooled format.

In order to verify that the T cell killing assay is a suitable tool to detect sgRNAs that target genes mediating resistance to T cell killing, I set up an experiment that aimed at recovering resistant *Tap1* KO cells co-cultured in an excess of non-resistant control cells. For that, *Tap1* KO cells were mixed with control cells (sgRosa26) at a ratio of 1:600. The sgTap1/sgRosa26 co-culture was used to perform the T cell killing assay and the enrichment of *Tap1* KO cells was determined via flow cytometry and NGS (**Figure 3.5 A and B**). In

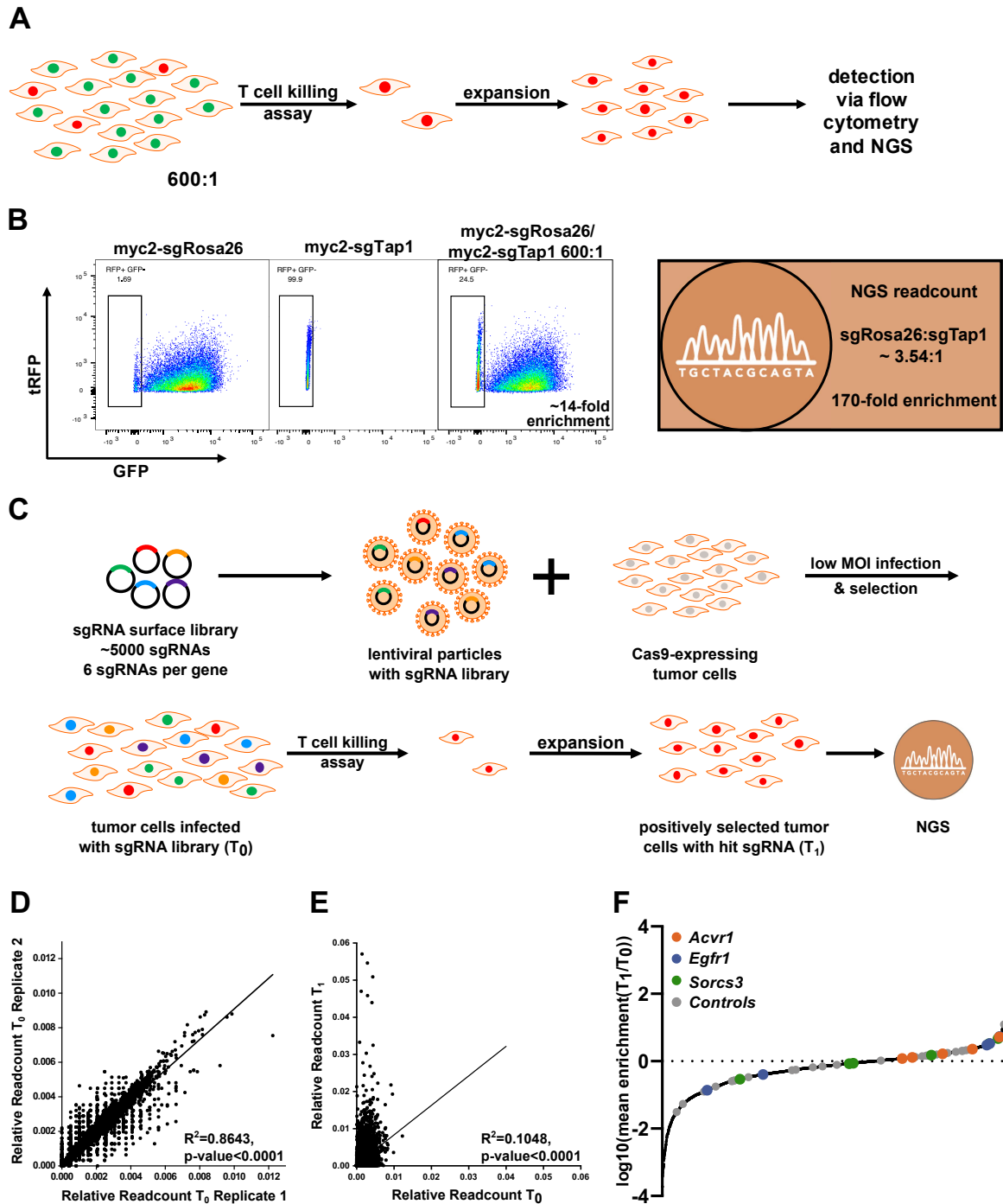


Figure 3.5. A pooled CRISPR/Cas9 screen to identify modulators of antigen-specific tumor cell killing. **A.** Graphic outline of a preliminary experiment designed to verify the detection efficiency of a positive control sgRNA in the T cell killing assay. tRFP-expressing *Tap1* KO cells were combined with GFP-expressing control cells (sgRosa26) in a ratio corresponding to that of a specific sgRNA in a pool comprising 600 sgRNAs (1:600). After co-culture with OT-I splenocytes and expansion, cells were subjected to flow cytometry and NGS analysis in order to determine the enrichment rate of the control RNA. **B.** Flow cytometrical and NGS analysis of MYC/sgTrp53 sgRosa26/sgTap1 cells subjected to T cell killing assay to recapture *Tap1* KO cells. **C.** Graphic outline of a lentiviral pooled CRISPR/Cas9 screen used in combination with the T cell killing assay. **D.-F.** Analysis of CRISPR/Cas9 screen performed with MYC/sgTrp53 cells. **D.** Scatter plot showing the correlation of relative readcounts at T_0 for 2 independent replicates. **E.** Representative scatter plot showing the correlation of relative readcounts of T_0 and T_1 for one of three independent replicates. **F.** Waterfall plot showing mean enrichment for individual sgRNAs. High-lighted data points indicate individual sgRNAs for selected genes and control sgRNAs.

order to discriminate *Tap1* KO cells from sgRosa26 control cells by flow cytometry, *Tap1* KO cells were modified to express the reporter gene tRFP, while sgRosa26 cells were expressing GFP. After performing the T cell killing assay, I was able to detect a distinctly enriched tRFP-positive cell population in the sgTap1/sgRosa26 co-culture. The tRFP-positive cell population constituted 24.5 % of the total cell population, resulting in an approx. 14-fold enrichment of *Tap1* KO cells by the T cell killing assay. Additionally, gDNA from cells that had been used in the T cell killing assay was isolated and DNA sequences coding for the sgRNA cassette were amplified and analyzed via NGS. The readcount ratio of sgRosa26 : sgTap1 was determined as approx. 3.54:1, indicating a 170-fold enrichment of *Tap1* KO cells (**Figure 3.5 B**). These results confirm that the T cell killing assay is a suitable tool to retrieve sgRNAs that lead to resistance to T cell killing, even if they are at a low presentation of 1:600.

The previous results demonstrated that a resistance-conferring sgRNA could be successfully recovered at a presentation of 1:600. Subsequently, I used the T cell killing assay to set up a lentiviral CRISPR/Cas9 screen in order to identify formerly unknown tumor cell-specific genes that affect the efficiency of T cell-mediated tumor cell killing. For that, an sgRNA library comprising all known genes of the surfaceome [232] was designed. This library consists of 5190 sgRNAs, targeting 865 different genes (6 independent sgRNAs per gene), and 36 non-targeting control sgRNAs. As previous experiments had established that an sgRNA could be recovered at a presentation of 1:600, the library was separated into 10 subpools with approx. 520 sgRNAs per pool.

In order to perform a lentiviral CRISPR/Cas9 screen in the context of the T cell killing assay, I transduced Cas9-expressing primary MYC/sgTrp53 cells with lentiviral particles containing the sgRNA library subpools. With the purpose of achieving a single sgRNA integration per cell, the transduction of each sgRNA subpool was performed with a low MOI (approx. 0.3) in technical triplicates. After completed selection, a fraction of cells was retained for the control time point T_0 and remaining tumor cells were subjected to T cell killing. Surviving cells were cultured one week for expansion and then harvested as T_1 samples. gDNA from T_0 and T_1 samples was isolated, the sgRNA cassette was amplified and tagged with barcodes via PCR, and amplicons were subjected to NGS analysis (**Figure 3.5 C**). *In silico* analysis of NGS data provided relative readcounts, which I further used to calculate the relative enrichment of each sgRNA. The relative T_0 readcounts correlated well within the three replicates, indicating a consistent representation of sgRNAs (**Figure 3.5 D**). However, when comparing relative readcounts of T_0 to T_1 samples, it became evident that several sgRNAs were highly enriched after T cell killing (**Figure 3.5 E**). The waterfall plot illustrates that the relative enrichment of individual sgRNAs is evenly distributed across the curve, indicating that the screen and analysis were not biased and did not result in shifted or clustered enrichment of sgRNAs. Moreover, control sgRNAs are randomly scattered across the curve, demonstrating that the enrichment or depletion of non-targeting sgRNAs was not shifted or clustered (**Figure 3.5 F**).

The criteria for hit calling and scoring of specific genes were chosen to account for sufficient presentation of sgRNAs at T_0 , reproducibility between replicates, off-target effects of single sgRNAs, and magnitude of enrichment. I employed three criteria to define genes as hits: (i) an absolute readcount for T_0 >100, (ii) relative enrichment in ≥ 2 out of 3 replicates, (iii) relative enrichment in ≥ 3 out of 6 sgRNAs per gene. These hits were then ranked according to a score defined by the mean enrichment of sgRNAs per gene multiplied by the amount of enriched sgRNAs per gene (**Table 7.2**). The 20 highest ranked genes are listed in **Table 3.1**.

Table 3.1. Overview of the 10 highest ranked hits of the CRISPR/Cas9 screen.

Gene	Score	Gene	Score
<i>Sostdc1</i>	54.910	<i>Bche</i>	22.621
<i>Egfr</i>	35.577	<i>Iglon5</i>	21.898
<i>Ldlr</i>	34.704	<i>Ab124611</i>	21.894
<i>Sdk2</i>	31.291	<i>Acvr1</i>	21.710
<i>C3ar1</i>	26.258	<i>Sorcs3</i>	21.607
<i>Lrrc4b</i>	25.831	<i>Cd164</i>	21.276
<i>Cacng8</i>	24.473	<i>Gpc1</i>	19.793
<i>Nlgn2</i>	23.920	<i>Pcdh15</i>	19.227
<i>Slc12a9</i>	23.517	<i>Col6a5</i>	18.519
<i>Ephb4</i>	22.767	<i>Igsf8</i>	18.333

In order to validate the 20 genes identified as highest-ranking hits, I used the two best performing sgRNAs for each gene were generate individual gene KO cell lines. These cell lines were then subjected to T cell killing in order to verify that the respective sgRNA-mediated gene KO reduces T cell killing efficiency (**Figure 3.6 A**). The results of the T cell killing assay revealed that not all tested sgRNAs reduced the killing efficiency compared to sgRosa26 control cells. In fact, several KO cell lines showed similar survival compared to sgRosa26 control cells, which allowed to exclude the associated genes as true hits. While for some examined genes neither sgRNA resulted in increased survival (e.g., *Sdk2*, *C3ar1*, *Sostdc1*), for others only one of the two tested sgRNAs conferred resistance to T cell killing (e.g., *Lrrc4b*, *Slc12a9*, *Nlgn2*). For the genes Epidermal growth factor receptor (*Egfr*), Activin A receptor type 1 (*Acvr1*), and Sortilin-related VPS10 domain containing receptor 3 (*Sorcs3*), both sgRNAs resulted in distinctly increased tumor cell survival compared to control cells. In order to further narrow down the list of potential hits, only genes for which both sgRNAs lead to distinctly reduced T cell killing efficiency were further considered for investigation.

Consequently, the three most promising gene candidates *Egfr*, *Acvr1*, and *Sorcs3* were selected for further verification. For that, I designed additional sgRNAs for each gene and examined their effectiveness to reduce T cell killing efficiency via T cell killing assay.

Surprisingly, the results showed that two sgRNAs targeting *Egfr* that had resulted in reduced T cell killing efficiency in previous experiments (i.e., sgEgfr.1 and sgEgfr.2) did not display differences in relative survival rates compared to sgRosa26 cells (**Figure 3.6 B and C**). Apart from those, all other tested sgRNAs caused a strong reduction in T cell killing efficiency for all three targeted genes. Quantification of the T cell killing assay revealed that KO of *Acvr1* lead to the highest resistance to T cell killing, displayed by an increase of relative survival rates to approx. 30 % - 40 %. Taken together, these results suggest that all three identified genes *Egfr*, *Acvr1*, and *Sorcs3* are potential regulators of T cell-mediated tumor cell killing. As *Acvr1* KO resulted in the highest resistance to T cell killing in three independent KO cell lines, *Acvr1* was identified as most promising hit and selected for further investigation.

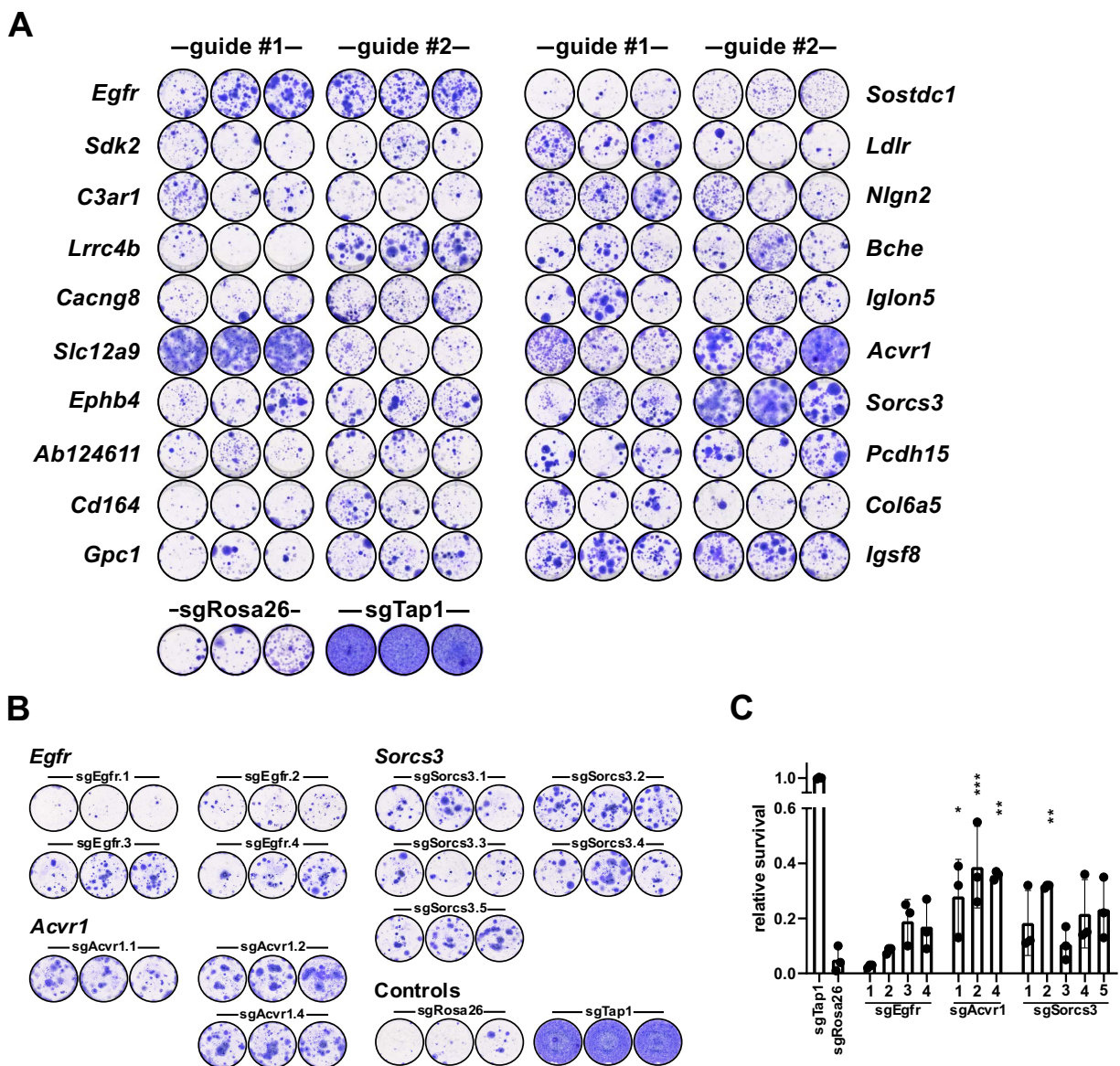


Figure 3.6. Validation of hits identified in the CRISPR/Cas9 screen. A. For each of the 20 highest scored genes, 2 individual sgRNAs used in the screen were used to perform KO cell lines in MYC/sgTrp53 cells. KO cells lines were subjected to T cell killing assay analysis to verify findings from the screen. Representative results from one of 3 independent replicates. **B** and **C.** T cell killing assay analysis with 3-5 individual sgRNA-mediated KO cell lines for *Egfr*, *Acvr1*, and *Sorcs3*. Representative results for one of 3 replicates. **C.** Quantification of T cell killing assay in **B**, shown are mean and s.d. Relative survival is defined as the relative stained area per well normalized to the relative stained area of untreated control wells (-OT-I) of the respective cell line. Statistical analysis was performed via one-way ANOVA. Asterisks indicate statistically significant differences from the control sgRosa26 (*: $p < 0.05$, **: $p < 0.01$, ***: $p < 0.001$).

3.3 *Acvr1* KO leads to reduced antigen-specific tumor cell killing

Since the results of the CRISPR/Cas9 screen suggested that *Acvr1* KO cells are less susceptible to antigen-mediated tumor cell killing by cytotoxic lymphocytes, I further characterized MYC/sgTrp53 *Acvr1* KO cells. For that, *Acvr1* KO cells were used to perform a T cell killing with increasing effector : target cell ratios. The results confirmed that more cells survived T cell-mediated killing in two different *Acvr1* KO cell lines compared to control cells expressing a non-targeting control sgRNA (sgRosa26) (**Figure 3.7 A**). Additionally,

quantification of the relative survival of the respective cell lines and a non-linear regression analysis confirmed that the IC_{50} value (the effector : target cell ration where 50 % survival was observed) of the *Acvr1* KO cell lines was similar or higher than that of the control cell line (Figure 3.7 B). This shows that a higher

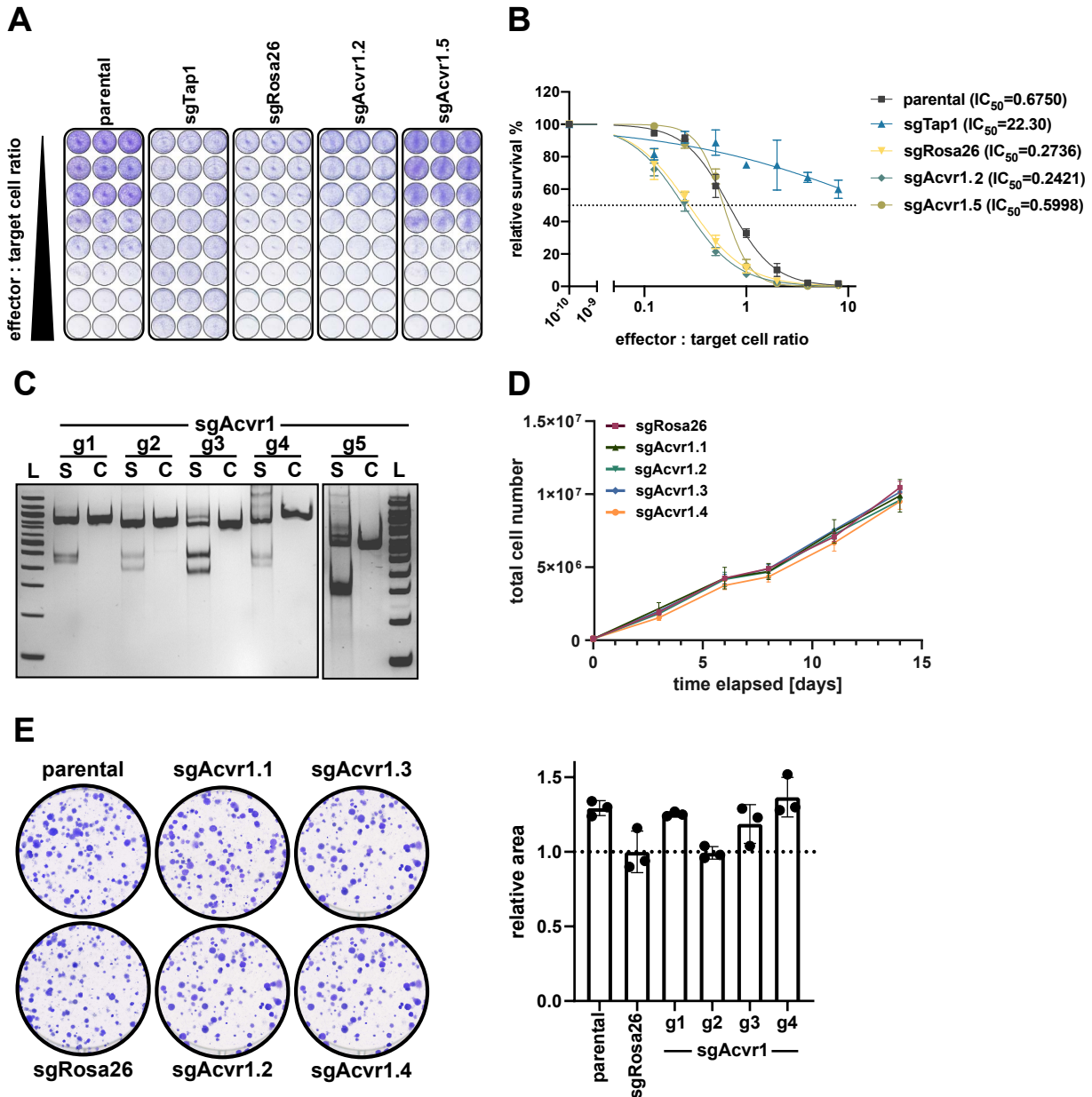


Figure 3.7. *Acvr1* KO leads to reduced T cell-mediated killing in MYC/sgTrp53 cells. **A** and **B**. T cell killing analysis in MYC/sgTrp53 cell lines with *Acvr1* KO. Relative survival is defined as the relative stained area per well normalized to the relative stained area of untreated control wells (-OT-I) of the respective cell line. Shown is one out of three independent replicates. Data in **B** is represented by mean and s.d. **C**. T7 endonuclease I assay of *Acvr1*-targeting sgRNAs used in this study. Cas9-expressing cells were transduced with a lentiviral plasmid encoding the respective sgRNA. L: DNA ladder, S: sample, C: control. **D**. Proliferation assay of *Acvr1* KO cells. Cells were plated in triplicate and the cell number was determined 2-3 days for 2 weeks. Shown are mean and s.d. as representative results from one of 3 independent replicates. **E**. Colony formation assay of *Acvr1* KO cells. Cells were plated in a low concentration in triplicates and after 7-21 days, cells were fixated and stained with crystal violet. Left panel: scanned wells, right panel: quantification of stained area, represented by mean and s.d. Shown is one out of 3 independent replicates.

RESULTS

effector : target cell ratio is needed to achieve 50 % of survival in *Acvr1* KO cells compared to control cells and further validates *Acvr1* as a hit of the CRISPR/Cas9 screen.

In order to verify the functionality of the used sgRNAs, I performed a T7 endonuclease I assay, which detects small insertions and deletions (indels) generated by sgRNA-guided Cas9 endonuclease activity. All cell lines transduced with *Acvr1*-targeting sgRNAs used in this study displayed distinct fragments in the genomic target region after T7 endonuclease I digest, which were absent in parental control cells (**Figure 3.7 C**). This suggests that all *Acvr1*-targeting sgRNAs are able to generate Cas9-mediated indels in the *Acvr1* locus, ultimately resulting in a loss of *Acvr1* gene function.

In order to exclude the possibility that the observed effect of *Acvr1* KO was caused by increased cell proliferation, KO and control cells were plated in specific concentrations and cultivated for 14 days, while the cell number was regularly determined (**Figure 3.7 D**). Thus, it became apparent that none of the used KO cell lines differed in proliferation compared to control cells. Additionally, I performed colony formation assays to study the colony formation capacity of *Acvr1* KO cells. For that, cells were seeded in low density for 7-21 days until detectable colonies had formed (**Figure 3.7 E**). No substantial difference between *Acvr1* KO cells and control cells was determined, indicating that *Acvr1* KO had no considerable effect on colony

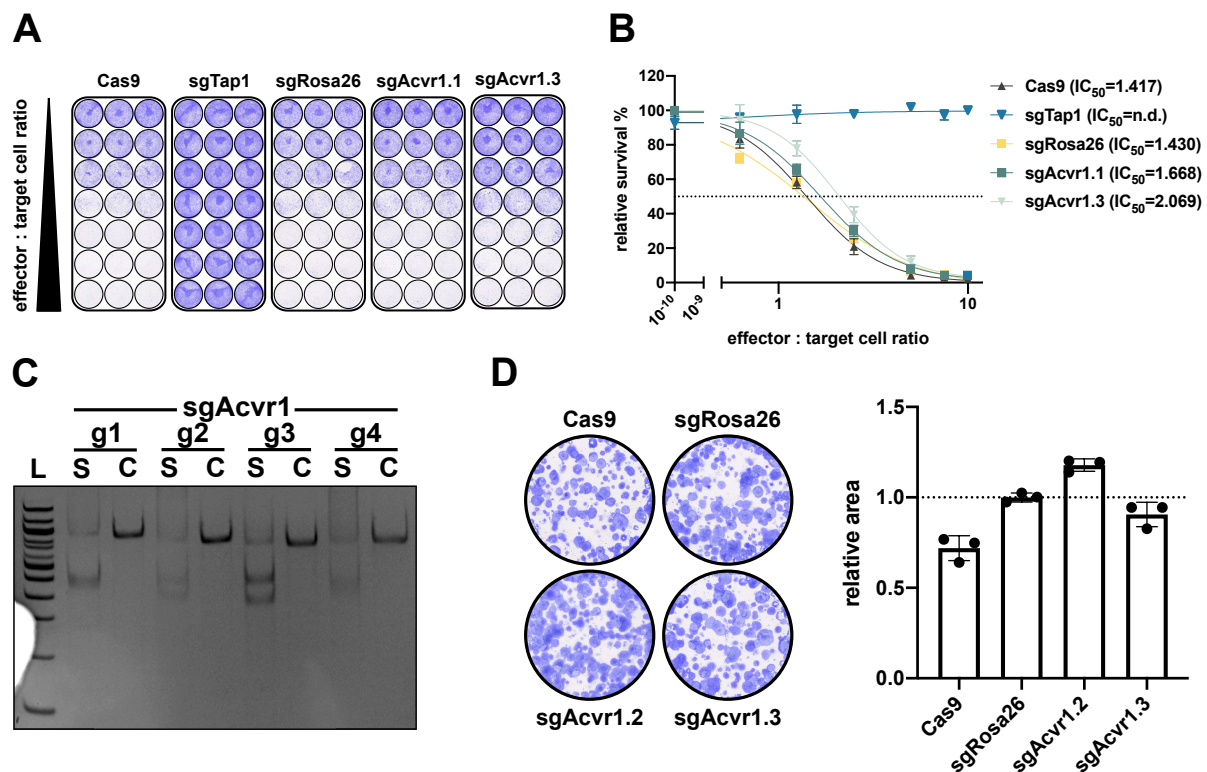


Figure 3.8. *Acvr1* KO leads to reduced T cell-mediated killing in *Kras*^{G12D}/*sgTrp53* cells. **A** and **B**. T cell killing analysis in *Kras*^{G12D}/*sgTrp53* cell lines with *Acvr1* KO. Relative survival is defined as the relative stained area per well normalized to the relative stained area of untreated control wells (-OT-I) of the respective cell line. Shown is one out of three independent replicates. Data in **B** is represented by mean and s.d. **C**. T7 endonuclease I assay of *Acvr1*-targeting sgRNAs used in this study. Cas9-expressing cells were transduced with a lentiviral plasmid encoding the respective sgRNA. L: DNA ladder, S: sample, C: control. **D**. Colony formation assay of *Acvr1* KO cells. Cells were plated in a low concentration in triplicates and after 7-21 days, cells were fixated and stained with crystal violet. Left panel: scanned wells, right panel: quantification of stained area, represented as mean and s.d. Shown is one out of 3 independent replicates. All data generated jointly with Philip Ohland, DKFZ.

formation capacity or proliferation rate. This leads to the conclusion that the increased survival rate of *Acvr1* KO cells in the T cell killing assay was no consequence of increased cell proliferation, but rather the result of a different mechanism.

In order to assess whether the observed effect is dependent to the oncogenic genotype of MYC/sgTrp53 cells, I used primary *Kras*^{G12D}/sgTrp53 cells to perform T cell killing assays (**Figure 3.8 A**). The non-linear regression analysis of the relative survival shows that the IC₅₀ value of *Acvr1* KO cell lines was higher than that of the control cell lines (**Figure 3.8 B**). This strongly suggests that *Acvr1* KO affects the tumor cell killing efficiency in *Kras*^{G12D}/sgTrp53 cells and that this effect is not restricted to MYC/sgTrp53-driven tumor cells. Additionally, I validated effective KO of *Acvr1* via T7 endonuclease I assay using *Kras*^{G12D}/sgTrp53 cells stably expressing *Acvr1*-targeting sgRNAs. T7 endonuclease I-digested DNA fragments were visible in all sgRNA-expressing, but not in control samples, implying that all used sgRNAs generated indels in the *Acvr1* locus of *Kras*^{G12D}/sgTrp53 cells (**Figure 3.8 C**). *Kras*^{G12D}/sgTrp53 *Acvr1* KO cells were further characterized with regard to their colony forming capacity (**Figure 3.8 D**). *Acvr1* KO cells did not exhibit a different colony forming capacity than control cells, which indicates that the observed resistance to T cell-mediated killing was not caused by increased clonogenic capacity of *Acvr1* KO cells.

Taken together, these results suggest that *Acvr1* KO in *Kras*^{G12D}/sgTrp53 cells causes an increased resistance to T cell-mediated tumor cell killing. Furthermore, this implies that this resistance is not a genotype-specific effect of MYC/sgTrp53-tumor cells, but could rather be a universal consequence of *Acvr1* KO.

3.4 *Acvr1* KO leads to changes in BMP signaling

ACVR1 is a type I receptor of the BMP signaling pathway. The pathway is activated by the binding of different BMPs to type II receptors, forming heterodimers with type I receptors. These are then activated through phosphorylation by type II receptors. Activated type I receptors phosphorylate the signaling proteins SMAD1/5/9, which subsequently form a complex with SMAD4 and translocate into the nucleus in order to activate the expression of specific genes like *Id1* [243,244].

In order to investigate the effect of *Acvr1* KO on BMP signaling, I performed immunoblotting analyses for downstream signaling components. For that, MYC/sgTrp53 cells were treated with BMP7 in order to activate BMP signaling and cell lysates were analyzed via Western blot. The results revealed that after treatment with BMP7, phosphorylated SMAD1/5/9 and ID1 protein levels were strongly increased in sgRosa26 control cells (**Figure 3.9 A**). In *Acvr1* KO cells, however, the extent of SMAD1/5/9 phosphorylation and the upregulation of *Id1* expression upon BMP7 treatment was markedly reduced compared to control cells (**Figure 3.9 A**). This observation is in accordance with previous reports, which state that BMP7 primarily leads to signaling via ACVR1 [245,246]. These results indicate that KO of *Acvr1* reduces BMP signaling transduction after treatment with BMP7.

Furthermore, to investigate whether this effect is cell type-specific, *Kras*^{G12D}/sgTrp53 were treated with known activators of the BMP pathway BMP2 or BMP7. The activation of BMP downstream signaling was analyzed via Western blot, which revealed that treatment of *Acvr1* KO cells with BMP2 or BMP7 resulted in distinctly reduced levels of phosphorylated SMAD1/5/9 compared to control cells (**Figure 3.9 B**). This suggests that *Acvr1* KO in *Kras*^{G12D}/sgTrp53 leads to reduced BMP pathway activation after treatment with BMP2 or BMP7. Notably, even though BMP2 is reported to primarily activate the pathway independent of

ACVR1, BMP2-induced phosphorylation of SMAD1/5/9 was also reduced in *Acvr1* KO cells [245]. This finding suggests that BMP2 is partly dependent on *Acvr1* to activate the signaling pathway. Taken together, these results demonstrate that *Acvr1* KO drastically reduces canonical BMP signaling and the expression of BMP downstream targets in two different primary liver cancer cell lines.

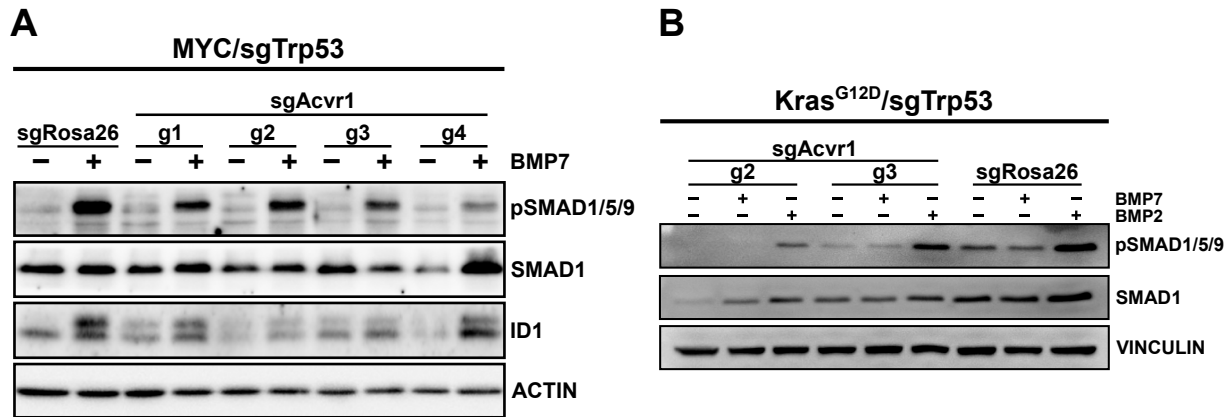


Figure 3.9. Activation of ACVR1 downstream targets is reduced in *Acvr1* KO cells. **A.** Western blot analysis of ACVR1 downstream signaling in MYC/sgTrp53 cells. *Acvr1* KO and control cells were treated with BMP7 (100 ng/ml, 1 h), harvested, and protein lysates were used for immunoblotting. **B.** Western blot analysis of ACVR1 downstream signaling in Kras^{G12D}/sgTrp53 cells. *Acvr1* KO and control cells were treated with BMP7 or BMP2 (50 ng/ml, 1 h), harvested, and protein lysates were used for immunoblotting. Data generated jointly with Philip Ohland, DKFZ.

In order to gain a deeper understanding of the effect of *Acvr1* KO on BMP signaling, I analyzed the transcriptomic profile of MYC/sgTrp53 *Acvr1* KO cells compared to sgRosa26 control cells via RNA sequencing. Differential gene expression analysis revealed that a considerable number of genes were up- or downregulated in *Acvr1* KO cells (**Figure 3.10 A and B**). Remarkably, the well-described target genes of ACVR1 signaling *Id1*, *Id2*, and *Id3* [247,248], as well as *Acvr1* itself were shown to be downregulated in *Acvr1* KO samples.

Further analysis of transcriptomic data revealed that numerous cell functions associated with BMP signaling were affected by *Acvr1* KO, demonstrating a phenotype that is consistent with known functions of *Acvr1* and BMP signaling. Ingenuity pathway analysis (IPA, QIAGEN Inc., [249]) identified several dysregulated pathways in *Acvr1* KO cells, connecting *Acvr1* to multiple processes involved in embryonal development and adult tissue homeostasis (**Figure 3.10 C**). These include embryonal stem cell pluripotency, osteogenesis, chondrogenesis, neural stem cell fate, cardiomyogenesis, wound healing, and fibrosis, which have all been linked to BMP signaling [250–257]. In addition to that, Gene Set Enrichment Analysis (GSEA) revealed differentially expressed gene sets (**Figure 3.10 D**). The three gene sets with the highest normalized enrichment score (NES) in *Acvr1* KO cells included epithelial-mesenchymal transition, genes downregulated as response to UV irradiation, and myogenesis. On the other hand, gene sets with highest NES in control cells – thus being the gene sets most depleted in *Acvr1* KO cells – were genes involved in oxidative phosphorylation, MYC target genes, and DNA repair genes. Consistently, all identified cellular processes affected by *Acvr1* KO were already described to be connected with BMP signaling [203,258–263].

Taken together, these results demonstrate that *Acvr1* KO leads to reduced BMP signaling. The transcriptomic analysis illustrates a phenotype of *Acvr1* KO cells that is coherent with already described functions of *Acvr1* and BMP signaling in embryonal development and adult tissue homeostasis and repair. Since

these processes are largely regulated by cell survival and apoptosis [264,265], it is conceivable that the observed influence of *Acvr1* on T cell-mediated tumor cell killing is mediated through one of the many downstream effects of BMP signaling.

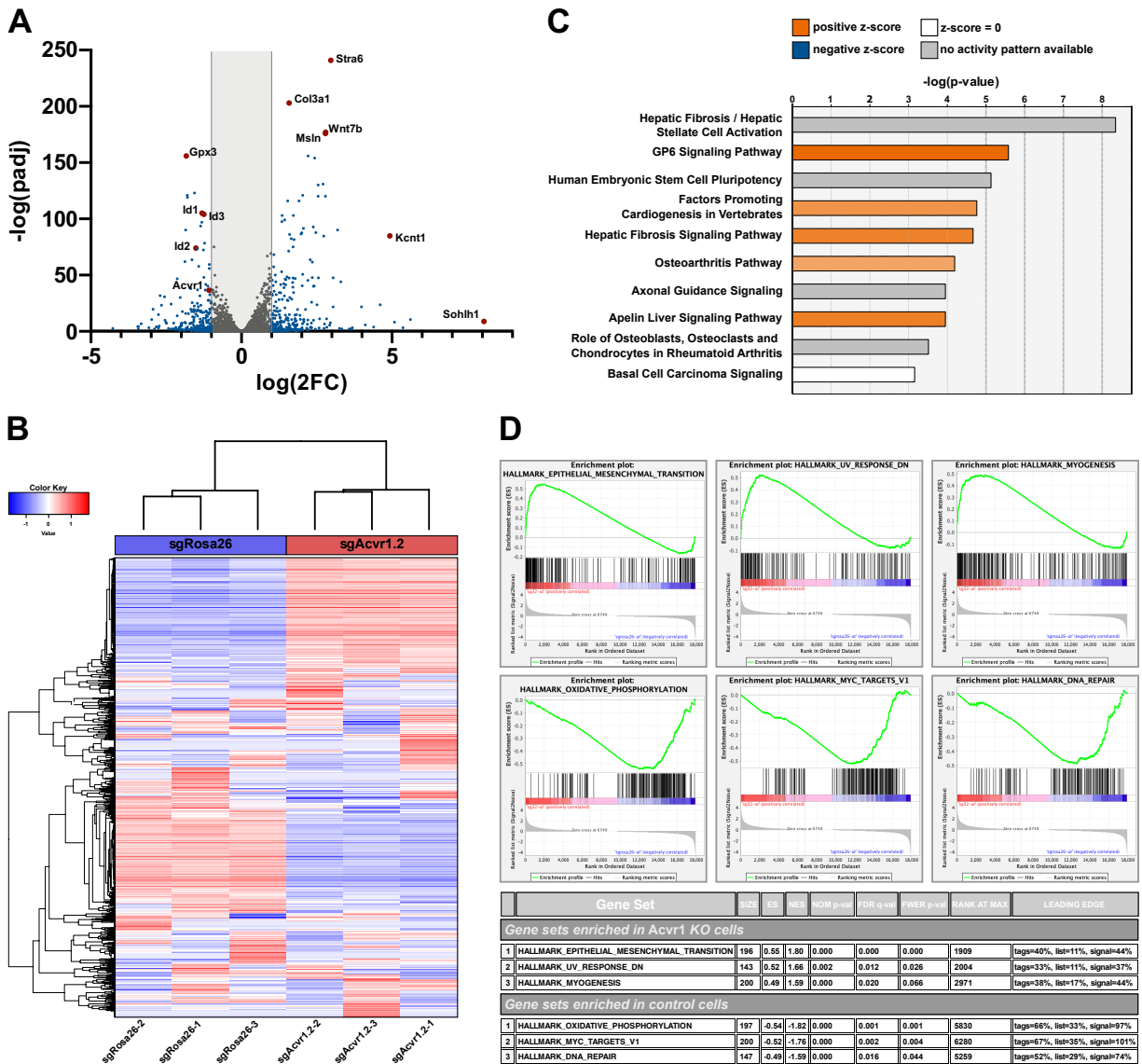


Figure 3.10. Gene expression analysis in *Acvr1* KO cells. **A.** Volcano plot of differentially expressed genes identified via RNA sequencing analysis. Genes were considered differentially expressed with an expression change > 2 and an adjusted p-value < 0.05 (blue and orange data points). **B.** Top ten pathways affected by *Acvr1* KO identified via Ingenuity Pathway Analysis. Positive z-score: upregulation of pathway, negative z-score: downregulation of pathway. **C.** Gene set enrichment analysis (GSEA) of top three hallmark gene sets altered in *Acvr1* KO or *sgRosa26* control cells. **D.** Heatmap of 1000 highest differentially expressed cells in *Acvr1* KO cells. Results show data from three independent replicates.

3.5 ACVR1 re-expression reverses the effects of *Acvr1* KO on T cell-mediated killing

As demonstrated by previous findings, *Acvr1* KO leads to increased resistance of T cell-mediated killing and reduced activation of BMP signaling. With the purpose of investigating whether re-expression of ACVR1 in *Acvr1* KO cells would reverse these effects, I stably transduced MYC/sgTrp53 *Acvr1* KO cells with retroviral plasmids encoding different versions of human ACVR1: wildtype ACVR1 (wtACVR1), constitutively active ACVR1 (caACVR1, mutated at Q207D), and kinase-dead ACVR1 (kdACVR1, mutated at K235R) [266]. Western blot analysis confirmed that the levels of pSMAD1/5/9 and ID1 were considerably higher in cells expressing wtACVR1 and caACVR1 compared to control cells (**Figure 3.11 A**). This suggests that re-expression of wt or constitutively active ACVR1 leads to activation of the BMP pathway even without further

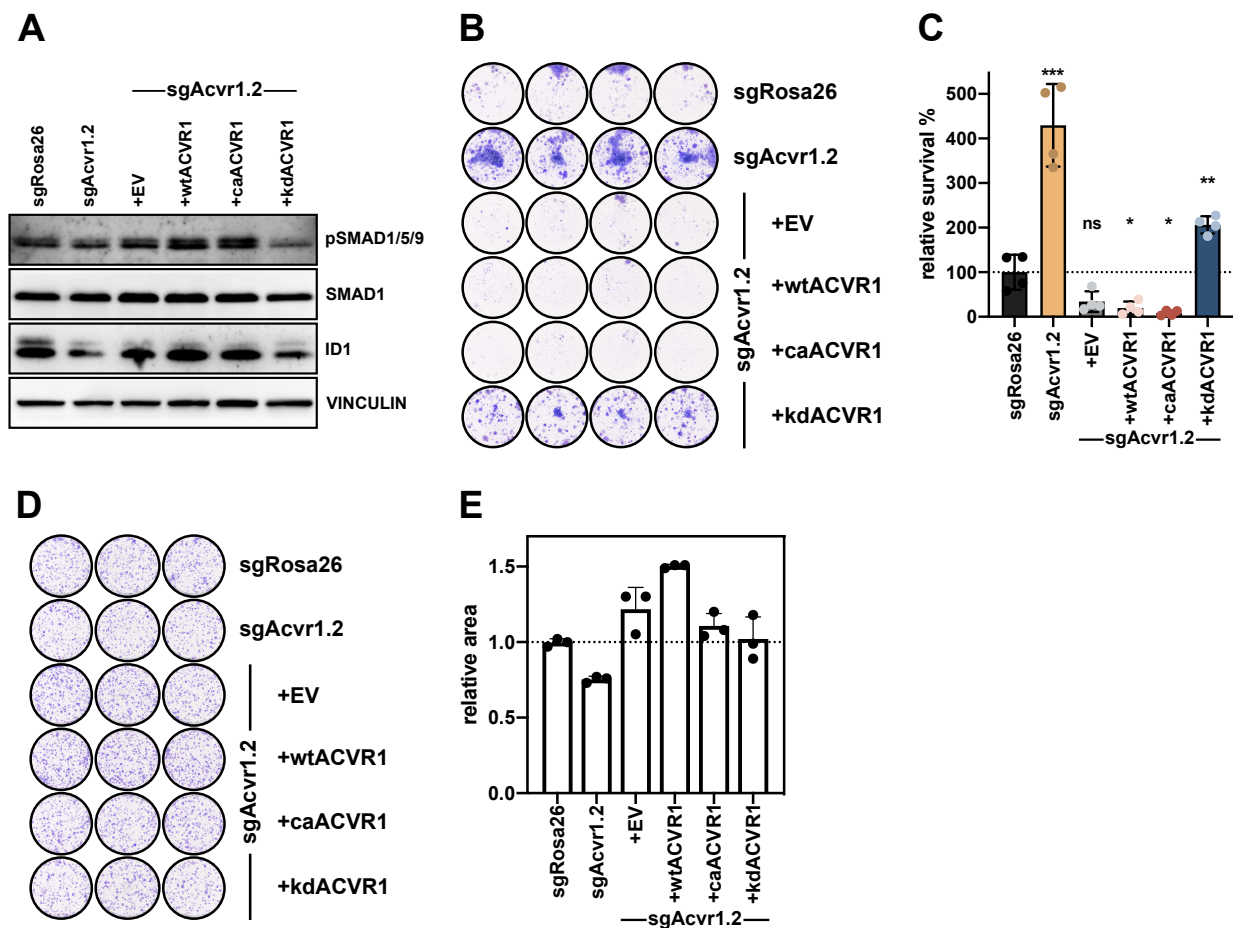


Figure 3.11. Expression of catalytically active ACVR1 versions reverses the effect of *Acvr1* KO on T cell-mediated killing in MYC/sgTrp53 cells. **A**. Western blot analysis of BMP downstream signaling in *Acvr1* KO cells stably expressing ACVR1 versions. *Acvr1* KO cells were stably transduced with retroviral pMSCV plasmids encoding human versions of ACVR1. EV: pMSCV empty vector control, wtACVR1: wildtype ACVR1, caACVR1: constitutively active version of ACVR1 (Q207D), kdACVR1: kinase-dead version of ACVR1 (K235R). **B** and **C**. T cell killing assay in MYC/sgTrp53 cell lines with *Acvr1* KO and expression of ACVR1 versions with effector : target cell ratio 2:1. Representative data from one out of three independent replicates. **C**. Quantification of T cell killing assay. Relative survival is defined as the relative stained area per well normalized to the relative stained area of untreated control wells (-OT-I) of the respective cell line. Shown are mean and s.d., statistical analysis was performed via one-way ANOVA. Asterisks indicate statistically significant differences from the control sgRosa26 (*:p<0.05, **:p<0.01, ***:p<0.001, ns: not significant). **D** and **E**. Colony formation assay of *Acvr1* KO and ACVR1-expressing cells. Cells were plated in low concentration in triplicates and after 7-21 days, cells were fixed and stained with crystal violet. Shown is one out of 3 independent replicates. **E**. Quantification of **D**. Shown are mean and s.d.

stimulation. On the other hand, empty vector (EV) control and kdACVR1 cells displayed pSMAD1/5/9 and ID1 levels similar to those of *Acvr1* KO cells, indicating that re-expression of ACVR1 without a functional kinase domain does not lead to activation of the BMP pathway (**Figure 3.11 A**). In the T cell killing assay, wtACVR1 and caACVR1 cells displayed relative survival rates that were lower than that of sgRosa26 control cells, while kdACVR1 cells exhibited higher survival rates compared to the control (**Figure 3.11 B and C**). Remarkably, the extent of this effect can be so pronounced, that the susceptibility to T cell-mediated killing exceeds even that of sgRosa26 control cells. Further investigating the effect of re-expression of *ACVR1* on MYC/sgTrp53 cells, I performed a colony formation assays (**Figure 3.11 D and E**). Re-expression of *ACVR1* did not result in a considerably altered clonogenic capacity, which further corroborates the results of the T cell killing assay.

Taken together, these results indicate that re-expression of *ACVR1* counteracts the resistance-conferring effects of *Acvr1* KO in T cell-mediated killing. Notably, this effect is only observed with *ACVR1* versions that have a functional kinase domain, which suggests that the effect of *Acvr1* on T cell killing efficiency is dependent on the ability of ACVR1 to transmit signals by phosphorylation. Moreover, these findings further confirm *Acvr1* as a mediator of T cell killing efficiency.

3.6 Investigating the effect of BMP signaling pathway pre-activation on T cell-mediated killing

Re-expression of *ACVR1* with a functional kinase domain resulted in increased BMP pathway activation, but decreased resistance to T cell-mediated killing. Therefore, I addressed whether BMP pathway activation via BMP7 treatment would have an effect on the survival rate in T cell-mediated killing.

For that, I treated MYC/sgTrp53 cells with BMP7 before co-culture with OT-I splenocytes in order to activate the signaling pathway. Surprisingly, treatment of sgRosa26 control cells with BMP7 did not lead to reduced, but rather increased survival rates compared to untreated cells (**Figure 3.12 A**). This effect was diminished, but not completely absent in *Acvr1* KO cell lines (**Figure 3.12 A**). Applying the same treatment in *Acvr1* KO cells with re-expression of different *ACVR1* versions, I observed a similar trend. While BMP7 treatment of EV control cells and kdACVR1 cells did not lead to any change in T cell killing efficiency compared to untreated cells, wtACVR1 and caACVR1 cells showed a slightly increased resistance to T cell killing when treated with BMP7 (**Figure 3.12 B**).

Taken together, these results suggest that BMP7-induced activation of the BMP signaling pathway leads to increased survival in MYC/sgTrp53 cells. This effect appears to be partly dependent on *Acvr1* expression, since KO of *Acvr1* leads to a less pronounced effect, while re-expression of kinase-active wtACVR1 or caACVR1 partially restores this effect.

These findings stand in contrast to the observation that re-expression of wtACVR1 or caACVR1 leads to increased T cell killing efficiency (3.5). However, BMP7 treatment is known to induce a multitude of different cellular functions, including increased proliferation in hepatocytes [267]. Thus, it is possible that survival-promoting effects of BMP7 treatment overshadowed the effect of *Acvr1* KO on T cell-mediated killing.

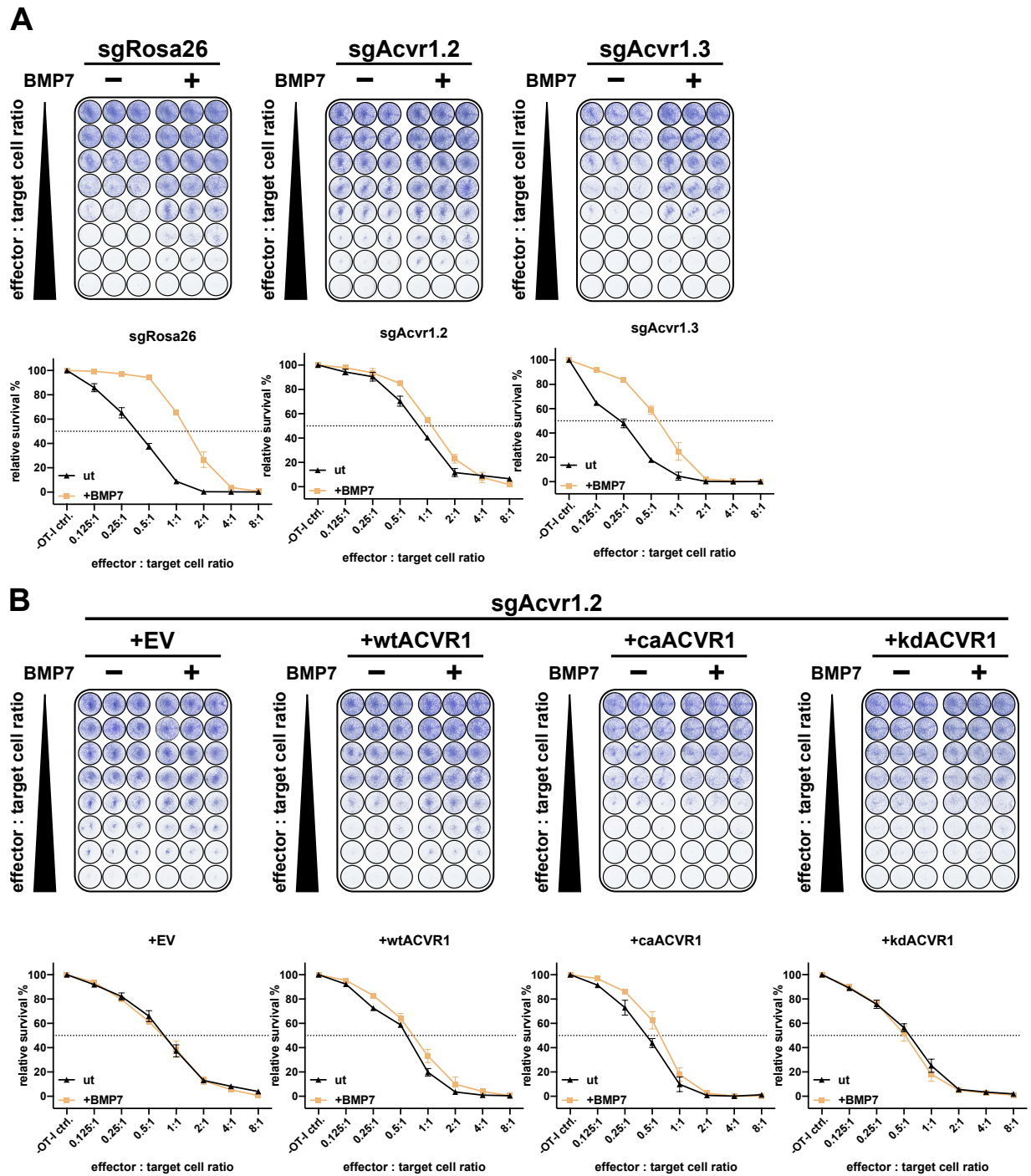


Figure 3.12. The effect of BMP7 treatment on T cell-mediated killing. A. and B. Tumor cells were treated with BMP7 (100 ng/ml) for 24 h prior to co-culture with activated OT-I splenocytes. T cell killing assay was performed in MYC/sgTrp53 cell lines with *Acvr1* KO (A) and expression of *ACVR1* versions (B). Representative data from one out of three independent replicates. Relative survival is defined as the relative stained area per well normalized to the relative stained area of untreated control wells (-OT-I) of the respective cell line. EV: pMSCV empty vector control, wtACVR1: wildtype *ACVR1*, caACVR1: constitutively active version of *ACVR1* (Q207D), kdACVR1: kinase-dead version of *ACVR1* (K235R). Shown are mean and s.d.

3.7 Unravelling the mechanistic effect of *Acvr1* on antigen-specific tumor cell killing

3.7.1 *Acvr1* KO does not affect antigen presentation in tumor cells

Antigen presentation by target cells and antigen recognition by T cells are crucial factors for efficient T cell-mediated killing [268]. Hence, I investigated the effect of *Acvr1* KO on antigen presentation. For that, cells were treated for 2 days with DOX and IFN γ in order to stimulate neoantigen expression and antigen presentation. Total surface MHC class I (H-2kb) and OVA-derived SIINFEKL bound to MHC class I were detected using flow cytometry. No substantial difference in either total surface MHC class I (**Figure 3.13 A**) or SIINFEKL:MHC class I complexes (**Figure 3.13 B**) were observed between control and *Acvr1* KO cells. *Tap1* KO cells showed strongly reduced surface presentation of total MHC class I and SIINFEKL bound to MHC class I. These observations lead to the conclusion that *Acvr1* KO does not result in reduced killing efficiency through downregulation of antigen presenting and subsequent diminished T cell activation. Instead, this suggests that *Acvr1* KO influences T cell killing efficiency through a different mechanism.

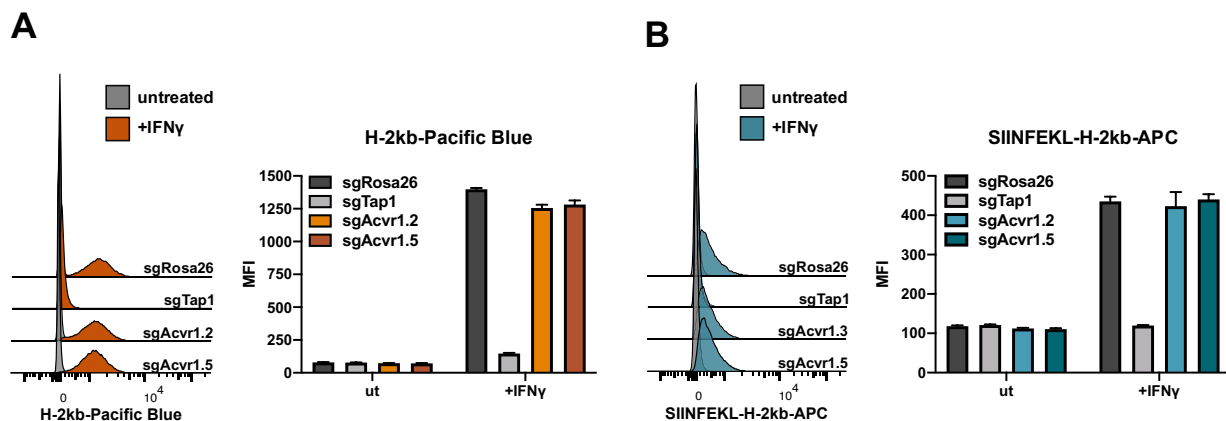


Figure 3.13. Neoantigen presentation in *Acvr1* KO cells. **A** and **B**. Flow cytometrical analysis of MYC/sGTrp53 *Acvr1* KO and control cells treated with IFN γ (300 U/ml for 2 days) and stained with antibodies against H-2kB (**A**) or SIINFEKL-H2kB (**B**). Left panels show representative histograms of 3 independent replicates. Right panels show mean and s.d. of median fluorescence intensity (MFI) for 3 replicates.

3.7.2 *Acvr1* KO diminishes *Fas* upregulation and leads to reduced apoptosis induction

Activated CD8⁺ T cells exert their cytotoxic function by the binding of FASLG to the FAS receptor of target cells, thereby activating the extrinsic apoptotic pathway [110]. Thus, I further examined *Fas* expression in *Acvr1* KO cells. As preliminary experiments revealed low basic levels of *Fas* expression, MYC/sGTrp53 cells were stimulated with IFN γ , TNF α , or both, thus inducing FAS surface expression [269,270]. The treatment protocol with IFN γ was similar to that included in the T cell killing assay, thereby recapitulating the same phenotype that facilitated the identification of *Acvr1*. TNF α treatment was described by Faletti *et al.* [271]. Moreover, both cytokines are secreted by cytotoxic lymphocytes upon activation, thus assisting effective target cell killing [272].

Consequently, I treated control and *Acvr1* KO cells with IFN γ , TNF α , or both, and examined the surface expression of FAS using flow cytometry (**Figure 3.14 A**). Untreated cells showed low levels of FAS surface expression, whereas treatment with cytokines increased FAS surface levels. The treatment of IFN γ resulted

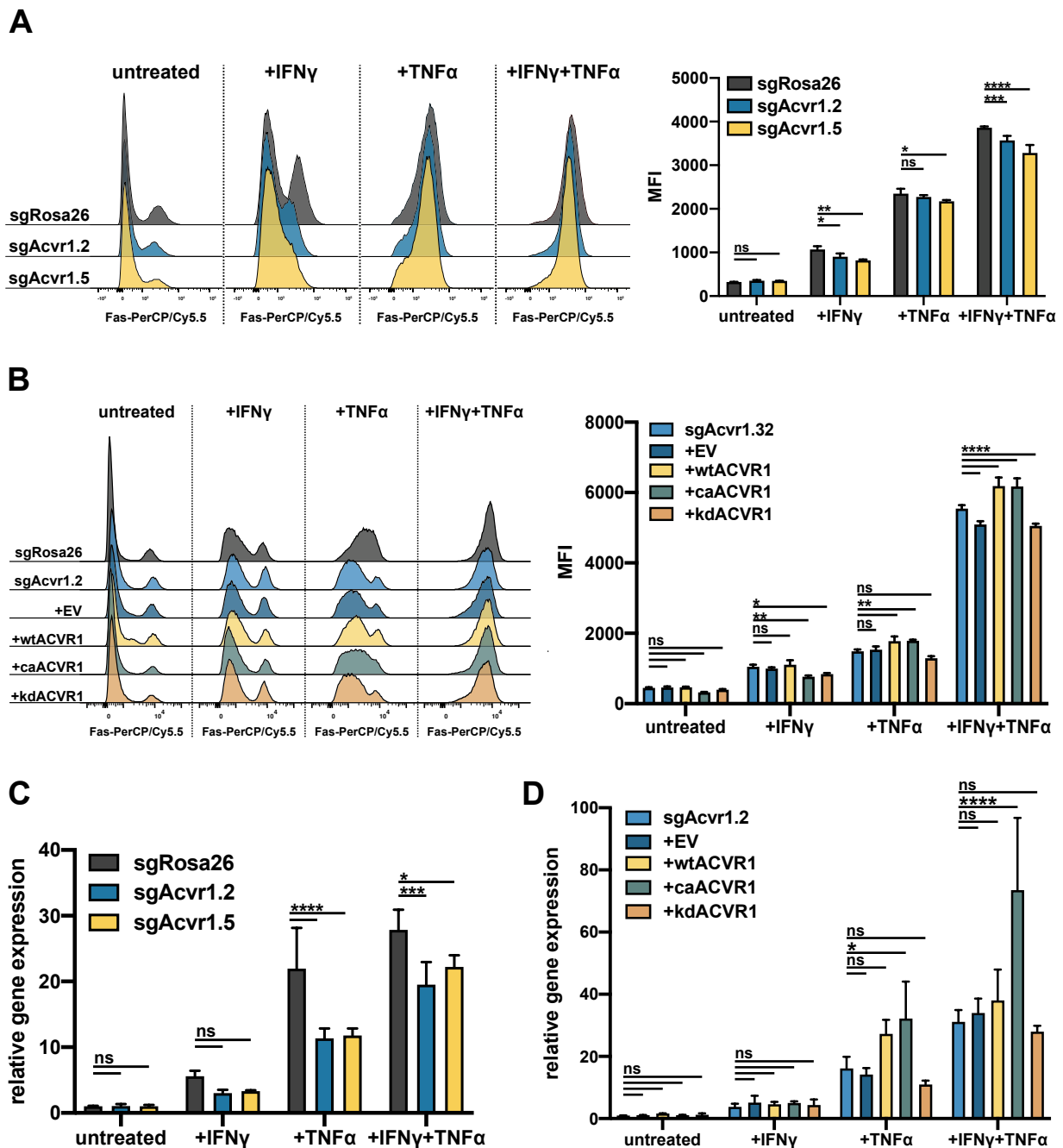


Figure 3.14. *Fas* surface presentation and gene expression in *Acvr1* KO and *ACVR1*-expressing cells. A and B. *FAS* surface expression in MYC/*sgTrp53* cells with *Acvr1* KO (A) and expression of *ACVR1* versions (B) treated with IFN γ (300 U/ml for 2 days), TNF α (20 ng/ml for 16 h), or both, and detected via flow cytometry. Left panels show representative histograms from 3 independent replicates. Right panels show mean and s.d. of median fluorescence intensity (MFI) for 3 replicates. **C and D.** Quantitative real-time PCR analysis of *Fas* gene expression in *Acvr1* KO (C) and *ACVR1*-expressing (D) MYC/*sgTrp53* cells treated with IFN γ (300 U/ml for 2 days), TNF α (20 ng/ml for 16 h), or both. Gene expression analysis was performed by $\Delta\Delta C_T$ method and normalized to *sgRosa26* untreated control (C) or *sgAcvr1.2* untreated control (D). Graphs show mean and s.d. of 3 replicates. EV: pMSCV empty vector control, wtACVR1: wildtype *ACVR1*, caACVR1: constitutively active version of *ACVR1* (Q207D), kdACVR1: kinase-dead version of *ACVR1* (K235R). Statistical testing was performed using 2-way ANOVA, compared to *sgRosa26* (C) or *sgAcvr1.2* (D) control cells with corresponding treatment (*: $p < 0.05$, **: $p < 0.01$, ***: $p < 0.001$).

in lower FAS surface expression compared to TNF α treatment, while the combined treatment of both cytokines caused the highest observed levels of surface FAS. Comparing FAS surface levels of control cells with two *Acvr1* KO cell lines, it became apparent that *Acvr1* KO cells displayed lower levels of FAS. Furthermore, this effect was more pronounced in cytokine-stimulated cells. These observations suggest that *Acvr1* KO leads to reduced FAS surface levels. Additionally, *Acvr1* KO resulted in a decreased induction of FAS surface expression upon IFN γ and TNF α treatment.

To substantiate these observations, FAS surface expression in *Acvr1* KO cells re-expressing different versions of *ACVR1* was examined (**Figure 3.14 B**). Compared to *Acvr1* KO alone, cells expressing wtACVR1 or caACVR1 displayed higher cytokine-induced FAS surface expression, while kdACVR1-expressing cells demonstrated lower FAS surface levels upon cytokine treatment. These results indicate that *Acvr1* expression and activity increase FAS surface levels, thus influencing T cell-mediated killing efficiency in *Acvr1* KO cells.

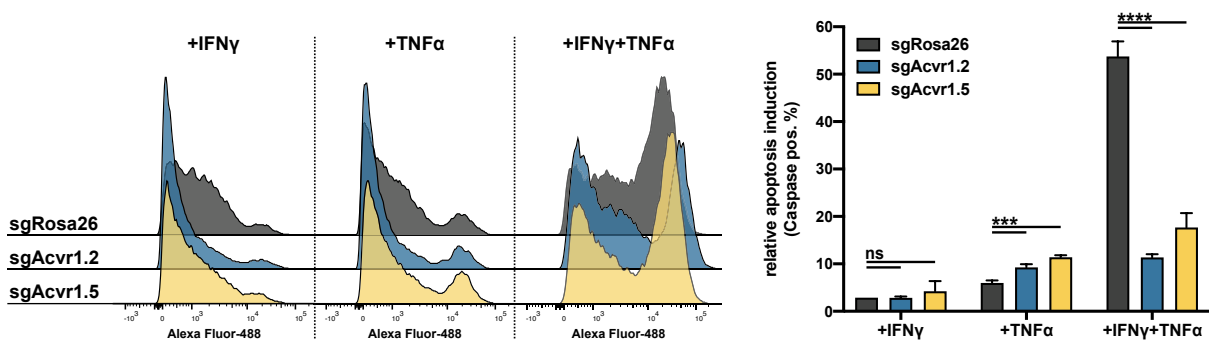
Furthermore, I determined *Fas* mRNA levels after cytokine treatment via qPCR in order to examine whether the reduction of FAS surface levels was a consequence of reduced *Fas* gene expression. *Acvr1* KO cells exhibited reduced cytokine-induced *Fas* expression (**Figure 3.14 C**). Notably, the effect was significant in cells treated with TNF α , but not IFN γ -treated cells, suggesting a stronger influence of TNF α . Additionally, cells re-expressing wtACVR1 or caACVR1 showed higher levels of cytokine-induced *Fas* expression compared to *Acvr1* KO cells, while re-expression of kdACVR1 did not affect *Fas* levels (**Figure 3.14 D**). Consistent with the observations in *Acvr1* KO cells, these effects were more pronounced in cells treated with TNF α or IFN γ +TNF α , suggesting a TNF α -dependent mechanism.

Taken together, these results show that *Acvr1* KO leads to reduced FAS surface levels and *Fas* gene expression upon cytokine treatment. The effects of *Acvr1* KO can be reversed by re-expressing *ACVR1* versions with functioning kinase domains. Furthermore, treatment with IFN γ alone results in lower *Fas* upregulation and is less affected by the *Acvr1* status of the cells, suggesting that the observed effects are primarily mediated through a TNF α -induced mechanism.

As FAS activation initiates the extrinsic apoptosis pathway, reduced *Fas* expression and presentation is likely to result in less apoptosis initiation. In order to examine this hypothesis, I first stimulated cells with IFN γ , TNF α , or both to upregulate *Fas*, and then treated cells with FASLG to induce apoptosis. The extent of apoptosis induction was determined using a detection reagent for activated caspase 3/7, which becomes fluorescent after cleavage by caspase 3/7 and is then detectable via flow cytometry. The results indicate that the magnitude of apoptosis induction was dependent on cytokine treatment and increased with IFN γ < TNF α < IFN γ +TNF α (**Figure 3.15 A**). This is coherent with previously observed increasing levels of *Fas* upregulation upon cytokine treatment, indicating that the extent of apoptosis induction is dependent on the level of *Fas* upregulation. Furthermore, apoptosis induction was dramatically reduced in *Acvr1* KO cells treated with IFN γ +TNF α compared to control cells, while the effect was less pronounced in cells treated with either IFN γ or TNF α alone (**Figure 3.15 A**).

Consistently, cells re-expressing different versions of *ACVR1* displayed a pattern of apoptosis induction similar to that of *Fas* upregulation. Especially the expression of caACVR1 resulted in increased apoptosis induction compared to control cells after treatment with TNF α alone or in combination with IFN γ , whereas re-expression of wtACVR1 or kdACVR1 had only minor effects on apoptosis induction (**Figure 3.15 B**).

A



B

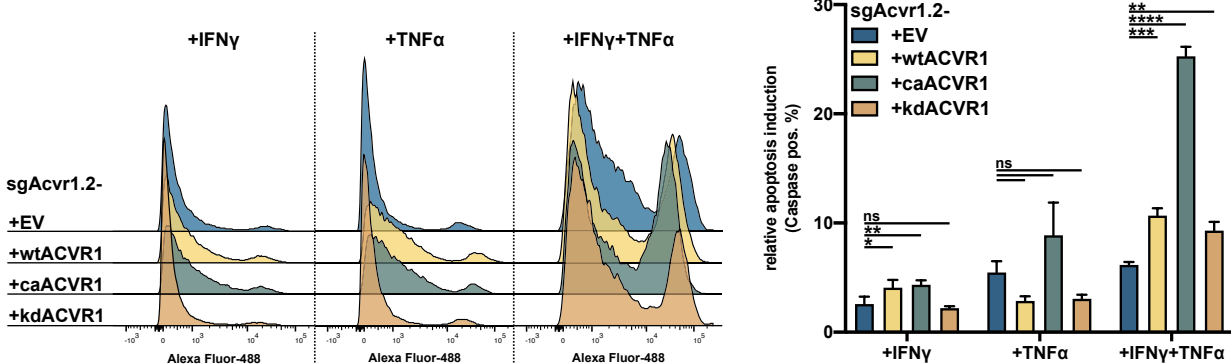


Figure 3.15. Cleaved caspase 3/7 assay with *Acvr1* KO and *ACVR1*-expressing cells. A and B. Flow cytometrical caspase assay MYC/*sgTrp53* cells with *Acvr1* KO (A) and expression of *ACVR1* versions (B). Cells were pre-treated with IFN γ (300 U/ml for 2 days), TNF α (20 ng/ml for 16 h), or both, and further treated with FASLG (5 ng/ml for 5 h) to induce apoptosis. Relative apoptosis induction is defined as the population of Alexa Fluor 488-positive cells normalized to control cells not treated with FASLG. EV: pMSCV empty vector control, wtACVR1: wildtype *ACVR1*, caACVR1: constitutively active version of *ACVR1* (Q207D), kdACVR1: kinase-dead version of *ACVR1* (K235R). Shown are mean and s.d. Statistical analysis was performed using one-way ANOVA with *sgRosa26* (A) or +EV as controls (B) (*: $p < 0.05$, **: $p < 0.01$, ***: $p < 0.001$).

These results suggest that *Acvr1* KO leads to reduced *Fas* surface levels and gene expression upon treatment with *Fas*-inducing cytokines, which consequently results in reduced apoptosis induction in *Acvr1* KO cells. Accordingly, cells that re-express caACVR1 display the opposite phenotype, *i.e.*, higher cytokine-induced *Fas* levels and increased apoptosis induction. Therefore, the increased resistance to T cell-mediated killing in *Acvr1* KO cells can be explained by reduced levels of cytokine-dependent *Fas* upregulation, which in turn result in decreased apoptosis induction.

To further elucidate the mechanistic link between *Acvr1* KO and *Fas* expression, I studied IFN γ - and TNF α -induced signaling pathways. Since IFN γ is known to stimulate *Fas* expression through activating Signal transducer and activator of transcription 1 (STAT1)-dependent signaling, the phosphorylation of STAT1 after IFN γ treatment was examined via Western blot analysis [273,274]. IFN γ treatment caused distinct phosphorylation of STAT1 at the phosphorylation sites Y701 and S727, however, there was no obvious difference in phosphorylation levels in *Acvr1* KO or re-expressing cells (Figure 3.16 A) [275,276]. This suggests that *Acvr1* does not influence the IFN γ -STAT1 signaling axis. These results are also in accordance with the previously made observations, which showed that the effect of IFN γ treatment on *Fas* upregulation or apoptosis induction was not as strong as the effect of TNF α treatment.

TNF α is reported to induce *Fas* expression via activation of the nuclear factor kappa-light-chain-enhancer of activated B cells (NF κ B) signaling pathway [271]. Hence, the activation of members of the NF κ B signaling pathway upon TNF α treatment was analyzed in control and *Acvr1* KO cells. No differences in phosphorylation levels of Inhibitor of nuclear factor kappa-B kinase (IKK) α/β or p65 could be observed, however, phosphorylation levels of NF κ B inhibitor α (I κ B α) were distinctly decreased in both *Acvr1* KO cell lines (Figure 3.16 B).

This could imply that *Acvr1* KO leads to reduced phosphorylation of I κ B α , which in turn would not be degraded and consequently would not result in NF κ B-induced gene expression. As a result of reduced NF κ B signaling, TNF α -induced *Fas* expression would be reduced in *Acvr1* KO cells in an I κ B α -dependent manner. However, these considerations are still hypothetical and further experiments are needed to unravel the underlying mechanism of *Acvr1*-mediated *Fas* expression.

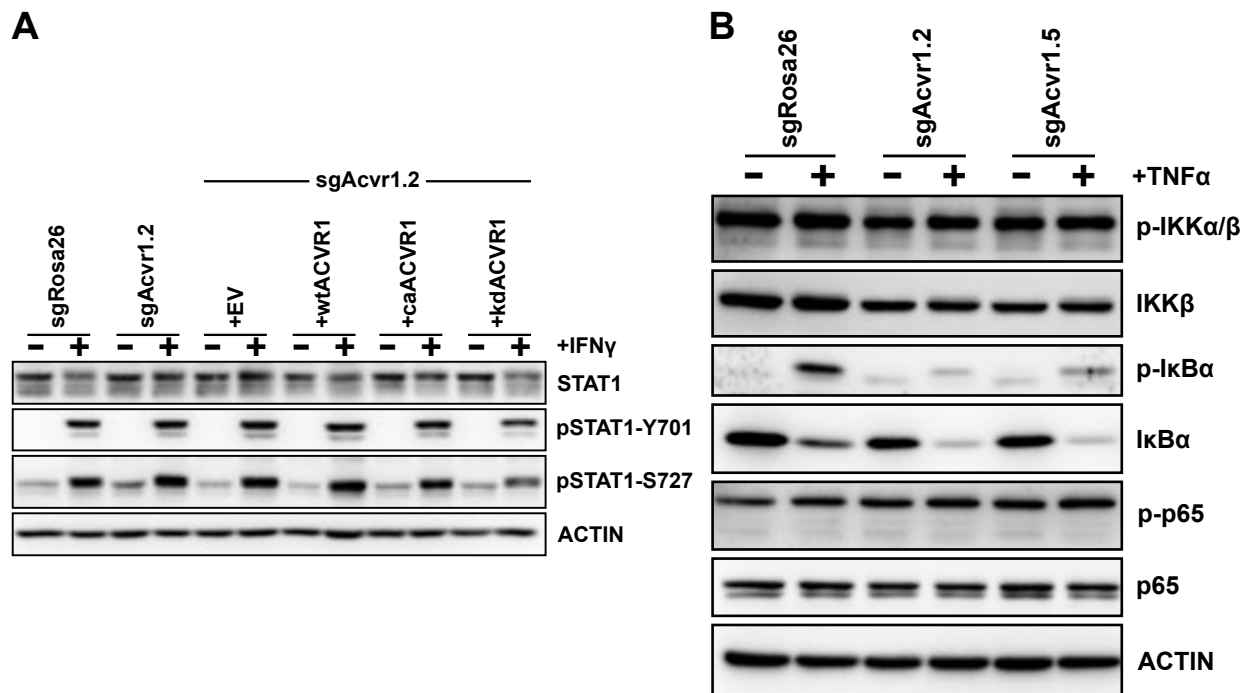


Figure 3.16. The impact of *Acvr1* on STAT1 and NF κ B signaling. **A.** Western blot analysis of *Acvr1* KO and *ACVR1*-expressing MYC/sgTrp53 cells investigating IFN γ -induced STAT1 signaling. Cells were treated with IFN γ (300 U/ml) for 30 min and protein lysates were used to analyze phosphorylation levels of STAT1. EV: pMSCV empty vector control, wtACVR1: wildtype *ACVR1*, caACVR1: constitutively active version of *ACVR1* (Q207D), kdACVR1: kinase-dead version of *ACVR1* (K235R). **B.** Western blot analysis of *Acvr1* KO MYC/sgTrp53 cells investigating TNF α -induced NF κ B signaling. Cells were treated with TNF α (20 ng/ml) for 30 min and protein lysates were used to analyze downstream activation of NF κ B signaling components.

3.8 Investigating the effect of other BMP signaling effectors on antigen-specific tumor cell killing

Since *Acvr1* was shown to influence the efficiency of T cell-mediated tumor cell killing, I further examined the influence of other BMP signaling receptors. For that, KO cell lines for different type I and type II receptors were generated using CRISPR/Cas9 technology. The efficacy of used sgRNAs was assessed with T7 endonuclease I assay, which displayed distinct T7 endonuclease I-digested DNA fragments, suggesting effective modification of targeted genes (**Figure 3.17 A**). The effect of the respective gene KO on T cell-mediated killing was then tested in T cell killing assays. The results show that KO of the investigated type II receptors BMP receptor type 2 (*Bmpr2*), *Acvr2a*, and *Acvr2b* did not result in significantly increased survival of tumor cells compared to sgRosa26 control cells (**Figure 3.17 B and C**). Interestingly, gene KO of the type I receptor *Bmpr1a* resulted in significantly increased survival after T cell-mediated killing compared to control cells, whereas *Bmpr1b* KO did not lead to increased survival (**Figure 3.17 C and D**).

These findings suggest that the investigated type II receptors did not affect T cell-mediated tumor cell killing, while KO of the type I receptor *Bmpr1a* resulted in enhanced resistance to T cell-mediated killing. However, these results are not conclusive and further investigation is needed to elucidate the role of other BMP receptors in T cell-mediated killing.

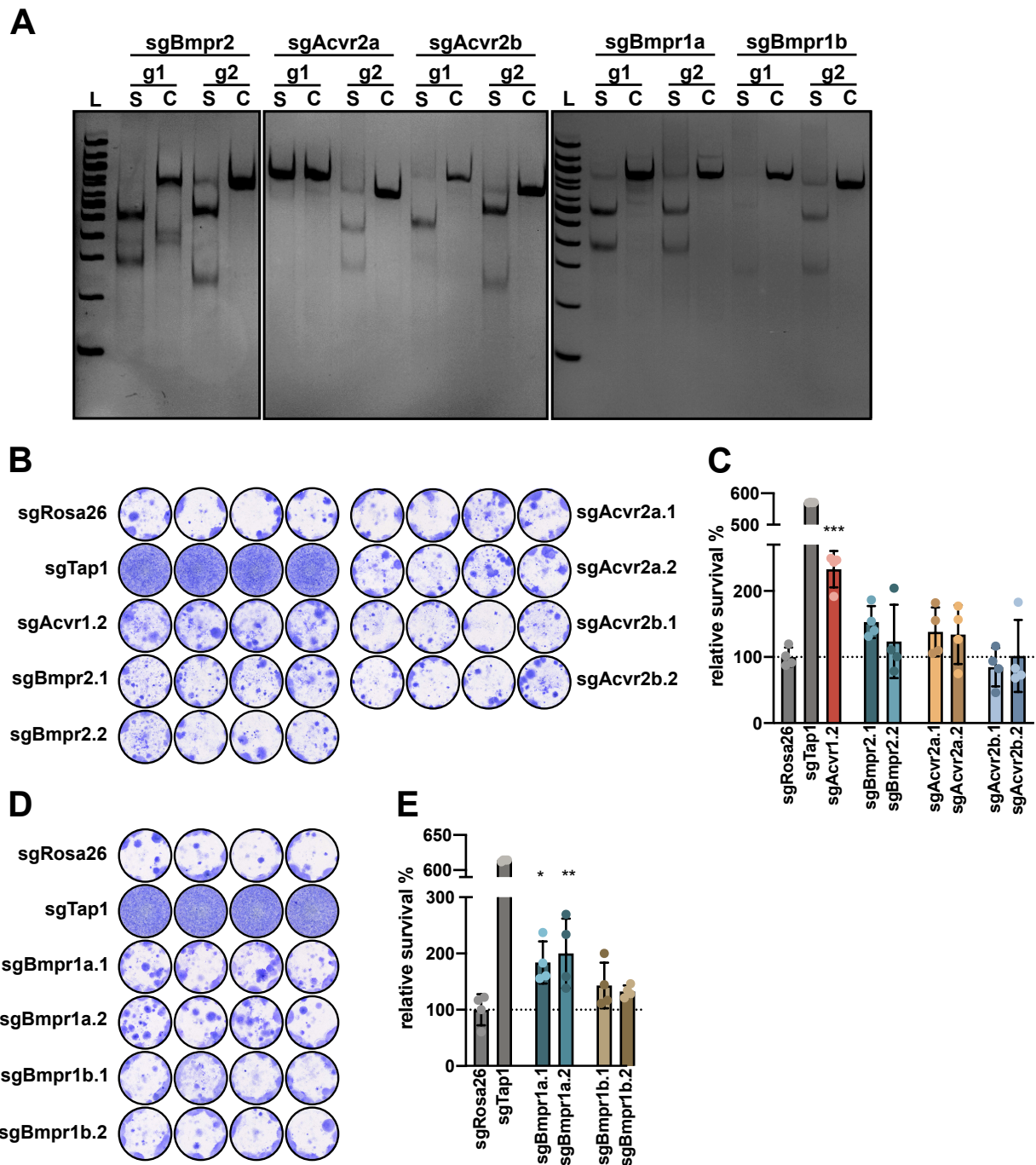


Figure 3.17. The effect of other BMP signaling receptor KOs on T cell-mediated killing in MYC/sgTrp53 cells. A. T7 endonuclease I assay of BMP signaling receptor-targeting sgRNAs used in this study. Cas9-expressing cells were transduced with a lentiviral plasmid encoding the respective sgRNA. L: DNA ladder, S: sample, C: control. **B.** T cell killing analysis in MYC/sgTrp53 cell lines with KO of BMP signaling type II receptors with effector : target cell ratio 2:1. Relative survival is defined as the relative stained area per well normalized to the relative stained area of untreated control wells (-OT-I) of the respective cell line. Representative data from one out of three independent replicates. Shown are mean and s. d., statistical analysis was performed via one-way ANOVA. Asterisks indicate statistically significant differences from the control sgRosa26 (***:p<0.001). **C.** T cell killing analysis in MYC/sgTrp53 cell lines with KO of respective BMP signaling type I receptors with effector : target cell ratio 2:1. Relative survival is defined as the relative stained area per well normalized to the relative stained area of untreated control wells (-OT-I) of the respective cell line. Shown are mean and s. d., statistical analysis was performed via one-way ANOVA. Asterisks indicate statistically significant differences from the control sgRosa26 (*:p<0.05, **:p<0.01). All data generated jointly with Philip Ohland, DKFZ.

3.9 KO of the ACVR1 downstream target *Id1* does not affect T cell killing efficiency

Activation of BMP signaling via ACVR1 leads to increased expression of *Id1* [248]. Furthermore, ID1 acts as transcription factor and plays a role in differentiation, cell cycle progression, apoptosis, and tumorigenesis [277]. Hence, it is conceivable that the increased resistance to T cell-mediated killing in *Acvr1* KO cells is mediated through downregulated *Id1* activation. In order to investigate this hypothesis, the effect of *Id1* KO on T cell-mediated killing and FAS surface expression was examined. For that, I used two *Id1*-targeting sgRNAs to create *Id1* KO cell lines. T7 endonuclease I assay confirmed effective targeted gene modification, which consequently resulted in complete gene KO of *Id1*, as verified by Western blot analysis (**Figure 3.18 A and B**). However, *Id1* KO did not lead to increased relative survival after T cell-mediated killing (**Figure 3.18 C and D**). Interestingly, the observation that BMP7 treatment resulted in increased resistance to T cell-mediated in control cells was completely abrogated by *Id1* KO (**Figure 3.18 D**). Consistent with the results that suggest no effect of *Id1* KO on T cell-mediated tumor cell killing, cytokine-stimulated upregulation of FAS surface levels was not affected by *Id1* KO (**Figure 3.18 E**).

Therefore, these results suggest that the effect of *Acvr1* on T cell killing efficiency is not mediated via *Id1*, but rather a consequence of a yet unknown mechanism, possibly involving TNF α -induced NF κ B signaling.

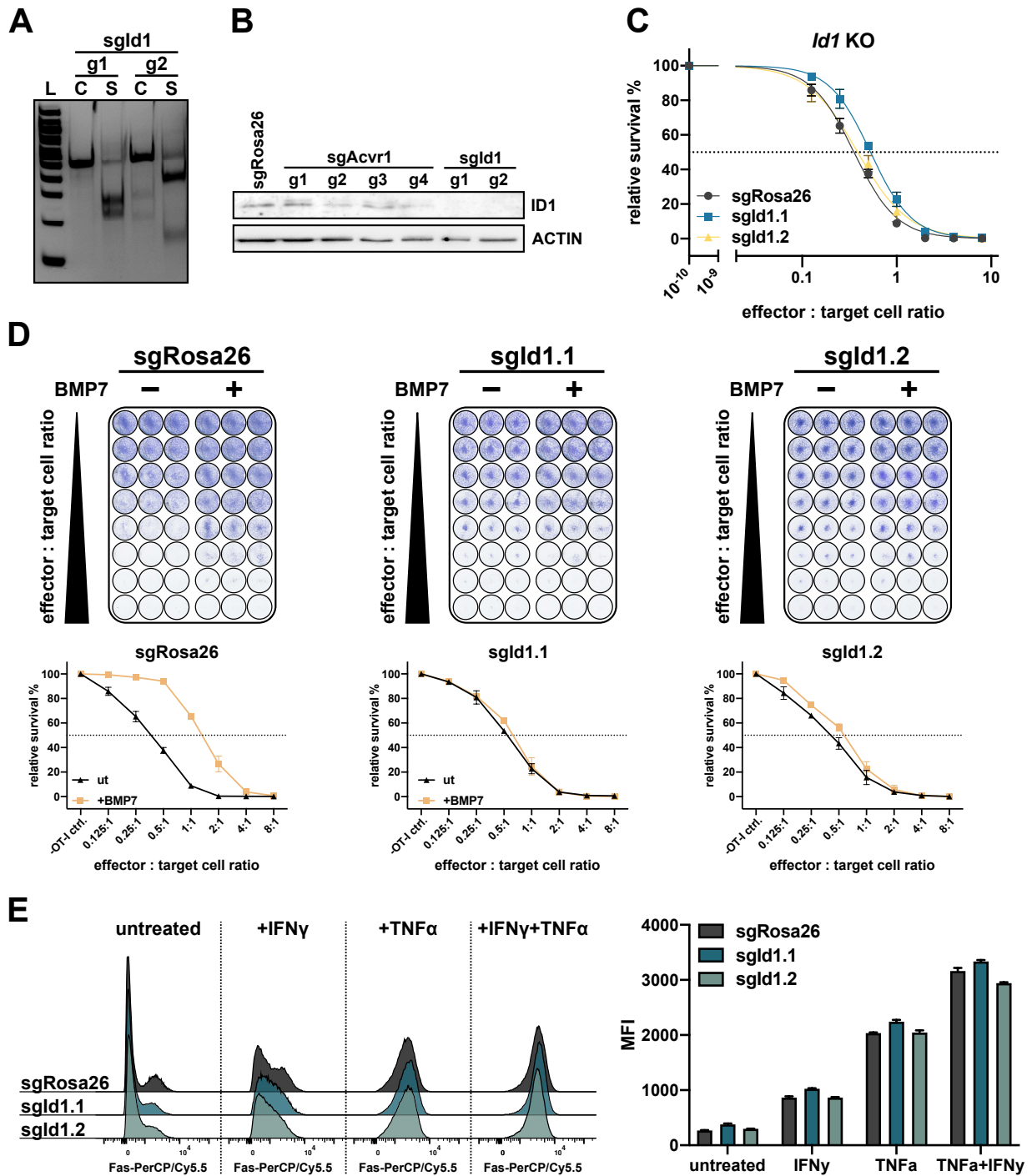


Figure 3.18. KO of the ACVR1 downstream target *Id1* does not affect T cell killing efficiency. **A.** T7 endonuclease I assay of *Id1*-targeting sgRNAs used in this study. Cas9-expressing MYC/sGTrp53 cells were transduced with a lentiviral plasmid encoding the respective sgRNA. L: DNA ladder, S: sample, C: control. **B.** Western blot analysis in *Id1* KO, *Acvr1* KO, and control MYC/sGTrp53 cells. **C.** Quantification of a T cell killing assay in MYC/sGTrp53 cell lines with *Id1* KO. **D.** T cell killing assay of MYC/sGTrp53 cells pre-treated with BMP7 (100 ng/ml for 24 h) before co-culture. Relative survival is defined as the relative stained area per well normalized to the relative stained area of untreated control wells (-OT-I) of the respective cell line. **E.** FAS surface expression in *Id1* KO MYC/sGTrp53 cells treated with IFN γ (300 U/ml for 2 days), TNF α (20 ng/ml for 16 h), or both, and detected via flow cytometry. Left panel shows representative histograms. Right panel shows mean and s.d. of median fluorescence intensity (MFI) for 3 replicates.

3.10 The effect of *ACVR1* KO on T cell killing efficiency in a human MART-1-specific killing assay

I further investigated the effect of *ACVR1* KO in a human context. For that, the human melanoma cell line COLO800, which expresses Melanoma antigen recognized by T-cells (*MART-1*), was used in a co-culture killing assay together with pre-activated genetically engineered, MART-1-specific human T cells (both cell types were kind gifts from Rafael Carretero, DKFZ).

sgRNAs targeting *TAP1* and *ACVR1* were designed and their functionality was confirmed by a T7 endonuclease assay (**Figure 3.19 A**). In addition to the generation of *TAP1* and *ACVR1* KOs, I stably transduced COLO800 cells with a retroviral plasmid coding for the different versions of *ACVR1* wt*ACVR1*, ca*ACVR1*, and kd*ACVR1*. The downstream signaling of *ACVR1* was examined via Western blot analysis, which verified that *ACVR1* KO and expression of kd*ACVR1* resulted in less phosphorylation of SMAD1/5/9 and lower ID1 levels, while expression of wt*ACVR1* and ca*ACVR1* caused similar or higher levels of pSMAD1/5/9 and ID1 compared to controls (**Figure 3.19 B**). Therefore, *ACVR1* KO and kd*ACVR1* cell lines displayed less activity of *ACVR1*, resulting in less downstream signaling, while cell lines expressing wt*ACVR1* and ca*ACVR1* exhibited increased *ACVR1* activity and pathway activation.

In order to establish a human MART-1-specific killing assay, COLO800 control, *TAP1* KO, and *ACVR1* KO cells were stimulated with IFN γ for 2 days and then co-cultured with pre-activated MART-1-specific T cells in increasing effector : target cell ratios (**Figure 3.19 C**). The results show that MART-1-specific T cells lead to effective killing of COLO800 cells and that the killing efficiency is dependent on T cell concentration. Additionally, *TAP1* KO cells displayed increased resistance to T cell-mediated killing, which lead to a higher relative survival of *TAP1* KO cells compared to control and *ACVR1* KO cells. Notably, *ACVR1* KO cells showed not altered relative survival compared to control cells, suggesting no influence of *ACVR1* KO on T cell killing efficiency. These results were substantiated by further MART-1-specific killing assays with an effector : target ratio of 2:1, where no differences in killing efficiency were observed between *ACVR1* KO cells, cells expressing different *ACVR1* versions, and control cells (**Figure 3.19 D and E**). Therefore, these results suggest that *ACVR1* does not influence the antigen-specific T cell killing efficiency in the context of human COLO800 cells.

Since *Acvr1* KO leads to decreased cytokine-induced upregulation of *Fas* in primary MYC/sgTrp53 cell lines, I further assessed the influence of *ACVR1* on *FAS* expression in COLO800 cells. For that, cells were treated with IFN γ , TNF α , or both and the amount of *FAS* mRNA was determined by qPCR. However, no consistent effect of *ACVR1* on *FAS* mRNA levels was detectable (**Figure 3.19 F**). Remarkably, only IFN γ , but not TNF α treatment was able to induce *FAS* expression, which indicates that upregulation of *FAS* in COLO800 cells is not dependent on TNF α signaling.

In summary, these results suggest that *ACVR1* does not affect the efficiency of T cell-mediated killing in COLO800 cells. Hence, the effect of *Acvr1* on primary MYC/sgTrp53 cells could not be recapitulated in COLO800 cells, suggesting that *Acvr1* plays different roles in different cell lines. This notion is in accordance with the observation that TNF α treatment in COLO800 cells does not induce *FAS* expression, while TNF α resulted in a strong induction of *Fas* expression in MYC/sgTrp53 cells. This finding indicates that the mechanism of *Fas* gene induction is cell type-dependent as well and further supports the hypothesis that *Acvr1* mediated *Fas* expression in a TNF α -dependent mechanism.

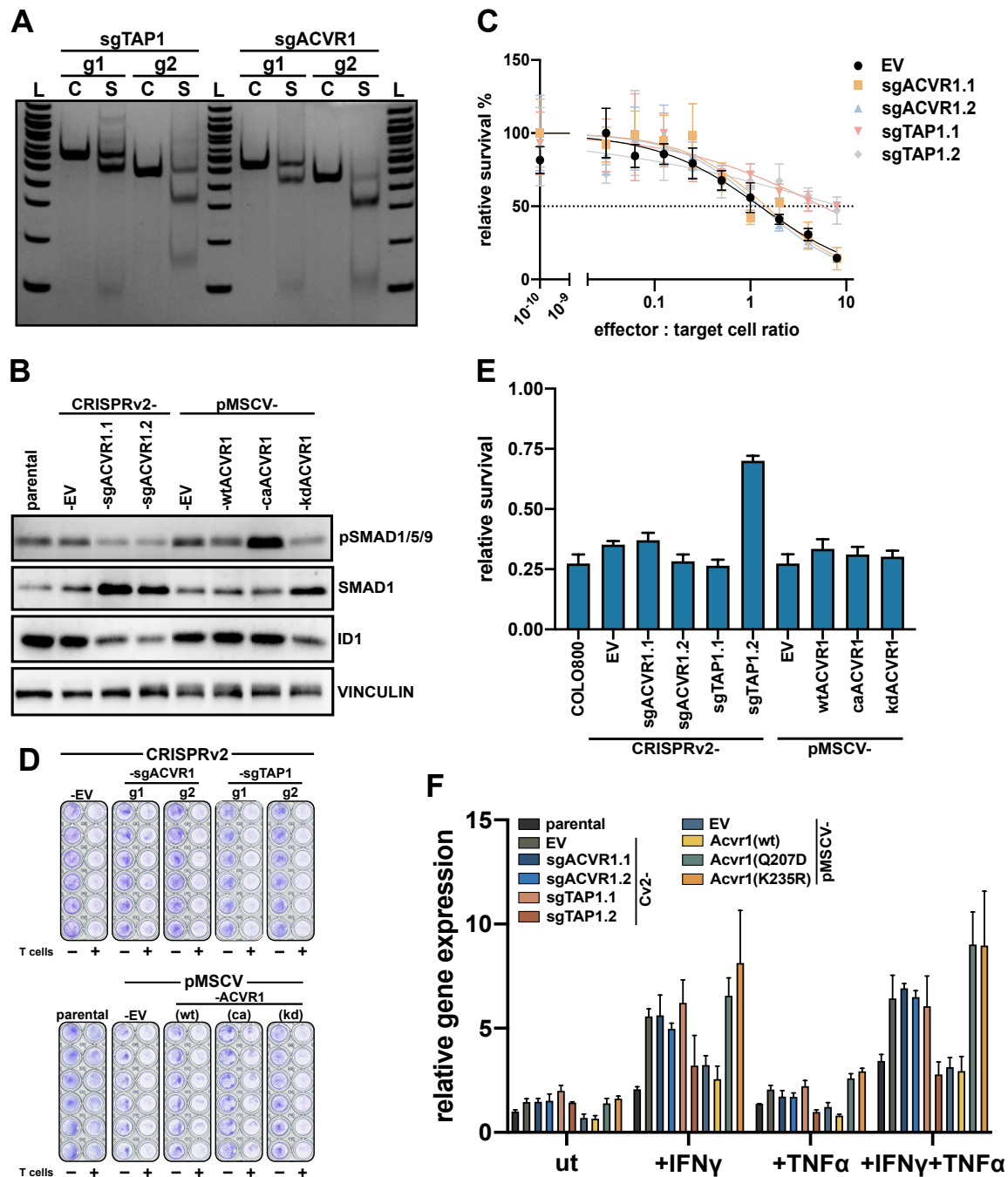


Figure 3.19. Human MART-1 co-culture assay with ACVR1 KO COLO800 cells. **A.** T7 endonuclease I assay of *ACVR1*-targeting sgRNAs. Cells were transduced with a lentiviral plasmid encoding the respective sgRNA and Cas9. L: DNA ladder, S: sample, C: control. **B.** Western blot analysis of *ACVR1* downstream signaling in cells with *ACVR1* KO or expression of *ACVR1* versions. **C-E.** MART-1 co-culture assay. COLO800 cells were plated in 96 well cell culture plates and treated with IFN γ (50 ng/ml) for 2 days prior to co-culture. Pre-activated MART-1-specific T cells were added in a dilution series (**C**) or an effector : target cell ratio of 2:1 (**D** and **E**). After one day, cells were fixated and stained with crystal violet. Relative survival is defined as the relative stained area per well normalized to the relative stained area of untreated control wells (-T cells) of the respective cell line. Representative data of one out of three independent replicates, shown as mean and s.d. **F.** Quantitative real-time PCR analysis of *FAS* gene expression in *ACVR1* KO and *ACVR1*-expressing COLO800 cells treated with IFN γ (50 ng/ml for 2 days), TNF α (20 ng/ml for 16 h), or both. Gene expression analysis was performed by $\Delta\Delta C_T$ method and normalized to parental untreated control. Graphs show mean and s.d. of 3 replicates. EV: pMSCV empty vector control, wtACVR1: wildtype *ACVR1*, caACVR1: constitutively active version of *ACVR1* (Q207D), kdACVR1: kinase-dead version of *ACVR1* (K235R).

4 Discussion

The notion of harnessing the patient's immune system to treat cancer has prompted the development of various immunotherapeutic approaches. Even though immunotherapy has shown promising results in a subset of patients and cancer types, the majority of patients does not respond to available immunotherapeutic treatments. The underlying mechanisms of immune evasion mechanisms by tumors are manifold and under ongoing investigation.

In order to shed light on new mechanisms conferring resistance to immunotherapy, this study pursued three objectives. First, I established an autochthonous liver cancer model with genetically defined cancer-driving gene modifications and conditional expression of the neoantigen OVA. This model proved to be a versatile and flexible tool to study immune-oncological questions *in vivo*. Second, a co-culture system using antigen-expressing primary tumor cells and antigen-specific T cells was developed that can be used to study antigen-dependent T cell-mediated tumor cell killing in defined *in vitro* conditions. Additionally, I used this system to perform a CRISPR/Cas9 screen, thus identifying and validating new genes mediating resistance to T cell-mediated killing. Lastly, *Acvr1* was identified, further investigated and validated as *bona fide* moderator of T cell-mediated killing. Furthermore, exploring the causative mechanism provided evidence that *Acvr1* mediates cytokine-induced *Fas* expression, possibly via the TNF α -NF κ B signaling axis.

Taken together, the presented findings strongly suggest an important role of *Acvr1* in influencing T cell-mediated tumor cell killing. Being part of the BMP signaling pathway, *Acvr1* influences pro- and anti-tumorigenic processes in a context-dependent manner. The role of *Acvr1* and BMP signaling in cancer has implications for future therapy approaches and BMP-targeting drugs are being investigated. This study links *Acvr1* to the efficiency of T cell-mediated killing, thus proposing that therapeutically targeting *Acvr1* could improve the outcome of immunotherapy.

4.1 A genetically defined autochthonous liver cancer model for the investigation of neoantigen-specific immune responses

The pressing need for suitable mouse models to study processes of liver cancer tumorigenesis and progression in an *in vivo* setting has resulted in the development of various murine cancer models [67,85,278–280]. Among these, the generation of genetically engineered mouse models via hydrodynamic delivery of plasmids employing transposon, CRISPR/Cas, or RNAi technologies is a well-established and widely used approach to study liver cancer in diverse contexts and backgrounds [67,85,278,281–284]. Genetic manipulation of hepatocytes through the stable integration of transposon plasmids expressing oncogenes and targeted KO of tumor suppressor genes via CRISPR/Cas9 plasmids has been used for fast generation of genetically defined tumors, which results in shortened survival [283,285,286]. Accordingly, after hydrodynamic injection of plasmids mediating tumor-driving genetic alterations, I observed rapid formation of genetically defined tumors, which led to euthanization shortly after tumor induction.

One advantage of this cancer model is its modularity, which enables the user to easily combine different tumor drivers and modify the genetic background of generated tumors. Thus, this model allows to comprehensively investigate the effects of specific genetic alterations in the context of liver cancer. In this study, two different tumor-driving combinations were used to induce liver tumors, *i.e.*, overexpression of

oncogenic *MYC* with CRISPR/Cas9-mediated KO of *Trp53*, and overexpression of constitutively active *Kras*^{G12D} combined with *Trp53* KO. Both genotype combinations led to rapid tumor formation and aggressiveness, thereby underlining the general scientific understanding that oncogenic *MYC* and *KRAS* are associated with cancer aggressiveness and reduced survival in patients [287,288]. Both oncogenes used in this study are known to influence mechanisms of tumorigenesis and tumor progression in a genotype-specific way, *e.g.*, by promoting angiogenesis, shaping of the microenvironment, and lineage commitment [289–292]. Moreover, *MYC* and *KRAS* have been shown to cooperate as oncogenes in order to drive immune evasion and maintain cancer cell viability [291,293]. Therefore, the presented approach to generate genetically defined liver tumors portrays a versatile model to investigate oncogene-specific and cooperative mechanisms of tumorigenesis, tumor progression, or immune evasion.

Thanks to its flexibility, this model offers the possibility to investigate neoantigen-mediated immune responses. Several studies have used HTVI-mediated mouse models in which transposon and CRISPR/Cas9 plasmids were delivered hydrodynamically to generate neoantigen-expressing liver tumors [285,286,294]. Although these models differed from each other and the model presented in this study with regard to used transposon plasmids, the used neoantigen, and the architecture of injected plasmids, the studies could show rapid generation of neoantigen-expressing liver tumors with defined genotypes and neoantigen-dependent immune responses.

For instance, Liu *et al.* generated *AKT*- and *Nras*-driven tumors expressing neoantigens derived from hepatitis B virus and OVA [285]. The authors could show that neoantigen-specific T cells accumulated in tumors expressing the neoantigen. Surprisingly, in this study, SIINFEL-specific T cells were only detected in a fraction of DOX-treated mice. This finding is consistent with my observation that not all analyzed ON DOX tumors displayed neoantigen expression in Western blot analysis, suggesting loss of antigen via immunoediting and selection against neoantigen-expressing tumor cells, as reported in other studies [295,296]. Moreover, the detection of SIINFEL-specific T cells in only a part of the analyzed samples could also point toward the possibility that the immune system of mice does not fully react to neoantigen-expressing tumors with the activation and expansion antigen-specific T cells. Considering the observed loss of OVA expression in some ON DOX tumors, however, it is more likely that tumors downregulate antigen expression to evade immune attacks. Another factor that needs to be taken into account is the site of blood withdrawal and thus immune cell collection. In this study, I collected peripheral blood from the submandibular vein. However, reports state that the detection of circulating neoantigen-specific T cell populations is challenging, as they are likely to accumulate at the tumor site and only a minor fraction of neoantigen-specific lymphocytes is found in peripheral blood [297]. Therefore, it is possible that SIINFEL-specific T cells in this mouse model are enriched in tumors and tumor-draining lymph nodes rather than peripheral blood, as it has been reported for SIINFEL-expressing sarcomas and lung cancer [295,296]. Consequently, it would be interesting to assess whether SIINFEL-specific T cells are detectable in lymph nodes and at the tumor site using different T cell isolation protocols.

Although Liu *et al.* detected neoantigen-specific T cells, they did not observe tumor regression due to T cell exhaustion and an overall immunosuppressive TME. In line with that, DOX-induced neoantigen expression in liver tumors did not result in prolonged survival in my hands, even though neoantigen expression is reported as a biomarker for prolonged survival in several tumor entities, including HCC [298–301]. Therefore,

transferring the observations made by Liu *et al.* to this model, it is possible that tumors displayed an immunosuppressive TME that obstructed tumor regression. Another possible explanation could be the observation that not all tumors grown in ON DOX conditions did express OVA. This proposed loss of antigen has been described as a mechanism of immunoediting in neoantigen-expressing autochthonous models of sarcoma and lung cancer, and it is conceivable that similar mechanisms counteracted a T cell-mediated tumor cell clearance in this model [295,296].

Taken together, the observations of Liu *et al.* are similar to my results and suggest that comparable survival rates in neoantigen-expressing and non-neoantigen-expressing control groups could be attributed to T cell exhaustion, which in turn would not result in tumor regression. Importantly, the tumor-driving genes used by Liu *et al.* were different compared to the oncogenes and tumor suppressor genes used in this study. As it was shown that immune cell infiltrates in HTVI-induced tumors are oncogene-dependent, the results of Liu *et al.* might only be partially comparable to my findings [294]. To determine whether antigen-specific T cells present an exhausted phenotype that fails to induce tumor regression in the presented model, tumors could be examined for the presence of infiltrating T cells, which could then be further characterized for their exhaustion status.

In contrast to observations made by Liu *et al.* and this study, Galarreta *et al.* observed increased survival in an HTVI-based mouse model of MYC/sgTrp53 tumors expressing the neoantigen OVA compared to the control group without neoantigen expression [286]. Considering that the authors used the same genetic alterations to induce liver tumors as this study, it seems surprising that the two studies obtained contradicting results. However, Galarreta *et al.* coupled the genetic sequence of OVA to the sequence of MYC, thereby ensuring that all cells that express oncogenic MYC also express the neoantigen. In contrast, I used a different plasmid design, in which OVA was encoded on an additional plasmid and was transcribed in a TRE-dependent manner. Using this design, it was ensured that OVA was only expressed in oncogenic MYC-expressing cells, while still allowing for selection against neoantigen-expressing tumor cells. Thus, my model allowed for selecting against cells that were not initially transfected with the OVA-encoding transposon plasmid. The genetic coupling of the neoantigen to the tumor-driving oncogene would explain why the model presented by Galarreta *et al.* resulted in prolonged survival of mice with neoantigen-expressing tumors. As stated by the authors, their design allows to investigate immune evasion mechanisms beside loss of antigen, like the upregulation of β -Catenin signaling found in that study. However, it might not sufficiently recapitulate tumor evolution and immune responses, and the authors propose that a system in which antigen expression is uncoupled from oncogene expression and conditionally inducible would help to further unravel immune evasion mechanisms.

Apart from Galarreta *et al.*, several other studies investigated autochthonous tumors with neoantigen expression and did not find neoantigen-dependent tumor regression, further supporting the findings of the presented project. Instead, those reports described immune evasion mechanisms and immunoediting, including loss of neoantigen, downregulation of MHC class I, and T cell tolerance via downregulation of TCR [295,296,302]. These reports suggest that immune evasion mechanisms might have also influenced the survival rates and tumor progression in the presented model. Further investigations will be needed to comprehensively analyze the mechanisms that prevent neoantigen-expressing tumor regression in this model.

Several efforts have been made to establish autochthonous neoantigen-expressing liver cancer models to study immunotherapeutic approaches [285,286,302,303]. However, most approaches using adoptive transfer of neoantigen-specific T cells did not result in tumor regression due to T cell exhaustion, an overall immunosuppressive TME, or downregulation of T cell receptors [285,302]. In contrast, I was able to demonstrate that adoptive transfer of pre-activated neoantigen-specific OT-I splenocytes and anti-CTLA4 immune checkpoint blockade therapy achieved partial or complete regression of nodules and increased survival in neoantigen-expressing mice compared to the control. Of note, this experiment was only performed with small sample sizes (n=2-3) and has thus only limited informative value. Nevertheless, the results show that this model is suited to model immunotherapeutic interventions and thus offers a previously unavailable opportunity for further investigation of immunotherapies in autochthonous liver cancers.

To summarize, the established model is well suited to generate autochthonous genotype-specific liver tumors in a short period of time. By including a neoantigen-expressing transposon sequence, this mouse model can also be used to address immuno-oncological research questions. Due to its autochthonous nature and genetically defined tumorigenesis, the model presents several advantages compared to other mouse models used in the immuno-oncological research area.

Compared to germline genetically-engineered mouse models, the HTVI model combined with transposon and CRISPR/Cas9 technology is less time consuming and less expensive, as it can be applied in wildtype mice and makes extensive breeding unnecessary. Additionally, the HTVI model provides more flexibility, as the used plasmids can be easily exchanged, so that a multitude of genetic alterations can be assessed in the context of liver cancer [278]. Subcutaneous transplantation of syngeneic tumor cells is a fast and easy way to generate *in vivo* tumors. However, these models do not recapitulate the TME of the liver, which is known to be a crucial factor in immuno-oncology [278]. Orthotopic transplantation of tumor tissue into the liver, on the other hand, involves elaborate surgery and imposes a great burden on the animals. Additionally, transplantation of established tumor cells does not sufficiently reflect tumorigenesis and malignant transformation of cells within the natural occurring hepatic microenvironment, as it is shown in autochthonous tumor models [278,279]. Carcinogen- and diet-induced tumor models sufficiently recapitulate the underlying causes of liver cancer development, like fibrosis, cirrhosis, or NASH. However, these models have a long latency (up to 12-18 months) and show a high heterogeneity in genetic alterations, which complicates the investigation of the involvement of specific genes in tumorigenic processes and tumor progression [278]. Nevertheless, the slow tumorigenesis in an inflammatory microenvironment shown in these models enables the development of immune, stromal, and vascular responses, and is thus thought to better reflect human carcinogenesis [278,279,304]. In this context, it would be interesting to combine diet-induced models that recreate a chronically inflamed liver microenvironment with my approach to investigate how an inflammatory TME influences effects of neoantigen-dependent immune responses and the outcome of immunotherapy. Each discussed model used in hepatic immuno-oncology research presents certain advantages and disadvantages concerning feasibility and the accuracy with which human liver cancer is recapitulated. Therefore, it is imperative to carefully choose the animal model that is best suited to solve posed research problems with regard to genetic heterogeneity, TME composition, tumorigenic processes, and cost and time expenditures.

In conclusion, autochthonous cancer models are considered to lead to aggressive tumor growth and immune evasion [101,286,296,305–307]. My findings are in line with this, and the reported selection against neoantigen-expressing tumors and the resulting lack of an adequate immune response could be explained by immune editing and immune evasion mechanisms. Considering that autochthonous tumor cells undergo gradual malignant transformation from somatic cells within the microenvironmental context of the affected organ, it is plausible that cells forming autochthonous tumors were able to evade the immune system during tumorigenesis and are thus less immunogenic. Therefore, the established model presents a versatile tool to investigate neoantigen-dependent immune responses and immune evasion mechanisms. Moreover, the shRNA construct, which was included to the TRE-controlled transposon plasmid but not used within this project, offers the possibility to use this model in conjunction with an RNAi screen to identify new genes that influence neoantigen-dependent immune responses *in vivo*. Taken together, the established model is a helpful new tool to investigate immuno-oncological processes in an autochthonous, genetically defined setting, which can be easily modified to unravel genotype-specific mechanisms of immune evasion *in vivo*.

4.2 A novel T cell killing assay identifies new mediators of tumor cell clearance

4.2.1 A novel T cell killing assay to study T cell-mediated tumor cell killing

Several antigen-specific co-culture assays have been used to investigate T cell-related research questions, demonstrating the versatility of this approach to explore T cell-dependent processes of tumor cell clearance [308–314]. Consistent with other assays, I could show that the established protocol caused antigen-specific tumor cell killing, which was dependent on the effector : target cell ratio. While antigen-presenting tumor cells were resistant to killing in OFF DOX conditions and only killed while ON DOX, sgTap1 control cells were not killed regardless of DOX conditions. However, increasing effector : target cell ratios resulted in minor killing of OFF DOX or sgTap1 cells. This effect could be caused by leakage of the TRE-promotor and incomplete *Tap1* KO. However, it is also conceivable that high effector : target cell ratios lead to unspecific tumor cell killing, as observed by Gee *et al.* [308]. In line with findings made by Patel *et al.*, no antigen-independent bystander killing occurred under the applied experimental conditions, since a small *Tap1* KO cell population could be recovered after performing the T cell killing assay with a mixed target cell population (**Figure 3.5 A and B**) [314,315].

Notably, while others used several different readout methods to assess T cell cytotoxicity, including chromium-51 release assays, impedance measurements, or multicolor flow cytometry, I made use of a crystal violet staining protocol [309,310,312,316,317]. This readout method allowed for time- and cost-effective quantification of surviving tumor cells in a large format. Thus, the readout methodology enabled the development of the T cell killing assay to be used in a high-throughput CRISPR/Cas9 screening format.

Overall, the established T cell killing assay presents a versatile method to investigate antigen-specific tumor cell killing. In general, co-culture assays offer a valuable methodology which facilitates investigating the interplay of specific cell types under defined cell culture conditions. Thereby, co-culture assays help to unravel basic mechanisms of cell type-specific interactions in a distinct system and can thus contribute to disentangle the highly complex interplay of various cell types within the tumor microenvironment. Many published studies describing co-culture assays use the well-established melanoma cell line B16 expressing

OVA as target cells [310–313]. In contrast, the here established assay used primary cell lines which had been derived from genetically defined autochthonous liver tumors. Therefore, this assay has the potential to be used with other primary tumor cells with different tumor drivers or even other model neoantigens in order to study genotype- or antigen-related effects interfering with T cell killing. Additionally, the utilized tumor cells developed autochthonously while being exposed to the murine hepatic microenvironment. Hence, established tumors that were used to generate primary cell lines already experienced selection pressure and immune editing [296]. In combination with the conditional neoantigen expression of the system, this offers the possibility to study primary and secondary escape mechanisms by using tumor cells that either developed under OFF DOX or ON DOX conditions [318].

In summary, the established T cell killing assay is a useful tool to study T cell-mediated tumor cell killing. By utilizing genetically defined primary liver cancer cell lines, the assay allows to investigate tumor cells with different cancer drivers or antigens. Thanks to the flexibility of the system, it provides the possibility to genetically modify target cells and to perform a high-throughput CRISPR/Cas9 screen, thus identifying new modulators of T cell-mediated tumor cell clearance.

4.2.2 A lentiviral CRISPR/Cas9 screen identifies new modulators of T cell-mediated tumor cell killing

Numerous scientific studies have been published in an effort to unravel immune evasion mechanisms, thereby identifying new angles for immunotherapy. Highlighting the persistent relevance of discovering genes influencing T cell-mediated tumor cell clearance, various studies have employed CRISPR/Cas-based high-throughput approaches *in vitro* and *in vivo* [308,311–314,319,320]. On the one hand, these studies were able to recover known mediators of antigen-dependent tumor cell killing, including genes involved in IFN γ signaling, antigen processing and presentation, or immune checkpoint ligands, like Interferon gamma receptor (*IFNGR*), *B2m*, or *PDL1* [311,313,319,321]. On the other hand, new genes mediating immune evasion could be identified, including the Apelin receptor (*Aplnr*), the chromatin regulators Polybromo 1 (*Pbrm1*) and AT-rich interaction domain 2 (*ARID2*), and the Protein tyrosine phosphatase non-receptor type 2 (*Ptpn2*) [313,319,321].

Surprisingly, out of the 20 highest scored enriched genes of this CRISPR/Cas9 KO screen, only one, the Complement C3a Receptor 1 (*C3ar1*), had been identified as mediator of immune evasion in a comparable screen (**Table 3.1**) [313]. However, in the study of Pan *et al.*, sgRNAs targeting *C3ar1* were found to be slightly depleted rather than enriched, indicating an opposing effect compared to this screen. Since Pan *et al.* used a different experimental setting by choosing a genome-wide CRISPR/Cas9 screen and targeting tumor cells with a low-affinity antigen, it is possible that the effect of *C3ar1* on T cell mediated killing is context-dependent and influenced by the target cell type and antigen.

The three most promising gene candidates identified by validation experiments were *Egfr*, *Acvr1*, and *Sorcs3*. While, to my knowledge, *Acvr1* and *Sorcs3* have not yet been associated with immune evasion mechanisms, *Egfr* is a known mediator of immune escape and has been reported to downregulate antigen presentation and upregulate PDL1 in tumor cells [322]. This finding is surprising, since the results obtained from this study suggest that KO of *Egfr* mediates immune evasion, rather than expression of *Egfr*. However, the tumor-driving genetic alterations of the used cell line are *MYC* overexpression and KO of *Trp53*, which

is therefore not dependent on *Egfr* expression. Being a known tumor driver itself, it is possible that immune-evasive effects of *Egfr* are only detectable in *Egfr*-dependent tumor cells and are thus cell line-specific [322].

Apart from *C3ar1* and *Egfr*, the screen did not identify already known mediators of immune evasion mechanisms. This can be partly explained with the design of the sgRNA library, which was created and prepared prior to this project. The library is based on the surfaceome library published by Bausch-Fluck *et al.*, who used a mass spectrometry-based experimental setup to capture and predict cellular surface proteins [232]. Surprisingly, this approach led to the exclusion of *Ifngr*, which could not be found in the library and explains why this known mediator of T cell-mediated killing could not be identified in the screen. Additionally, constituents of MHC class I and II complexes, *i.e.*, H-2 genes and *B2m*, had been manually removed from the surface library. This was done in order to avoid that sgRNAs targeting MHC components would enrich to such a strong degree that other sgRNAs mediating weaker phenotypes would be undetectable. Moreover, some sgRNAs targeting the known checkpoint ligand *PDL1* displayed enrichment after T cell killing, but did not meet the overall criteria for hit calling.

Importantly, the used library only targeted genes encoding surface proteins. On the one hand, this design complicates the discovery of cellular processes and signaling pathways which include not only surface proteins, but also intracellular proteins. For instance, using a surfaceome library, changes in antigen processing and presenting mechanisms can only be detected on cell surface levels, while whole-genome screens were also able to recover IFN γ -induced intracellular Janus kinase (JAK)-STAT signaling components and TAP-associated genes [311,319,321]. On the other hand, the use of the surface library allowed for identifying formerly unknown mechanisms of T cell-mediated killing, which was only possible since already established strong mediators of immune evasion (*e.g.*, antigen processing and presentation) were not included in the library.

Notably, with known mediators of T cell killing absent from the sgRNA library, the library did not include positive controls that could have confirmed that the experimental setup was indeed able to recover sgRNAs mediating immune resistance. However, the preliminary experiment using *Tap1* KO cells as positive control demonstrated that the T cell killing system was able to recover a resistant cell population with low presentation in conditions similar to the screening system (**Figure 3.5 A and B**). Thus, this experiment supports the use of the T cell killing assay as a screening system. However, as the preliminary experiment was performed independent from the screen, and internal positive controls were not included to the screen itself, some uncertainty regarding the experimental performance remains. Nevertheless, due to the high-throughput approach of the CRISPR/Cas9 screen, identified hits can only provide suggestions as to which genes are true hits and mediate immune resistance. Therefore, it is necessary to validate the potential hits in subsequent examinations using single gene KO cell lines [323].

Taken together, the CRISPR/Cas9 screen performed in conjunction with the T cell killing assay revealed previously undescribed mediators of T cell-mediated killing, which could be validated in downstream experiments. Thus, the results of the screen are able to add to existing knowledge by identifying formerly unknown effectors of T cell-mediated killing. Remarkably, the cells used in this screen were primary cell lines derived from tumors that had been generated using HTVI and transposon technology. Thus, these cells have genetically defined tumor-driving alterations that possibly influence how specific genes mediate immune cell evasion. Thanks to the modularity of the underlying mouse model, this system offers the

possibility to generate various primary cell lines with different genetic drivers and to investigate the effect of specific cancer-driving genes on immune evasion mechanisms. Additionally, it is important to mention that the tumor cells developed autochthonously within the context of the hepatic tumor microenvironment. These circumstances most likely play a role in the evolution of malignant cells, and it is possible that antigen-presenting tumor cells underwent immune editing during tumorigenesis and tumor progression [17]. Therefore, this system also allows to compare if cells derived from antigen-presenting tumors show different immune evasion mechanisms compared to cells derived from tumors that did not present the model antigen. In this context, it would be interesting to perform the screen with tumor cells grown in ON DOX vs. OFF DOX conditions in order to assess primary and secondary immune escape mechanisms [311]. In addition to that, the T cell killing assay can be modified in a way that reduces T cell killing efficiency by decreasing the effector : target cell ratio. A screen performed under those conditions could be used to identify not only enriched, but also depleted sgRNAs, thus discovering genes that mediate susceptibility to T cell killing. Alternatively, the system could be utilized to perform a CRISPRa/dCas9 screen to further uncover new target genes for immunotherapy, as described by Zhang *et al.* [320]. In conclusion, the established T cell killing assay offers versatile opportunities in combination with high-throughput approaches and can therefore be used to investigate antigen-specific immune evasion mechanisms.

4.3 The role of *Acvr1* in T cell-mediated tumor cell killing

4.3.1 *Acvr1* as new mediator of T cell-mediated cytotoxicity

The findings of this study strongly suggest that *Acvr1* is a mediator of T cell-mediated tumor cell killing. ACVR1 (also known as ALK2) is a type I receptor of the BMP signaling pathway and is activated upon binding of BMP5,-6,-7, and -8 [324]. After formation of heterotetrameric signaling complexes with the type II receptors ACVR2A, ACVR2B, or BMPR2, it induces phosphorylation of the downstream effectors SMAD1/5/9, which in turn associate with SMAD4 in order to regulate gene expression [179]. BMP signaling is known to regulate various cellular processes of embryonal development and adult tissue homeostasis, including embryonal stem cell pluripotency, osteogenesis, chondrogenesis, neural stem cell fate, cardiomyogenesis, wound healing, and fibrosis [203,243,258–263]. In line with current knowledge of ACVR1- and BMP-mediated signaling, immunoblotting and transcriptional analyses of *Acvr1* KO cells resulted in decreased activation of downstream SMAD1-dependent signaling and reduced activation of BMP-mediated cellular pathways. However, gene expression analysis could not provide further insight into underlying mechanisms that might confer resistance to T cell killing upon *Acvr1* KO.

In the context of diseases, *ACVR1* is primarily known as the underlying genetic cause of fibrodysplasia ossificans progressiva (FOP), a rare genetic disease which leads to spontaneous or trauma-induced heterotopic ossification. In this process called skeletal metamorphosis, connective tissue slowly transforms into bone, which results in gradual immobilization and premature death of patients [325]. Activating mutations of *ACVR1* have been identified as the genetic cause for FOP, leading to increased responsiveness to BMP stimulation and dysregulation of BMP signaling [243,326]. In addition to that, activating *ACVR1* mutations could be found in up to 30 % of all cases of diffuse intrinsic pontine glioma (DIPG), suggesting that *ACVR1* is an oncogenic driver in this disease [327].

Furthermore, *ACVR1* has been associated with a variety of other cancer types, including multiple myeloma as well as ovarian, endometrial, and prostate cancer [243]. While *ACVR1* has been shown to function as oncogenic driver in various backgrounds, other studies have described tumor suppressive functions of *ACVR1*. For instance, dysregulated BMP signaling via *ACVR1* promotes proliferation of ovarian cancer cells and hyperactivating mutations of *ACVR1* are found endometrial cancer [328–330]. In contrast, in multiple myeloma, glioblastoma, and eye lens tumor, *ACVR1* is thought to act as tumor suppressor by mediating apoptosis and growth arrest [331–333]. Additionally, copy number gains of *ACVR1* are linked to increased survival in head and neck squamous cell carcinoma [334]. With regard to these studies and the reported dual role of BMP signaling in cancer, it is conceivable that *ACVR1* itself can act as both oncogene and tumor suppressor, depending on the cellular background and microenvironment [243]. The majority of the findings made in this study suggest a tumor suppressing role for *Acvr1*, as *Acvr1* KO resulted in increased survival of tumor cells after T cell-mediated killing. Accordingly, re-expression of *ACVR1* increased the susceptibility of tumor cells towards cytotoxic T cells. In contrast, treatment with BMP7 prior to T cell killing resulted in higher survival rates compared to untreated control cells, indicating a tumor-promoting role of BMP7-mediated signaling. As BMP7 is known to act as a growth factor in several cell types, including hepatocytes and breast cancer cell lines, it is conceivable that the effect of BMP7 on proliferation was stronger than the effect on resistance to T cell-mediated killing [202,243,267]. However, this raises the question if BMP7 is the right ligand to investigate the effect of *ACVR1* signaling on T cell killing, or whether another BMP factor would elicit different effects. As BMP7 is known to primarily bind to *ACVR1*, it was chosen to examine the effect of *ACVR1*-mediated BMP signaling on T cell killing [335]. Nevertheless, it would be interesting to compare the effects of BMP7 stimulation to other BMP signaling factors, like BMP2 or BMP6. Taken together, the opposing results of BMP pathway activation via *ACVR1* overexpression vs. BMP7 stimulation illustrate the complex pleiotropic effects of *ACVR1*-mediated BMP signaling on tumorigenesis and tumor progression reported in the literature and emphasize the necessity to comprehensively unravel BMP-mediated signaling in various contexts [168].

With regard to the effects of *ACVR1* on immuno-oncological mechanisms, little is known about the role of *ACVR1* itself. However, BMP signaling in general is considered to exert immunoregulatory functions in the TME by affecting activation, proliferation, and cytokine signaling of innate and adaptive immune cells [169,171,172]. Interestingly, Cortez *et al.* found that BMP7-secreting tumor cells confer resistance to immune checkpoint blockade therapy by influencing BMP-mediated signaling in macrophages and T helper cells and inhibiting pro-inflammatory responses [170]. In contrast, to my knowledge, there is no account of BMP signaling within tumor cells that could be associated with immune evasion or modulation of tumor-infiltrating immune cells. Therefore, my findings suggest a yet undescribed immune evasion mechanism of *ACVR1*-mediated BMP signaling in tumor cells.

Notably, the phenotype of *Acvr1* KO displays only a modest effect on killing efficiency and BMP signaling in the presented study and is dependent on the used sgRNA. On the one hand, this could be explained with incomplete KO, which cannot be entirely ruled out, as there are no commercially available *ACVR1*-specific antibodies that could be used to confirm the KO on protein level. On the other hand, the BMP signaling pathway can be activated by a multitude of ligand and receptor combinations, all resulting in phosphorylation of SMAD1/5/9 [191,324]. Therefore, it is possible that other BMP receptors aside from *ACVR1* lead to activation of BMP signaling, thereby reducing the observed effect of *Acvr1* KO. This shows that careful

experimental design and independent replicates are imperative to obtain reliable results. Since the experiments were performed with a set of independent sgRNAs and suitable controls and repeated independently, I was able to demonstrate that the observed phenotype of *Acvr1* KO, though modest, is robust and reproducible. In order to achieve a stronger phenotype, future experiments could aim at knocking out one pivotal effector of BMP signaling, like *Smad1*, or performing double- or triple KOs of *Acvr1* and other BMP receptors simultaneously.

In conclusion, my findings provide strong evidence for a role of *Acvr1* in modulating the efficiency of T cell-mediated killing. In order to substantiate these results, future studies are needed that will contextualize the effect of *Acvr1* and BMP signaling in immuno-oncological research. BMP signaling is a crucial factor of tumor development influencing pro- as well as anti-tumorigenic processes depending on the cellular context and microenvironment [168]. Thus, it will be interesting to assess the role of *Acvr1* in different cellular and cancer backgrounds in order to identify contributing factors that influence *Acvr1*-mediated BMP signaling. Additionally, *in vivo* studies and investigations of human samples will be needed to further corroborate the proposed role of *ACVR1*.

4.3.2 The role of other BMP signaling effectors on T cell-mediated tumor cell killing

The previous results provide evidence that *Acvr1* KO affects T cell-mediated killing. Beside *Acvr1*, two other type I and three type II receptors mediate BMP signaling [191]. This raises the question if the observed effect of *Acvr1* KO is specific or a general result of downregulated BMP signaling. Therefore, I performed exploratory experiments investigating the T cell killing efficiency with sgRNA-mediated KO cell lines for *Bmpr2*, *Acvr2a*, *Acvr2b*, *Bmpr1a*, and *Bmpr1b*. The results suggest that the tested type II receptors did not affect killing efficiency, while KO of the type I receptor *Bmpr1a* resulted in slightly increased survival after T cell killing. Importantly, these findings are still preliminary and have to be validated with further studies, but indicate that *Bmpr1a* might act similar to *Acvr1*. Accordingly, analysis of the CRISPR/Cas9 screen did not find sgRNAs targeting *Acvr2a* and *Acvr2b* to be enriched. In contrast, *Bmpr2*-targeting sgRNAs were enriched, but did not score high enough to be further investigated. *Bmpr1a* and *Bmpr1b* could not be found in the library of Bausch-Fluck *et al.*, so that no enrichment data is available for these genes.

Based on these results, it is possible that other BMP signaling effectors influence T cell-mediated killing in a similar way than *Acvr1*. However, even though a receptor redundancy in BMP signaling has been proposed, different ligand-receptor combinations are able to result in specific and differential gene expression [191]. It is therefore conceivable that different BMP ligands and receptors have specific functions in tumorigenesis, and that the effect of *Acvr1* on T cell killing cannot be recapitulated by other BMP receptors. Additionally, *Acvr1* plays a distinct role in the development of FOP and DIPG, while other BMP receptors do not contribute to these diseases [243,326,327]. This further supports the notion that *Acvr1* has specific functions, and that other BMP receptors might not have comparable effects on T cell-mediated killing.

In order to unravel the role of BMP receptors in T cell-mediated killing, further experiments are needed. In addition to generating cell lines with a single KO of a BMP effector, it would be interesting to investigate if knocking-out more than one member of the BMP pathway would result in synergistic effects on T cell-mediated killing. Alternatively, a focused CRISPR/Cas9 screen targeting BMP effectors could provide further insight and could help to identify additional mediators of T cell killing.

4.3.3 A potential mechanism of *Acvr1*-mediated resistance to T cell killing involves *Fas* and NFκB signaling

The mechanisms of how cytotoxic T cells mediate antigen-specific tumor cell clearance are well known. Besides secreting exocytotic granules comprising PRF1 and GZMs, T cells employ the FAS/FASLG axis in order to kill target cells [110]. Consequently, it is plausible that decreased *Fas* expression leads to less apoptosis induction and increased survival, as shown in this study. Additionally, downregulation of *FAS* is a known mechanism of tumor cells to evade apoptotic stimuli and cell death [336–339]. In line with that, the results of this study provide strong evidence that the observed resistance to T cell killing in *Acvr1* KO cells is mediated through a role of *Acvr1* in the regulation of cytokine-induced *Fas* expression.

The current understanding of BMP-related signaling does not provide an adequate explanation for *Acvr1*-mediated *Fas* expression. Even though the presented results do not provide sufficient evidence to comprehensively elucidate the mechanistic link between *Acvr1* and *Fas*, they nevertheless suggest a role of dysregulated NFκB signaling as mediator. Indeed, NFκB signaling might be a downstream target of non-canonical BMP signaling, mediated by *TAK1* [88]. *TAK1* is activated by TGFβ or BMP signaling and has been shown to be a critical mediator of TNFα-induced NFκB signaling [340,341]. Additionally, the effects of *Acvr1* KO on T cell-mediated killing and *Fas* expression could not be recapitulated by KO of *Id1*, a major downstream target of canonical BMP signaling, which further suggests that effects on *Fas* expression are mediated by non-canonical signaling (**Figure 3.18**) [247]. Taken together, these results provide plausible evidence that *Acvr1* KO reduces *TAK1*-mediated activation of NFκB signaling, which in turn results in reduced *Fas* transcription.

The role of NFκB in cancer is intensively investigated, and NFκB signaling has been found to affect a multitude of cellular processes [342–344]. NFκB is best known to activate pro-inflammatory and anti-apoptotic mechanisms, however, several studies have demonstrated upregulation of pro-apoptotic target genes upon NFκB signaling, including *Fas* [271,345,346]. Additionally, NFκB signaling has been identified in two previously discussed CRISPR/Cas9 screens, suggesting a role in immune evasion [313,319].

Interestingly, reports show that not only BMP signaling influences NFκB activation, but that NFκB conversely affects BMP-mediated signaling as well. For instance, *BMP2* and *BMP4* are both target genes of NFκB [347,348]. Additionally, the NFκB subunit p65 has been shown to inhibit the DNA binding of *SMAD1-SMAD4* complexes, thereby regulating BMP-mediated gene expression [349,350]. This demonstrates that BMP and NFκB signaling engage in complex crosstalk, further underlining the diversity of the complicated mechanistical network of both signaling pathways.

Even though these results show that *Acvr1* KO leads to increased resistance to T cell killing by downregulating *Fas*, *Fas* itself was not enriched in the CRISPR/Cas9 screen. This is surprising, as *Fas* KO should decrease killing efficiency of cytotoxic T cells. Therefore, it is possible that the results of the screen regarding *Fas* were false negative, which is a frequent phenomenon in large-scale screening approaches [351]. Alternatively, *Fas* downregulation might not be the primary effect of *Acvr1* KO mediating immune evasion. Thus, it is conceivable that another, still unidentified downstream effect of *Acvr1* KO contributes to the resistance to T cell killing.

Taken together, the presented results suggest a previously undescribed involvement of *Acvr1* in the NFκB-mediated upregulation of *Fas*. Importantly, the role of NFκB signaling is not completely unraveled and needs to be further investigated in detail. Future studies should involve KO experiments of *Tak1* and NFκB signaling effectors like *p65* in order to ascertain the crosstalk between BMP and NFκB signaling pathways. In this regard, it would be interesting to investigate whether ligands activating BMP signaling also (directly or indirectly) affect NFκB signaling and *vice versa*. As *Fas* downregulation might not be the only resistance-conferring mechanism of *Acvr1* KO, additional downstream effects of *Acvr1* KO on T cell killing have the potential to be identified in the future.

4.4 Unravelling the role of BMP signaling in different cellular contexts

Previous studies investigating the role BMP signaling in tumorigenesis include numerous accounts of cell- and context-specific roles of BMP signaling and BMP signaling effectors have been proposed as both oncogenes and tumor suppressor genes depending on the context [168,352,353]. Remarkably, even within the same tumor entity, contradicting reports demonstrate opposing effects of BMP signaling. For instance, both pro- and anti-tumorigenic properties have been reported for BMP4 in breast cancer cell lines [200,205]. Additionally, in the context of HCC, BMP ligands can inhibit as well as promote migration of tumor cells [354,355]. These findings illustrate that the role BMP signaling in cancer has to be meticulously investigated with regard to cellular background and studied signaling effectors [168,202]. Therefore, future experiments should be carefully designed to account for the influence of different cell lines and genetic backgrounds on BMP signaling and include various BMP signaling effectors.

With the purpose of recapitulating the findings of this study in the genetic context of a human melanoma cell line, I performed exploratory experiments with an antigen-specific T cell killing assay using COLO800 melanoma cells and T cells specific for the MART-1 antigen constitutively expressed in COLO800 cells. Even though co-culturing antigen-expressing target cells with pre-activated antigen-specific T cells resulted in concentration-dependent tumor cell killing, *ACVR1* KO or overexpression did not have an effect on T cell killing efficiency (**Figure 3.19**). Further experiments assessing cytokine-stimulated *FAS* expression revealed that COLO800 cells did not respond to TNFα treatment by upregulating *FAS*. This finding, even though preliminary, reinforces the hypothesis that *Acvr1*-mediated signaling regulates *Fas* expression by affecting the TNFα-NFκB signaling axis. In addition to that, the observation that *ACVR1* appears to have no effect on T cell killing efficiency in this co-culture system further underlines the context-dependency of *ACVR1* signaling. Therefore, future investigations should compare the effect of *ACVR1* and BMP signaling in different cellular contexts. In this regard, it would be interesting to assess which cell lines respond to *ACVR1* KO by increasing resistance to T cell killing, and to identify causative mechanisms of this effect.

In order to translate these findings to a clinical application, it will be essential to investigate the effect of *Acvr1* in an *in vivo* cancer model. The model established within this project would be suitable system, as it can be easily modified to generate an sgRNA-mediated KO of *Acvr1* or to stably integrate *Acvr1*-encoding cDNA to hepatocytes. Importantly, it is possible that due to its dependency on the cellular context, *Acvr1* and BMP signaling might cause different effects *in vivo* compared to *in vitro* systems, since cells of the microenvironment could also influence the outcome of BMP signaling.

Lastly, the clinical relevance of these findings could be further corroborated by analyzing patient samples and data for aberrant BMP signaling. Particularly the effect of immunotherapies on BMP signaling levels could provide helpful insight into the role of *ACVR1* or other BMP effectors in immune evasion mechanisms. For instance, comparing levels of BMP signaling in tumors that are responsive vs. non-responsive to immunotherapy could indicate if BMP signaling is correlated with resistance or responsiveness to immunotherapeutical approaches.

4.5 Clinical applications for *ACVR1* as mediator of antigen-specific tumor cell killing

The presented findings provide convincing evidence for a role of *Acvr1* in T cell-mediated tumor cell killing. *Acvr1* KO leads to increased resistance to cytotoxic lymphocytes, whereas (re-)expression of kinase-active versions of *ACVR1* results in stronger susceptibility to T cell killing. Tumor cell killing by cytotoxic T cells is a major mechanisms of immune-mediated tumor regression, illustrated by the common downregulation of CTL effector function as a mechanism of immune evasion. Thus, the involvement of *Acvr1* in T cell-mediated killing efficiency offers new possibilities to increase the efficiency of immunotherapy.

In fact, the role of BMP signaling in tumorigenesis and tumor progression has led to the exploration of BMP signaling as new therapeutic target for cancer therapy [352,353,356]. The inhibition of BMP receptor kinases via specific small molecule inhibitors has shown promising results in ovarian, lung, and breast cancer by reducing proliferation, inducing apoptosis, and inhibiting metastasis [215,353,356–361].

However, in the context of this study, reducing BMP signaling via *Acvr1* KO was shown to be beneficial for the survival of tumor cells. Thus, therapy approaches that lead to increased activation of BMP signaling might result in a more desirable outcome in the used system. As BMPs are known to have context-dependent pro- and anti-tumorigenic effects, therapy approaches that aim at activating BMP signaling are being investigated [352]. For instance, by inhibiting the SMAD ubiquitination regulatory factor-1 (SMURF1), a negative regulator of BMP signaling, it is possible to increase BMP signaling [362]. Additionally, studies in brain and breast cancer cells demonstrated promising effects of treatment with recombinant BMP ligands by reducing tumorigenic potential and invasiveness and facilitating tumor regression [363–366]. Furthermore, treatment with BMP2 reverses chemoresistance in ovarian cancer and glioblastoma, underlining the potential of combinational therapy using BMP ligands [359,367].

Unexpectedly, even though downregulation of BMP signaling via *Acvr1* KO resulted in increased resistance to T cell killing, activation of BMP signaling via treatment with BMP7 showed similar effects. This further demonstrates the pleiotropic pro- and anti-tumorigenic effects of BMP signaling and underlines the necessity to comprehensively investigate the role of BMP signaling in different contexts and cell types [352,353]. Nevertheless, it would be interesting to combine BMP-targeting drugs with immunotherapeutical approaches in order to assess potential synergistic effects.

In addition to the approach using BMP signaling as a drug target for cancer therapy, several studies provide evidence that members of the signaling pathway can be used as therapeutical and prognostic biomarker [168,368,369]. Particularly, expression of BMP signaling genes was suggested as biomarker in prostate, breast, and ovarian cancer [369–372]. In accordance with the dual role of BMP signaling in cancer, both high and low expression of BMP effectors were associated with poor prognosis and increased aggressiveness, depending on the context.

Overall, exploiting the therapeutic potential of BMP signaling in cancer shows great promise and is subject of intensive research. Nevertheless, the diverse pro- and anti-tumorigenic effects of BMP signaling in different contexts are still not fully understood. Future research will have to comprehensively decipher the role of BMP signaling in specific contexts in order to develop effective cancer therapies targeting BMP signaling.

5 Conclusion

Immunotherapeutic approaches to treat cancer have shown promising results and initiated the development of new therapies and research fields. Nevertheless, the clinical success of immunotherapies has been dampened by unsatisfactory response rates, highlighting the need to investigate tumor cell-specific mechanisms of immune evasion.

In this study, I developed and employed state-of-the-art *in vivo* and *in vitro* systems to identify new tumor cell-specific mediators of T cell-dependent killing. Thus, I was able to discover a new role for the BMP receptor type I *Acvr1* in antigen-specific killing. Further studies revealed that the underlying mechanism of *Acvr1* KO-mediated resistance to T cell killing involved downregulation of the death receptor *Fas* and indicated a connection to dysregulated NF κ B signaling.

These findings suggest a formerly unknown mechanism of immune evasion through *Acvr1*-mediated signaling in tumor cells. Additionally, this study illustrates the pleiotropic cell type- and context-dependent effects of BMP signaling, thereby underlining the requirement to comprehensively explore the role of BMP signaling in pro- and anti-tumorigenic processes. The prospective exploitation of ACVR1 and other BMP signaling effectors as cancer drug targets offers the potential to improve the outcome of immunotherapeutic approaches by inhibiting ACVR1-mediated mechanisms of immune evasion. To eventually increase the response rate to immunotherapy, however, future research is necessary that further assesses the role of ACVR1 and other BMP signaling effectors as potential drug targets.

6 References

1. Bakin AV, Tomlinson AK, Bhowmick NA, Moses HL, Arteaga CL. Phosphatidylinositol 3-Kinase Function Is Required for Transforming Growth Factor β -mediated Epithelial to Mesenchymal Transition and Cell Migration*. *Journal of Biological Chemistry*. 2000;275: 36803–36810. doi:10.1074/jbc.M005912200
2. Global Cancer Observatory. [cited 18 Nov 2021]. Available: <https://gco.iarc.fr/>
3. Cancer. [cited 18 Nov 2021]. Available: <https://www.who.int/westernpacific/health-topics/cancer>
4. Hanahan D, Weinberg RA. The Hallmarks of Cancer. *Cell*. 2000;100: 57–70. doi:10.1016/S0092-8674(00)81683-9
5. Hanahan D, Weinberg RA. Hallmarks of Cancer: The Next Generation. *Cell*. 2011;144: 646–674. doi:10.1016/j.cell.2011.02.013
6. Ponder BAJ. Cancer genetics. *Nature*. 2001;411: 336–341. doi:10.1038/35077207
7. Prevalence and penetrance of BRCA1 and BRCA2 mutations in a population-based series of breast cancer cases. *Br J Cancer*. 2000;83: 1301–1308. doi:10.1054/bjoc.2000.1407
8. Stratton MR, Campbell PJ, Futreal PA. The cancer genome. *Nature*. 2009;458: 719–724. doi:10.1038/nature07943
9. Chakravarthi BVSK, Nepal S, Varambally S. Genomic and Epigenomic Alterations in Cancer. *Am J Pathol*. 2016;186: 1724–1735. doi:10.1016/j.ajpath.2016.02.023
10. Feinberg AP, Tycko B. The history of cancer epigenetics. *Nat Rev Cancer*. 2004;4: 143–153. doi:10.1038/nrc1279
11. Dawson MA, Kouzarides T. Cancer Epigenetics: From Mechanism to Therapy. *Cell*. 2012;150: 12–27. doi:10.1016/j.cell.2012.06.013
12. Chang Y, Moore PS, Weiss RA. Human oncogenic viruses: nature and discovery. *Philos Trans R Soc Lond B Biol Sci*. 2017;372: 20160264. doi:10.1098/rstb.2016.0264
13. Zapatka M, Borozan I, Brewer DS, Iskar M, Grundhoff A, Alawi M, et al. The landscape of viral associations in human cancers. *Nat Genet*. 2020;52: 320–330. doi:10.1038/s41588-019-0558-9
14. Kontomanolis EN, Koutras A, Syllaios A, Schizas D, Mastoraki A, Garmpis N, et al. Role of Oncogenes and Tumor-suppressor Genes in Carcinogenesis: A Review. *Anticancer Research*. 2020;40: 6009–6015. doi:10.21873/anticancer.14622
15. Weinberg RA. Oncogenes and tumor suppressor genes. *CA: A Cancer Journal for Clinicians*. 1994;44: 160–170. doi:10.3322/canjclin.44.3.160
16. Pylayeva-Gupta Y, Grabocka E, Bar-Sagi D. RAS oncogenes: weaving a tumorigenic web. *Nat Rev Cancer*. 2011;11: 761–774. doi:10.1038/nrc3106
17. Timar J, Kashofer K. Molecular epidemiology and diagnostics of KRAS mutations in human cancer. *Cancer Metastasis Rev*. 2020;39: 1029–1038. doi:10.1007/s10555-020-09915-5
18. Cox AD, Der CJ. Ras history. *Small GTPases*. 2010;1: 2–27. doi:10.4161/sgtp.1.1.12178
19. Rodriguez-Viciana P, Warne PH, Khwaja A, Marte BM, Pappin D, Das P, et al. Role of Phosphoinositide 3-OH Kinase in Cell Transformation and Control of the Actin Cytoskeleton by Ras. *Cell*. 1997;89: 457–467. doi:10.1016/S0092-8674(00)80226-3
20. Bourne HR, Sanders DA, McCormick F. The GTPase superfamily: conserved structure and molecular mechanism. *Nature*. 1991;349: 117–127. doi:10.1038/349117a0
21. Bos JL. The ras gene family and human carcinogenesis. *Mutation Research/Reviews in Genetic Toxicology*. 1988;195: 255–271. doi:10.1016/0165-1110(88)90004-8

REFERENCES

22. Scheffzek K, Ahmadian MR, Kabsch W, Wiesmüller L, Lautwein A, Schmitz F, et al. The Ras-RasGAP Complex: Structural Basis for GTPase Activation and Its Loss in Oncogenic Ras Mutants. *Science*. 1997;277: 333–339. doi:10.1126/science.277.5324.333
23. Meichle A, Philipp A, Eilers M. The functions of Myc proteins. *Biochimica et Biophysica Acta (BBA) - Reviews on Cancer*. 1992;1114: 129–146. doi:10.1016/0304-419X(92)90011-M
24. Dang CV, O'Donnell KA, Zeller KI, Nguyen T, Osthus RC, Li F. The c-Myc target gene network. *Semin Cancer Biol*. 2006;16: 253–264. doi:10.1016/j.semcancer.2006.07.014
25. Meyer N, Penn LZ. Reflecting on 25 years with MYC. *Nat Rev Cancer*. 2008;8: 976–990. doi:10.1038/nrc2231
26. Vita M, Henriksson M. The Myc oncoprotein as a therapeutic target for human cancer. *Seminars in Cancer Biology*. 2006;16: 318–330. doi:10.1016/j.semcancer.2006.07.015
27. Blackwell TK, Kretzner L, Blackwood EM, Eisenman RN, Weintraub H. Sequence-Specific DNA Binding by the c-Myc Protein. *Science*. 1990;250: 1149–1151. doi:10.1126/science.2251503
28. Blackwood EM, Eisenman RN. Max: A Helix-Loop-Helix Zipper Protein That Forms a Sequence-Specific DNA-Binding Complex with Myc. *Science*. 1991;251: 1211–1217. doi:10.1126/science.2006410
29. Finver SN, Nishikura K, Finger LR, Haluska FG, Finan J, Nowell PC, et al. Sequence analysis of the MYC oncogene involved in the t(8;14)(q24;q11) chromosome translocation in a human leukemia T-cell line indicates that putative regulatory regions are not altered. *Proc Natl Acad Sci U S A*. 1988;85: 3052–3056.
30. Boxer LM, Dang CV. Translocations involving c-myc and c-myc function. *Oncogene*. 2001;20: 5595–5610. doi:10.1038/sj.onc.1204595
31. Favera RD, Wong-Staal F, Gallo RC. onc gene amplification in promyelocytic leukaemia cell line HL-60 and primary leukaemic cells of the same patient. *Nature*. 1982;299: 61–63. doi:10.1038/299061a0
32. Alitalo K, Schwab M, Lin CC, Varmus HE, Bishop JM. Homogeneously staining chromosomal regions contain amplified copies of an abundantly expressed cellular oncogene (c-myc) in malignant neuroendocrine cells from a human colon carcinoma. *PNAS*. 1983;80: 1707–1711. doi:10.1073/pnas.80.6.1707
33. Schaub FX, Dhankani V, Berger AC, Trivedi M, Richardson AB, Shaw R, et al. Pan-cancer Alterations of the MYC Oncogene and Its Proximal Network across the Cancer Genome Atlas. *Cell Systems*. 2018;6: 282-300.e2. doi:10.1016/j.cels.2018.03.003
34. Cooper GM. Tumor Suppressor Genes. *The Cell: A Molecular Approach* 2nd edition. 2000 [cited 23 Nov 2021]. Available: <https://www.ncbi.nlm.nih.gov/books/NBK9894/>
35. Wang L-H, Wu C-F, Rajasekaran N, Shin YK. Loss of Tumor Suppressor Gene Function in Human Cancer: An Overview. *CPB*. 2018;51: 2647–2693. doi:10.1159/000495956
36. Knudson AG. Mutation and cancer: statistical study of retinoblastoma. *Proc Natl Acad Sci U S A*. 1971;68: 820–823. doi:10.1073/pnas.68.4.820
37. Friend SH, Bernards R, Rogelj S, Weinberg RA, Rapaport JM, Albert DM, et al. A human DNA segment with properties of the gene that predisposes to retinoblastoma and osteosarcoma. *Nature*. 1986;323: 643–646. doi:10.1038/323643a0
38. Dyson NJ. RB1: a prototype tumor suppressor and an enigma. *Genes Dev*. 2016;30: 1492–1502. doi:10.1101/gad.282145.116
39. Li FP, Fraumeni JF, Mulvihill JJ, Blattner WA, Dreyfus MG, Tucker MA, et al. A Cancer Family Syndrome in Twenty-four Kindreds. *Cancer Res*. 1988;48: 5358–5362.
40. Malkin D, Li FP, Strong LC, Fraumeni JF, Nelson CE, Kim DH, et al. Germ Line p53 Mutations in a Familial Syndrome of Breast Cancer, Sarcomas, and Other Neoplasms. *Science*. 1990;250: 1233–1238. doi:10.1126/science.1978757

41. Kastan MB, Onyekwere O, Sidransky D, Vogelstein B, Craig RW. Participation of p53 protein in the cellular response to DNA damage. *Cancer Res.* 1991;51: 6304–6311.
42. Lowe SW. Activation of p53 by oncogenes. *Endocrine-Related Cancer.* 1999;6: 45–48.
43. Toufekhtchan E, Toledo F. The Guardian of the Genome Revisited: p53 Downregulates Genes Required for Telomere Maintenance, DNA Repair, and Centromere Structure. *Cancers (Basel).* 2018;10: 135. doi:10.3390/cancers10050135
44. El-Deiry WS, Tokino T, Velculescu VE, Levy DB, Parsons R, Trent JM, et al. WAF1, a potential mediator of p53 tumor suppression. *Cell.* 1993;75: 817–825. doi:10.1016/0092-8674(93)90500-P
45. Olivier M, Hollstein M, Hainaut P. TP53 Mutations in Human Cancers: Origins, Consequences, and Clinical Use. *Cold Spring Harb Perspect Biol.* 2010;2: a001008. doi:10.1101/cshperspect.a001008
46. Soussi T, Lozano G. p53 mutation heterogeneity in cancer. *Biochem Biophys Res Commun.* 2005;331: 834–842. doi:10.1016/j.bbrc.2005.03.190
47. Cancer today. [cited 24 Nov 2021]. Available: <http://gco.iarc.fr/today/home>
48. Petrick JL, McGlynn KA. The Changing Epidemiology of Primary Liver Cancer. *Curr Epidemiol Rep.* 2019;6: 104–111. doi:10.1007/s40471-019-00188-3
49. Sia D, Villanueva A, Friedman SL, Llovet JM. Liver Cancer Cell of Origin, Molecular Class, and Effects on Patient Prognosis. *Gastroenterology.* 2017;152: 745–761. doi:10.1053/j.gastro.2016.11.048
50. Llovet JM, Kelley RK, Villanueva A, Singal AG, Pikarsky E, Roayaie S, et al. Hepatocellular carcinoma. *Nat Rev Dis Primers.* 2021;7: 1–28. doi:10.1038/s41572-020-00240-3
51. Global Burden of Disease Liver Cancer Collaboration. The Burden of Primary Liver Cancer and Underlying Etiologies From 1990 to 2015 at the Global, Regional, and National Level: Results From the Global Burden of Disease Study 2015. *JAMA Oncology.* 2017;3: 1683–1691. doi:10.1001/jamaoncol.2017.3055
52. Wang J, Chenivresse X, Henglein B, Bréchet C. Hepatitis B virus integration in a cyclin A gene in a hepatocellular carcinoma. *Nature.* 1990;343: 555–557. doi:10.1038/343555a0
53. Marrero JA, Kulik LM, Sirlin CB, Zhu AX, Finn RS, Abecassis MM, et al. Diagnosis, Staging, and Management of Hepatocellular Carcinoma: 2018 Practice Guidance by the American Association for the Study of Liver Diseases. *Hepatology.* 2018;68: 723–750. doi:10.1002/hep.29913
54. Campbell JS, Hughes SD, Gilbertson DG, Palmer TE, Holdren MS, Haran AC, et al. Platelet-derived growth factor C induces liver fibrosis, steatosis, and hepatocellular carcinoma. *PNAS.* 2005;102: 3389–3394. doi:10.1073/pnas.0409722102
55. Kang T-W, Yevsa T, Woller N, Hoenicke L, Wuestefeld T, Dauch D, et al. Senescence surveillance of pre-malignant hepatocytes limits liver cancer development. *Nature.* 2011;479: 547–551. doi:10.1038/nature10599
56. Ringelhan M, Pfister D, O’Connor T, Pikarsky E, Heikenwalder M. The immunology of hepatocellular carcinoma. *Nat Immunol.* 2018;19: 222–232. doi:10.1038/s41590-018-0044-z
57. Schulze K, Imbeaud S, Letouzé E, Alexandrov LB, Calderaro J, Rebouissou S, et al. Exome sequencing of hepatocellular carcinomas identifies new mutational signatures and potential therapeutic targets. *Nat Genet.* 2015;47: 505–511. doi:10.1038/ng.3252
58. Guichard C, Amaddeo G, Imbeaud S, Ladeiro Y, Pelletier L, Maad IB, et al. Integrated analysis of somatic mutations and focal copy-number changes identifies key genes and pathways in hepatocellular carcinoma. *Nat Genet.* 2012;44: 694–698. doi:10.1038/ng.2256
59. Cerami E, Gao J, Dogrusoz U, Gross BE, Sumer SO, Aksoy BA, et al. The cBio cancer genomics portal: an open platform for exploring multidimensional cancer genomics data. *Cancer Discov.* 2012;2: 401–404. doi:10.1158/2159-8290.CD-12-0095

REFERENCES

60. Gao J, Aksoy BA, Dogrusoz U, Dresdner G, Gross B, Sumer SO, et al. Integrative analysis of complex cancer genomics and clinical profiles using the cBioPortal. *Sci Signal*. 2013;6: pl1. doi:10.1126/scisignal.2004088
61. The Cancer Genome Atlas Program - National Cancer Institute. 13 Jun 2018 [cited 8 Dec 2021]. Available: <https://www.cancer.gov/about-nci/organization/ccg/research/structural-genomics/tcga>
62. Banales JM, Marin JGG, Lamarca A, Rodrigues PM, Khan SA, Roberts LR, et al. Cholangiocarcinoma 2020: the next horizon in mechanisms and management. *Nat Rev Gastroenterol Hepatol*. 2020;17: 557–588. doi:10.1038/s41575-020-0310-z
63. Khan SA, Tavolari S, Brandi G. Cholangiocarcinoma: Epidemiology and risk factors. *Liver International*. 2019;39: 19–31. doi:10.1111/liv.14095
64. Huang W-C, Tsai C-C, Chan C-C. Mutation analysis and copy number changes of KRAS and BRAF genes in Taiwanese cases of biliary tract cholangiocarcinoma. *Journal of the Formosan Medical Association*. 2017;116: 464–468. doi:10.1016/j.jfma.2016.07.015
65. Simbolo M, Vicentini C, Ruzzenente A, Brunelli M, Conci S, Fassan M, et al. Genetic alterations analysis in prognostic stratified groups identified TP53 and ARID1A as poor clinical performance markers in intrahepatic cholangiocarcinoma. *Sci Rep*. 2018;8: 7119. doi:10.1038/s41598-018-25669-1
66. Vandamme TF. Use of rodents as models of human diseases. *J Pharm Bioallied Sci*. 2014;6: 2–9. doi:10.4103/0975-7406.124301
67. Carlessi R, Köhn-Gaone J, Olynyk JK, Tirnitz-Parker JEE. Mouse Models of Hepatocellular Carcinoma. In: Tirnitz-Parker JEE, editor. *Hepatocellular Carcinoma*. Brisbane (AU): Codon Publications; 2019. Available: <http://www.ncbi.nlm.nih.gov/books/NBK549197/>
68. Corbin KD, Zeisel SH. Choline metabolism provides novel insights into nonalcoholic fatty liver disease and its progression. *Curr Opin Gastroenterol*. 2012;28: 159–165. doi:10.1097/MOG.0b013e32834e7b4b
69. Lau JKC, Zhang X, Yu J. Animal models of non-alcoholic fatty liver disease: current perspectives and recent advances. *J Pathol*. 2017;241: 36–44. doi:10.1002/path.4829
70. Gaemers IC, Stallen JM, Kunne C, Wallner C, van Werven J, Nederveen A, et al. Lipotoxicity and steatohepatitis in an overfed mouse model for non-alcoholic fatty liver disease. *Biochim Biophys Acta*. 2011;1812: 447–458. doi:10.1016/j.bbadis.2011.01.003
71. Tetri LH, Basaranoglu M, Brunt EM, Yerian LM, Neuschwander-Tetri BA. Severe NAFLD with hepatic necroinflammatory changes in mice fed trans fats and a high-fructose corn syrup equivalent. *Am J Physiol Gastrointest Liver Physiol*. 2008;295: G987–G995. doi:10.1152/ajpgi.90272.2008
72. Dowman JK, Hopkins LJ, Reynolds GM, Nikolaou N, Armstrong MJ, Shaw JC, et al. Development of Hepatocellular Carcinoma in a Murine Model of Nonalcoholic Steatohepatitis Induced by Use of a High-Fat/Fructose Diet and Sedentary Lifestyle. *Am J Pathol*. 2014;184: 1550–1561. doi:10.1016/j.ajpath.2014.01.034
73. Charlton M, Krishnan A, Viker K, Sanderson S, Cazanave S, McConico A, et al. Fast food diet mouse: novel small animal model of NASH with ballooning, progressive fibrosis, and high physiological fidelity to the human condition. *Am J Physiol Gastrointest Liver Physiol*. 2011;301: G825–G834. doi:10.1152/ajpgi.00145.2011
74. Verna L, Whysner J, Williams GM. N-nitrosodiethylamine mechanistic data and risk assessment: bioactivation, DNA-adduct formation, mutagenicity, and tumor initiation. *Pharmacol Ther*. 1996;71: 57–81. doi:10.1016/0163-7258(96)00062-9
75. Sánchez-Pérez Y, Carrasco-Legleu C, García-Cuellar C, Pérez-Carreón J, Hernández-García S, Salcido-Neyoy M, et al. Oxidative stress in carcinogenesis. Correlation between lipid peroxidation and induction of preneoplastic lesions in rat hepatocarcinogenesis. *Cancer Lett*. 2005;217: 25–32. doi:10.1016/j.canlet.2004.07.019
76. Dong S, Chen Q-L, Song Y-N, Sun Y, Wei B, Li X-Y, et al. Mechanisms of CCl4-induced liver fibrosis with combined transcriptomic and proteomic analysis. *J Toxicol Sci*. 2016;41: 561–572. doi:10.2131/jts.41.561

77. Johansson I, Ingelman-Sundberg M. Carbon tetrachloride-induced lipid peroxidation dependent on an ethanol-inducible form of rabbit liver microsomal cytochrome P-450. *FEBS Lett.* 1985;183: 265–269. doi:10.1016/0014-5793(85)80790-0
78. Suda T, Liu D. Hydrodynamic Gene Delivery: Its Principles and Applications. *Molecular Therapy.* 2007;15: 2063–2069. doi:10.1038/sj.mt.6300314
79. Kamimura K, Yokoo T, Abe H, Kobayashi Y, Ogawa K, Shinagawa Y, et al. Image-Guided Hydrodynamic Gene Delivery: Current Status and Future Directions. *Pharmaceutics.* 2015;7: 213–223. doi:10.3390/pharmaceutics7030213
80. Liu F, Song YK, Liu D. Hydrodynamics-based transfection in animals by systemic administration of plasmid DNA. *Gene Ther.* 1999;6: 1258–1266. doi:10.1038/sj.gt.3300947
81. Ivics Z, Hackett PB, Plasterk RH, Izsvák Z. Molecular Reconstruction of Sleeping Beauty, a Tc1-like Transposon from Fish, and Its Transposition in Human Cells. *Cell.* 1997;91: 501–510. doi:10.1016/S0092-8674(00)80436-5
82. Dupuy AJ, Akagi K, Largaespada DA, Copeland NG, Jenkins NA. Mammalian mutagenesis using a highly mobile somatic Sleeping Beauty transposon system. *Nature.* 2005;436: 221–226. doi:10.1038/nature03691
83. Hubner EK, Lechler C, Rösner TN, Kohnke-Ertel B, Schmid RM, Ehmer U. Constitutive and Inducible Systems for Genetic In Vivo Modification of Mouse Hepatocytes Using Hydrodynamic Tail Vein Injection. *J Vis Exp.* 2018; 56613. doi:10.3791/56613
84. Adli M. The CRISPR tool kit for genome editing and beyond. *Nat Commun.* 2018;9: 1911. doi:10.1038/s41467-018-04252-2
85. Chen X, Calvisi DF. Hydrodynamic Transfection for Generation of Novel Mouse Models for Liver Cancer Research. *Am J Pathol.* 2014;184: 912–923. doi:10.1016/j.ajpath.2013.12.002
86. Padma VV. An overview of targeted cancer therapy. *Biomedicine (Taipei).* 2015;5: 19. doi:10.7603/s40681-015-0019-4
87. Zhong L, Li Y, Xiong L, Wang W, Wu M, Yuan T, et al. Small molecules in targeted cancer therapy: advances, challenges, and future perspectives. *Sig Transduct Target Ther.* 2021;6: 1–48. doi:10.1038/s41392-021-00572-w
88. Sorafenib Tosylate - National Cancer Institute. 5 Oct 2006 [cited 3 Jan 2022]. Available: <https://www.cancer.gov/about-cancer/treatment/drugs/sorafenibtosylate>
89. Anonymous. Nexavar. In: European Medicines Agency [Internet]. 17 Sep 2018 [cited 3 Jan 2022]. Available: <https://www.ema.europa.eu/en/medicines/human/EPAR/nexavar>
90. Keating GM, Santoro A. Sorafenib. *Drugs.* 2009;69: 223–240. doi:10.2165/00003495-200969020-00006
91. Hormone Therapy for Breast Cancer | Breast Cancer Treatment. [cited 3 Jan 2022]. Available: <https://www.cancer.org/cancer/breast-cancer/treatment/hormone-therapy-for-breast-cancer.html>
92. Targeted Cancer Therapies Fact Sheet - National Cancer Institute. 6 Dec 2021 [cited 22 Dec 2021]. Available: <https://www.cancer.gov/about-cancer/treatment/types/targeted-therapies/targeted-therapies-fact-sheet>
93. The Nobel Prize in Physiology or Medicine 2018. In: NobelPrize.org [Internet]. [cited 4 Jan 2022]. Available: <https://www.nobelprize.org/prizes/medicine/2018/summary/>
94. Waldman AD, Fritz JM, Lenardo MJ. A guide to cancer immunotherapy: from T cell basic science to clinical practice. *Nat Rev Immunol.* 2020;20: 651–668. doi:10.1038/s41577-020-0306-5
95. Immune System Modulators for Cancer Therapy - National Cancer Institute. 24 Sep 2019 [cited 7 Jan 2022]. Available: <https://www.cancer.gov/about-cancer/treatment/types/immunotherapy/immune-system-modulators>
96. Srivastava PK. Neoepitopes of Cancers: Looking Back, Looking Ahead. *Cancer Immunol Res.* 2015;3: 969–977. doi:10.1158/2326-6066.CIR-15-0134

REFERENCES

97. Janelle V, Rulleau C, Del Testa S, Carli C, Delisle J-S. T-Cell Immunotherapies Targeting Histocompatibility and Tumor Antigens in Hematological Malignancies. *Frontiers in Immunology*. 2020;11. Available: <https://www.frontiersin.org/article/10.3389/fimmu.2020.00276>
98. Kessler JH, Melief CJM. Identification of T-cell epitopes for cancer immunotherapy. *Leukemia*. 2007;21: 1859–1874. doi:10.1038/sj.leu.2404787
99. Kotsias F, Cebrian I, Alloatti A. Chapter Two - Antigen processing and presentation. In: Lhuillier C, Galluzzi L, editors. *International Review of Cell and Molecular Biology*. Academic Press; 2019. pp. 69–121. doi:10.1016/bs.ircmb.2019.07.005
100. Janeway CA. The T cell receptor as a multicomponent signalling machine: CD4/CD8 coreceptors and CD45 in T cell activation. *Annu Rev Immunol*. 1992;10: 645–674. doi:10.1146/annurev.iy.10.040192.003241
101. Hewitt EW. The MHC class I antigen presentation pathway: strategies for viral immune evasion. *Immunology*. 2003;110: 163–169. doi:10.1046/j.1365-2567.2003.01738.x
102. Acuto O, Michel F. CD28-mediated co-stimulation: a quantitative support for TCR signalling. *Nat Rev Immunol*. 2003;3: 939–951. doi:10.1038/nri1248
103. Murphy K, Weaver C. *Janeway's Immunobiology*. 9th edition. Garland Science; 2016.
104. Schoenborn JR, Wilson CB. Regulation of Interferon- γ During Innate and Adaptive Immune Responses. *Advances in Immunology*. Academic Press; 2007. pp. 41–101. doi:10.1016/S0065-2776(07)96002-2
105. Ratner A, Clark WR. Role of TNF-alpha in CD8+ cytotoxic T lymphocyte-mediated lysis. *J Immunol*. 1993;150: 4303–4314.
106. Bossi G, Griffiths GM. CTL secretory lysosomes: biogenesis and secretion of a harmful organelle. *Seminars in Immunology*. 2005;17: 87–94. doi:10.1016/j.smim.2004.09.007
107. Voskoboinik I, Smyth MJ, Trapani JA. Perforin-mediated target-cell death and immune homeostasis. *Nat Rev Immunol*. 2006;6: 940–952. doi:10.1038/nri1983
108. Voskoboinik I, Thia M-C, De Bono A, Browne K, Cretney E, Jackson JT, et al. The Functional Basis for Hemophagocytic Lymphohistiocytosis in a Patient with Co-inherited Missense Mutations in the Perforin (PFN1) Gene. *J Exp Med*. 2004;200: 811–816. doi:10.1084/jem.20040776
109. Chowdhury D, Lieberman J. Death by a Thousand Cuts: Granzyme Pathways of Programmed Cell Death. *Annu Rev Immunol*. 2008;26: 389–420. doi:10.1146/annurev.immunol.26.021607.090404
110. Martínez-Lostao L, Anel A, Pardo J. How Do Cytotoxic Lymphocytes Kill Cancer Cells? *Clin Cancer Res*. 2015;21: 5047–5056. doi:10.1158/1078-0432.CCR-15-0685
111. Anel A, Buferne M, Boyer C, Schmitt-Verhulst AM, Golstein P. T cell receptor-induced Fas ligand expression in cytotoxic T lymphocyte clones is blocked by protein tyrosine kinase inhibitors and cyclosporin A. *Eur J Immunol*. 1994;24: 2469–2476. doi:10.1002/eji.1830241032
112. Rudd CE, Taylor A, Schneider H. CD28 and CTLA-4 coreceptor expression and signal transduction. *Immunol Rev*. 2009;229: 12–26. doi:10.1111/j.1600-065X.2009.00770.x
113. Francisco LM, Sage PT, Sharpe AH. The PD-1 Pathway in Tolerance and Autoimmunity. *Immunol Rev*. 2010;236: 219–242. doi:10.1111/j.1600-065X.2010.00923.x
114. Han Y, Liu D, Li L. PD-1/PD-L1 pathway: current researches in cancer. *Am J Cancer Res*. 2020;10: 727–742.
115. Blank C, Gajewski TF, Mackensen A. Interaction of PD-L1 on tumor cells with PD-1 on tumor-specific T cells as a mechanism of immune evasion: implications for tumor immunotherapy. *Cancer Immunol Immunother*. 2005;54: 307–314. doi:10.1007/s00262-004-0593-x

116. Solinas C, Aiello M, Rozali E, Lambertini M, Willard-Gallo K, Migliori E. Programmed Cell Death-Ligand 2: A Neglected But Important Target in the Immune Response to Cancer? *Transl Oncol.* 2020;13: 100811. doi:10.1016/j.tranon.2020.100811
117. DailyMed - YERVOY- ipilimumab injection. [cited 5 Jan 2022]. Available: <https://dailymed.nlm.nih.gov/dailymed/drugInfo.cfm?setid=2265ef30-253e-11df-8a39-0800200c9a66>
118. DailyMed - OPDIVO- nivolumab injection. [cited 5 Jan 2022]. Available: <https://dailymed.nlm.nih.gov/dailymed/drugInfo.cfm?setid=f570b9c4-6846-4de2-abfa-4d0a4ae4e394>
119. Kumar V, Chaudhary N, Garg M, Floudas CS, Soni P, Chandra AB. Current Diagnosis and Management of Immune Related Adverse Events (irAEs) Induced by Immune Checkpoint Inhibitor Therapy. *Front Pharmacol.* 2017;8: 49. doi:10.3389/fphar.2017.00049
120. Zhu C, Anderson AC, Schubart A, Xiong H, Imitola J, Khoury SJ, et al. The Tim-3 ligand galectin-9 negatively regulates T helper type 1 immunity. *Nat Immunol.* 2005;6: 1245–1252. doi:10.1038/ni1271
121. He Y, Rivard CJ, Rozeboom L, Yu H, Ellison K, Kowalewski A, et al. Lymphocyte-activation gene-3, an important immune checkpoint in cancer. *Cancer Sci.* 2016;107: 1193–1197. doi:10.1111/cas.12986
122. Wang L, Rubinstein R, Lines JL, Wasiuk A, Ahonen C, Guo Y, et al. VISTA, a novel mouse Ig superfamily ligand that negatively regulates T cell responses. *J Exp Med.* 2011;208: 577–592. doi:10.1084/jem.20100619
123. Rosenberg SA, Spiess P, Lafreniere R. A New Approach to the Adoptive Immunotherapy of Cancer with Tumor-Infiltrating Lymphocytes. *Science.* 1986 [cited 6 Jan 2022]. doi:10.1126/science.3489291
124. Wang S, Sun J, Chen K, Ma P, Lei Q, Xing S, et al. Perspectives of tumor-infiltrating lymphocyte treatment in solid tumors. *BMC Medicine.* 2021;19: 140. doi:10.1186/s12916-021-02006-4
125. Huang J, Khong HT, Dudley ME, El-Gamil M, Li YF, Rosenberg SA, et al. Survival, Persistence, and Progressive Differentiation of Adoptively Transferred Tumor-Reactive T Cells Associated with Tumor Regression. *J Immunother.* 2005;28: 258–267.
126. Powell DJ, Dudley ME, Robbins PF, Rosenberg SA. Transition of late-stage effector T cells to CD27+ CD28+ tumor-reactive effector memory T cells in humans after adoptive cell transfer therapy. *Blood.* 2005;105: 241–250. doi:10.1182/blood-2004-06-2482
127. Kuwana Y, Asakura Y, Utsunomiya N, Nakanishi M, Arata Y, Itoh S, et al. Expression of chimeric receptor composed of immunoglobulin-derived V regions and T-cell receptor-derived C regions. *Biochemical and Biophysical Research Communications.* 1987;149: 960–968. doi:10.1016/0006-291X(87)90502-X
128. Maher J, Brentjens RJ, Gunset G, Rivière I, Sadelain M. Human T-lymphocyte cytotoxicity and proliferation directed by a single chimeric TCR ζ /CD28 receptor. *Nat Biotechnol.* 2002;20: 70–75. doi:10.1038/nbt0102-70
129. Kuhn NF, Purdon TJ, van Leeuwen DG, Lopez AV, Curran KJ, Daniyan AF, et al. CD40 Ligand-Modified Chimeric Antigen Receptor T Cells Enhance Antitumor Function by Eliciting an Endogenous Antitumor Response. *Cancer Cell.* 2019;35: 473-488.e6. doi:10.1016/j.ccell.2019.02.006
130. Finney HM, Akbar AN, Lawson ADG. Activation of resting human primary T cells with chimeric receptors: costimulation from CD28, inducible costimulator, CD134, and CD137 in series with signals from the TCR zeta chain. *J Immunol.* 2004;172: 104–113. doi:10.4049/jimmunol.172.1.104
131. Imai C, Mihara K, Andreansky M, Nicholson IC, Pui C-H, Geiger TL, et al. Chimeric receptors with 4-1BB signaling capacity provoke potent cytotoxicity against acute lymphoblastic leukemia. *Leukemia.* 2004;18: 676–684. doi:10.1038/sj.leu.2403302
132. Chmielewski M, Kopecky C, Hombach AA, Abken H. IL-12 release by engineered T cells expressing chimeric antigen receptors can effectively Muster an antigen-independent macrophage response on tumor cells that have shut down tumor antigen expression. *Cancer Res.* 2011;71: 5697–5706. doi:10.1158/0008-5472.CAN-11-0103

REFERENCES

133. T-cell Transfer Therapy - Immunotherapy - National Cancer Institute. 24 Sep 2019 [cited 6 Jan 2022]. Available: <https://www.cancer.gov/about-cancer/treatment/types/immunotherapy/t-cell-transfer-therapy>
134. Maus MV, June CH. Making Better Chimeric Antigen Receptors for Adoptive T-cell Therapy. *Clin Cancer Res.* 2016;22: 1875–1884. doi:10.1158/1078-0432.CCR-15-1433
135. Majzner RG, Theruvath JL, Nellan A, Heitzeneder S, Cui Y, Mount CW, et al. CAR T Cells Targeting B7-H3, a Pan-Cancer Antigen, Demonstrate Potent Preclinical Activity Against Pediatric Solid Tumors and Brain Tumors. *Clin Cancer Res.* 2019;25: 2560–2574. doi:10.1158/1078-0432.CCR-18-0432
136. Neelapu SS, Tummala S, Kebriaei P, Wierda W, Gutierrez C, Locke FL, et al. Chimeric antigen receptor T-cell therapy — assessment and management of toxicities. *Nat Rev Clin Oncol.* 2018;15: 47–62. doi:10.1038/nrclinonc.2017.148
137. Sahin U, Türeci Ö. Personalized vaccines for cancer immunotherapy. *Science.* 2018 [cited 7 Jan 2022]. doi:10.1126/science.aar7112
138. Conlon KC, Miljkovic MD, Waldmann TA. Cytokines in the Treatment of Cancer. *J Interferon Cytokine Res.* 2019;39: 6–21. doi:10.1089/jir.2018.0019
139. Reang P, Gupta M, Kohli K. Biological Response Modifiers in Cancer. *MedGenMed.* 2006;8: 33.
140. Borchering N, Kolb R, Gullicksrud J, Vikas P, Zhu Y, Zhang W. Keeping tumors in check: a mechanistic review of clinical response and resistance to immune checkpoint blockade in cancer. *J Mol Biol.* 2018;430: 2014–2029. doi:10.1016/j.jmb.2018.05.030
141. Sermer D, Brentjens R. CAR T-cell therapy: Full speed ahead. *Hematological Oncology.* 2019;37: 95–100. doi:10.1002/hon.2591
142. Beatty GL, Gladney WL. Immune Escape Mechanisms as a Guide for Cancer Immunotherapy. *Clin Cancer Res.* 2015;21: 687–692. doi:10.1158/1078-0432.CCR-14-1860
143. Hegde PS, Chen DS. Top 10 Challenges in Cancer Immunotherapy. *Immunity.* 2020;52: 17–35. doi:10.1016/j.immuni.2019.12.011
144. Whiteside TL, Demaria S, Rodriguez-Ruiz ME, Zarour HM, Melero I. Emerging Opportunities and Challenges in Cancer Immunotherapy. *Clin Cancer Res.* 2016;22: 1845–1855. doi:10.1158/1078-0432.CCR-16-0049
145. Sambhi M, Bagheri L, Szewczuk MR. Current Challenges in Cancer Immunotherapy: Multimodal Approaches to Improve Efficacy and Patient Response Rates. *Journal of Oncology.* 2019;2019: e4508794. doi:10.1155/2019/4508794
146. Perea F, Bernal M, Sánchez-Palencia A, Carretero J, Torres C, Bayarri C, et al. The absence of HLA class I expression in non-small cell lung cancer correlates with the tumor tissue structure and the pattern of T cell infiltration. *International Journal of Cancer.* 2017;140: 888–899. doi:10.1002/ijc.30489
147. Pereira C, Gimenez-Xavier P, Pros E, Pajares MJ, Moro M, Gomez A, et al. Genomic Profiling of Patient-Derived Xenografts for Lung Cancer Identifies B2M Inactivation Impairing Immunorecognition. *Clin Cancer Res.* 2017;23: 3203–3213. doi:10.1158/1078-0432.CCR-16-1946-T
148. Snyder A, Makarov V, Merghoub T, Yuan J, Zaretsky JM, Desrichard A, et al. Genetic basis for clinical response to CTLA-4 blockade in melanoma. *N Engl J Med.* 2014;371: 2189–2199. doi:10.1056/NEJMoa1406498
149. Apetoh L, Smyth MJ, Drake CG, Abastado J-P, Apte RN, Ayyoub M, et al. Consensus nomenclature for CD8+ T cell phenotypes in cancer. *Oncoimmunology.* 2015;4: e998538. doi:10.1080/2162402X.2014.998538
150. Taube JM, Anders RA, Young GD, Xu H, Sharma R, McMiller TL, et al. Colocalization of inflammatory response with B7-h1 expression in human melanocytic lesions supports an adaptive resistance mechanism of immune escape. *Sci Transl Med.* 2012;4: 127ra37. doi:10.1126/scitranslmed.3003689

151. Taube JM, Klein A, Brahmer JR, Xu H, Pan X, Kim JH, et al. Association of PD-1, PD-1 ligands, and other features of the tumor immune microenvironment with response to anti-PD-1 therapy. *Clin Cancer Res.* 2014;20: 5064–5074. doi:10.1158/1078-0432.CCR-13-3271
152. Kerkar SP, Restifo NP. Cellular Constituents of Immune Escape within the Tumor Microenvironment. *Cancer Res.* 2012;72: 3125–3130. doi:10.1158/0008-5472.CAN-11-4094
153. Labani-Motlagh A, Ashja-Mahdavi M, Loskog A. The Tumor Microenvironment: A Milieu Hindering and Obstructing Antitumor Immune Responses. *Front Immunol.* 2020;11: 940. doi:10.3389/fimmu.2020.00940
154. van Kempen LCLT, Ruiters DJ, van Muijen GNP, Coussens LM. The tumor microenvironment: a critical determinant of neoplastic evolution. *European Journal of Cell Biology.* 2003;82: 539–548. doi:10.1078/0171-9335-00346
155. Yu P, Rowley DA, Fu Y-X, Schreiber H. The role of stroma in immune recognition and destruction of well-established solid tumors. *Current Opinion in Immunology.* 2006;18: 226–231. doi:10.1016/j.coi.2006.01.004
156. de la Rosa M, Rutz S, Dorninger H, Scheffold A. Interleukin-2 is essential for CD4+CD25+ regulatory T cell function. *European Journal of Immunology.* 2004;34: 2480–2488. doi:10.1002/eji.200425274
157. Fehérvári Z, Sakaguchi S. CD4+ Tregs and immune control. *J Clin Invest.* 2004;114: 1209–1217. doi:10.1172/JCI200423395
158. Zou W. Regulatory T cells, tumour immunity and immunotherapy. *Nat Rev Immunol.* 2006;6: 295–307. doi:10.1038/nri1806
159. Romano M, Fanelli G, Albany CJ, Giganti G, Lombardi G. Past, Present, and Future of Regulatory T Cell Therapy in Transplantation and Autoimmunity. *Frontiers in Immunology.* 2019;10. Available: <https://www.frontiersin.org/article/10.3389/fimmu.2019.00043>
160. Gabrilovich DI, Nagaraj S. Myeloid-derived-suppressor cells as regulators of the immune system. *Nat Rev Immunol.* 2009;9: 162–174. doi:10.1038/nri2506
161. Noy R, Pollard JW. Tumor-associated macrophages: from mechanisms to therapy. *Immunity.* 2014;41: 49–61. doi:10.1016/j.immuni.2014.06.010
162. Hegde PS, Karanikas V, Evers S. The Where, the When, and the How of Immune Monitoring for Cancer Immunotherapies in the Era of Checkpoint Inhibition. *Clin Cancer Res.* 2016;22: 1865–1874. doi:10.1158/1078-0432.CCR-15-1507
163. Pai SI, Cesano A, Marincola FM. The Paradox of Cancer Immune Exclusion: Immune Oncology Next Frontier. *Cancer Treat Res.* 2020;180: 173–195. doi:10.1007/978-3-030-38862-1_6
164. Herbst RS, Soria J-C, Kowanetz M, Fine GD, Hamid O, Gordon MS, et al. Predictive correlates of response to the anti-PD-L1 antibody MPDL3280A in cancer patients. *Nature.* 2014;515: 563–567. doi:10.1038/nature14011
165. Bagaev A, Kotlov N, Nomie K, Svekolkina V, Gafurov A, Isaeva O, et al. Conserved pan-cancer microenvironment subtypes predict response to immunotherapy. *Cancer Cell.* 2021;39: 845–865.e7. doi:10.1016/j.ccell.2021.04.014
166. Thorsson V, Gibbs DL, Brown SD, Wolf D, Bortone DS, Yang T-HO, et al. The Immune Landscape of Cancer. *Immunity.* 2018;48: 812–830.e14. doi:10.1016/j.immuni.2018.03.023
167. Blank CU, Haanen JB, Ribas A, Schumacher TN. The “cancer immunogram.” *Science.* 2016 [cited 20 Jan 2022]. doi:10.1126/science.aaf2834
168. Bach D-H, Park HJ, Lee SK. The Dual Role of Bone Morphogenetic Proteins in Cancer. *Mol Ther Oncolytics.* 2017;8: 1–13. doi:10.1016/j.omto.2017.10.002
169. Chen W, ten Dijke P. Immunoregulation by members of the TGF β superfamily. *Nat Rev Immunol.* 2016;16: 723–740. doi:10.1038/nri.2016.112
170. Cortez MA, Masrourpour F, Ivan C, Zhang J, Younes AI, Lu Y, et al. Bone morphogenetic protein 7 promotes resistance to immunotherapy. *Nat Commun.* 2020;11: 4840. doi:10.1038/s41467-020-18617-z

REFERENCES

171. Kuczma M, Kurczewska A, Kraj P. Modulation of Bone Morphogenetic Protein Signaling in T-Cells for Cancer Immunotherapy. *J Immunotoxicol.* 2014;11: 319–327. doi:10.3109/1547691X.2013.864736
172. Sconocchia T, Sconocchia G. Regulation of the Immune System in Health and Disease by Members of the Bone Morphogenetic Protein Family. *Front Immunol.* 2021;12: 802346. doi:10.3389/fimmu.2021.802346
173. Hemmati-Brivanlou A, Thomsen GH. Ventral mesodermal patterning in *Xenopus* embryos: expression patterns and activities of BMP-2 and BMP-4. *Dev Genet.* 1995;17: 78–89. doi:10.1002/dvg.1020170109
174. Zou H, Niswander L. Requirement for BMP Signaling in Interdigital Apoptosis and Scale Formation. *Science.* 1996 [cited 22 Jan 2022]. doi:10.1126/science.272.5262.738
175. Kobayashi T, Lyons KM, McMahon AP, Kronenberg HM. BMP signaling stimulates cellular differentiation at multiple steps during cartilage development. *Proc Natl Acad Sci U S A.* 2005;102: 18023–18027. doi:10.1073/pnas.0503617102
176. Tsuji K, Bandyopadhyay A, Harfe BD, Cox K, Kakar S, Gerstenfeld L, et al. BMP2 activity, although dispensable for bone formation, is required for the initiation of fracture healing. *Nat Genet.* 2006;38: 1424–1429. doi:10.1038/ng1916
177. Huang Z, Wang D, Ihida-Stansbury K, Jones PL, Martin JF. Defective pulmonary vascular remodeling in Smad8 mutant mice. *Hum Mol Genet.* 2009;18: 2791–2801. doi:10.1093/hmg/ddp214
178. Wang RN, Green J, Wang Z, Deng Y, Qiao M, Peabody M, et al. Bone Morphogenetic Protein (BMP) signaling in development and human diseases. *Genes & Diseases.* 2014;1: 87–105. doi:10.1016/j.gendis.2014.07.005
179. Heldin C-H, Miyazono K, ten Dijke P. TGF- β signalling from cell membrane to nucleus through SMAD proteins. *Nature.* 1997;390: 465–471. doi:10.1038/37284
180. Miyazono K, Kamiya Y, Morikawa M. Bone morphogenetic protein receptors and signal transduction. *The Journal of Biochemistry.* 2010;147: 35–51. doi:10.1093/jb/mvp148
181. Heldin C-H, Moustakas A. Role of Smads in TGF β signaling. *Cell Tissue Res.* 2012;347: 21–36. doi:10.1007/s00441-011-1190-x
182. Feng X-H, Derynck R. SPECIFICITY AND VERSATILITY IN TGF- β SIGNALING THROUGH SMADS. *Annual Review of Cell and Developmental Biology.* 2005;21: 659–693. doi:10.1146/annurev.cellbio.21.022404.142018
183. Derynck R, Zhang YE. Smad-dependent and Smad-independent pathways in TGF- β family signalling. *Nature.* 2003;425: 577–584. doi:10.1038/nature02006
184. Atfi A, Djelloul S, Chastre E, Davis R, Gespach C. Evidence for a role of Rho-like GTPases and stress-activated protein kinase/c-Jun N-terminal kinase (SAPK/JNK) in transforming growth factor beta-mediated signaling. *J Biol Chem.* 1997;272: 1429–1432. doi:10.1074/jbc.272.3.1429
185. Glise B, Noselli S. Coupling of Jun amino-terminal kinase and Decapentaplegic signaling pathways in *Drosophila* morphogenesis. *Genes Dev.* 1997;11: 1738–1747. doi:10.1101/gad.11.13.1738
186. Mulder KM, Morris SL. Activation of p21ras by transforming growth factor beta in epithelial cells. *J Biol Chem.* 1992;267: 5029–5031.
187. Lou J, Tu Y, Li S, Manske PR. Involvement of ERK in BMP-2 Induced Osteoblastic Differentiation of Mesenchymal Progenitor Cell Line C3H10T1/2. *Biochemical and Biophysical Research Communications.* 2000;268: 757–762. doi:10.1006/bbrc.2000.2210
188. Hanafusa H, Ninomiya-Tsuji J, Masuyama N, Nishita M, Fujisawa J, Shibuya H, et al. Involvement of the p38 Mitogen-activated Protein Kinase Pathway in Transforming Growth Factor- β -induced Gene Expression*. *Journal of Biological Chemistry.* 1999;274: 27161–27167. doi:10.1074/jbc.274.38.27161
189. Iwasaki S, Iguchi M, Watanabe K, Hoshino R, Kohno M, Tsujimoto M. Specific Activation of the p38 Mitogen-activated Protein Kinase Signaling Pathway and Induction of Neurite Outgrowth in PC12 Cells by Bone Morphogenetic Protein-2*. *Journal of Biological Chemistry.* 1999;274: 26503–26510. doi:10.1074/jbc.274.37.26503

190. Yamaguchi K, Shirakabe K, Shibuya H, Irie K, Oishi I, Ueno N, et al. Identification of a Member of the MAPKKK Family as a Potential Mediator of TGF- β Signal Transduction. *Science*. 1995 [cited 26 Jan 2022]. doi:10.1126/science.270.5244.2008
191. Nickel J, Mueller TD. Specification of BMP Signaling. *Cells*. 2019;8: 1579. doi:10.3390/cells8121579
192. Petritsch C, Beug H, Balmain A, Oft M. TGF- β inhibits p70 S6 kinase via protein phosphatase 2A to induce G1 arrest. *Genes Dev*. 2000;14: 3093–3101.
193. Colak S, Ten Dijke P. Targeting TGF- β Signaling in Cancer. *Trends Cancer*. 2017;3: 56–71. doi:10.1016/j.trecan.2016.11.008
194. Massagué J. TGF β in Cancer. *Cell*. 2008;134: 215–230. doi:10.1016/j.cell.2008.07.001
195. Guinney J, Dienstmann R, Wang X, de Reyniès A, Schlicker A, Sonesson C, et al. The consensus molecular subtypes of colorectal cancer. *Nat Med*. 2015;21: 1350–1356. doi:10.1038/nm.3967
196. Calon A, Lonardo E, Berenguer-Llergo A, Espinet E, Hernando-Momblona X, Iglesias M, et al. Stromal gene expression defines poor-prognosis subtypes in colorectal cancer. *Nat Genet*. 2015;47: 320–329. doi:10.1038/ng.3225
197. Herbertz S, Sawyer JS, Stauber AJ, Gueorguieva I, Driscoll KE, Estrem ST, et al. Clinical development of galunisertib (Ly2157299 monohydrate), a small molecule inhibitor of transforming growth factor-beta signaling pathway. *Drug Design, Development and Therapy*. 2015;9: 4479–4499. doi:10.2147/DDDT.S86621
198. Liu S, Ren J, ten Dijke P. Targeting TGF β signal transduction for cancer therapy. *Sig Transduct Target Ther*. 2021;6: 1–20. doi:10.1038/s41392-020-00436-9
199. Ning J, Zhao Y, Ye Y, Yu J. Opposing roles and potential antagonistic mechanism between TGF- β and BMP pathways: Implications for cancer progression. *EBioMedicine*. 2019;41: 702–710. doi:10.1016/j.ebiom.2019.02.033
200. Guo D, Huang J, Gong J. Bone morphogenetic protein 4 (BMP4) is required for migration and invasion of breast cancer. *Mol Cell Biochem*. 2012;363: 179–190. doi:10.1007/s11010-011-1170-1
201. Paez-Pereda M, Giacomini D, Refojo D, Nagashima AC, Hopfner U, Grubler Y, et al. Involvement of bone morphogenetic protein 4 (BMP-4) in pituitary prolactinoma pathogenesis through a Smad/estrogen receptor crosstalk. *Proc Natl Acad Sci U S A*. 2003;100: 1034–1039. doi:10.1073/pnas.0237312100
202. Alarmo E-L, Pärssinen J, Ketolainen JM, Savinainen K, Karhu R, Kallioniemi A. BMP7 influences proliferation, migration, and invasion of breast cancer cells. *Cancer Lett*. 2009;275: 35–43. doi:10.1016/j.canlet.2008.09.028
203. Frey P, Devisme A, Schrempp M, Andrieux G, Boerries M, Hecht A. Canonical BMP Signaling Executes Epithelial-Mesenchymal Transition Downstream of SNAIL1. *Cancers (Basel)*. 2020;12: 1019. doi:10.3390/cancers12041019
204. Ye L, Kynaston H, Jiang WG. Bone Morphogenetic Protein-10 Suppresses the Growth and Aggressiveness of Prostate Cancer Cells Through a Smad Independent Pathway. *Journal of Urology*. 2009;181: 2749–2759. doi:10.1016/j.juro.2009.01.098
205. Cao Y, Slaney CY, Bidwell BN, Parker BS, Johnstone CN, Rautela J, et al. BMP4 inhibits breast cancer metastasis by blocking myeloid-derived suppressor cell activity. *Cancer Research*. 2014;74: 5091–5102. doi:10.1158/0008-5472.CAN-13-3171
206. RocherCrystal, SinglaReetu, K S, ParthasarathySampath, K S. Bone morphogenetic protein 7 polarizes THP-1 cells into M2 macrophages. *Canadian Journal of Physiology and Pharmacology*. 2012 [cited 27 Jan 2022]. doi:10.1139/y2012-102
207. Lee J-H, Lee GT, Woo SH, Ha Y-S, Kwon SJ, Kim W-J, et al. BMP-6 in renal cell carcinoma promotes tumor proliferation through IL-10-dependent M2 polarization of tumor-associated macrophages. *Cancer Res*. 2013;73: 3604–3614. doi:10.1158/0008-5472.CAN-12-4563
208. Hong JH, Lee GT, Lee JH, Kwon SJ, Park SH, Kim SJ, et al. Effect of bone morphogenetic protein-6 on macrophages. *Immunology*. 2009;128: e442–e450. doi:10.1111/j.1365-2567.2008.02998.x

REFERENCES

209. Martínez VG, Hernández-López C, Valencia J, Hidalgo L, Entrena A, Zapata AG, et al. The canonical BMP signaling pathway is involved in human monocyte-derived dendritic cell maturation. *Immunol Cell Biol.* 2011;89: 610–618. doi:10.1038/icb.2010.135
210. Robson NC, Hidalgo L, Mc Alpine T, Wei H, Martínez VG, Entrena A, et al. Optimal effector functions in human natural killer cells rely upon autocrine bone morphogenetic protein signaling. *Cancer Res.* 2014;74: 5019–5031. doi:10.1158/0008-5472.CAN-13-2845
211. Aoki M, Ishigami S, Uenosono Y, Arigami T, Uchikado Y, Kita Y, et al. Expression of BMP-7 in human gastric cancer and its clinical significance. *Br J Cancer.* 2011;104: 714–718. doi:10.1038/sj.bjc.6606075
212. Motoyama K, Tanaka F, Kosaka Y, Mimori K, Uetake H, Inoue H, et al. Clinical significance of BMP7 in human colorectal cancer. *Ann Surg Oncol.* 2008;15: 1530–1537. doi:10.1245/s10434-007-9746-4
213. Megumi K, Ishigami S, Uchikado Y, Kita Y, Okumura H, Matsumoto M, et al. Clinicopathological Significance of BMP7 Expression in Esophageal Squamous Cell Carcinoma. *Ann Surg Oncol.* 2012;19: 2066–2071. doi:10.1245/s10434-011-2024-5
214. Rodriguez-Martinez A, Alarmo E-L, Saarinen L, Ketolainen J, Nousiainen K, Hautaniemi S, et al. Analysis of BMP4 and BMP7 signaling in breast cancer cells unveils time-dependent transcription patterns and highlights a common synexpression group of genes. *BMC Med Genomics.* 2011;4: 80. doi:10.1186/1755-8794-4-80
215. Owens P, Pickup MW, Novitskiy SV, Giltneane JM, Gorska AE, Hopkins CR, et al. Inhibition of BMP signaling suppresses metastasis in mammary cancer. *Oncogene.* 2015;34: 2437–2449. doi:10.1038/onc.2014.189
216. Alarmo E-L, Kallioniemi A. Bone morphogenetic proteins in breast cancer: dual role in tumorigenesis? *Endocrine-Related Cancer.* 2010;17: R123–R139. doi:10.1677/ERC-09-0273
217. Sanjana NE, Shalem O, Zhang F. Improved vectors and genome-wide libraries for CRISPR screening. *Nat Methods.* 2014;11: 783–784. doi:10.1038/nmeth.3047
218. Raja E, Tzavlaki K, Vuilleumier R, Edlund K, Kahata K, Zieba A, et al. The protein kinase LKB1 negatively regulates bone morphogenetic protein receptor signaling. *Oncotarget.* 2016;7: 1120–1143. doi:10.18632/oncotarget.6683
219. Cong L, Ran FA, Cox D, Lin S, Barretto R, Habib N, et al. Multiplex genome engineering using CRISPR/Cas systems. *Science.* 2013;339: 819–823. doi:10.1126/science.1231143
220. CHOPCHOP. [cited 9 Sep 2021]. Available: <https://chopchop.cbu.uib.no/>
221. Montague TG, Cruz JM, Gagnon JA, Church GM, Valen E. CHOPCHOP: a CRISPR/Cas9 and TALEN web tool for genome editing. *Nucleic Acids Research.* 2014;42: W401–W407. doi:10.1093/nar/gku410
222. Labun K, Montague TG, Gagnon JA, Thyme SB, Valen E. CHOPCHOP v2: a web tool for the next generation of CRISPR genome engineering. *Nucleic Acids Res.* 2016;44: W272–W276. doi:10.1093/nar/gkw398
223. Labun K, Montague TG, Krause M, Torres Cleuren YN, Tjeldnes H, Valen E. CHOPCHOP v3: expanding the CRISPR web toolbox beyond genome editing. *Nucleic Acids Research.* 2019;47: W171–W174. doi:10.1093/nar/gkz365
224. Analysis of Relative Gene Expression Data Using Real-Time Quantitative PCR and the 2- $\Delta\Delta$ CT Method - ScienceDirect. [cited 13 Sep 2021]. Available: <https://www.sciencedirect.com/science/article/abs/pii/S1046202301912629?via%3Dihub>
225. Pear WS, Nolan GP, Scott ML, Baltimore D. Production of high-titer helper-free retroviruses by transient transfection. *Proc Natl Acad Sci U S A.* 1993;90: 8392–8396. doi:10.1073/pnas.90.18.8392
226. Swift S, Lorens J, Achacoso P, Nolan GP. Rapid production of retroviruses for efficient gene delivery to mammalian cells using 293T cell-based systems. *Curr Protoc Immunol.* 2001;Chapter 10: Unit 10.17C. doi:10.1002/0471142735.im1017cs31
227. Retroviral Systems. [cited 15 Sep 2021]. Available: https://web.stanford.edu/group/nolan/_OldWebsite/retroviral_systems/retsyst.html

228. Franken NAP, Rodermond HM, Stap J, Haveman J, van Bree C. Clonogenic assay of cells in vitro. *Nat Protoc.* 2006;1: 2315–2319. doi:10.1038/nprot.2006.339
229. Hogquist KA, Jameson SC, Heath WR, Howard JL, Bevan MJ, Carbone FR. T cell receptor antagonist peptides induce positive selection. *Cell.* 1994;76: 17–27. doi:10.1016/0092-8674(94)90169-4
230. Clarke SR, Barnden M, Kurts C, Carbone FR, Miller JF, Heath WR. Characterization of the ovalbumin-specific TCR transgenic line OT-I: MHC elements for positive and negative selection. *Immunol Cell Biol.* 2000;78: 110–117. doi:10.1046/j.1440-1711.2000.00889.x
231. Guzmán C, Bagga M, Kaur A, Westermarck J, Abankwa D. ColonyArea: An ImageJ Plugin to Automatically Quantify Colony Formation in Clonogenic Assays. *PLOS ONE.* 2014;9: e92444. doi:10.1371/journal.pone.0092444
232. Bausch-Fluck D, Hofmann A, Bock T, Frei AP, Cerciello F, Jacobs A, et al. A Mass Spectrometric-Derived Cell Surface Protein Atlas. *PLoS One.* 2015;10. doi:10.1371/journal.pone.0121314
233. Winter J, Schwering M, Pelz O, Rauscher B, Zhan T, Heigwer F, et al. CRISPRAnalyzer: Interactive analysis, annotation and documentation of pooled CRISPR screens. *bioRxiv.* 2017; 109967. doi:10.1101/109967
234. Anders S, Pyl PT, Huber W. HTSeq—a Python framework to work with high-throughput sequencing data. *Bioinformatics.* 2015;31: 166–169. doi:10.1093/bioinformatics/btu638
235. Love MI, Huber W, Anders S. Moderated estimation of fold change and dispersion for RNA-seq data with DESeq2. *Genome Biology.* 2014;15: 550. doi:10.1186/s13059-014-0550-8
236. Talmadge JE, Singh RK, Fidler IJ, Raz A. Murine Models to Evaluate Novel and Conventional Therapeutic Strategies for Cancer. *Am J Pathol.* 2007;170: 793–804. doi:10.2353/ajpath.2007.060929
237. Zheng K, Cubero FJ, Nevzorova YA. c-MYC—Making Liver Sick: Role of c-MYC in Hepatic Cell Function, Homeostasis and Disease. *Genes (Basel).* 2017;8: 123. doi:10.3390/genes8040123
238. Hill MA, Alexander WB, Guo B, Kato Y, Patra K, O’Dell MR, et al. Kras and Tp53 Mutations Cause Cholangiocyte- and Hepatocyte-Derived Cholangiocarcinoma. *Cancer Res.* 2018;78: 4445–4451. doi:10.1158/0008-5472.CAN-17-1123
239. Brunt EM. Histopathologic features of hepatocellular carcinoma. *Clinical Liver Disease.* 2012;1: 194–199. doi:10.1002/cld.98
240. Schlageter M, Terracciano LM, D’Angelo S, Sorrentino P. Histopathology of hepatocellular carcinoma. *World J Gastroenterol.* 2014;20: 15955–15964. doi:10.3748/wjg.v20.i43.15955
241. Meyer-Ficca ML, Meyer RG, Kaiser H, Brack AR, Kandolf R, Küpper J-H. Comparative analysis of inducible expression systems in transient transfection studies. *Analytical Biochemistry.* 2004;334: 9–19. doi:10.1016/j.ab.2004.07.011
242. Mizuguchi H, Hayakawa T. Characteristics of adenovirus-mediated tetracycline-controllable expression system. *Biochimica et Biophysica Acta (BBA) - General Subjects.* 2001;1568: 21–29. doi:10.1016/S0304-4165(01)00195-7
243. Valer JA, Sánchez-de-Diego C, Pimenta-Lopes C, Rosa JL, Ventura F. ACVR1 Function in Health and Disease. *Cells.* 2019;8: 1366. doi:10.3390/cells8111366
244. López-Rovira T, Chaux E, Massagué J, Rosa JL, Ventura F. Direct Binding of Smad1 and Smad4 to Two Distinct Motifs Mediates Bone Morphogenetic Protein-specific Transcriptional Activation of *Id1* Gene *. *Journal of Biological Chemistry.* 2002;277: 3176–3185. doi:10.1074/jbc.M106826200
245. ten Dijke P, Yamashita H, Sampath TK, Reddi AH, Estevez M, Riddle DL, et al. Identification of type I receptors for osteogenic protein-1 and bone morphogenetic protein-4. *J Biol Chem.* 1994;269: 16985–16988.
246. Yu PB, Beppu H, Kawai N, Li E, Bloch KD. Bone Morphogenetic Protein (BMP) Type II Receptor Deletion Reveals BMP Ligand-specific Gain of Signaling in Pulmonary Artery Smooth Muscle Cells*. *Journal of Biological Chemistry.* 2005;280: 24443–24450. doi:10.1074/jbc.M502825200

REFERENCES

247. Hollnagel A, Oehlmann V, Heymer J, Rütter U, Nordheim A. Id Genes Are Direct Targets of Bone Morphogenetic Protein Induction in Embryonic Stem Cells *. *Journal of Biological Chemistry*. 1999;274: 19838–19845. doi:10.1074/jbc.274.28.19838
248. Miyazono K, Miyazawa K. Id: A Target of BMP Signaling. *Science's STKE*. 2002;2002: pe40–pe40. doi:10.1126/stke.2002.151.pe40
249. Krämer A, Green J, Pollard J, Tugendreich S. Causal analysis approaches in Ingenuity Pathway Analysis. *Bioinformatics*. 2014;30: 523–530. doi:10.1093/bioinformatics/btt703
250. Li Z, Chen Y-G. Functions of BMP signaling in embryonic stem cell fate determination. *Exp Cell Res*. 2013;319: 113–119. doi:10.1016/j.yexcr.2012.09.016
251. Rahman MS, Akhtar N, Jamil HM, Banik RS, Asaduzzaman SM. TGF- β /BMP signaling and other molecular events: regulation of osteoblastogenesis and bone formation. *Bone Res*. 2015;3: 1–20. doi:10.1038/boneres.2015.5
252. Yoon BS, Lyons KM. Multiple functions of BMPs in chondrogenesis. *J Cell Biochem*. 2004;93: 93–103. doi:10.1002/jcb.20211
253. Bond AM, Bhalala OG, Kessler JA. The dynamic role of bone morphogenetic proteins in neural stem cell fate and maturation. *Dev Neurobiol*. 2012;72: 1068–1084. doi:10.1002/dneu.22022
254. Jamali M, Karamboulas C, Rogerson PJ, Skerjanc IS. BMP signaling regulates Nkx2-5 activity during cardiomyogenesis. *FEBS Lett*. 2001;509: 126–130. doi:10.1016/s0014-5793(01)03151-9
255. Kaiser S, Schirmacher P, Philipp A, Protschka M, Moll I, Nicol K, et al. Induction of Bone Morphogenetic Protein-6 in Skin Wounds. Delayed Reepitheliazation and Scar Formation in BMP-6 Overexpressing Transgenic Mice. *Journal of Investigative Dermatology*. 1998;111: 1145–1152. doi:10.1046/j.1523-1747.1998.00407.x
256. Xu F, Liu C, Zhou D, Zhang L. TGF- β /SMAD Pathway and Its Regulation in Hepatic Fibrosis. *J Histochem Cytochem*. 2016;64: 157–167. doi:10.1369/0022155415627681
257. Zou G-L, Zuo S, Lu S, Hu R-H, Lu Y-Y, Yang J, et al. Bone morphogenetic protein-7 represses hepatic stellate cell activation and liver fibrosis via regulation of TGF- β /Smad signaling pathway. *World J Gastroenterol*. 2019;25: 4222–4234. doi:10.3748/wjg.v25.i30.4222
258. Knöchel S, Schuler-Metz A, Knöchel W. c-Jun (AP-1) activates BMP-4 transcription in *Xenopus* embryos. *Mech Dev*. 2000;98: 29–36. doi:10.1016/s0925-4773(00)00448-2
259. Ono Y, Calhabeu F, Morgan JE, Katagiri T, Amthor H, Zammit PS. BMP signalling permits population expansion by preventing premature myogenic differentiation in muscle satellite cells. *Cell Death Differ*. 2011;18: 222–234. doi:10.1038/cdd.2010.95
260. Sexton KE. The generalized effect of BMP-2 on oxidative phosphorylation. 2019 [cited 9 Nov 2021]. Available: <https://open.bu.edu/handle/2144/36636>
261. Holien T, Våtsveen TK, Hella H, Rampa C, Brede G, Grøseth L a. G, et al. Bone morphogenetic proteins induce apoptosis in multiple myeloma cells by Smad-dependent repression of MYC. *Leukemia*. 2012;26: 1073–1080. doi:10.1038/leu.2011.263
262. Liu H, Bao D, Xia X, Chau JFL, Li B. An Unconventional Role of BMP-Smad1 Signaling in DNA Damage Response: A Mechanism for Tumor Suppression. *Journal of Cellular Biochemistry*. 2014;115: 450–456. doi:10.1002/jcb.24698
263. Vattulainen-Collanus S, Southwood M, Yang XD, Moore S, Ghatpande P, Morrell NW, et al. Bone morphogenetic protein signaling is required for RAD51-mediated maintenance of genome integrity in vascular endothelial cells. *Commun Biol*. 2018;1: 1–15. doi:10.1038/s42003-018-0152-1
264. Gudipaty SA, Conner CM, Rosenblatt J, Montell DJ. Unconventional Ways to Live and Die: Cell Death and Survival in Development, Homeostasis, and Disease. *Annu Rev Cell Dev Biol*. 2018;34: 311–332. doi:10.1146/annurev-cellbio-100616-060748

265. Voss AK, Strasser A. The essentials of developmental apoptosis. *F1000Res*. 2020;9: F1000 Faculty Rev-148. doi:10.12688/f1000research.21571.1
266. Raja E, Tzavlaki K, Vuilleumier R, Edlund K, Kahata K, Zieba A, et al. The protein kinase LKB1 negatively regulates bone morphogenetic protein receptor signaling. *Oncotarget*. 2015;7: 1120–1143. doi:10.18632/oncotarget.6683
267. Sugimoto H, Yang C, LeBleu VS, Soubasakos MA, Giraldo M, Zeisberg M, et al. BMP-7 functions as a novel hormone to facilitate liver regeneration. *The FASEB Journal*. 2007;21: 256–264. doi:10.1096/fj.06-6837com
268. Smith-Garvin JE, Koretzky GA, Jordan MS. T Cell Activation. *Annu Rev Immunol*. 2009;27: 591–619. doi:10.1146/annurev.immunol.021908.132706
269. Leithäuser F, Dhein J, Mechtersheimer G, Koretz K, Brüderlein S, Henne C, et al. Constitutive and induced expression of APO-1, a new member of the nerve growth factor/tumor necrosis factor receptor superfamily, in normal and neoplastic cells. *Lab Invest*. 1993;69: 415–429.
270. Möller P, Koretz K, Leithäuser F, Brüderlein S, Henne C, Quentmeier A, et al. Expression of APO-1 (CD95), a member of the NGF/TNF receptor superfamily, in normal and neoplastic colon epithelium. *International Journal of Cancer*. 1994;57: 371–377. doi:10.1002/ijc.2910570314
271. Faletti L, Peintner L, Neumann S, Sandler S, Grabinger T, Mac Nelly S, et al. TNF α sensitizes hepatocytes to FasL-induced apoptosis by NF κ B-mediated Fas upregulation. *Cell Death Dis*. 2018;9: 1–14. doi:10.1038/s41419-018-0935-9
272. Charles A Janeway J, Travers P, Walport M, Shlomchik MJ. T cell-mediated cytotoxicity. *Immunobiology: The Immune System in Health and Disease* 5th edition. 2001 [cited 29 Oct 2021]. Available: <https://www.ncbi.nlm.nih.gov/books/NBK27101/>
273. Chin YE, Kitagawa M, Kuida K, Flavell RA, Fu XY. Activation of the STAT signaling pathway can cause expression of caspase 1 and apoptosis. *Mol Cell Biol*. 1997;17: 5328–5337.
274. Xu X, Fu X-Y, Plate J, Chong AS-F. IFN- γ Induces Cell Growth Inhibition by Fas-mediated Apoptosis: Requirement of STAT1 Protein for Up-Regulation of Fas and FasL Expression. *Cancer Res*. 1998;58: 2832–2837.
275. Shuai K, Schindler C, Prezioso VR, Darnell JE. Activation of Transcription by IFN- γ : Tyrosine Phosphorylation of a 91-kD DNA Binding Protein. *Science*. 1992;258: 1808–1812. doi:10.1126/science.1281555
276. Wen Z, Zhong Z, Darnell JE. Maximal activation of transcription by stat1 and stat3 requires both tyrosine and serine phosphorylation. *Cell*. 1995;82: 241–250. doi:10.1016/0092-8674(95)90311-9
277. Sikder HA, Devlin MK, Dunlap S, Ryu B, Alani RM. Id proteins in cell growth and tumorigenesis. *Cancer Cell*. 2003;3: 525–530. doi:10.1016/S1535-6108(03)00141-7
278. Bresnahan E, Lindblad KE, Galarreta MR de, Lujambio A. Mouse Models of Oncoimmunology in Hepatocellular Carcinoma. *Clin Cancer Res*. 2020;26: 5276–5286. doi:10.1158/1078-0432.CCR-19-2923
279. Zitvogel L, Pitt JM, Daillère R, Smyth MJ, Kroemer G. Mouse models in oncoimmunology. *Nat Rev Cancer*. 2016;16: 759–773. doi:10.1038/nrc.2016.91
280. Caviglia JM, Schwabe RF. Mouse Models of Liver Cancer. In: Eferl R, Casanova E, editors. *Mouse Models of Cancer: Methods and Protocols*. New York, NY: Springer; 2015. pp. 165–183. doi:10.1007/978-1-4939-2297-0_8
281. Xue W, Chen S, Yin H, Tammela T, Papagiannakopoulos T, Joshi NS, et al. CRISPR-mediated direct mutation of cancer genes in the mouse liver. *Nature*. 2014;514: 380–384. doi:10.1038/nature13589
282. Tschaharganeh DF, Xue W, Calvisi DF, Evert M, Michurina TV, Dow LE, et al. p53-dependent Nestin regulation links tumor suppression to cellular plasticity in liver cancer. *Cell*. 2014;158: 579–592. doi:10.1016/j.cell.2014.05.051
283. Revia S, Seretny A, Wendler L, Banito A, Eckert C, Breuer K, et al. Histone H3K27 demethylase KDM6A is an epigenetic gatekeeper of mTORC1 signalling in cancer. *Gut*. 2021 [cited 9 Feb 2022]. doi:10.1136/gutjnl-2021-325405

REFERENCES

284. Breinig M, Schweitzer AY, Herianto AM, Revia S, Schaefer L, Wendler L, et al. Multiplexed orthogonal genome editing and transcriptional activation by Cas12a. *Nat Methods*. 2019;16: 51–54. doi:10.1038/s41592-018-0262-1
285. Liu Y-T, Tseng T-C, Soong R-S, Peng C-Y, Cheng Y-H, Huang S-F, et al. A novel spontaneous hepatocellular carcinoma mouse model for studying T-cell exhaustion in the tumor microenvironment. *J Immunother Cancer*. 2018;6: 144. doi:10.1186/s40425-018-0462-3
286. Galarreta MR de, Bresnahan E, Molina-Sánchez P, Lindblad KE, Maier B, Sia D, et al. β -Catenin Activation Promotes Immune Escape and Resistance to Anti-PD-1 Therapy in Hepatocellular Carcinoma. *Cancer Discov*. 2019;9: 1124–1141. doi:10.1158/2159-8290.CD-19-0074
287. Lin C-P, Liu C-R, Lee C-N, Chan T-S, Liu HE. Targeting c-Myc as a novel approach for hepatocellular carcinoma. *World J Hepatol*. 2010;2: 16–20. doi:10.4254/wjh.v2.i1.16
288. Perincheri S, Hui P. KRAS mutation testing in clinical practice. *Expert Review of Molecular Diagnostics*. 2015;15: 375–384. doi:10.1586/14737159.2015.986102
289. Wang G, Wang Q, Liang N, Xue H, Yang T, Chen X, et al. Oncogenic driver genes and tumor microenvironment determine the type of liver cancer. *Cell Death Dis*. 2020;11: 1–13. doi:10.1038/s41419-020-2509-x
290. Gabay M, Li Y, Felsher DW. MYC Activation Is a Hallmark of Cancer Initiation and Maintenance. *Cold Spring Harb Perspect Med*. 2014;4: a014241. doi:10.1101/cshperspect.a014241
291. Ischenko I, D’Amico S, Rao M, Li J, Hayman MJ, Powers S, et al. KRAS drives immune evasion in a genetic model of pancreatic cancer. *Nat Commun*. 2021;12: 1482. doi:10.1038/s41467-021-21736-w
292. Carvalho PD, Guimarães CF, Cardoso AP, Mendonça S, Costa ÂM, Oliveira MJ, et al. KRAS Oncogenic Signaling Extends beyond Cancer Cells to Orchestrate the Microenvironment. *Cancer Res*. 2018;78: 7–14. doi:10.1158/0008-5472.CAN-17-2084
293. Ischenko I, Zhi J, Hayman MJ, Petrenko O. KRAS-dependent suppression of MYC enhances the sensitivity of cancer cells to cytotoxic agents. *Oncotarget*. 2017;8: 17995–18009. doi:10.18632/oncotarget.14929
294. Juric V, Ruffell B, Evason KJ, Hu J, Che L, Wang L, et al. Monocytes promote liver carcinogenesis in an oncogene-specific manner. *Journal of Hepatology*. 2016;64: 881–890. doi:10.1016/j.jhep.2015.11.025
295. DuPage M, Cheung AF, Mazumdar C, Winslow MM, Bronson R, Schmidt LM, et al. Endogenous T cell responses to antigens expressed in lung adenocarcinomas delay malignant tumor progression. *Cancer Cell*. 2011;19: 72–85. doi:10.1016/j.ccr.2010.11.011
296. DuPage M, Mazumdar C, Schmidt LM, Cheung AF, Jacks T. Expression of tumour-specific antigens underlies cancer immunoediting. *Nature*. 2012;482: 405–409. doi:10.1038/nature10803
297. Fehlings M, Jhunjhunwala S, Kowanetz M, O’Gorman WE, Hegde PS, Sumatoh H, et al. Late-differentiated effector neoantigen-specific CD8+ T cells are enriched in peripheral blood of non-small cell lung carcinoma patients responding to atezolizumab treatment. *Journal for ImmunoTherapy of Cancer*. 2019;7: 249. doi:10.1186/s40425-019-0695-9
298. Zhang J, Caruso FP, Sa JK, Justesen S, Nam D-H, Sims P, et al. The combination of neoantigen quality and T lymphocyte infiltrates identifies glioblastomas with the longest survival. *Commun Biol*. 2019;2: 135. doi:10.1038/s42003-019-0369-7
299. Miller A, Asmann Y, Cattaneo L, Braggio E, Keats J, Auclair D, et al. High somatic mutation and neoantigen burden are correlated with decreased progression-free survival in multiple myeloma. *Blood Cancer J*. 2017;7: e612. doi:10.1038/bcj.2017.94
300. Ren Y, Cherukuri Y, Wickland DP, Sarangi V, Tian S, Carter JM, et al. HLA class-I and class-II restricted neoantigen loads predict overall survival in breast cancer. *Oncoimmunology*. 2020;9: 1744947. doi:10.1080/2162402X.2020.1744947

301. Petrizzo A, Tagliamonte M, Mauriello A, Costa V, Aprile M, Esposito R, et al. Unique true predicted neoantigens (TPNAs) correlates with anti-tumor immune control in HCC patients. *J Transl Med.* 2018;16: 286. doi:10.1186/s12967-018-1662-9
302. Ney JT, Schmidt T, Kurts C, Zhou Q, Eckert D, Felsher DW, et al. Autochthonous liver tumors induce systemic T cell tolerance associated with T cell receptor down-modulation. *Hepatology.* 2009;49: 471–481. doi:10.1002/hep.22652
303. Morales-Kastresana A, Sanmamed MF, Rodriguez I, Palazon A, Martinez-Forero I, Labiano S, et al. Combined Immunostimulatory Monoclonal Antibodies Extend Survival in an Aggressive Transgenic Hepatocellular Carcinoma Mouse Model. *Clin Cancer Res.* 2013;19: 6151–6162. doi:10.1158/1078-0432.CCR-13-1189
304. Connor F, Rayner TF, Aitken SJ, Feig C, Lukk M, Santoyo-Lopez J, et al. Mutational landscape of a chemically-induced mouse model of liver cancer. *J Hepatol.* 2018;69: 840–850. doi:10.1016/j.jhep.2018.06.009
305. Willimsky G, Blankenstein T. Sporadic immunogenic tumours avoid destruction by inducing T-cell tolerance. *Nature.* 2005;437: 141–146. doi:10.1038/nature03954
306. Embleton MJ, Heidelberger C. Antigenicity of clones of mouse prostate cells transformed in vitro. *International Journal of Cancer.* 1972;9: 8–18. doi:10.1002/ijc.2910090103
307. Brown ZJ, Heinrich B, Greten TF. Mouse models of hepatocellular carcinoma: an overview and highlights for immunotherapy research. *Nat Rev Gastroenterol Hepatol.* 2018;15: 536–554. doi:10.1038/s41575-018-0033-6
308. Gee S, Nelson N, Bornot A, Carter N, Cuomo ME, Dovedi SJ, et al. Developing an Arrayed CRISPR-Cas9 Co-Culture Screen for Immuno-Oncology Target ID. *SLAS DISCOVERY: Advancing the Science of Drug Discovery.* 2020;25: 581–590. doi:10.1177/2472555220916457
309. Olivo Pimentel V, Yaromina A, Marcus D, Dubois LJ, Lambin P. A novel co-culture assay to assess anti-tumor CD8+ T cell cytotoxicity via luminescence and multicolor flow cytometry. *Journal of Immunological Methods.* 2020;487: 112899. doi:10.1016/j.jim.2020.112899
310. Lakins MA, Ghorani E, Munir H, Martins CP, Shields JD. Cancer-associated fibroblasts induce antigen-specific deletion of CD8 + T Cells to protect tumour cells. *Nat Commun.* 2018;9: 948. doi:10.1038/s41467-018-03347-0
311. Han P, Dai Q, Fan L, Lin H, Zhang X, Li F, et al. Genome-Wide CRISPR Screening Identifies JAK1 Deficiency as a Mechanism of T-Cell Resistance. *Frontiers in Immunology.* 2019;10. Available: <https://www.frontiersin.org/article/10.3389/fimmu.2019.00251>
312. Kearney CJ, Vervoort SJ, Hogg SJ, Ramsbottom KM, Freeman AJ, Lalaoui N, et al. Tumor immune evasion arises through loss of TNF sensitivity. *Science Immunology.* 2018 [cited 17 Feb 2022]. doi:10.1126/sciimmunol.aar3451
313. Pan D, Kobayashi A, Jiang P, Andrade LF de, Tay RE, Luoma AM, et al. A major chromatin regulator determines resistance of tumor cells to T cell-mediated killing. *Science.* 2018 [cited 17 Feb 2022]. doi:10.1126/science.aao1710
314. Patel SJ, Sanjana NE, Kishton RJ, Eidizadeh A, Vodnala SK, Cam M, et al. Identification of essential genes for cancer immunotherapy. *Nature.* 2017;548: 537–542. doi:10.1038/nature23477
315. Spiotto MT, Rowley DA, Schreiber H. Bystander elimination of antigen loss variants in established tumors. *Nat Med.* 2004;10: 294–298. doi:10.1038/nm999
316. Peper JK, Schuster H, Löffler MW, Schmid-Horch B, Rammensee H-G, Stevanović S. An impedance-based cytotoxicity assay for real-time and label-free assessment of T-cell-mediated killing of adherent cells. *Journal of Immunological Methods.* 2014;405: 192–198. doi:10.1016/j.jim.2014.01.012
317. Brunner KT, Mauel J, Cerottini J-C, Chapuis B. Quantitative assay of the lytic action of immune lymphoid cells of 51Cr-labelled allogeneic target cells in vitro; inhibition by isoantibody and by drugs. *Immunology.* 1968;14: 181–196.

REFERENCES

318. Kim JM, Chen DS. Immune escape to PD-L1/PD-1 blockade: seven steps to success (or failure). *Annals of Oncology*. 2016;27: 1492–1504. doi:10.1093/annonc/mdw217
319. Manguso RT, Pope HW, Zimmer MD, Brown FD, Yates KB, Miller BC, et al. In vivo CRISPR screening identifies Ptpn2 as a cancer immunotherapy target. *Nature*. 2017;547: 413–418. doi:10.1038/nature23270
320. Zhang J, Späth SS, Katz SG. Genome-Wide CRISPRi/a Screening in an In Vitro Coculture Assay of Human Immune Cells with Tumor Cells. *Methods Mol Biol*. 2020;2097: 231–252. doi:10.1007/978-1-0716-0203-4_15
321. Patel SJ, Sanjana NE, Kishton RJ, Eidizadeh A, Vodnala SK, Cam M, et al. Identification of essential genes for cancer immunotherapy. *Nature*. 2017;548: 537–542. doi:10.1038/nature23477
322. Concha-Benavente F, Ferris RL. Reversing EGFR Mediated Immunoescape by Targeted Monoclonal Antibody Therapy. *Frontiers in Pharmacology*. 2017;8. Available: <https://www.frontiersin.org/article/10.3389/fphar.2017.00332>
323. Miles LA, Garippa RJ, Poirier JT. Design, execution, and analysis of pooled in vitro CRISPR/Cas9 screens. *The FEBS Journal*. 2016;283: 3170–3180. doi:10.1111/febs.13770
324. Yadin D, Knaus P, Mueller TD. Structural insights into BMP receptors: Specificity, activation and inhibition. *Cytokine & Growth Factor Reviews*. 2016;27: 13–34. doi:10.1016/j.cytogfr.2015.11.005
325. Kaplan FS, Shen Q, Lounev V, Seemann P, Groppe J, Katagiri T, et al. Skeletal metamorphosis in fibrodysplasia ossificans progressiva (FOP). *J Bone Miner Metab*. 2008;26: 521–530. doi:10.1007/s00774-008-0879-8
326. Shore EM, Xu M, Feldman GJ, Fenstermacher DA, Cho T-J, Choi IH, et al. A recurrent mutation in the BMP type I receptor ACVR1 causes inherited and sporadic fibrodysplasia ossificans progressiva. *Nat Genet*. 2006;38: 525–527. doi:10.1038/ng1783
327. Wu G, Diaz AK, Paugh BS, Rankin SL, Ju B, Li Y, et al. The genomic landscape of diffuse intrinsic pontine glioma and pediatric non-brainstem high-grade glioma. *Nat Genet*. 2014;46: 444–450. doi:10.1038/ng.2938
328. Tsai C-L, Tsai C-N, Lin C-Y, Chen H-W, Lee Y-S, Chao A, et al. Secreted Stress-Induced Phosphoprotein 1 Activates the ALK2-SMAD Signaling Pathways and Promotes Cell Proliferation of Ovarian Cancer Cells. *Cell Reports*. 2012;2: 283–293. doi:10.1016/j.celrep.2012.07.002
329. Herrera B, van Dinther M, ten Dijke P, Inman GJ. Autocrine Bone Morphogenetic Protein-9 Signals through Activin Receptor-like Kinase-2/Smad1/Smad4 to Promote Ovarian Cancer Cell Proliferation. *Cancer Research*. 2009;69: 9254–9262. doi:10.1158/0008-5472.CAN-09-2912
330. Zhao B, Pritchard JR. Inherited Disease Genetics Improves the Identification of Cancer-Associated Genes. *PLOS Genetics*. 2016;12: e1006081. doi:10.1371/journal.pgen.1006081
331. Olsen OE, Wader KF, Misund K, Våtsveen TK, Rø TB, Mylin AK, et al. Bone morphogenetic protein-9 suppresses growth of myeloma cells by signaling through ALK2 but is inhibited by endoglin. *Blood Cancer Journal*. 2014;4: e196–e196. doi:10.1038/bcj.2014.16
332. Raja E, Komuro A, Tanabe R, Sakai S, Ino Y, Saito N, et al. Bone morphogenetic protein signaling mediated by ALK-2 and DLX2 regulates apoptosis in glioma-initiating cells. *Oncogene*. 2017;36: 4963–4974. doi:10.1038/onc.2017.112
333. Wiley LA, Rajagopal R, Dattilo LK, Beebe DC. The tumor suppressor gene Trp53 protects the mouse lens against posterior subcapsular cataracts and the BMP receptor Acvr1 acts as a tumor suppressor in the lens. *Disease Models & Mechanisms*. 2011;4: 484–495. doi:10.1242/dmm.006593
334. Ambrosio EP, Drigo SA, Bérnago NA, Rosa FE, Bertonha FB, de Abreu FB, et al. Recurrent copy number gains of ACVR1 and corresponding transcript overexpression are associated with survival in head and neck squamous cell carcinomas. *Histopathology*. 2011;59: 81–89. doi:10.1111/j.1365-2559.2011.03885.x

335. Macías-Silva M, Hoodless PA, Tang SJ, Buchwald M, Wrana JL. Specific Activation of Smad1 Signaling Pathways by the BMP7 Type I Receptor, ALK2*. *Journal of Biological Chemistry*. 1998;273: 25628–25636. doi:10.1074/jbc.273.40.25628
336. Ivanov VN, Bergami PL, Maulit G, Sato T-A, Sassoon D, Ronai Z. FAP-1 Association with Fas (Apo-1) Inhibits Fas Expression on the Cell Surface. *Molecular and Cellular Biology*. 2003;23: 3623–3635. doi:10.1128/MCB.23.10.3623-3635.2003
337. Ivanov VN, Ronai Z, Hei TK. Opposite Roles of FAP-1 and Dynamin in the Regulation of Fas (CD95) Translocation to the Cell Surface and Susceptibility to Fas Ligand-mediated Apoptosis. *J Biol Chem*. 2006;281: 1840–1852. doi:10.1074/jbc.M509866200
338. Peter ME, Hadji A, Murmann AE, Brockway S, Putzbach W, Pattanayak A, et al. The role of CD95 and CD95 ligand in cancer. *Cell Death Differ*. 2015;22: 549–559. doi:10.1038/cdd.2015.3
339. Bullani RR, Wehrli P, Viard-Leveugle I, Rimoldi D, Cerottini J-C, Saurat J-H, et al. Frequent downregulation of Fas (CD95) expression and function in melanoma. *Melanoma Res*. 2002;12: 263–270. doi:10.1097/00008390-200206000-00010
340. Takaesu G, Surabhi RM, Park K-J, Ninomiya-Tsuji J, Matsumoto K, Gaynor RB. TAK1 is Critical for I κ B Kinase-mediated Activation of the NF- κ B Pathway. *Journal of Molecular Biology*. 2003;326: 105–115. doi:10.1016/S0022-2836(02)01404-3
341. Barruet E, Morales BM, Cain CJ, Ton AN, Wentworth KL, Chan TV, et al. NF- κ B/MAPK activation underlies ACVR1-mediated inflammation in human heterotopic ossification. *JCI Insight*. 2018;3. doi:10.1172/jci.insight.122958
342. Zinatizadeh MR, Schock B, Chalbatani GM, Zarandi PK, Jalali SA, Miri SR. The Nuclear Factor Kappa B (NF- κ B) signaling in cancer development and immune diseases. *Genes & Diseases*. 2021;8: 287–297. doi:10.1016/j.gendis.2020.06.005
343. Taniguchi K, Karin M. NF- κ B, inflammation, immunity and cancer: coming of age. *Nat Rev Immunol*. 2018;18: 309–324. doi:10.1038/nri.2017.142
344. Verzella D, Pescatore A, Capece D, Vecchiotti D, Ursini MV, Franzoso G, et al. Life, death, and autophagy in cancer: NF- κ B turns up everywhere. *Cell Death Dis*. 2020;11: 1–14. doi:10.1038/s41419-020-2399-y
345. Galenkamp KM, Carriba P, Urresti J, Planells-Ferrer L, Coccia E, Lopez-Soriano J, et al. TNF α sensitizes neuroblastoma cells to FasL-, cisplatin- and etoposide-induced cell death by NF- κ B-mediated expression of Fas. *Molecular Cancer*. 2015;14: 62. doi:10.1186/s12943-015-0329-x
346. Chan H, Bartos DP, Owen-Schaub LB. Activation-dependent transcriptional regulation of the human Fas promoter requires NF- κ B p50-p65 recruitment. *Mol Cell Biol*. 1999;19: 2098–2108. doi:10.1128/MCB.19.3.2098
347. Feng JQ, Xing L, Zhang J-H, Zhao M, Horn D, Chan J, et al. NF- κ B specifically activates BMP-2 gene expression in growth plate chondrocytes in vivo and in a chondrocyte cell line in vitro. *J Biol Chem*. 2003;278: 29130–29135. doi:10.1074/jbc.M212296200
348. Fukui N, Ikeda Y, Ohnuki T, Hikita A, Tanaka S, Yamane S, et al. Pro-inflammatory cytokine tumor necrosis factor- α induces bone morphogenetic protein-2 in chondrocytes via mRNA stabilization and transcriptional up-regulation. *J Biol Chem*. 2006;281: 27229–27241. doi:10.1074/jbc.M603385200
349. Yamazaki M, Fukushima H, Shin M, Katagiri T, Doi T, Takahashi T, et al. Tumor Necrosis Factor α Represses Bone Morphogenetic Protein (BMP) Signaling by Interfering with the DNA Binding of Smads through the Activation of NF- κ B. *J Biol Chem*. 2009;284: 35987–35995. doi:10.1074/jbc.M109.070540
350. Jimi E, Hirata S, Shin M, Yamazaki M, Fukushima H. Molecular mechanisms of BMP-induced bone formation: Cross-talk between BMP and NF- κ B signaling pathways in osteoblastogenesis. *Japanese Dental Science Review*. 2010;46: 33–42. doi:10.1016/j.jdsr.2009.10.003
351. Dede M, Kim E, Hart T. Biases and Blind-Spots in Genome-Wide CRISPR Knockout Screens. 2020. p. 2020.01.16.909606. doi:10.1101/2020.01.16.909606

REFERENCES

352. Davis H, Raja E, Miyazono K, Tsubakihara Y, Moustakas A. Mechanisms of action of bone morphogenetic proteins in cancer. *Cytokine & Growth Factor Reviews*. 2016;27: 81–92. doi:10.1016/j.cytogfr.2015.11.009
353. Jiramongkolchai P, Owens P, Hong CC. Emerging roles of the bone morphogenetic protein pathway in cancer: potential therapeutic target for kinase inhibition. *Biochem Soc Trans*. 2016;44: 1117–1134. doi:10.1042/BST20160069
354. Zheng Y, Wang X, Wang H, Yan W, Zhang Q, Chang X. Bone morphogenetic protein 2 inhibits hepatocellular carcinoma growth and migration through downregulation of the PI3K/AKT pathway. *Tumour Biol*. 2014;35: 5189–5198. doi:10.1007/s13277-014-1673-y
355. Maegdefrau U, Bosserhoff A-K. BMP activated Smad signaling strongly promotes migration and invasion of hepatocellular carcinoma cells. *Experimental and Molecular Pathology*. 2012;92: 74–81. doi:10.1016/j.yexmp.2011.10.004
356. Fukuda T, Fukuda R, Miyazono K, Heldin C-H. Tumor Promoting Effect of BMP Signaling in Endometrial Cancer. *International Journal of Molecular Sciences*. 2021;22: 7882. doi:10.3390/ijms22157882
357. Fotinos A, Nagarajan N, Martins AS, Fritz DT, Garsetti D, Lee AT, et al. Bone morphogenetic protein-focused strategies to induce cytotoxicity in lung cancer cells. *Anticancer Res*. 2014;34: 2095–2104.
358. Langenfeld E, Hong CC, Lanke G, Langenfeld J. Bone morphogenetic protein type I receptor antagonists decrease growth and induce cell death of lung cancer cell lines. *PLoS One*. 2013;8: e61256. doi:10.1371/journal.pone.0061256
359. Ali JL, Lagasse BJ, Minuk AJ, Love AJ, Moraya AI, Lam L, et al. Differential cellular responses induced by dorsomorphin and LDN-193189 in chemotherapy-sensitive and chemotherapy-resistant human epithelial ovarian cancer cells. *Int J Cancer*. 2015;136: E455–469. doi:10.1002/ijc.29220
360. Hover LD, Young CD, Bholra NE, Wilson AJ, Khabele D, Hong CC, et al. Small molecule inhibitor of the bone morphogenetic protein pathway DMH1 reduces ovarian cancer cell growth. *Cancer Lett*. 2015;368: 79–87. doi:10.1016/j.canlet.2015.07.032
361. Garulli C, Kalogris C, Pietrella L, Bartolacci C, Andreani C, Falconi M, et al. Dorsomorphin reverses the mesenchymal phenotype of breast cancer initiating cells by inhibition of bone morphogenetic protein signaling. *Cell Signal*. 2014;26: 352–362. doi:10.1016/j.cellsig.2013.11.022
362. Cao Y, Wang C, Zhang X, Xing G, Lu K, Gu Y, et al. Selective Small Molecule Compounds Increase BMP-2 Responsiveness by Inhibiting Smurf1-mediated Smad1/5 Degradation. *Sci Rep*. 2014;4: 4965. doi:10.1038/srep04965
363. Buijs JT, van der Horst G, van den Hoogen C, Cheung H, de Rooij B, Kroon J, et al. The BMP2/7 heterodimer inhibits the human breast cancer stem cell subpopulation and bone metastases formation. *Oncogene*. 2012;31: 2164–2174. doi:10.1038/onc.2011.400
364. Piccirillo SGM, Reynolds BA, Zanetti N, Lamorte G, Binda E, Broggi G, et al. Bone morphogenetic proteins inhibit the tumorigenic potential of human brain tumour-initiating cells. *Nature*. 2006;444: 761–765. doi:10.1038/nature05349
365. Reguera-Núñez E, Roca C, Hardy E, de la Fuente M, Csaba N, Garcia-Fuentes M. Implantable controlled release devices for BMP-7 delivery and suppression of glioblastoma initiating cells. *Biomaterials*. 2014;35: 2859–2867. doi:10.1016/j.biomaterials.2013.12.001
366. Duggal R, Geissinger U, Zhang Q, Aguilar J, Chen NG, Binda E, et al. Vaccinia virus expressing bone morphogenetic protein-4 in novel glioblastoma orthotopic models facilitates enhanced tumor regression and long-term survival. *Journal of Translational Medicine*. 2013;11: 155. doi:10.1186/1479-5876-11-155
367. Persano L, Pistollato F, Rampazzo E, Della Puppa A, Abbadi S, Frasson C, et al. BMP2 sensitizes glioblastoma stem-like cells to Temozolomide by affecting HIF-1 α stability and MGMT expression. *Cell Death Dis*. 2012;3: e412–e412. doi:10.1038/cddis.2012.153

-
368. Md Mizanur Rahman CCM. An Update of Bone Morphogenetic Proteins as Biomarker and Therapy for Cancer. *J Carcinog Mutagen*. 2015;06. doi:10.4172/2157-2518.1000e114
369. Gul S, Murad S, Ehsan N, Bloodsworth P, Sultan A, Faheem M. Transcriptional up-regulation of BMP-4 and BMPRII genes in the peripheral blood of breast cancer patients: A pilot study. *Cancer Biomark*. 2015;15: 551–557. doi:10.3233/CBM-150494
370. Horvath LG, Henshall SM, Kench JG, Turner JJ, Golovsky D, Brenner PC, et al. Loss of BMP2, Smad8, and Smad4 Expression in Prostate Cancer Progression. *Prostate*. 2004;59: 234–242. doi:10.1002/pros.10361
371. Morrissey C, Brown LG, Pitts TEM, Vessella RL, Corey E. Bone Morphogenetic Protein 7 Is Expressed in Prostate Cancer Metastases and Its Effects on Prostate Tumor Cells Depend on Cell Phenotype and the Tumor Microenvironment. *Neoplasia*. 2010;12: 192–205. doi:10.1593/neo.91836
372. Ma Y, Ma L, Guo Q, Zhang S. Expression of bone morphogenetic protein-2 and its receptors in epithelial ovarian cancer and their influence on the prognosis of ovarian cancer patients. *Journal of Experimental & Clinical Cancer Research*. 2010;29: 85. doi:10.1186/1756-9966-29-85

7 Appendix

Table 7.1. List of genes included in the sgRNA surface library.

1600012H06Rik	Cpm	Itgad	Ptprn2
1810055G02Rik	Cpxm1	Itgae	Ptprs
2410131K14Rik	Cr1l	Itgal	Pttg1ip
5330417C22Rik	Cr2	Itgam	Pxdn
9330182L06Rik	Crb2	Itgav	Qsox2
A2m	Crhr1	Itgax	Rack1
AB124611	Crim1	Itgb1	Raet1a
Abca7	Crlf1	Itgb2	Raet1b
Abcb1a	Crtap	Itgb3	Raet1c
Abcc1	Csf1	Itgb4	Raet1e
Ace	Csf1r	Itgb5	Ramp3
Ace2	Csf2ra	Itgb7	Reck
Ackr3	Csmd1	Itih5	Rgma
Acp2	Cspg4	Itrip	Rnf13
Acvr1	Cspg5	Izumo1r	Robo1
Acvr2a	Ctla4	Jag1	Robo2
Acvr2b	Ctsb	Jam2	Robo3
Adam10	Ctsd	Jam3	Ror1
Adam12	Cxadr	Jaml	Ror2
Adam17	Cxcr5	Kdr	Rpn1
Adam22	Dag1	Kirrel	Rpn2
Adam23	Dcbld1	Kirrel3	Rtn4r
Adam9	Dcbld2	Kit	Ryk
Adamtsl4	Dcc	Kitl	S1pr1
Adcyap1r1	Dcn	L1cam	S1pr2
Adgra2	Dgcr2	Lag3	S1pr3
Adgra3	Dkk3	Lair1	S1pr4
Adgrb3	Dner	Lama1	Scarb1
Adgre1	Dpep1	Lama2	Scn2b
Adgre5	Dpep2	Lama4	Scpep1
Adgrg1	Dpp4	Lama5	Scube2
Adgrg6	Dsc2	Lamb1	Scube3
Adgrl1	Dse	Lamb2	Sdk1
Adgrl2	Dsg2	Lamc1	Sdk2
Adgrl3	Ece1	Lamp1	Sel1l
Adgrv1	Ecm1	Lamp2	Sell
Adora2b	Ednra	Lamp5	Sema3a
Adra1b	Ednrb	Ldlr	Sema3c

Adra2a	Efna2	Lgals3bp	Sema4b
Afp	Efna3	Lgi2	Sema4c
Agtr1a	Efnb1	Lgr4	Sema4d
Agtr2	Efnb3	Lifr	Sema4g
Ahsg	Egfr	Lilr4b	Sema5b
AI593442	Elfn1	Lilrb4a	Sema7a
Alcam	Elfn2	Lingo1	Sez6
Alk	Emb	Lingo3	Sez6l
Alpl	Emc1	Lipg	Sez6l2
Amigo1	Emid1	Lman2	Sgcb
Angpt1	Emilin1	Lman2l	Sgcd
Angptl2	Emilin2	Lnpep	Sgce
Angptl4	Eng	Loxl2	Shisa7
Ank2	Eno1	Lpar1	Sidt1
Ano1	Enpp1	Lpar2	Sidt2
Ano6	Enpp3	Lpar4	Siglec1
Ano9	Enpp4	Lpar6	Sirpa
Antxr1	Enpp5	Lpl	Slamf1
Antxr2	Epcam	Lrfn2	Slamf6
Anxa2	Epdr1	Lrfn4	Slamf9
Ap2m1	Epha1	Lrig1	Slc12a5
Art2b	Epha10	Lrig2	Slc12a6
Asah2	Epha2	Lrp1	Slc12a7
Asic1	Epha3	Lrp11	Slc12a9
Aspn	Epha4	Lrp1b	Slc17a7
Astn1	Ephb1	Lrp2	Slc20a2
Astn2	Ephb2	Lrp4	Slc22a5
Atp1a1	Ephb3	Lrp5	Slc23a2
Atp1a3	Ephb4	Lrrc24	Slc24a3
Atp1b1	ErbB2	Lrrc25	Slc24a4
Atp1b2	ErbB3	Lrrc4	Slc29a1
Atp1b3	ErbB4	Lrrc4b	Slc29a4
Atp6ap1	Esam	Lrrn1	Slc2a1
Atp6v0a2	Eva1c	Lrrn4	Slc2a4
Atraid	Evc2	Lrrn4cl	Slc2a8
Atrn	F11r	Lrrtm3	Slc30a1
Axl	F2r	Lsamp	Slc38a1
Bace2	F3	Ltbp1	Slc38a2
Bcam	F5	Ltbp4	Slc38a3
Bcan	Fam171a2	Ltbr	Slc38a5

APPENDIX

Bche	Fap	Lum	Slc39a10
Bdkrb2	Fas	Ly6h	Slc39a14
Bgn	Fasl	Ly75	Slc39a4
Bmp1	Fat3	Ly9	Slc39a6
Bmp3	Fat4	Lypd8	Slc3a2
Bmpr2	Fbln2	M6pr	Slc44a1
Boc	Fbn1	Masp1	Slc46a1
Brinp2	Fbn2	Mbtps1	Slc4a10
Bsg	Fcer1a	Mc2r	Slc4a11
Bst1	Fcer2a	Mcam	Slc4a7
Bst2	Fcgr1	Mcoln1	Slc52a2
Btbd17	Fcgr2b	Mdga1	Slc6a6
Btd	Fgf17	Mdga2	Slc8a1
Btla	Fgfr1	Megf10	Slc8b1
C1qa	Fgfr2	Megf8	Slco1a4
C3ar1	Fgfr3	Megf9	Slco1a5
Cachd1	Fgfrl1	Melft	Slco1c1
Cacna1c	Fkrp	Mertk	Slco2a1
Cacna2d1	Flt1	Met	Slco3a1
Cacna2d2	Flt4	Mfap3l	Slco4a1
Cacng8	Fmod	Mfap4	Slco4c1
Cadm1	Fn1	Mfap5	Slit1
Cadm2	Fndc4	Mfge8	Slit2
Cadm3	Fndc5	Mfsd2a	Slit3
Cadm4	Folh1	Milr1	Slitrk2
Calcr	Folr1	Mme	Slitrk4
Calcr1	Folr2	Mmp15	Smo
Calu	Fras1	Mmrn1	Smpdl3b
Car12	Frem2	Moxd1	Sorcs2
Car4	Fstl1	Mpz	Sorcs3
Casd1	Fzd5	Mpzl1	Sorl1
Casr	Fzd9	Mpzl2	Sort1
Ccdc80	Gabbr1	Mrc1	Sostdc1
Cckbr	Gabbr2	Mrc2	Spock2
Ccr4	Gabra3	Mrgprf	Spon1
Ccr7	Gabra6	Ms4a1	Sppl2a
Cd101	Gabrb3	Msln	Sppl2b
Cd109	Gabrg1	Muc1	Ssr1
Cd14	Gabrg2	Muc15	Ssr2
Cd163	Galnt1	Mug1	St3gal1

Cd164	Gdf3	Mxra8	Stab1
Cd164l2	Gdpd2	Nagpa	Steap4
Cd180	Gfra1	Ncam1	Stim1
Cd19	Gfra2	Ncam2	Sts
Cd2	Gfra3	Ncan	Suco
Cd200	Ggh	Ncln	Susd2
Cd200r1	Ginm1	Ncstn	Sv2a
Cd200r4	Glg1	Nectin1	Sv2b
Cd22	Glmp	Nectin2	Sv2c
Cd226	Glp1r	Nectin3	Svep1
Cd244	Gp5	Negr1	Synpr
Cd24a	Gp9	Neo1	Syp
Cd27	Gpa33	Nfasc	Tacstd2
Cd274	Gpc1	Nid1	Tapbpl
Cd276	Gpc3	Nid2	Tbxa2r
Cd28	Gpc4	Nkain4	Tctn1
Cd302	Gpm6a	Nlgn1	Tctn2
Cd320	Gpm6b	Nlgn2	Tctn3
Cd33	Gpnmb	Nlgn3	Tek
Cd34	Gpr158	Notch1	Tenm2
Cd3d	Gpr176	Notch2	Tex101
Cd3g	Gpr37l1	Npc1	Tfpi
Cd4	Gpr39	Npr2	Tfrc
Cd40	Gria1	Npr3	Tgfb1
Cd44	Gria2	Nptn	Tgfbr1
Cd47	Gria3	Nptx2	Tgfbr2
Cd48	Gria4	Nrcam	Tgfbr3
Cd5	Grid1	Nrp1	Tgoln1
Cd6	Grid2	Nrp2	Thbd
Cd63	Grik2	Nrxn1	Thsd4
Cd79a	Grin1	Nt5e	Thsd7a
Cd79b	Grin2a	Ntm	Thy1
Cd80	Grin2b	Ntn1	Timp1
Cd84	Grm3	Ntng2	Tlr1
Cd86	Grm5	Ntrk2	Tlr13
Cd8a	Grm7	Ntrk3	Tlr2
Cd8b1	Grn	Nup210	Tlr4
Cd93	Gzma	Olfm1	Tlr6
Cd96	Havcr2	Olfm2	Tlr8
Cdcp1	Hepacam	Omg	Tm2d1

APPENDIX

Cdh1	Hepacam2	Osmr	Tm2d3
Cdh10	Heph	Ostm1	Tm9sf1
Cdh11	Hfe	P2rx7	Tm9sf3
Cdh13	Hhip	P2ry10	Tm9sf4
Cdh15	Hnrnpk	P3h1	Tmed4
Cdh17	Hspg2	Panx1	Tmed9
Cdh2	Htr2c	Pcdh15	Tmeff1
Cdh20	Hyal2	Pcdh19	Tmem108
Cdh3	Icam1	Pdcd1	Tmem130
Cdh4	Icam2	Pdcd1lg2	Tmem132a
Cdh5	Icosl	Pdgfc	Tmem132c
Cdh6	Ifnar1	Pdgfra	Tmem132e
Cdhr1	Ifnar2	Pdgfrb	Tmem150a
Cdon	Igdcc3	Pdpn	Tmem231
Ceacam1	Igdcc4	Pecam1	Tmem27
Celsr1	Igf1r	Pigt	Tmem67
Celsr2	Igf2r	Pilrb2	Tmem87a
Celsr3	Igfbp3	Pkd1	Tmem87b
Chl1	IgG6	Pla2g7	Tmem9
Chrdl1	Ighg1	Plat	Tmem9b
Chrm4	Iglon5	Plaur	Tmx3
Chrna4	Igsf1	Plpp1	Tnc
Ckap4	Igsf10	Pltp	Tnfrsf10b
Clcn5	Igsf21	Plxdc1	Tnfrsf18
Clec12a	Igsf3	Plxdc2	Tnfrsf26
Clec2d	Igsf8	Plxna1	Tnfrsf4
Clic1	Igsf9	Plxna2	Tnfrsf8
Clmp	Il10rb	Plxna4	Tnfrsf9
Clstn2	Il12rb1	Plxnb1	Tnfsf11
Clu	Il12rb2	Plxnb3	Tor2a
Cma1	Il17ra	Plxnc1	Tpbg
Cmklr1	Il17rd	Podxl	Trem2
Cnm2	Il18r1	Podxl2	Tril
Cnm4	Il1r1	Pon1	Trpv2
Cnr1	Il1r2	Postn	Trpv4
Cnr2	Il1rap	Prg4	Ttyh1
Cntfr	Il21r	Prl7d1	Ttyh2
Cntn1	Il27ra	Prnp	Ttyh3
Cntn2	Il2ra	Procr	Txndc15
Cntn3	Il2rg	Prom1	Tyro3

Cntn6	Il31ra	Prom2	Unc5a
Cntnap1	Il3ra	Prss23	Unc5b
Cntnap4	Il4ra	Prtg	Unc5c
Col12a1	Il6ra	Psap	Vasn
Col16a1	Il6st	Psca	Vcam1
Col18a1	Il7r	Ptafr	Vcan
Col1a1	Insr	Ptchd1	Vdac1
Col2a1	Islr	Ptgfrn	Vnn1
Col3a1	Itfg1	Pth1r	Vsir
Col5a1	Itga1	Ptk7	Vtcn1
Col6a1	Itga11	Ptprc	Vtn
Col6a2	Itga2	Ptprd	Wnt1
Col6a5	Itga3	Ptprf	Wnt5a
Col6a6	Itga4	Ptprg	Wnt7a
Copb1	Itga5	Ptprj	Wnt7b
Cp	Itga6	Ptprk	Wnt8a
Cpd	Itga7	Ptprm	Ybx1
Cpe	Itga8	Ptprn	Zp3

Table 7.2. Genes identified as hits in the CRISPR/Cas9 screen.

Gene	Score	Gene	Score	Gene	Score
Sostdc1	54.910281	Neo1	15.8748162	Itga11	11.8063792
Egfr	35.5771181	Mfap5	15.8187488	Cd302	11.5891222
Ldlr	34.7044041	Bcam	15.5971365	Pttg1ip	11.4629655
Sdk2	31.2911701	Fras1	15.585465	Dsc2	11.2774465
C3ar1	26.2582884	Vasn	15.5457458	Gp5	11.2714103
Lrrc4b	25.8309419	Psca	15.4375876	Lrp1	11.1790961
Cacng8	24.4729609	Gpr37l1	15.3661651	Lamc1	11.1147071
Nlgn2	23.9197022	Col6a1	15.2901536	Clic1G	10.9381293
Slc12a9	23.5171788	Lrp5	15.2419407	Lgals3bp	10.844621
Ephb4	22.7666505	Nfasc	15.1701596	Cnm2	10.834775
Bche	22.6208356	Tbxa2r	15.167656	Slco4c1	10.7488806
Igln5	21.8977466	Fbln2	15.164482	Cd28	10.6070375
AB12461	21.8942478	Slc20a2	15.0489248	Npr2	10.5641896
Acvr1	21.7099777	Rtn4r	14.8930412	Plaur	10.5622591
Sorcs3	21.5068041	Itga3	14.7974683	Tmeff1	10.4186514
Cd164	21.2764174	Col6a2	14.7193622	Tgfbr2	10.3974166
Gpc1	19.7927931	Ntrk3	14.1798334	Wnt7b	10.0689707
S1pr4	19.3907991	Tacstd2	14.1722301	Itgb3	9.92506908
Pcdh15	19.2270335	Itga7	14.155158	Sorcs2	9.87937679
Mpz	19.0804324	Jaml	13.9886667	Erbp2	9.78670305
Col6a5	18.519053	Gp9	13.9497463	Cd33	9.43239281
Igsf8	18.3331566	Igdcc4	13.8660988	Bmp3	9.3898315
Ncan	17.9760121	Emilin2	13.7834087	Il17ra	9.36092847
Efna2	17.9302102	Ceacam1	13.6425044	Ahsg	9.31469273
Mfge8	17.8043819	Itrip1	13.3047528	Ptprn2	9.2821482
Cntn6	17.7841935	Nectin1	13.209601	Cdh6	9.25407064
Emilin1	17.778275	Cd6	13.0637281	Pdcd1G	8.82974302
Anxa2	17.1508754	Gabbr3	12.8251378	Ggh	8.74570559
Melf	17.143358	Unc5b	12.7950776	Adamtsl4	8.73817624
Lamb2	16.8168345	Epha4	12.5492616	Cd5	8.72073006
Epha1	16.8119089	Itgb7	12.374013	Tlr6	8.6680382
Il17rd	16.7761505	Slc39a4	12.3357904	Cd320	8.63720966
Lrrtm3	16.7681249	Fn1	12.2443388	Bmpr2	7.79228943
S1pr2	16.6143576	Lpar4	12.1672121	Vcan	7.60316444
Grid2	16.5496134	Dag1	12.0310872	Btbd17	7.28339265
Brinp2	16.5481302	Slco3a1	11.961038	Adam23	6.86549636
Ostm1	16.198133	Icam1	11.9293763	Cdon	6.65987919
Shisa7	16.0434253	Notch2	11.83418	Itga2	5.77256638
Nrp2	16.013865	Lrrn4	11.8259246	Icosl	4.83657073